Oil & Natural Gas Technology

DOE Award No.: DE-NT0006553

Progress Report
First Half 2011

ConocoPhillips Gas Hydrate
Production Test

Submitted by:
ConocoPhillips
700 G Street
Anchorage, AK 99501
Principal Investigator: David Schoderbek

Prepared for:
United States Department of Energy
National Energy Technology Laboratory

July 31, 2011

Office of Fossil Energy

Executive Summary

Accomplishments

- Continuation Application submitted by COP and approved by NETL/DOE
- Final Well Design and draft Test Design completed and reviewed by NETL/DOE
- Hydrate test well (COP-Iġnik Sikumi #1) was drilled, logged, completion installed, cemented, and temporarily suspended with no health, safety, or environmental incidents.

Current Status

- Securing permits for well testing activities in Q1/Q2 2012
- Designing 2012 activities including perforating, injection, drawdown, data gathering/management, and abandonment activities, and engineering design of high-pressure injection, metering, and data systems.
- Simulation to predict reservoir performance

Introduction

Work began on the ConocoPhillips Gas Hydrates Production Test (DE-NT0006553) on October 1, 2008. This report is the eighth progress report for the project and summarizes project activities from January 1, 2011 to June 31, 2011. The most significant milestone in this period was drilling, logging, completion installation and temporary suspension of Iġnik Sikumi #1 in Prudhoe Bay Unit, Alaska North Slope (see Figure 1). Another major milestone was approval of Continuation Application to close Phase 2 and enter Phase 3A.

Detailed work on the well design resulted in the well being reconfigured for injection of CO_2 at low rates required by low in-situ reservoir permeability. The redesigned wellbore was reviewed with NETL on December 1, 2010. To accommodate the reconfiguration and minimize technical uncertainty, the test will now be conducted over two winter seasons. The well was drilled and completed in 2011, with perforation, injection, flow back, and depressurization to be conducted in 2012.
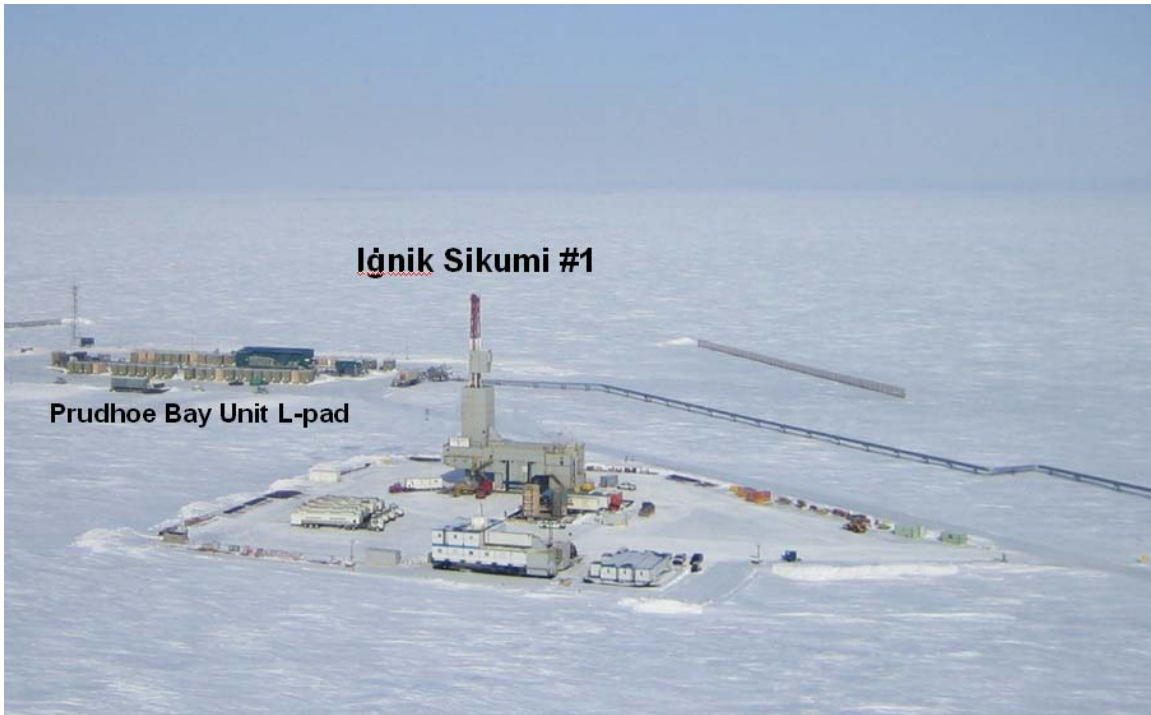
Figure 1: Iġnik Skiumi #1

Task 5 (Phase 2): Detailed Well Planning/Engineering: UNDERWAY
Well planning and engineering for Iġnik Sikumi #1 were completed prior to April 9 spud.
Several critical engineering challenges were encountered and accommodated during
drilling, logging, and casing operations, summarized under Task 8.

Design and planning for winter 2012 injection, flowback, and drawdown operations
continued through the reporting period, are still in progress, and are summarized below:

Basis of Design (BOD) for the 2012 field trial was completed in February 2011.
Equipment will be sourced to handle the following injection and flowback rates:

	N2 (gpm)	CO2 (gpm)
Injection	0.25 – 2	0.25 – 2

	Qg (MCFPD)	Qw (BWPD)
Flowback Above P_{GHS}	7.5 – 100	0 – 50
Flowback Below P_{GHS}	50 – 140	50 – 400

Artificial Lift options to provide drawdown and lifting of produced fluids include a
hydraulic-drive mechanical pump and a reverse jet pump. The hydraulic-drive
mechanical pump will utilize the ¾"chemical injection line to supply power fluid and the
lower end of a conventional sucker-rod pump. One advantage of hydraulic-drive pump,
which has a maximum capacity estimated at 75 BWPD (with limited gas capacity), is the
ability to pump fluid without contact between and mixing of power fluid and pumped
fluid. The reverse jet pump will straddle the gas lift mandrel and will accommodate the

upper range of produced water and gas capacity to meet the Basis Of Design. Power fluid for the reverse jet pump will be recycled produced water, pumped down the annulus and into the gas-lift mandrel.

Process Flow Diagram, graphically describing surface equipment, is under development and is a key planning tool for illustrating the field trial flow handling requirements.

High Pressure Pumping Skid is in detailed engineering design. The HPP skid will provide high pressure pumping for N_2, CO_2, wellbore heating fluid circulation, and reverse jet pump power fluid.

Flow Back system is a standard well testing package including a 1440 psi separator, produced water tanks, metering/gas chromatographs, and flare stack.

Distributed Temperature Sensor (DTS) Cable and Down-Hole Gauges will be continuously monitored by a DTS engineer during the field trial to manage downhole temperature and pressure, key feedback elements for injection, flowback, and drawdown testing. Periodic surveillance of DTS and down-hole gauges is ongoing.

Camp has been identified to provide onsite accommodations for operations personnel.

Task 6 (Phase 2): Pre-Drill Estimation of Reservoir Behavior: COMPLETED
Two important aspects of predictive reservoir behavior have been recently completed. Six laboratory experiments designed to evaluate issues relevant to the Winter 2012 Field Trial were completed during Q1/Q2 2011, testing N_2 and mixed CO_2/N_2 gas injection into hydrate-bearing sandstones and sandpacks. Results confirmed that mixed CO_2/N_2 gas exchanges more efficiently than liquid CO_2, on a mole-per-mole basis, despite its lower CO_2 concentration. Q1/Q2 2011 laboratory results are summarized in Appendix 1.

Modeling of phase behavior inside wellbore tubulars, between the surface and the reservoir, was performed with Prosper^{TM} software. Results confirm that at low injection rates, the relatively long residence time in the tubing is sufficient to condition injected fluids to reservoir temperature, provided liquid/vapor phase transitions in the wellbore are avoided. Wellbore tubular modeling details are presented in Appendix 2.

Task 7 (Phase 3A): Establishment of Test Site Infrastructure: COMPLETED
Initial surveying Iġnik Sikumi #1 location was completed October 21, 2010. Pre-construction staking was completed March 2 (see Figure 2). Federal, State and local permits acquisition was completed March 7, and icepad construction started March 3. Ice pad construction was completed March 15 (see Figure 3), and conductor/cellar setting operations were completed March 22 (see Figure 4). Pre-construction survey, post-construction icepad survey, and final "as-built" survey plats are included as Figures 5, 6, and 7, respectively.
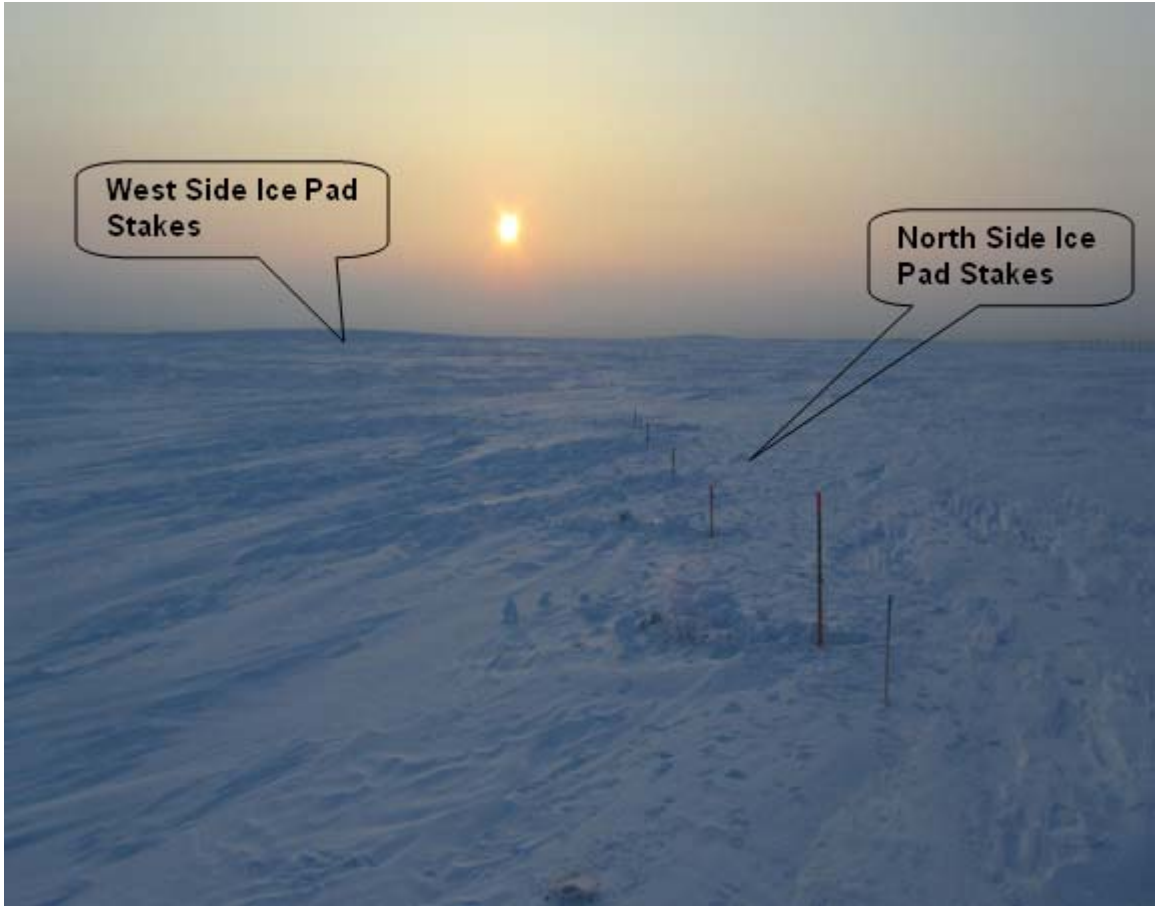
Figure 2: Pre-construction surveying

Figure 3: Ice-pad construction completion

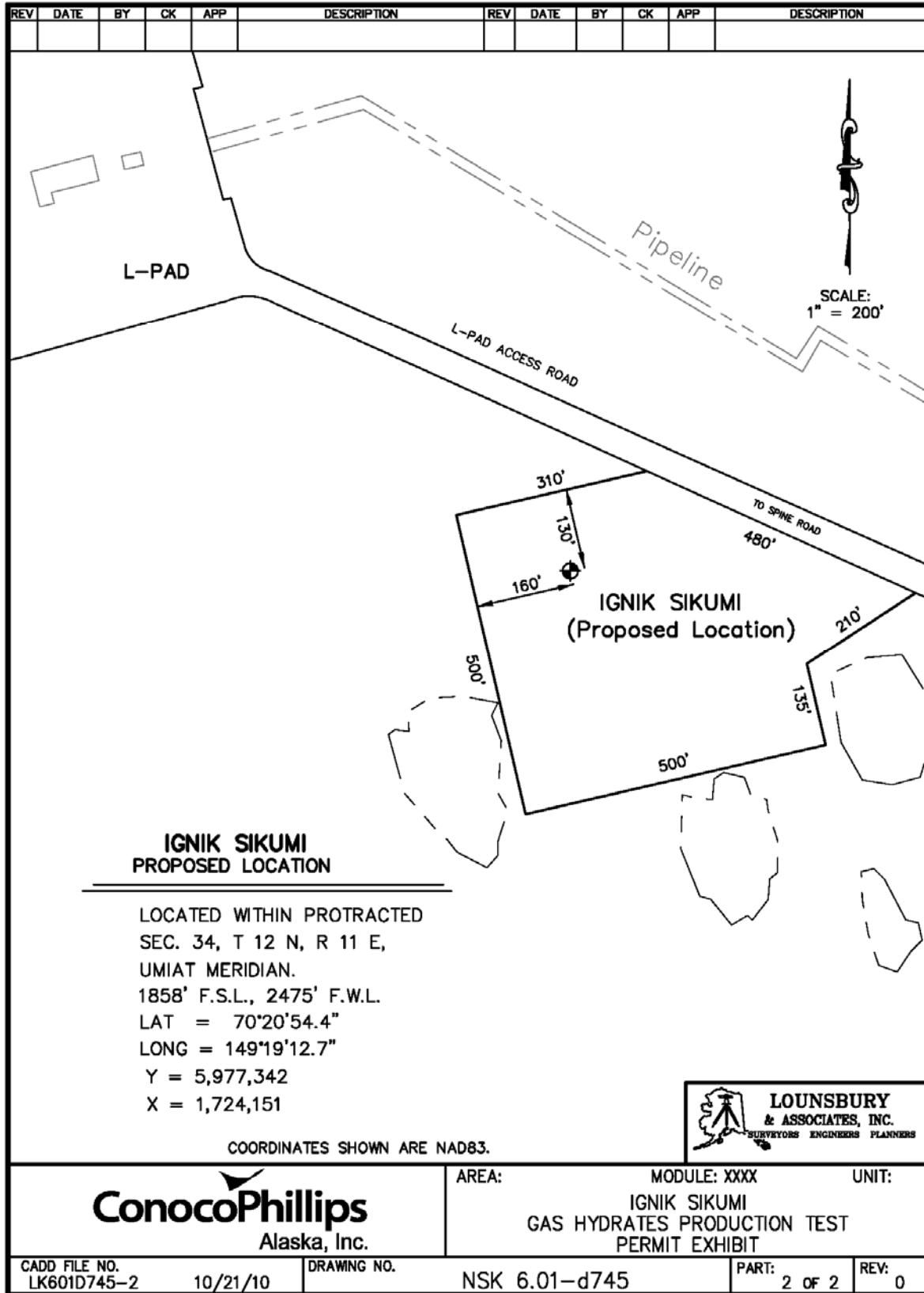Figure 4: Cellar-setting operation; PBU L-pad facilities in background

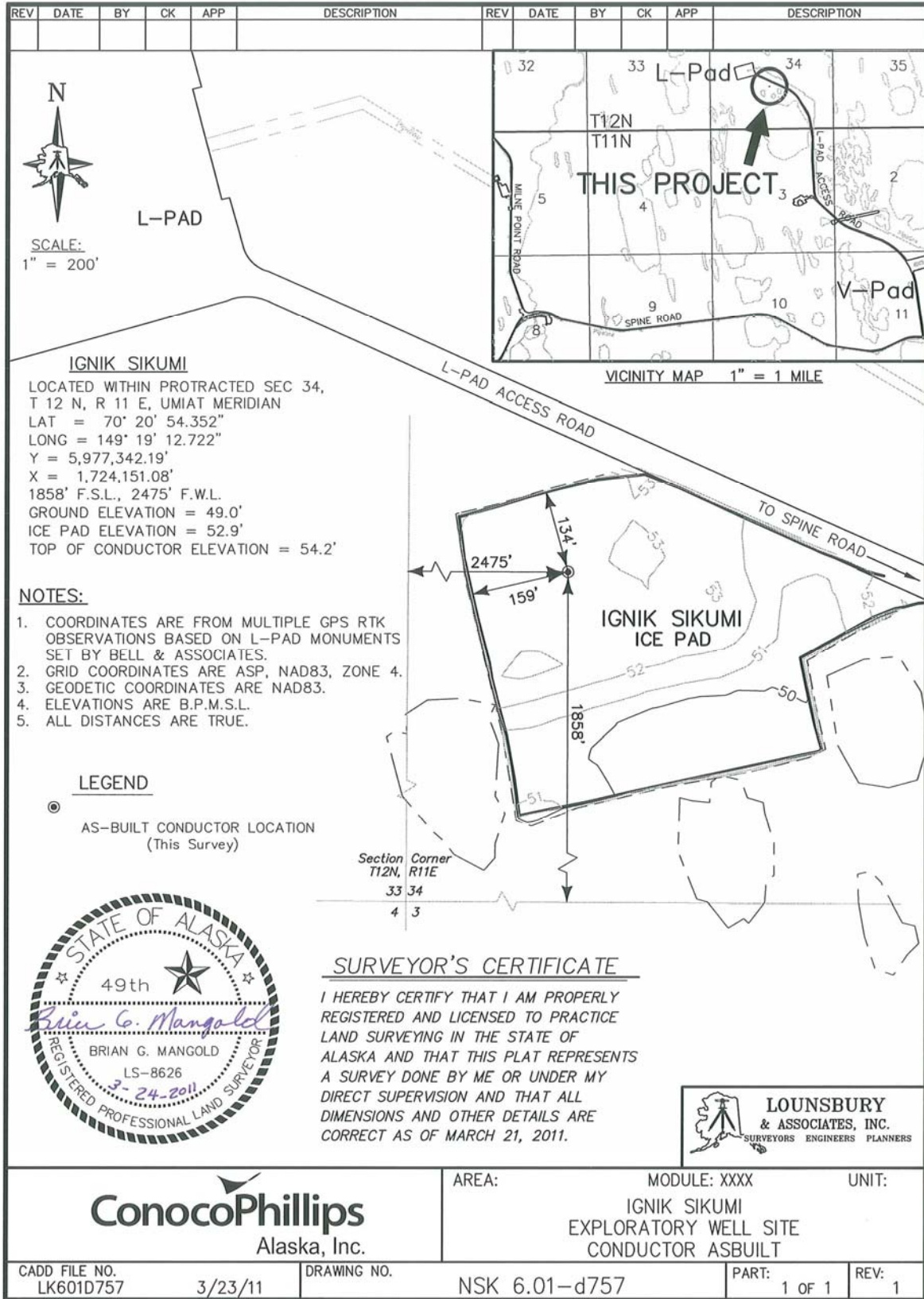Figure 5: Iġnik Sikumi #1 Pre-construction survey plat

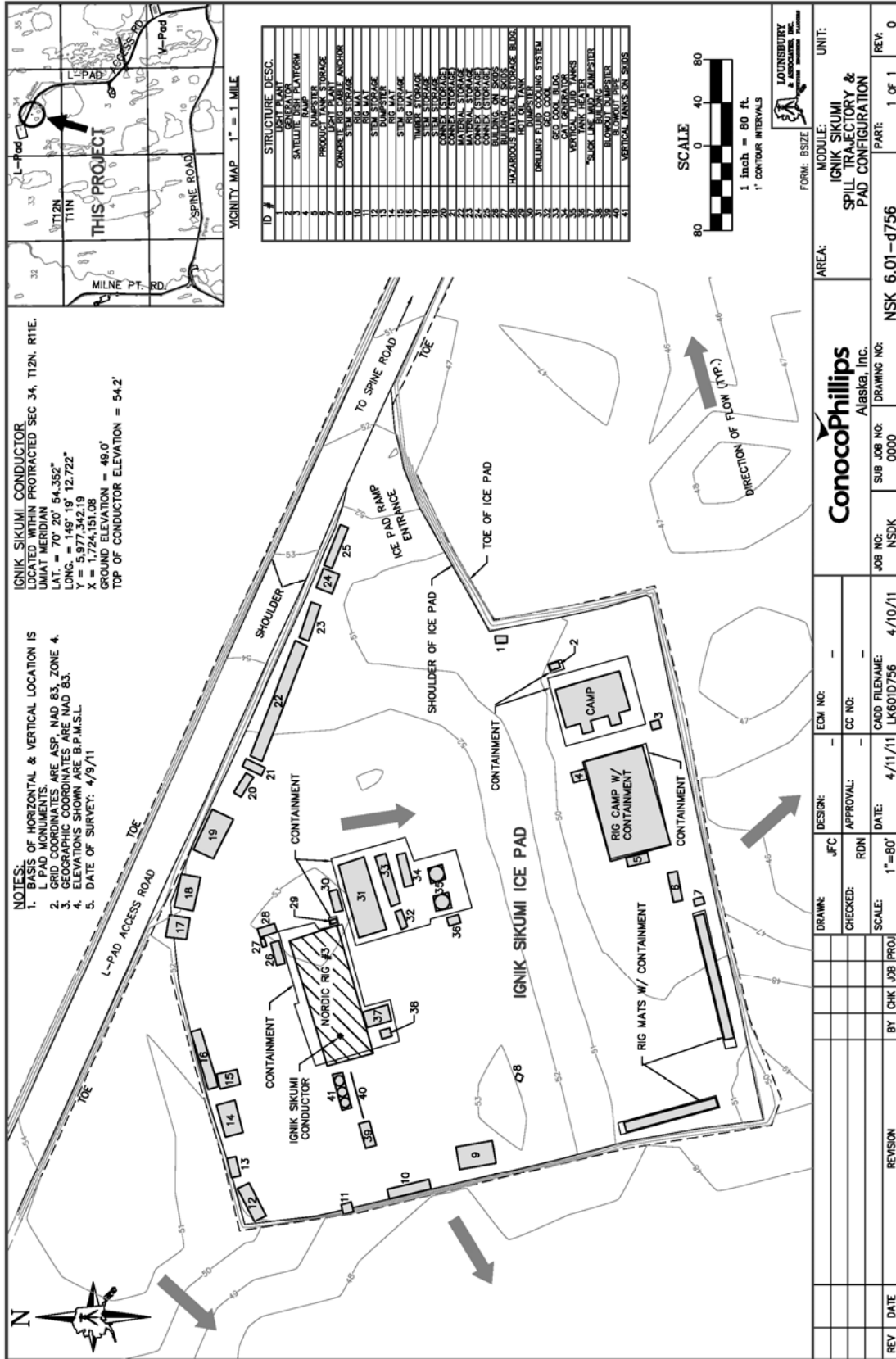Figure 6: Iġnik Sikumi #1 Post-icepad construction plat

Figure 7: Iġnik Sikumi #1 "As-built" survey plat

Task 8 (Phase 3A): Drilling of Production Test Well: COMPLETED
Most significant milestone in report period was drilling, logging, completion installation and temporary suspension of Iġnik Sikumi #1 in Prudhoe Bay Unit, Alaska North Slope, accomplished without any health, safety, or environmental incidents. Iġnik Sikumi #1 was spud by Nordic-Calista Rig 3 on April 9 and reached TD (2597ft MD) April 16. Openhole logging was completed April 21, lower completion was cemented April 25, and rig moved off after release April 28. Mudlogging, logging-while-drilling (LWD), and openhole wireline and drillpipe-conveyed logging results are described in Task 9.

Numerous engineering challenges developed during drilling that required creative resolution, but mud-chilling was the most relevant to project objectives. Drilling with OBM (oil-based mud) commenced with drill-out of 10¾" surface casing at 1473ft MD. Plans called for pumping 20°F chilled OBM and monitoring mud temperature coming out of the hole to ensure sub-freezing (30°F) returns. After several attempts to cool OBM back into 20°F/30°F specifications by pulling up and circulating inside casing, bottomhole assembly (BHA) was tripped to eliminate two heat sources: mud motor and small bit nozzles. Mud motor was eliminated from BHA and larger jets were installed in bit. Upon resumption of drilling, mud continued to warm outside of design criteria and consensus was reached to relax outcoming mud criteria to 40°F return temperature. Drilling proceeded cautiously ahead with several cycles of pulling back up into casing and circulating through mud chillers until mud was back in specifications before resuming drilling. Since drilling deeper exposed incrementally warmer strata, and hydrate/water contact had already been imaged and identified by LWD measurements, consensus was reached to call TD at 2597ft MD instead of drilling ahead to 2825ft and risking dissociation of hydrate-bearing sandstones and further melting of overlying ice-bearing sandstones already exposed in the wellbore.

Task 9 (Phase 3A): Pre-Test Reservoir Characterization (logging): COMPLETED
Mudlogging, logging-while-drilling (LWD) of 13½" hole and 9⅞"hole, and full wireline logging suite in 9⅞"hole, were performed according to plans. Mudlogging, under the supervision of ConocoPhillips wellsite geologist, was conducted from bottom of conductor (110ft MD) to total depth of 2597ft. Mudloggers caught samples for real-time geologist review, archival storage, and to fulfill USGS geochemical sampling protocol. Preserved wet cuttings were canned every 60ft above surface casing point (1482ft MD) and every 30ft from surface casing point to TD (2597ft MD), treated with biocide, frozen, and sent to USGS for headspace gas analysis. In addition, canisters of gas agitated from the mud stream (Isotubes) were recovered with the same frequency and shipped to IsoTech Laboratories for compositional and isotopic analysis, per USGS sampling protocol. Mudlog over hydrate-bearing interval of Sagavanirktok sandstones, depicting rate of penetration, interpreted lithology, quantitative gas-show measurements, and sample description, is Figure 8.
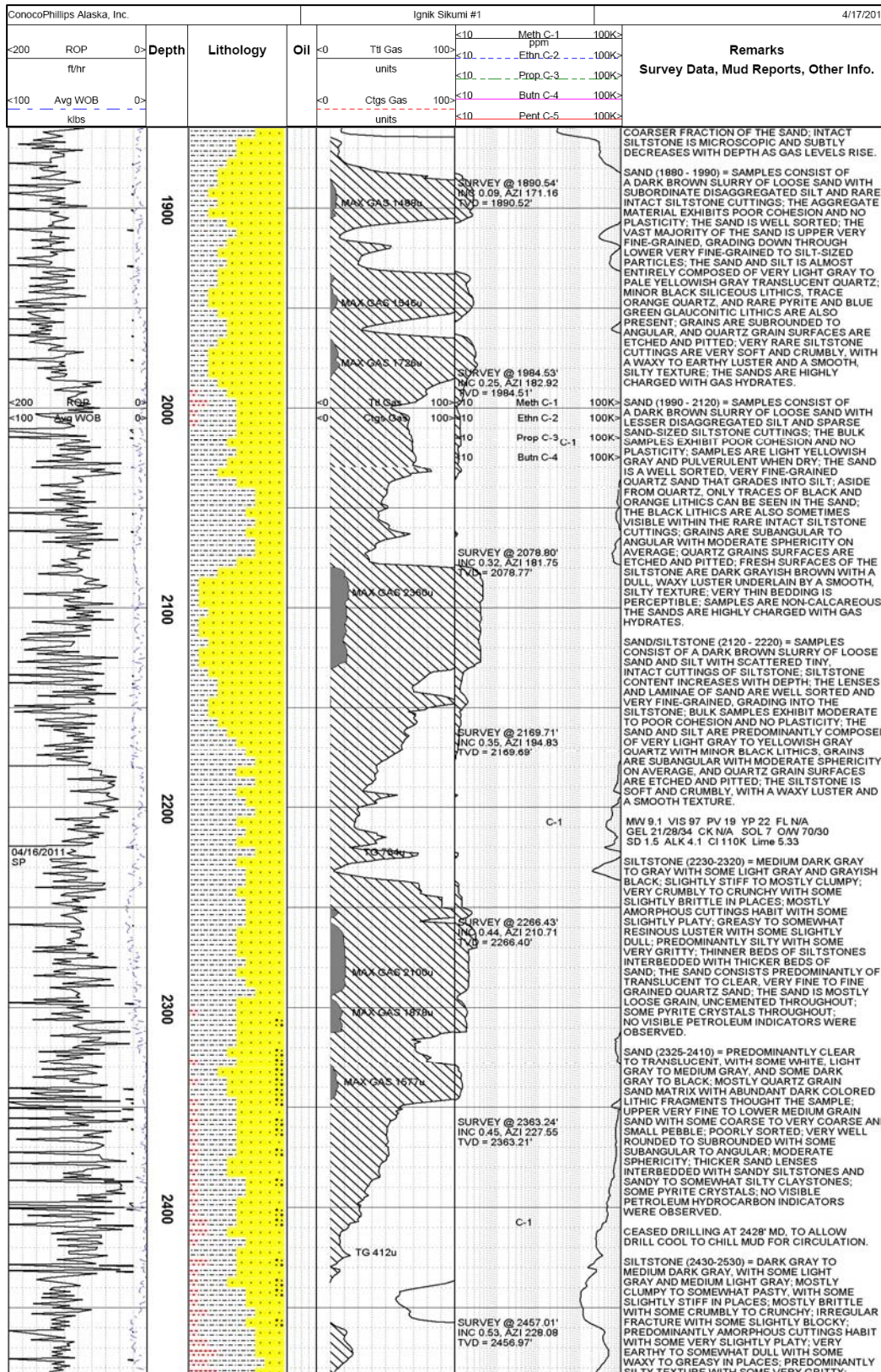
ROP ft/hr <200 — 0> ; Avg WOB klbs <100 — 0>	Depth	Lithology	Oil	Ttl Gas units <0 — 100> ; Ctgs Gas units <0 — 100>	Meth C-1 ppm <10 — 100K> ; Ethn C-2 <10 — 100K> ; Prop C-3 <10 — 100K> ; Butn C-4 <10 — 100K> ; Pent C-5 <10 — 100K>	Remarks Survey Data, Mud Reports, Other Info.

Remarks column text:

COARSER FRACTION OF THE SAND; INTACT SILTSTONE IS MICROSCOPIC AND SUBTLY DECREASES WITH DEPTH AS GAS LEVELS RISE.

SAND (1880 - 1990) = SAMPLES CONSIST OF A DARK BROWN SLURRY OF LOOSE SAND WITH SUBORDINATE DISAGGREGATED SILT AND RARE INTACT SILTSTONE CUTTINGS; THE AGGREGATE MATERIAL EXHIBITS POOR COHESION AND NO PLASTICITY; THE SAND IS WELL SORTED; THE VAST MAJORITY OF THE SAND IS UPPER VERY FINE-GRAINED, GRADING DOWN THROUGH LOWER VERY FINE-GRAINED TO SILT-SIZED PARTICLES; THE SAND AND SILT IS ALMOST ENTIRELY COMPOSED OF VERY LIGHT GRAY TO PALE YELLOWISH GRAY TRANSLUCENT QUARTZ; MINOR BLACK SILICEOUS LITHICS, TRACE ORANGE QUARTZ, AND RARE PYRITE AND BLUE GREEN GLAUCONITIC LITHICS ARE ALSO PRESENT; GRAINS ARE SUBROUNDED TO ANGULAR, AND QUARTZ GRAIN SURFACES ARE ETCHED AND PITTED; VERY RARE SILTSTONE CUTTINGS ARE VERY SOFT AND CRUMBLY, WITH A WAXY TO EARTHY LUSTER AND A SMOOTH, SILTY TEXTURE; THE SANDS ARE HIGHLY CHARGED WITH GAS HYDRATES.

SAND (1990 - 2120) = SAMPLES CONSIST OF A DARK BROWN SLURRY OF LOOSE SAND WITH LESSER DISAGGREGATED SILT AND SPARSE SAND-SIZED SILTSTONE CUTTINGS; THE BULK SAMPLES EXHIBIT POOR COHESION AND NO PLASTICITY; SAMPLES ARE LIGHT YELLOWISH GRAY AND PULVERULENT WHEN DRY; THE SAND IS A WELL SORTED, VERY FINE-GRAINED QUARTZ SAND THAT GRADES INTO SILT; ASIDE FROM QUARTZ, ONLY TRACES OF BLACK AND ORANGE LITHICS CAN BE SEEN IN THE SAND; THE BLACK LITHICS ARE ALSO SOMETIMES VISIBLE WITHIN THE RARE INTACT SILTSTONE CUTTINGS; GRAINS ARE SUBANGULAR TO ANGULAR WITH MODERATE SPHERICITY ON AVERAGE; QUARTZ GRAINS SURFACES ARE ETCHED AND PITTED; FRESH SURFACES OF THE SILTSTONE ARE DARK GRAYISH BROWN WITH A DULL, WAXY LUSTER UNDERLAIN BY A SMOOTH, SILTY TEXTURE; VERY THIN BEDDING IS PERCEPTIBLE; SAMPLES ARE NON-CALCAREOUS; THE SANDS ARE HIGHLY CHARGED WITH GAS HYDRATES.

SAND/SILTSTONE (2120 - 2220) = SAMPLES CONSIST OF A DARK BROWN SLURRY OF LOOSE SAND AND SILT WITH SCATTERED TINY, INTACT CUTTINGS OF SILTSTONE; SILTSTONE CONTENT INCREASES WITH DEPTH; THE LENSES AND LAMINAE OF SAND ARE WELL SORTED AND VERY FINE-GRAINED, GRADING INTO THE SILTSTONE; BULK SAMPLES EXHIBIT MODERATE TO POOR COHESION AND NO PLASTICITY; THE SAND AND SILT ARE PREDOMINANTLY COMPOSED OF VERY LIGHT GRAY TO YELLOWISH GRAY QUARTZ WITH MINOR BLACK LITHICS; GRAINS ARE SUBANGULAR WITH MODERATE SPHERICITY ON AVERAGE, AND QUARTZ GRAIN SURFACES ARE ETCHED AND PITTED; THE SILTSTONE IS SOFT AND CRUMBLY, WITH A WAXY LUSTER AND A SMOOTH TEXTURE.

MW 9.1 VIS 97 PV 19 YP 22 FL N/A GEL 21/28/34 CK N/A SOL 7 O/W 70/30 SD 1.5 ALK 4.1 Cl 110K Lime 5.33

SILTSTONE (2230-2320) = MEDIUM DARK GRAY TO GRAY WITH SOME LIGHT GRAY AND GRAYISH BLACK; SLIGHTLY STIFF TO MOSTLY CLUMPY; VERY CRUMBLY TO CRUNCHY WITH SOME SLIGHTLY BRITTLE IN PLACES; MOSTLY AMORPHOUS CUTTINGS HABIT WITH SOME SLIGHTLY PLATY; GREASY TO SOMEWHAT RESINOUS LUSTER WITH SOME SLIGHTLY DULL; PREDOMINANTLY SILTY WITH SOME VERY GRITTY; THINNER BEDS OF SILTSTONES INTERBEDDED WITH THICKER BEDS OF SAND; THE SAND CONSISTS PREDOMINANTLY OF TRANSLUCENT TO CLEAR, VERY FINE TO FINE GRAINED QUARTZ SAND; THE SAND IS MOSTLY LOOSE GRAIN, UNCEMENTED THROUGHOUT; SOME PYRITE CRYSTALS THROUGHOUT; NO VISIBLE PETROLEUM INDICATORS WERE OBSERVED.

SAND (2325-2410) = PREDOMINANTLY CLEAR TO TRANSLUCENT, WITH SOME WHITE, LIGHT GRAY TO MEDIUM GRAY, AND SOME DARK GRAY TO BLACK; MOSTLY QUARTZ GRAIN SAND MATRIX WITH ABUNDANT DARK COLORED LITHIC FRAGMENTS THOUGHT THE SAMPLE; UPPER VERY FINE TO LOWER MEDIUM GRAIN SAND WITH SOME COARSE TO VERY COARSE AND SMALL PEBBLE; POORLY SORTED; VERY WELL ROUNDED TO SUBROUNDED WITH SOME SUBANGULAR TO ANGULAR; MODERATE SPHERICITY; THICKER SAND LENSES INTERBEDDED WITH SANDY SILTSTONES AND SANDY TO SOMEWHAT SILTY CLAYSTONES; SOME PYRITE CRYSTALS; NO VISIBLE PETROLEUM HYDROCARBON INDICATORS WERE OBSERVED.

CEASED DRILLING AT 2428' MD, TO ALLOW DRILL COOL TO CHILL MUD FOR CIRCULATION.

SILTSTONE (2430-2530) = DARK GRAY TO MEDIUM DARK GRAY, WITH SOME LIGHT GRAY AND MEDIUM LIGHT GRAY; MOSTLY CLUMPY TO SOMEWHAT PASTY, WITH SOME SLIGHTLY STIFF IN PLACES; MOSTLY BRITTLE WITH SOME CRUMBLY TO CRUNCHY; IRREGULAR FRACTURE WITH SOME SLIGHTLY BLOCKY; PREDOMINANTLY AMORPHOUS CUTTINGS HABIT WITH SOME VERY SLIGHTLY PLATY; VERY EARTHY TO SOMEWHAT DULL WITH SOME WAXY TO GREASY IN PLACES; PREDOMINANTLY SILTY TEXTURE WITH SOME VERY GRITTY;

Survey / gas annotations:
SURVEY @ 1890.54' INC 0.09, AZI 171.16 TVD = 1890.52'
MAX GAS 1488u
MAX GAS 1546u
MAX GAS 1738u
SURVEY @ 1984.53' INC 0.25, AZI 182.92 TVD = 1984.51'
SURVEY @ 2078.80' INC 0.32, AZI 181.75 TVD = 2078.77'
MAX GAS 2360u
SURVEY @ 2169.71' INC 0.35, AZI 194.83 TVD = 2169.69'
C-1
TG 784u
SURVEY @ 2266.43' INC 0.44, AZI 210.71 TVD = 2266.40'
MAX GAS 2100u
MAX GAS 1878u
MAX GAS 1677u
SURVEY @ 2363.24' INC 0.45, AZI 227.55 TVD = 2363.21'
C-1
TG 412u
SURVEY @ 2457.01' INC 0.53, AZI 228.08 TVD = 2456.97'

04/16/2011 SP

Figure 8: Mudlog through hydrate-bearing Sagavanirktok sandstones

Schlumberger's Platform Express (PEX), Combinable Magnetic Resonance (CMR), Pressure Express (XPT) and Modular Dynamic Tool (MDT) were run as planned, with slight revisions to depths, as summarized in Table 1. Surface casing was set in 13½" hole at 1473ft MD, landed in the 150ft-thick mudstone just above the ice-saturated "Sagavanirktok F" sands. Subsequent "production hole" was drilled with a 9⅞" bit and chilled oil-based drilling mud (OBM) to 2597ft MD, slightly shallower than planned 2825ft TD, because mud-chilling was not as effective as expected. After logging, a tapered 7⅝" x 4½" casing string was run and cemented with low heat-of-hydration cement.

Logging Run	Vendor	Hole Size	Tool	Measurement	Interval
Mudlogging	CanRig/Epoch	13½" & 9⅞"	Mudlogger	ROP, mudgas, sample descriptions	110ft-2597ft
LWD Run 1	Sperry (Halliburton)	13½"	Gamma Ray	GR	110ft-1482ft
			Resistivity	pre-invasion R_t	110ft-1482ft
			Density-Neutron	Φ_D, Φ_N	110ft-1482ft
LWD Run 2	Sperry (Halliburton)	9⅞"	Gamma Ray	GR	1473ft-2597ft
			Resistivity	pre-invasion R_t	1473ft-2597ft
Wireline Run 1	Schlumberger	9⅞"	Gamma Ray	GR	1473ft-2597ft
			Sonic Scanner	Δt_C, Δt_S	1473ft-2597ft
			OBMI (+ GPIT)	Hi-Res image	1473ft-2597ft
			Rt Scanner	Vertical & horizontal resistivity	1473ft-2597ft
Wireline Run 2	Schlumberger	9⅞"	PEX	Φ_D, Φ_N	1473ft-2597ft
			HNGS	natural gamma spectroscopy	1473ft-2597ft
			CMR	distribution of relaxation times	1473ft-2597ft
			XPT	P, T, fluid mobility	selected points
Drillpipe	Schlumberger	9⅞"	TLC	Drillpipe conveyance	
			Gamma Ray	GR	
		Run 3A	MDT mini-Frac	P, T, fluid sampling	selected points
		Run 3B	MDT mini-DST	frac/breakdown pressures	selected points

Table 1: Iġnik Sikumi #1 Openhole Data Collection

Task 10 (Phase 3A): Initial Log Data Review: COMPLETED
Initial Log Data Review was completed and results presented at ConocoPhillips Houston offices on May 25. Tim Collett (USGS), Ray Boswell (DOE/NETL), and ConocoPhillips stakeholders/petrophysicists were joined by Schlumberger's Richard Birchwood and Ahmad Latifzai, who summarized their processing and interpretation of MDT MiniFrac and XPT/MDT Drawdown Test results, respectively. MDT Mini-Frac interpretation is summarized in Appendix 4 and XPT/MDT Mini-DST/Drawdown analyses are summarized in Appendix 5. Schlumberger also provided interpretation of OBMI, Rt Scanner, Sonic Scanner, and CMR datasets, reported in Appendix 6. ConocoPhillips presented preliminary log analyses focused on hydrate saturation calculations (see Figure 9) and Tim Collett summarized initial isotube compositional analyses (see Figure 10).
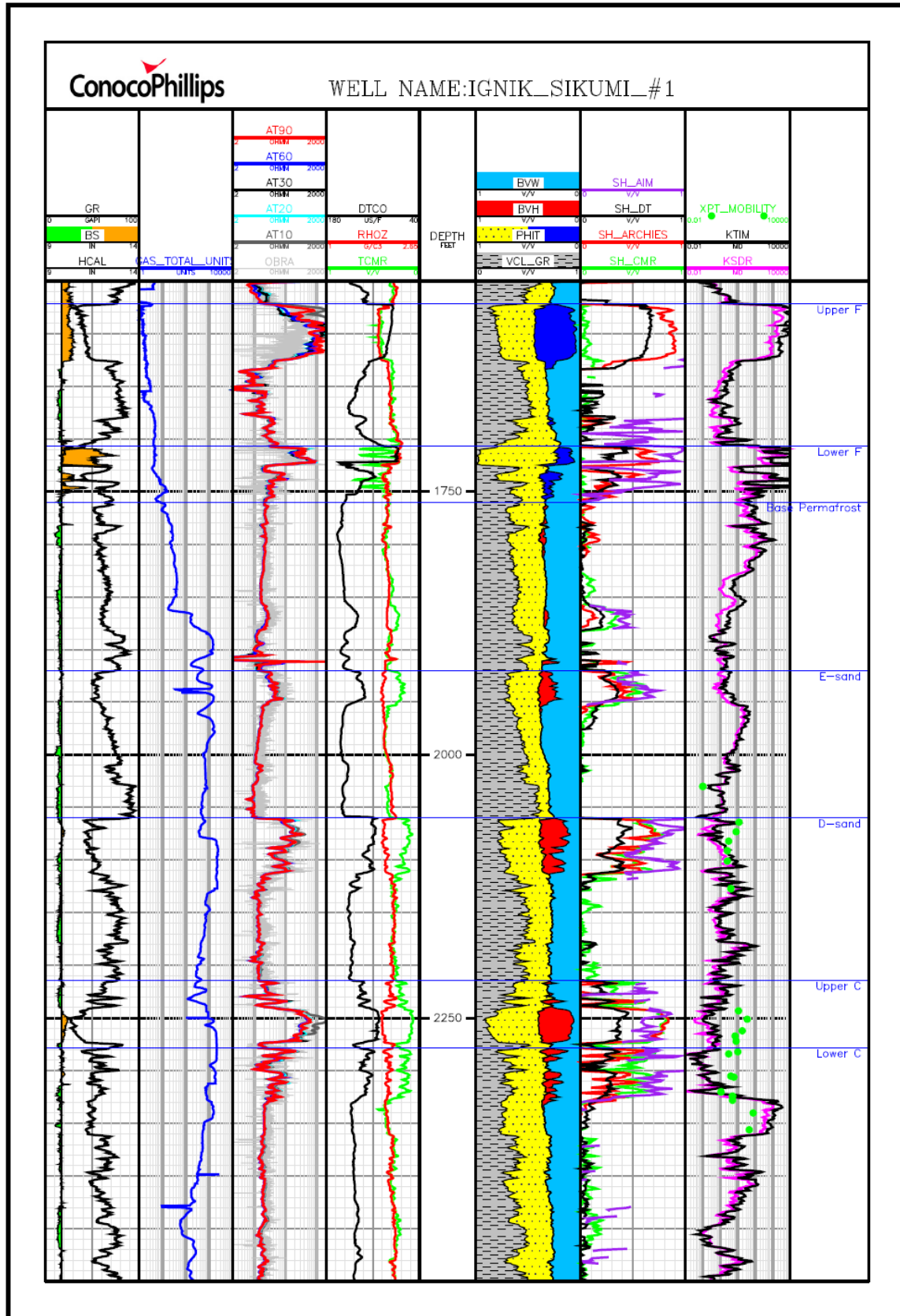
Figure 9: Initial petrophysical evaluation: COP - Iġnik Sikumi #1
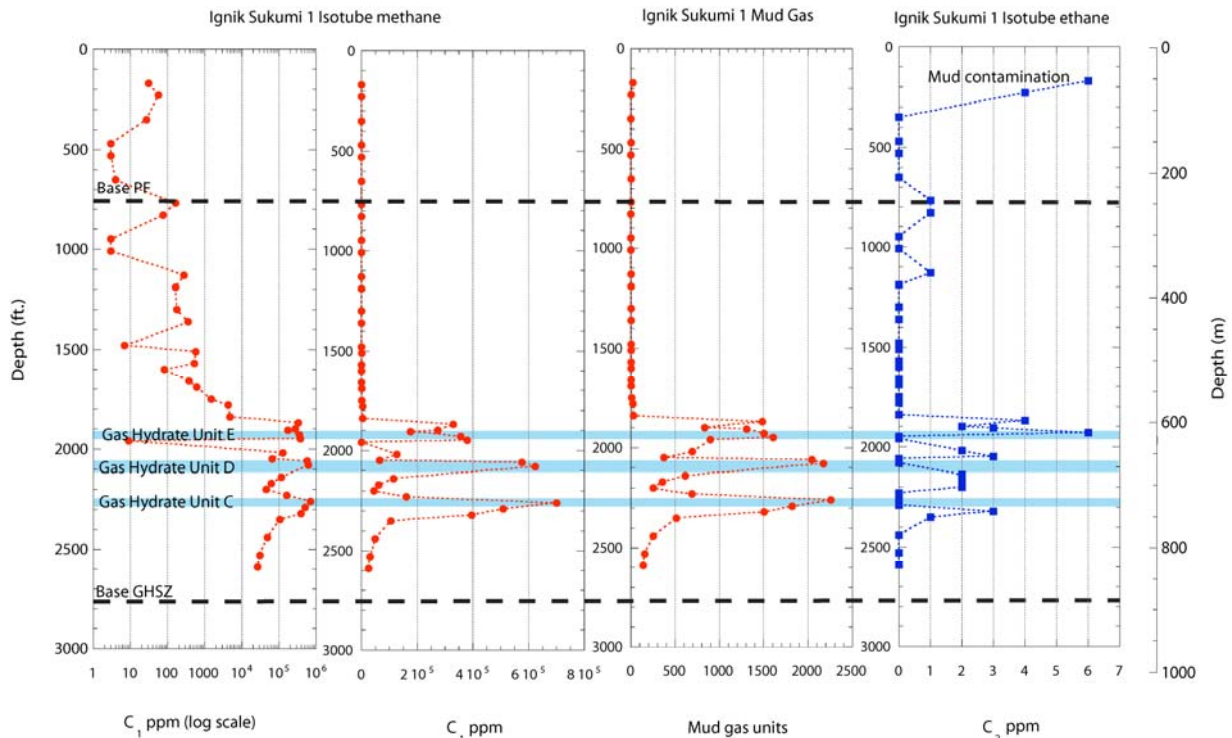
Figure 10: Iġnik Sikumi #1 isotube gas composition analyses (source: USGS)

Task 11 (Phase 3A)– Well Preparation and Completion: COMPLETED

Upon completion of openhole logging operations, well was re-entered with drillstring, circulated with OBM (oil-based mud) and prepared for completion installation. Production casing, consisting of cemented 7⅝" x 4½" tapered and instrumented casing string, is referred to as "lower completion." "Upper completion" refers to 4½" tubing , connected to lower completion by seal bore assembly, creating 4½" monobore from surface to plugged-back TD (PBTD 2371ft MD). Figure 11 summarizes completion as installed.

The lower completion, which was cemented (with full cement returns to surface) with low heat-of-hydration cement, includes fiber-optic Distributed Temperature Sensor (DTS) cable, carefully clamped outside the tapered casing, which extends from TD to surface. Three surface-readout pressure/temperature gauges, ported to the casing interior, were run on the 4½" casing. Electronic lines for gauges were also clamped to the outside of the tapered string. The bottom gauge (2285ft MD), located below planned Sagavanirktok Upper C Sand perforations, is deployed primarily to monitor fluid fill-up during completion and production testing operations. Both the upper (2034ft MD) and central (2226ft MD) gauge were positioned above the planned perforation interval in Upper C sand. The central gauge is placed between the 3.735" nipple at 2224ft MD and the 3.675" polish-bore receptacle at 2278ft MD, which reflect the top and bottom of a sand-control screen to be run prior to the final depressurization step. The central gauge will allow pressure and temperature monitoring behind the sand-control screen. The upper gauge will allow pressure and temperature monitoring above the sand-control screen.

Hydrate Well Final

4-1/2" Completion String

ConocoPhillips

Drilling & Wells
ConocoPhillips
Alaska

16" 164.82#/ft
SCH100
@ +/- 110' MD

4 ½" 12.6#/ft L-80 IBT- mod tubing
Special Drift: 3.886" I.D.
Turned Down Couplings: 4.92" O.D.

10 ¾" 45.5#/ft
L-80 BTC
to 1,511' MD

Two red tubes represent ¾" injection lines for circulating hot
fluid in annulus. Black background indicates "triple flatpack"
with ¾" chemical injection line (blue tube) connected to KBMG-
LTS Chemical Injection Mandrel

4 ½" Camco 'DB' Nipple w/3.91" No-Go Profile, IBT mod, at
1,927' MD (3.875" min ID)

4 ½" KBMG-LTS Chemical Injection Mandrel with 3/4" line,
IBT mod, at 1,929' MD

7 ⅝" 29.7#/ft
L-80 BTCM
to 1,974' MD

4 ½" Camco 'DB' Nipple w/3.843" No-Go Profile, IBT mod,
at 1,942' MD (3.813" min ID)

4 ½" KBMG GLM with SOV installed, IBT mod, at 1,944' MD

4 ½" Camco 'DB' Nipple w/3.785" No-Go Profile, IBT mod,
at 1,957' MD (3.750" min ID)

4 ½" x 7 ⅝" Cross-over and 18' long 5 ½" SBE with 4.75" seal
bore at 1,974' MD

Yellow line is encapsulated fiber-optic DTS cable
Black line is encapsulated electronic cable

4 ½" 12.6#/ft
L-80 IBT- mod

4 ½" Pressure and Temperature Gauge, IBT mod, at 2,034' MD

4 ½" Camco 'DB' Nipple w/3.735" No-Go Profile, IBT mod,
at 2,224' MD (3.687" min ID)

4 ½" Pressure and Temperature Gauge, IBT mod, at 2,226' MD

4 ½" Polished Bore Receptacle with 3.625" polished bore at 2,278' MD

4 ½" Pressure and Temperature Gauge, IBT mod, at 2,285' MD

4 ½" Baker Packoff Bushing at 2,371' MD (PBTD)

2,597' MD

9 ⅞" hole

Figure 11: Completion Installation

Electronic lines for pressure-temperature gauges and fiber-optic DTS cables were monitored during running to ensure integrity. Monitoring continued until the well was temporarily suspended; gauges/DTS were also interrogated May 30. Once the lower completion was installed, the 2⅞" tubing string was picked-up and circulation was re-established with chilled OBM. Initial plans to use a cement retainer had been upgraded to packoff/stringer combination, and 2⅞" was subsequently stung into packoff bushing (2371ft MD) to displace OBM and slightly warm and pre-condition annulus prior to cementing.

Cementing of 7⅝" x 4½" tapered casing "lower completion" proceeded mostly according to plan, although emplaced cement was warmer than designed. Cementing plans called for mixing -5°F bulk cement with 37°F lake water to yield a 40°F slurry. Upon mixing of ingredients and shearing to ensure uniform properties, slurry temperature at the surface rose to nearly 80°F before decision was made to pump cement downhole. Data capture from DTS cable during cementing (and all subsequent wellsite operations) documented maximum recorded temperature of 75°F at 2483ft MD. Hydrate-bearing strata in the Sagavanirktok Upper C Sandstone naturally cooled back into the hydrate stability zone within 18 hours.

Shortly after cement circulation in the annulus ceased, 2⅞" tubing was pulled up the hole to 1800ft MD (above hydrate-bearing Sagavanirktok sandstones) and circulation was reestablished inside the casing with 90°F OBM to inhibit pre-hydration cement freezing in the annulus. Circulation of warm OBM proceeded for 10 hours, followed by displacement of OBM in casing (at 2364ft MD, near PBTD) with corrosion-inhibited KCl brine. KCl brine was specified for pumping at 50°F, and cold lake water was again used. Unfortunately heat of mixing, heat of salt dissolution, and frictional heating inside 2⅞" tubing combined to yield fluid warmer than design. Maximum temperature measured downhole by DTS is 64°F at 2338ft MD. Temperatures recorded outside the casing opposite hydrate-bearing strata were above 50°F for 12hours, though hydrated cement thermally insulated prospective targets from warm wellbore fluids. Each operational event after installation of DTS cable with lower completion is well-documented by DTS data (see Figure 12).
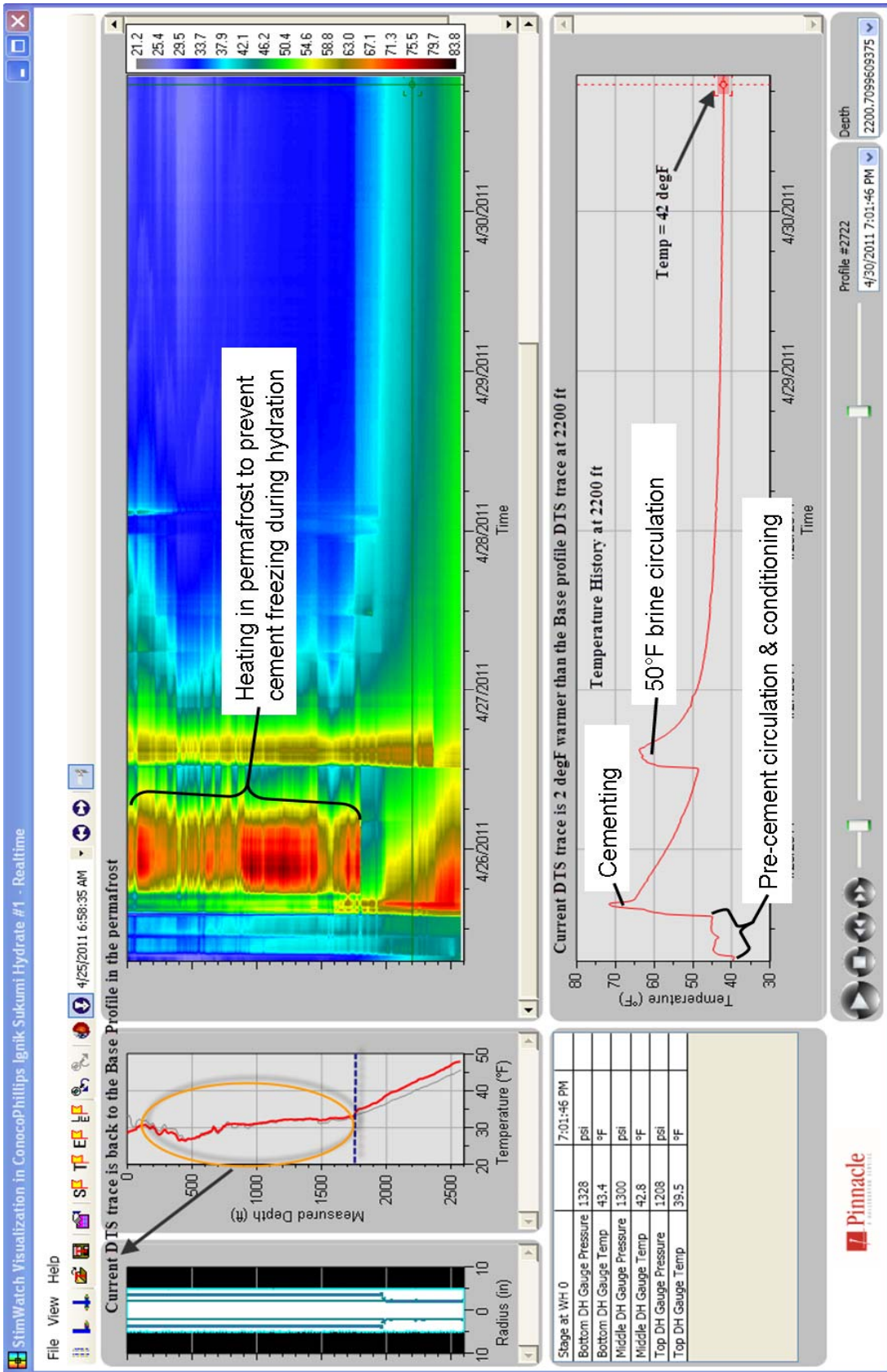
Figure 12: Ignik Sikumi #1 DTS data: April 26-April 30, 2011

Following cementing of 7⅝" x 4½" tapered casing, the upper completion was installed on 4½" tubing. This tubing string, when stung into a polish-bore receptacle seal assembly (at the 7⅝" x 4½" crossover) converts the wellbore to a 4½" monobore which simplifies perforation, injection, and flowback testing. Clamped to the outside of the tubing, bound together in a triple flatpack, are three ¾" tubing strings. Two ¾" strings (shown in red) are run open-ended to facilitate fluid circulation and heating of the annulus. This "heater string" allows the 7⅝" x 4½" annulus to act as a heat exchanger, facilitating the delivery of injected fluids at the desired temperature. The chemical injection mandrel (shown in red) has a variable back-pressure valve, which is critical to the delivery of injected fluids to the perforations at sub-breakdown pressure. The chemical injection mandrel is connected to the third ¾" tubing string (shown in blue). This line facilitates the delivery of injection fluids at low to moderate rates. The gas-lift mandrel (shown in blue) serves four functions: evacuation of fluid from the annulus, artificial lift of fluid in the 4½" tubing, installation of an additional pressure-temperature gauge, and as a circulation port for cementing during plug and abandonment (P&A) operations.

Following installation of upper completion, Cement Bond Logs (Halliburton CBL and CASTM tools) were run May 1 to confirm casing-to-annular-cement and annular cement-to-formation bonding. CBL indicated excellent bonding throughout the length of the cemented lower completion.

Task 12 – Temporary Well Suspension: COMPLETED

Iġnik Sikumi #1 was temporarily suspended May 5, 2011. Lower completion (from 1957ft MD to 2371ft MD (PBTD)) is filled with 9.5ppg corrosion-inhibited 6% KCl brine. Following installation of upper completion, 7⅝" by 4½" annulus was displaced over to 6.8ppg diesel for freeze protection. Electronic line and fiber-optic DTS cable were terminated with plug-ins for surface readout, and wellhead was "raven-proofed" with heavy duty plastic sheeting (see Fig 13). The icepad was bladed to remove surface spots with removed material hauled to Kuparuk River Unit for disposal. ConocoPhillips KRU environmental staff has "closed out" pad for season. Interim readings of DTS cable and electronic gauges are anticipated. Iġnik Sikumi #1 is temporarily suspended until planned reentry for injection/flowback/drawdown production testing under Phase 3B.
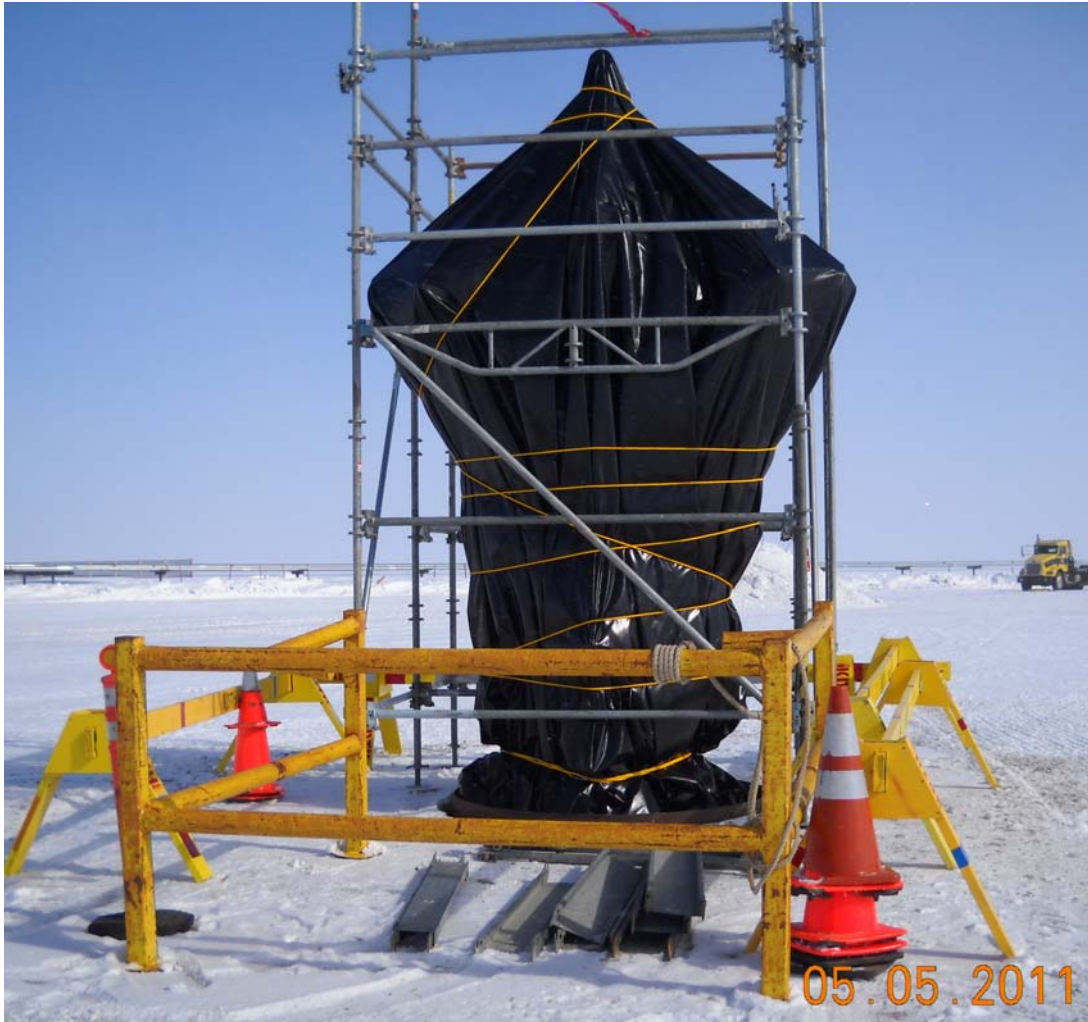
Figure 13: Iġnik Sikumi wellhead prepared for Temporary Suspension (scaffolding/barricades/cones have been removed)

Cost Status

Expenses incurred during this period were below the Baseline Cost Plan as shown in Exhibit 1.

COST PLAN/STATUS											
Project Phase ==>	Phase 1, Site Ident.		Phase 2, Field Test Planning								
Baseline Reporting Quarter ==>	Q408	Q109	Q209	Q309	Q409	Q110	Q210	Q310	Q410	Q111	Q211
BASELINE COST PLAN											
Federal Share	-	-	60,000	1,450,000	-	-	-	-	-	-	6,123,125
Non-Federal Share	325,100	499,172	390,875	333,875	170,699	-	-	-	-	2,219,272	-
Total Planned	325,100	499,172	450,875	1,783,875	170,699	-	-	-	-	2,219,272	6,123,125
Cumulative Baseline Cost	325,100	824,272	1,275,147	3,059,022	3,229,721	3,229,721	3,229,721	3,229,721	3,229,721	5,448,993	11,572,118
ACTUAL INCURRED COSTS											
Federal Share	-	-	-	-	-	-	-	-	-	-	4,520,635
Non-Federal Share	121,012	186,099	275,348	354,447	254,734	358,001	250,044	255,579	308,855	548,124	945,485
Total Incurred Cost	121,012	186,099	275,348	354,447	254,734	358,001	250,044	255,579	308,855	548,124	5,466,119
Cumulative Incurred Cost	121,012	307,111	582,459	936,906	1,191,640	1,549,641	1,799,685	2,055,264	2,364,119	2,912,243	8,378,362
VARIANCE											
Federal Share	-	-	(60,000)	(1,450,000)	-	-	-	-	-	-	(1,602,490)
Non-Federal Share	(204,088)	(313,073)	(115,527)	20,572	84,035	358,001	250,044	255,579	308,855	(1,671,148)	945,485
Total Variance	(204,088)	(313,073)	(175,527)	(1,429,428)	84,035	358,001	250,044	255,579	308,855	(1,671,148)	(657,006)
Cumulative Variance	(204,088)	(517,161)	(692,688)	(2,122,116)	(2,038,081)	(1,680,080)	(1,430,036)	(1,174,457)	(1,371,225)	(3,101,184)	(1,831,463)

Exhibit 1: Cost Plan/Status

Milestone Status

The Milestone Status is shown in Exhibit 2 below.

MILESTONE STATUS REPORT						
#	Task/Subtask Description	Planned Start Date	Planned End Date	Actual Start Date	Actual End Date	Comments
Task 2	Field trial site selected	1-Oct-08	31-Mar-09	1-Oct-08	3-Apr-09	Complete
Task 3	Partner negotiations completed	15-Feb-09	31-Mar-09	17-Mar-09	29-Oct-10	Complete
Task 4	Evaluation of synergies with DOE-BP project	1-Mar-09	31-Mar-09	30-Mar-09	9-Jul-10	Complete
Task 5	Detailed well planning/engineering (test plan)	1-Apr-09	30-Sep-09	10-Mar-09		Ongoing
Task 6	Pre-drill estimation of reservoir behavior	1-Jul-09	31-Dec-09	22-Jun-09	9-Apr-11	Complete
Task 7	Establishment of test site infrastructure	1-Jan-10	31-Dec-10	21-Oct-10	22-Mar-11	Complete
Task 8	Drilling of production test well	1-Apr-10	30-Apr-10	9-Apr-11	16-Apr-11	Complete
Task 9	Pre-test reservoir characterization (logging)	1-May-10	31-Dec-10	17-Apr-11	21-Apr-11	Complete
Task 10	Initial log data review	15-Mar-11	1-May-11	21-Apr-11	25-May-11	Complete
Task 11	Well preparation and completion	15-Mar-11	20-Mar-11	22-Apr-11	28-Apr-11	Complete
Task 12	Temporary well suspension	21-Mar-11	1-Apr-11	29-Apr-11	5-May-11	Complete
Task 13	Update of production test plan	1-Jan-11	31-Dec-11	21-Apr-11		Ongoing
Task 14	Establishment of test site infrastructure	15-Dec-11	15-Jan-12			
Task 15	Pre-test operations (logging, perforating)	15-Jan-12	20-Jan-12			
Task 16	CO2 injection and gas production monitoring	21-Jan-12	30-Apr-12			

Exhibit 2: Milestone Status

Appendix 1: Laboratory Experimental Results
Prepared by James Howard and Keith Hester, ConocoPhillips (Bartlesville)

A series of experiments were completed in Q1/Q2 2011 to evaluate several issues associated with the North Slope hydrate exchange field trial (see Table 1-1). The first set of lab tests addressed challenges associated with adding a hydrate-forming fluid into hydrate-bearing sediments containing excess water, which increases the potential for blockage in the near-well region. A second set of experiments dealt with the operational issue of replacing liquid CO_2 as the injectant with a CO_2/N_2 gas mixture. This issue evolved when it was determined that supplying liquid CO2 to the reservoir would be difficult, both in terms of the temperature of the liquid and the pressure due to the weight of the liquid column in the borehole. At reservoir conditions the CO_2/N_2 mixture falls in the gas region of the phase diagram, reducing the pressure due to the head in the borehole while still retaining sufficient amounts of CO_2 to affect the exchange with the hydrate.

Test	Sample	Swi	Fluid	Remarks
Feb_2011	Sandstone	0.5	N_2	Inject N_2 to displace excess water
Mar_2011	Sandstone	1.0	N_2; $CO_{2(l)}$	Inject 1 PV N_2 preflush followed by $CO_{2(l)}$
April_2011	Sandpack	0.26	CO_2/N_2	Test of DTS, CO_2 leakage around rubber sleeve
May_2011_A	Sandpack	0.45		Test of new 4-port cell and DTS Formed hydrate, numerous leaks.
May_2011_B	Sandpack	0.63	CO_2/N_2	60/40 CO_2/N_2 injected at various flow rates
June_2011_A	Sandpack	0.58	$CO_{2(l)}$	Compare with CO_2/N_2 mixture

Table 1.1: Q1/Q2 Laboratory Experiments

Additional tests were completed in March and April to evaluate the experimental cell setup, in particular the use of Teflon shrink-wrap. Standard coreflood cells use rubber sleeves to ensure a tight fit between the sample and the pressure-containment cell. Rubber sleeves are very sensitive to CO_2, which either corrodes the sleeve or permeates through it. Experiments conducted in prior years utilized Teflon shrink-wrap instead of rubber sleeves, since the former is impervious to CO_2. Teflon shrink-wrap worked well on sandstone core plugs that were relatively rigid and easy to shrink the Teflon around. The introduction of unconsolidated sandpacks resulted in poor fits between the Teflon and the sample, which led to leakage of the confining fluid into the sample. Testing of rubber sleeves yielded no acceptable materials; final resolution involved use of a thinner, more flexible Teflon as the seal.

The Feb_2011 experiment was designed to test the effectiveness of N_2 pre-flush to displace excess water in the hydrate-saturated pore system. Methane hydrate was formed in a Bentheim sandstone whole core with an initial water saturation of 50% at a pore pressure of 8.3 MPa (1200 psi) and 4°C. Most of the available water was converted to hydrate (Figure 1-1A). After hydrate formation, the core was flooded with 20 cm^3 of water at an injection rate of 0.5cm^3/min. MRI images document a uniform distribution of water in the core (Figure 1-1B). Nitrogen was injected at a low rate, 0.05cm^3/min, for several days. After three days the MRI images show evidence of hydrate dissociation, particularly at the inlet end (Figure 1-1C).
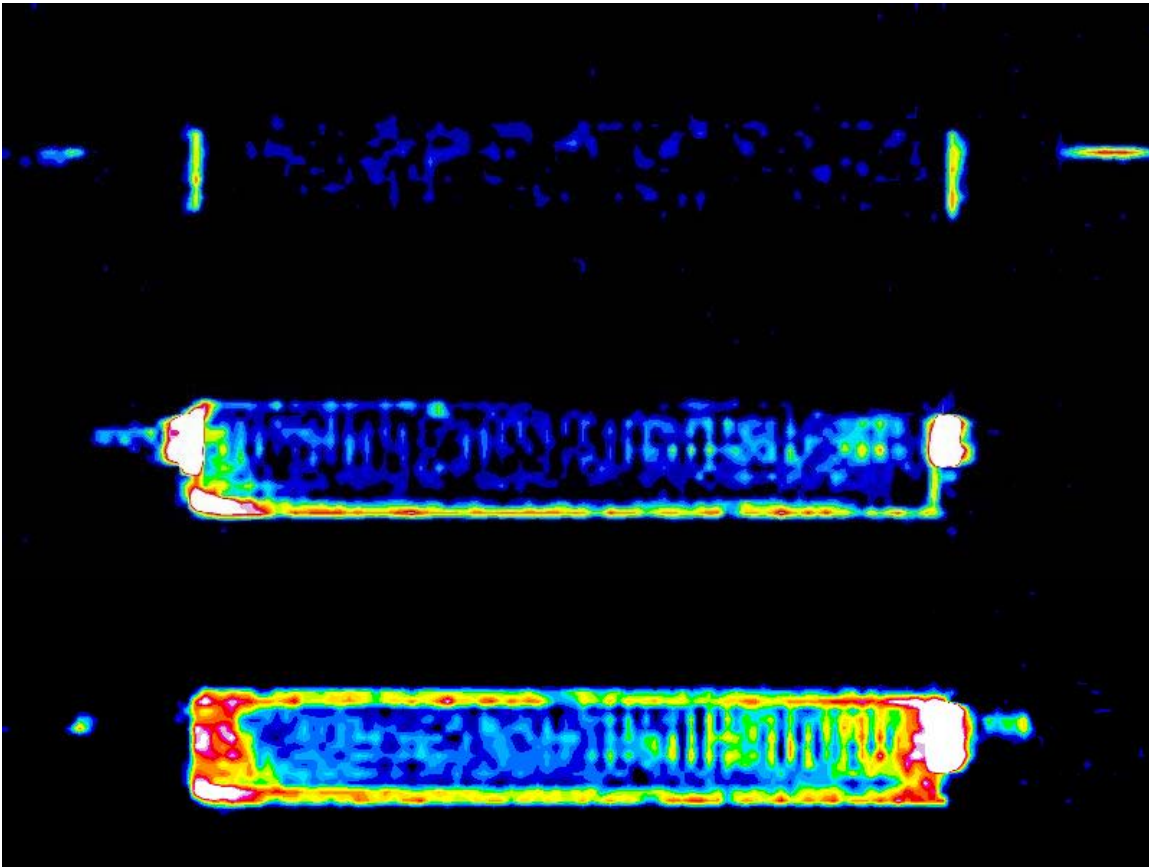
Figure 1-1A-C (top-bottom): MRI 2-D sagittal images of sandstone core at several stages of hydrate formation and fluid injection. Presence of hydrate shown by the absence of signal, while water and methane are the sources of MRI intensity. End of hydrate formation (top) shows remaining water distributed uniformly along length of core with excess methane in spacers at each end. Subsequent injection of additional water (middle) produces additional signal, especially along the inlet end (left) and along the bottom of sleeve. The injection of nitrogen (bottom) resulted in hydrate dissociation into its components of water and methane.

The Mar_2011 experiment extended testing of a nitrogen pre-flush stage to displace excess water in the hydrate-saturated pores. Approximately 1 pore volume was injected over a short period of time prior to injection of CO_2. Several modifications to the experimental apparatus were added to this test, including a wire in the outlet end platen designed to heat the lines in case of line blockage. The small N_2 pre-flush did not cause any significant dissociation of the hydrate or displacement of the water (Figure 1-2). Injection of CO_2 resulted in almost immediate blockage, most likely in the flowlines. Additional N_2 was injected in an effort to remove the blockages, but with limited success. A review of the pump pressures suggested that a bypass between the sample and sleeve was created, and the experiment was terminated.
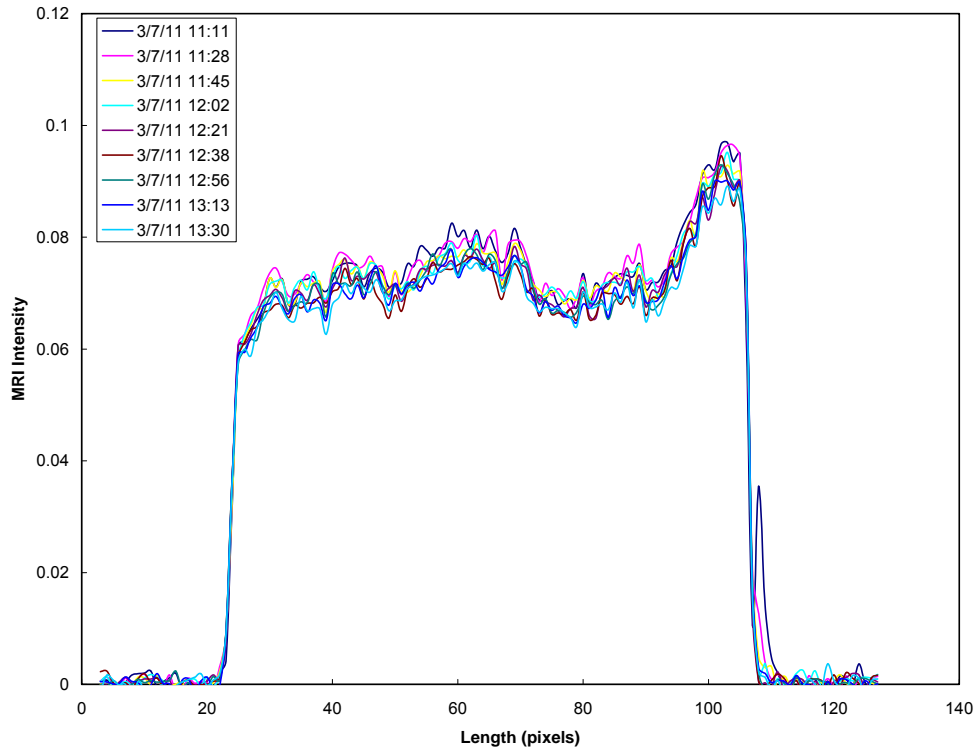
Figure 1-2: 1-D profiles along length of core during 2-hour injection of N_2 pre-flush. Nearly uniform magnetic resonance intensity indicates no dissociation of hydrate nor appreciable displacement of excess water.

The Apr_2011 experiment was the first to include installation of a fiber-optic distributed temperature sensor (DTS) wire, which was inserted down the length of the sandpack. The fiber-optic system uses a back-scattered reflectance method to determine temperature (and potentially strain) at 1cm spatial resolution and with $0.1^{o}C$ detection limit. Several alternative approaches to embedding the thin fiber (165 micron diameter) in the sandpack without damaging it or subjecting it to excessive and/or variable stress were attempted. The optimal design included building the sandpack around a thin thermoplastic (PEEK) tube, stretched along the length of the core-holder, upon which the sample was packed. The optical fiber threaded into the tube with relative ease, providing the tube remained straight and without kinks. This sandpack test with a low initial water saturation (26%) and formed methane hydrate quickly. A power failure in the lab shortly after the initiation of the 60/40 CO_2/N_2 gas injection unfortunately compromised much of the subsequent data. Leaking around the rubber sleeve led to termination of the test after CO_2/N_2 injection.

The May_2011_A experiment was the first to evaluate a new four-port sample holder along with the DTS system. The multiple inlets on the end pieces allow for greater flexibility in setting up experiments, with two ports dedicated to fluids, one port for the DTS, and the fourth for connections to ultrasonic transducers or resistivity electrodes. During hydrate formation the heats of formation were sensed by the DTS system in the center of the core and at positions in front and back platens. The sensor in the core even

measured the heat of solution as methane was dissolved into the water. The thermal perturbations matched changes in the CH_4 consumption curve as methane was dissolved in the water, followed by two periods of hydrate growth (Figure 1-3).
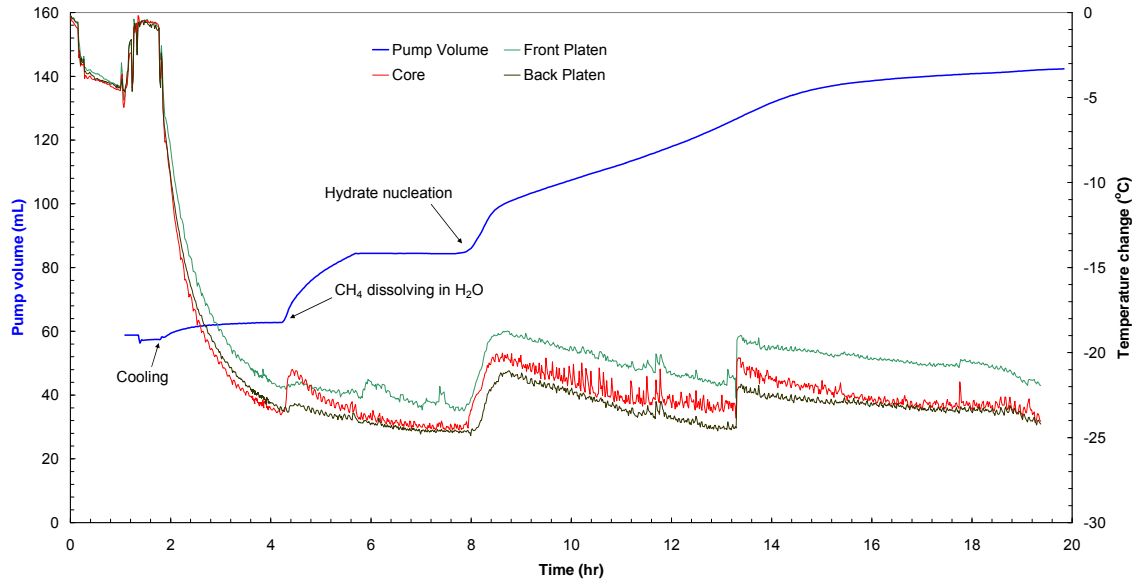
Figure 1-3: Temperature in the sandpack and sample end pieces during hydrate formation in May_2011 experiment. The temperature curves are compared with the CH_4 volume curve generated as methane was consumed during solution and hydrate formation.

The May_2011_B experiment continued efforts with the new sample holder to measure the effectiveness of CO_2/N_2 mixed gas on the exchange with methane hydrate. Initial water saturation was 63%, which converted to an initial hydrate saturation of 58%, since not all of the water converted to hydrate. There was no excess water in the sandpack, rather the remaining pore space was filled with gas. The introduction of CO_2/N_2 mixture started before the initial CH_4 hydrate formation had stabilized, though much of the original water clearly had already converted into hydrate (Figure 1-4). The CO_2/N_2 mixture did not alter the water and hydrate saturation in any appreciable manner, in part due to the low free water saturation at this point (Figure 1-5).
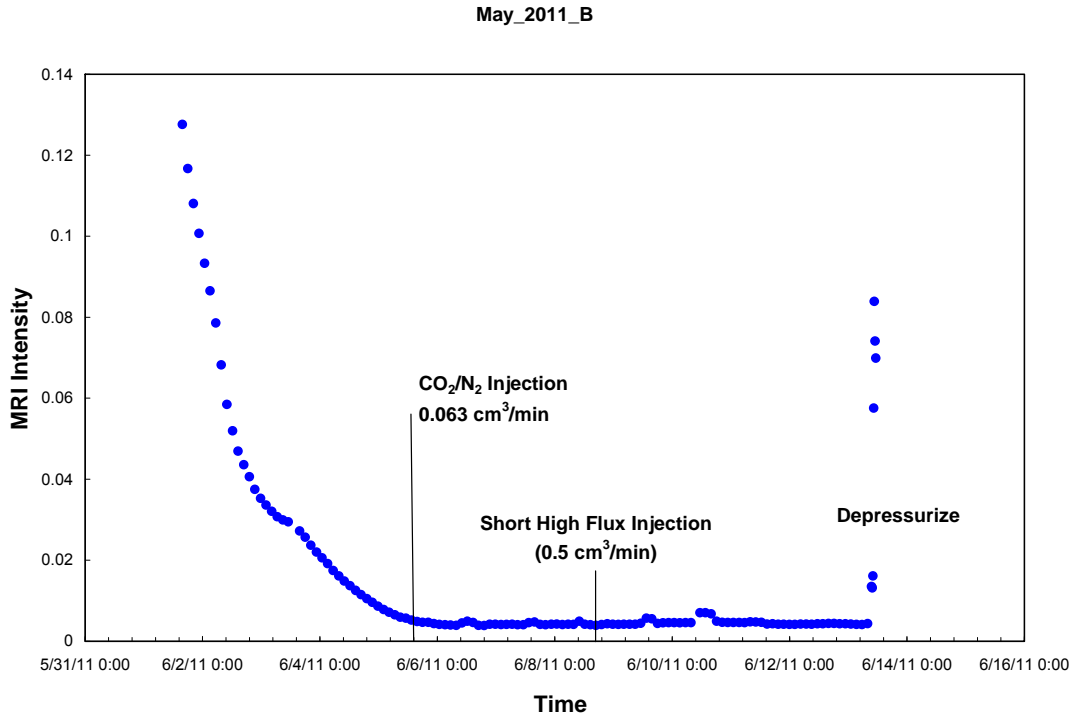
Figure 1-4: Progress of May_2011_B experiment as monitored with MRI.
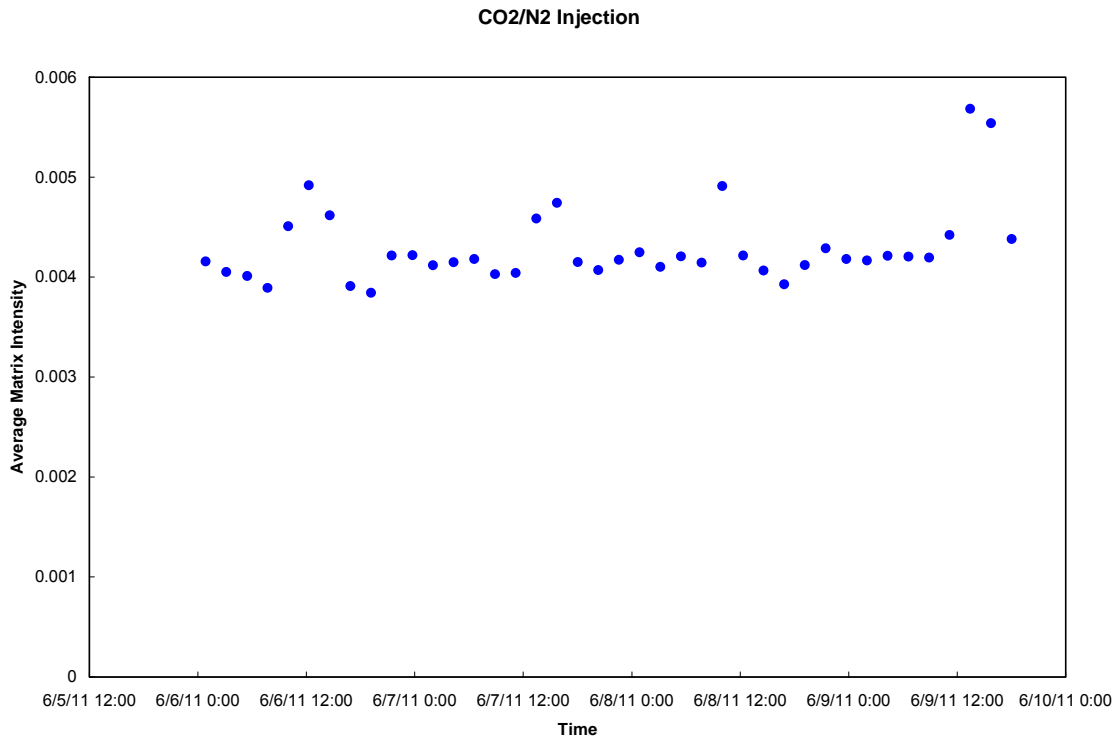
Figure 1-5. MRI intensity in May_2011_2 sandpack after hydrate formation and during the initial stages of CO_2/N_2 injection. The absence of change in intensity indicates that no additional hydrate formed upon introduction of CO_2.

The June_2011_A experiment was a continuation of the tests to evaluate the effectiveness of the mixed CO_2/N_2 gas versus liquid CO_2 for CO_2/CH_4 exchange. The initial parameters were very similar to those used in the May_2011_B test, but in this case liquid CO_2 was used. No excess water was introduced into the sandpack after hydrate formation. After initial hydrate formation, liquid CO_2 was injected at of $0.01 cm^3/min$. Pressure buildup developed when the rate was increased to $0.05 cm^3/min$, a result of back-pressure regulator failure due to diaphragm expansion from contact with CO_2. The diaphragm was replaced with a Teflon seal and the CO_2 injection continued. The introduction of CO_2 converted remaining water in the system to CO_2-hydrate, indicated by additional loss of MRI intensity (Figure 1-6).
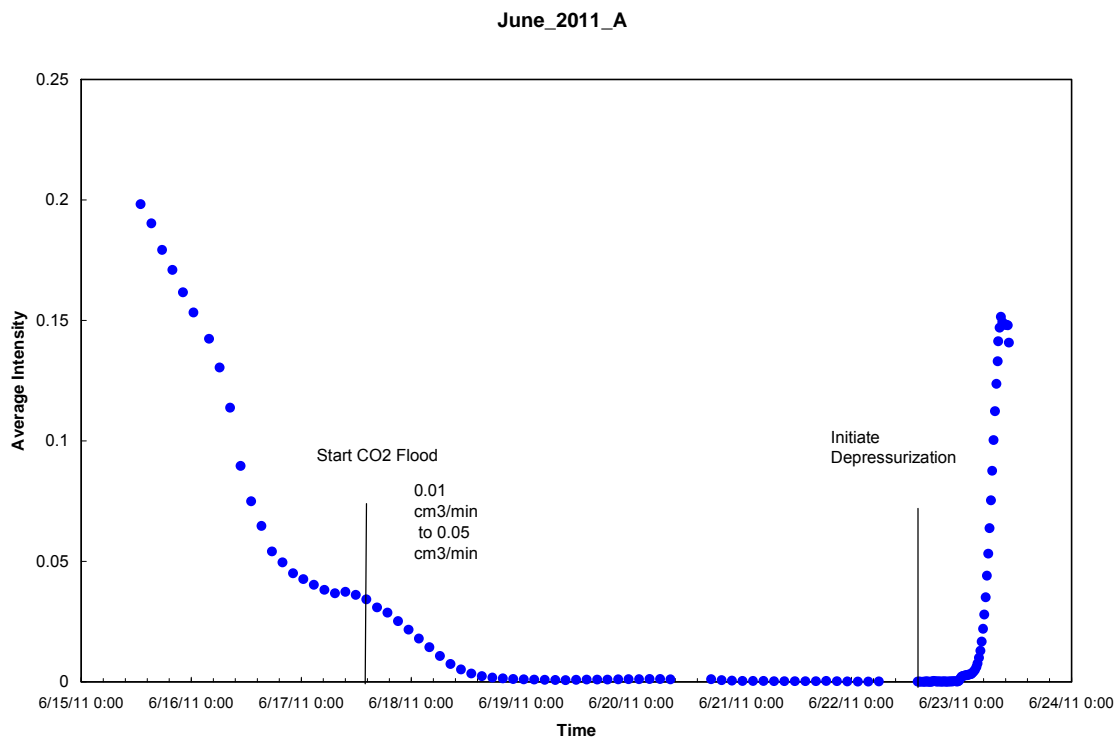
June_2011_A

Figure 1-6: Progress of June_2011_A experiment as monitored by MRI intensity.

A comparison of the produced methane from the two experiments suggests that the CO_2/N_2 60-40 mixture is as efficient as liquid CO_2 with respect to the rate and extent of exchange with methane hydrate (Figure 1-7). The initial displacement of methane from pores is independent of injectant volume, corrected for experimental conditions. After that initial displacement stage, injection of liquid CO_2 yielded the same molar volume of CH_4 as the CO_2/N_2 mixture, but with one-quarter of the injected volume.
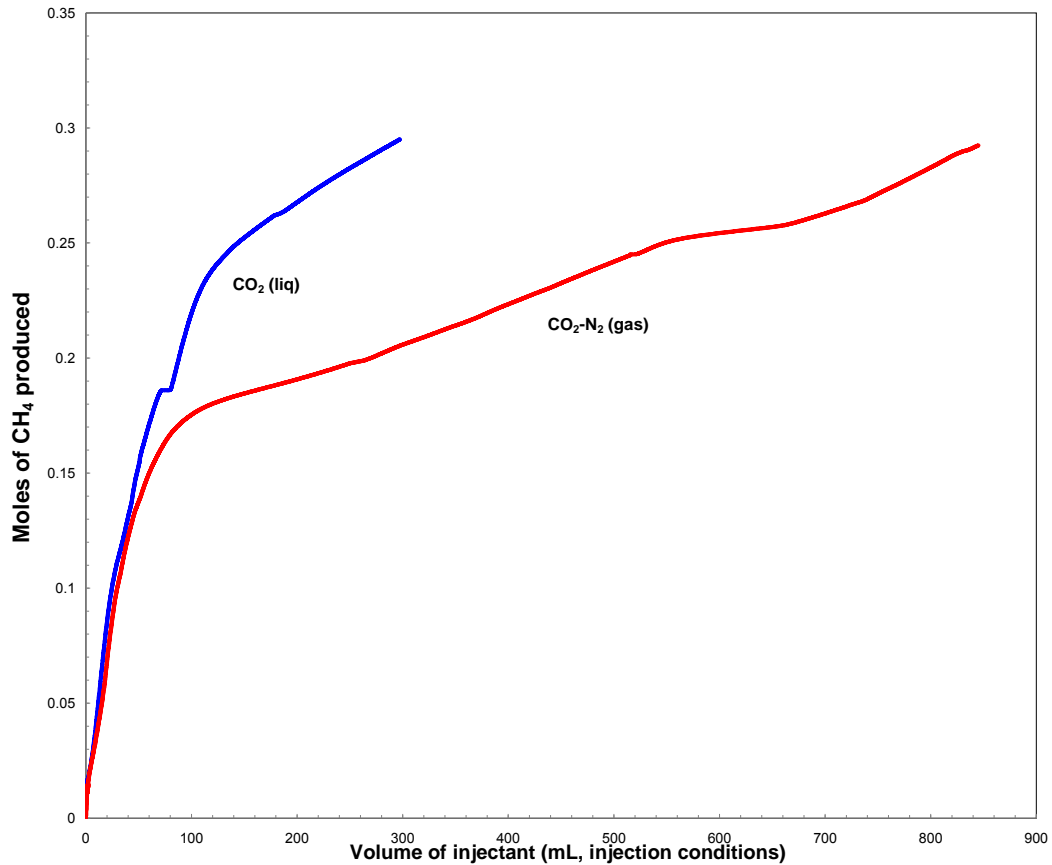
Figure 1-7: Volumetric comparison of methane production from experimental injection of liquid CO_2 and CO_2/N_2 gas mixture.

When the injected volumes of the liquid and gas mixture are converted into moles of CO_2, the gas mixture appears more efficient in terms of total moles of available CO_2 in the production of the CH_4 (Figure 1-8). In this experiment much of the liquid CO_2 was forced through the system before it had time it interact with CH_4-hydrate sites, thereby limiting its exchange efficiency.
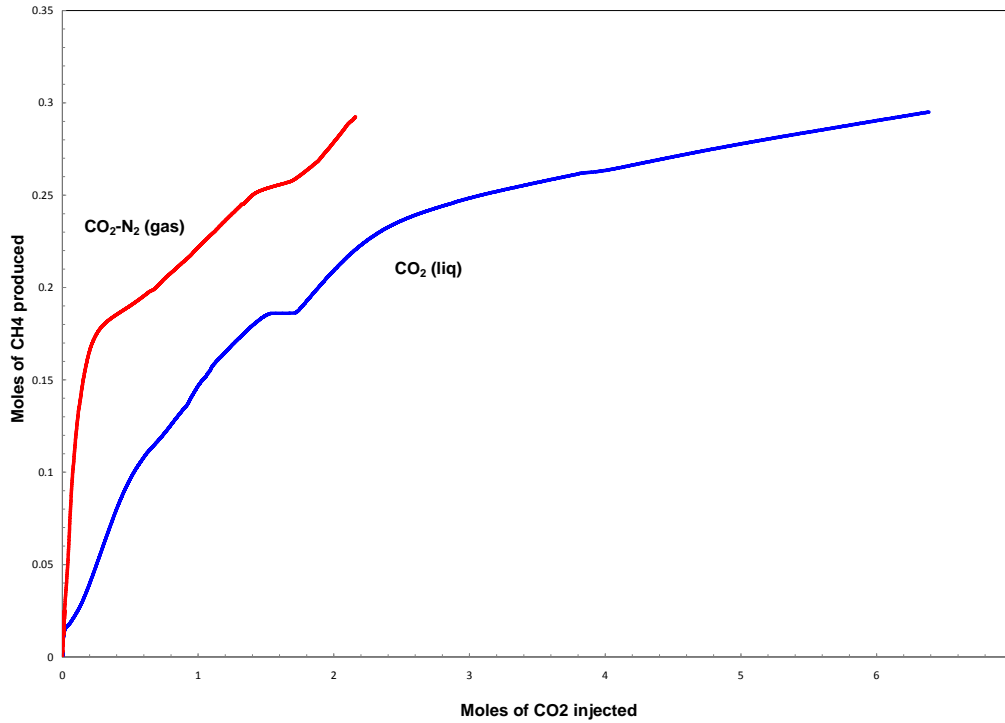
Figure 1-8: Molar comparison of methane production from experimental injection of liquid CO_2 and CO_2/N_2 mixed gas.

Similar exchange rates indicate that, after the initial sweep of free CH_4 from pores, mixed CO_2/N_2 gas is just as efficient as denser liquid CO_2. This comparison indicates that the exchange process is less affected by the driving force, as represented by the moles of available CO_2, than by the reactivity. Surface area and abundance of interfaces as determined by S_{Wi} are the same for these both tests.

Appendix 2: Wellbore Tubular (Prosper^{TM}) Modeling
Prepared by Suntichai Silpngarmlert, ConocoPhillips (Houston)

Gas hydrates in nature exist in a relatively narrow range of (low) temperature and (high) pressure, and their stability is very sensitive to pressure and temperature. If temperature of injected fluid (when it enters formation) is warmer than ~50°F, it could trigger hydrate dissociation in the formation. On the other hand, if the fluid temperature is too low, it could freeze free water in the formation resulting in significant injectivity reduction. It is important, therefore, to maintain injected fluid temperatures within a narrow range to avoid these problems.

Fluid temperatures at surface during pumping and at the perforation/completion depth are different due to heat generation from friction and heat transfer between fluid in the wellbore and the tubing and surrounding annular materials. Wellbore modeling was used to estimate fluid temperature at the completion depth for a range of surface fluid temperatures, injection rates, and fluid compositions.

The main objective of this simulation study is to calculate fluid temperature at the completion zone based on different inlet temperatures, injection rates, and fluid compositions. This information will be used to determine the required heating capacity of heat exchanger system at the surface (the estimated surface temperature is 15°F during the test).

First of all, benchmarking study of three wellbore simulators was conducted to determine the best simulator for this study. The three simulators are: 1) Prosper^{TM}, 2) WellCat^{TM}, and 3) CO2Well (research code developed by CSIRO, Australia). The benchmark study indicates that Prosper^{TM} is the best tool as the other two simulators do not accurately represent phase transition (from single gas phase to gas and liquid phase) prediction inside the wellbore. Therefore, this wellbore simulation study was conducted using Prosper^{TM}. Tables 2-1and 2-2 summarize formation thermal properties and temperature gradients used in this study. Thermal conductivity of cement and casing used in this study are 0.5 BTU/hr-ft-^{o}F and 26 BTU/hr-ft-^{o}F, respectively. Wellbore schematic of the test is illustrated in Figure 2-1. Annular fluid is modeled as water, since Prosper^{TM} does not support modeling of water/glycol mixture, which will be in the annulus during injection/flowback operations.

Bottomhole fluid temperature has been determined in this study based on different inlet temperatures (fluid temperature at surface), injection rates, and injected fluid compositions (CO_2/N_2). In this study, the bottom-hole pressure (BHP) was fixed 1385 psi for all simulation cases. Note that BHP value was only used for calculating fluid pressure within the wellbore. It was not used to calculate the injection rate (i.e., BHP and injection rate are not related), both BHP and injection rate are independent variables.

Figure 2-2 compares temperature and pressure profiles at different inlet temperatures when injection rate is 0.2 MMSCF/day and fluid composition is 60% CO_2 and 40% N_2 (weight %). The results indicate that even though the inlet temperatures are different, the

predicted bottom hole fluid temperatures are very close to formation temperature (42°F). This matches expectations, since high inlet-temperature case experiences higher heat transfer (cools down faster) than low inlet-temperature case.

Figure 2-3 shows temperature and pressure profiles at different injection rates when inlet temperature is 35°F and fluid composition is 60% CO_2 and 40% N_2 (weight %). The results illustrate that slower injection rate case cools down faster (in permafrost zone) as it has more time for heat transfer. But again, the plot shows that predicted bottom hole fluid temperature are very close to formation temperature and are not very sensitive to injection rate.

Table 2-1: Formation thermal properties

Formation type	Bottom depth (ft)	Thermal conductivity (BTU/hr-ft-$^{\circ}$F)	Specific heat (BTU/hr-ft)
Permafrost	1790	2.30	0.216
Siltstone/Shale	1900	1.50	0.239
Hydrate	1950	1.07	0.387
Siltstone/Shale	2050	1.50	0.239
Hydrate	2100	1.07	0.387
Hydrate	2250	1.07	0.387
Hydrate	2400	1.07	0.387
Sandstone/Siltstone/Shale	3525	1.50	0.239

Table 2: Formation temperatures

True Vertical Depth (ft)	Temperature ($^{\circ}$F)
0	15
1790	32
2280	42
2825	54

Hydrate Well

4-1/2" Completion String

ConocoPhillips

Drilling & Wells

ConocoPhillips Alaska

16" 164.82#
SCH100
@ +/- 110' MD

4 ½" 12.6# L-80 IBT- mod tubing

10-3/4" L-80 BTC to
1,475' MD

Two red lines are ¾ injection lines for circulating hot fluid in annulus. Black background indicates that they are flatpacked with the ¾ Chemical injection line that goes to the KBMG-LTS Mandrel

4 ½" Camco 'DB' Nipple w/ 3.843" No-Go Profile, IBT mod, at ~1,908' MD (3.813" min ID)

4-1/2" KBMG-LTS Chemical Injection Mandrel with 3/4 line, IBT mod, located 1,968' MD

7-5/8" 29.7#
L-80 BTCM
To 2,008' MD

4-1/2" KBMG GLM with SOV installed, IBT mod, located at 1,988' MD

4-1/2" x 7 5/8" X-Over (2,008' MD)

Yellow line is DTS
Black line is electronic

4 ½" Pressure and Temperature Gauge, IBT mod, at ~2,025' MD

4 ½" Camco 'DB' Nipple w/ 3.785" No-Go Profile, IBT mod, at ~2,184' MD (3.75" min ID)

4 ½" Pressure and Temperature Gauge, IBT mod, at ~2,190' MD

4 ½" 12.6#
L-80 IBT- mod

4 ½" Seal bore receptacle with 3.625" polished bore 2,235' MD

4 ½" Pressure and Temperature Gauge, IBT mod, at ~2,257' MD

4 ½" Stab in float collar 2,366' MD (PBTD)

2,820' MD

9 7/8 hole

Figure 2-1: Wellbore schematic of the test

Figure 2-4 shows temperature and pressure profiles at different injected fluid compositions when inlet temperature is 35^oF and injection rate is 0.2 MMSCF/day. In this case, the profiles become more different when phase change takes place (from single gas phase to gas + liquid phase) in the wellbore. However, the results still indicate that predicted bottom hole fluid temperature will be very close to formation temperature.

Conclusions

A fundamental design criterion of ConocoPhillips' CO_2/CH_4 exchange test is that bottom hole temperature of injected fluid is close to ambient formation temperature, a condition inside the hydrate stability field. These analyses demonstrate that fluids (mixed CO_2 and N_2 gas) injected at different inlet temperatures, at different rates, or with different fluid compositions all reach formation temperature by the time they reach the perforations. Based on the rates modeled in these analyses, injected fluid only requires heating up to the temperature that achieves single phase condition at the surface (which depends on fluid composition) to avoid any technical challenges related to managing two-phase fluid at the perforations.
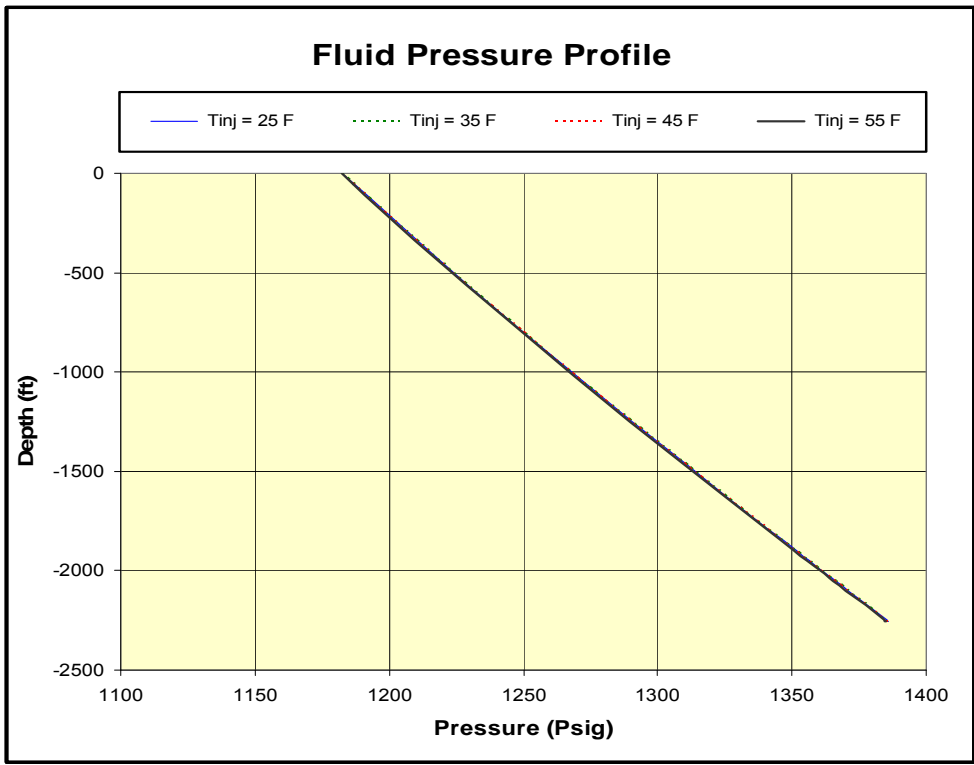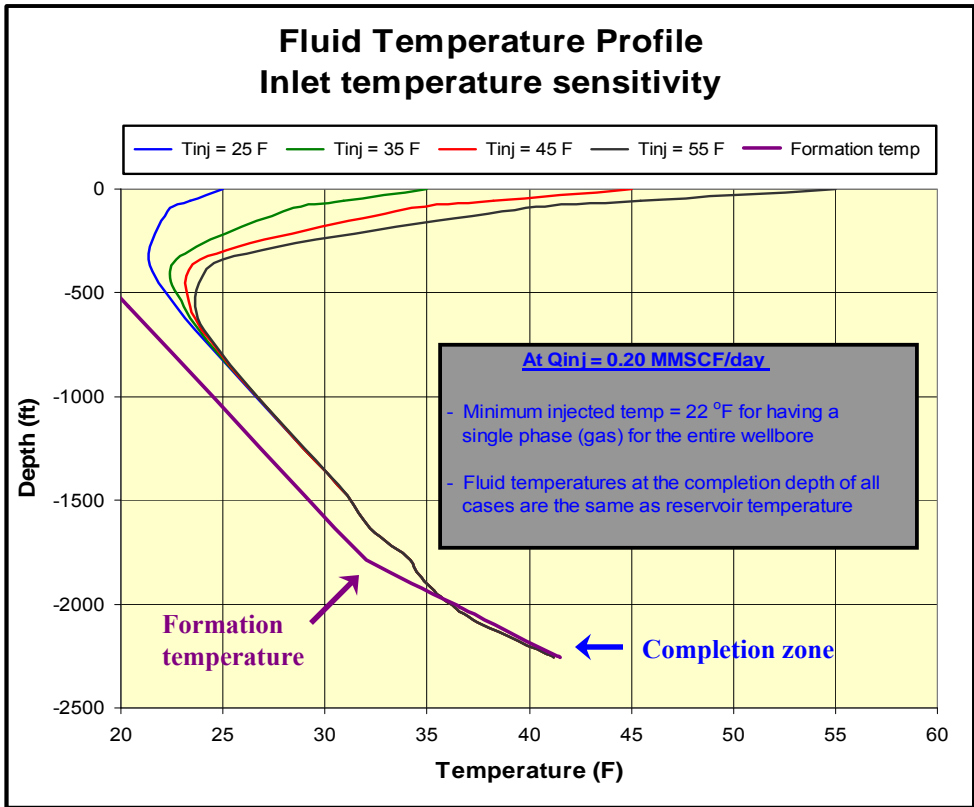
Figure 2-2: Temperature and pressure profiles at various inlet temperatures
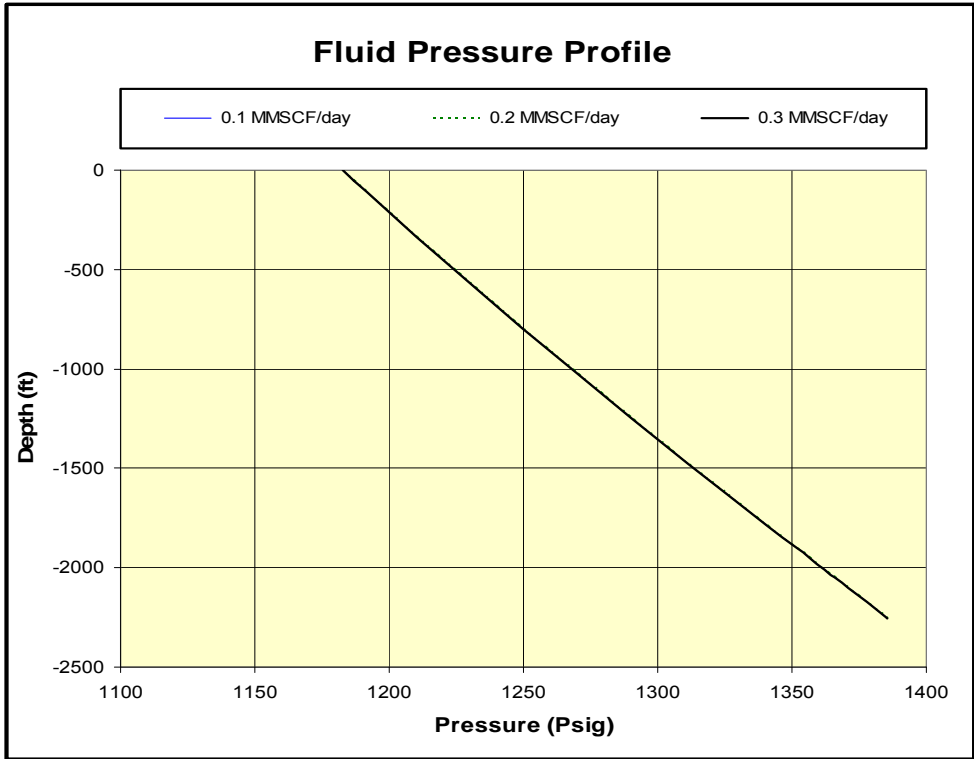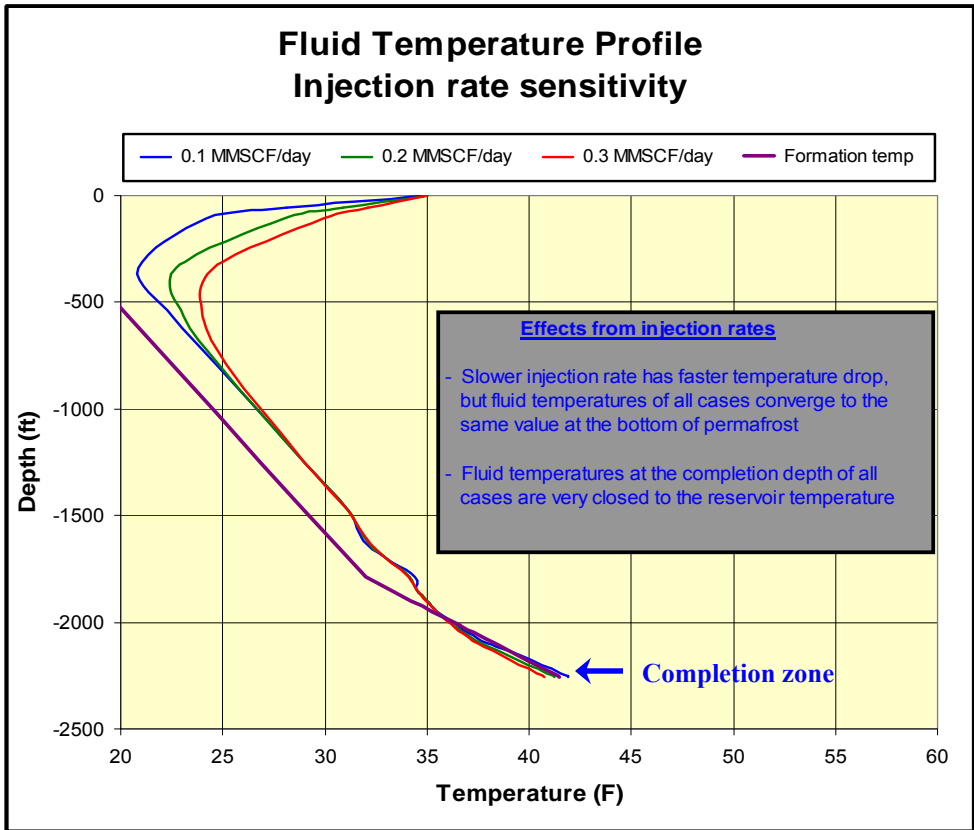
Figure 2-3: Temperature and pressure profiles at various injection rates
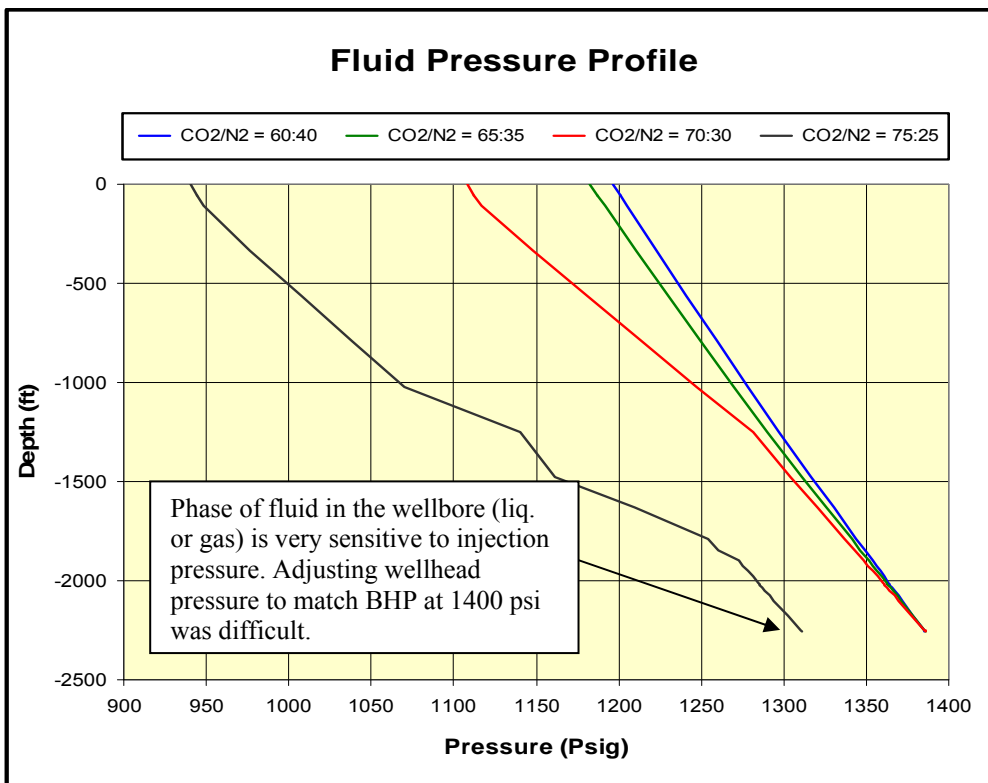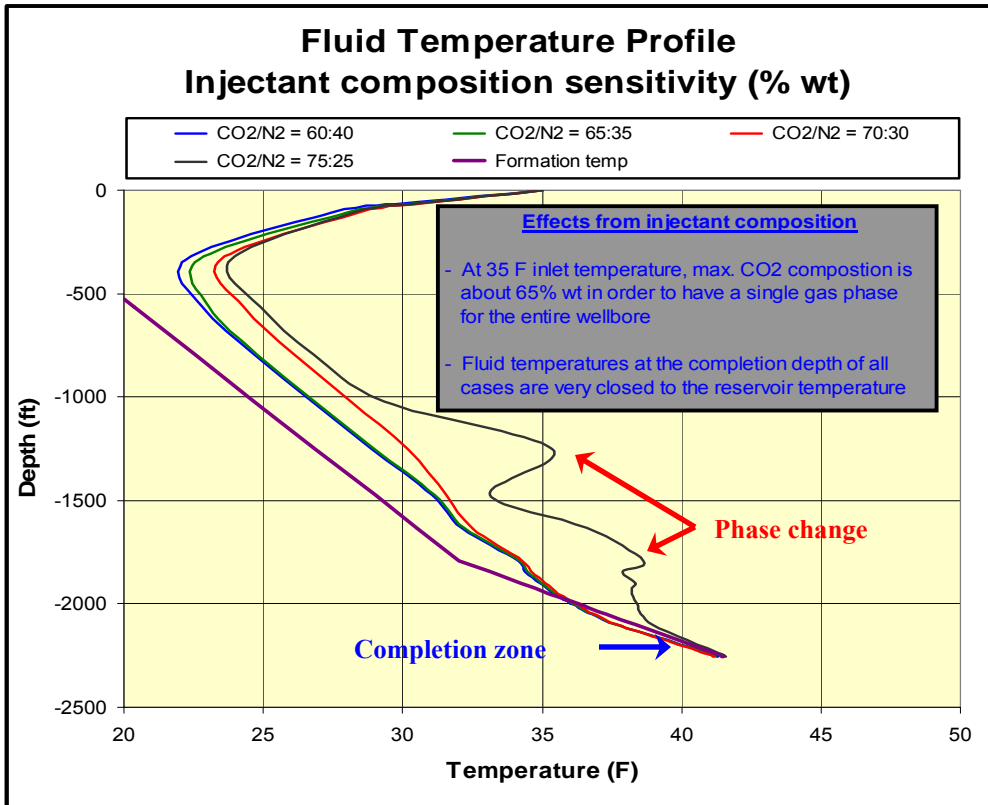
Figure 2-4: Temperature and pressure profiles at various injected fluid composition

Appendix 3: Iġnik Sikumi Daily Operations Summaries

ConocoPhillips
Wellview Web Reporting

24 Hr Summary Report

Report Header					
Well: IGNIK SIKUMI 1	**Field:** PRUDHOE BAY UNIT	**Job Type:** DRILLING ORIGINAL	**Rig Name:** NORDIC 3	**Rig Supervisor:** Brett Packer	
Rig Accept: 4/5/2011 4:30:00 PM	**Rig Release:** 4/28/2011 9:00:00 PM				

Date	24 hr Summary:
04/04/2011	Move rig from 2V pad to CPF-2. Crew changeout. Check air in tires, grease planetaries. Move rig from CPF-2 to Oliktok Y. Standby w/ crews for CPAI crew changeout. Move Rig from Oliktok Y to KCC. Set rig down, grease planetaries, check tires. Move rig from KCC towards 1D pad.
04/05/2011	Moved Rig to 1J access road. Greased planetaries and check tires, service rig. Moved rig from 1J access road to Milne Pt. turnoff. Check equipment, meet w/ security. Move rig f/ Milne Pt. turnoff to Ignik Sikumi #1. Lay out herculite & T-mats, stack double rig mats. Continue to double stack rig mats and build ramp. PJSM, move rig over well. Spot & level rig. Rig Accepted at 16:30 hrs on 4/5/11. NU diverter, spot equipment, berm equipment.
04/06/2011	Finish NU diverter. Changeout saver sub & grabber box dies. Spot Drill Cool units w/ crane & berm up around Drill Cool units. Cont. to spot MI filter unit, MI vac unit, and other 3rd party equipment around rig. Spot upright tanks and berm up. Load MWD tools, load casing spider slips w/ crane. Offload 5" HWDP & 5" DP. Load 5" drillpipe into pipe shed, rack & tally drillpipe. Load tools, troubleshoot stabbing board, now functioning properly.
04/07/2011	Function test stabbing board. Install wood steps over wires running to MWD shack. Install 4" valve on conductor. PJSM. Pick up drillpipe, calibrate MWD to block height. PU 5" drillpipe, torque up and rack back in derrick. Load 290 bbls spud mud into upright tank. PJSM. Slip & cut drilling line. Test Diverter. RIH tag cement at 96.44'. Est. 12' cement to conductor shoe. PJSM. Rack & tally 5" HWDP. PJSM. Rack & tally 10-3/4" casing. Pressure test mud pumpst to 2000 psi.
04/08/2011	Load casing, rack & tally. MU & break out new HWDP, drift to 2.867. Service top drive, washpipe. Install Totco monitors in mud shack and MWD shack. Load casing equipment, bring cement head to rig floor. Load hanger into pipe shed. Continue to load spud mud into pits. Load 20' casing pup and Landing Joint. PJSM. PU & MU BHA #1, fill hole w/ water. Dry run 10-3/4" fluted hanger and land. Top of Landing Ring at 30.88' RKB, top of load shoulder at 31.25' RKB. Work on Totco system, fix stroke counter and flapper sensor. Other Totco functions failed. Stroke counter and gain/loss functions won't zero. Troubleshooting Totco.
04/09/2011	Continue troubleshooting Totco system. Swapped computer module for older version, reloaded Totco and re-input well info. Totco fixed. Function tested Totco sensors, loaded 10 bbls into trip tank, tested PVT, block height, traveling speed. Verified can zero stroke counter and gain/loss functions. PJSM. Spudded well at 02:45 am. Cleanout conductor shoe track f/ 96' to 108'. Drilling ahead f/ 108' to 239'. Back ream out of hole f/ 239' to 165' Blow down top drive. POOH f/ 239' to surface. PU & MU BHA #2 and TIH to 132'. Upload MWD. PU single & pulse test. Bring pumps online and survey at 132'. Service Rig. PJSM on radioactive sources. Load MWD radioactive source and RIH to 170'. Survey at 170'. RBIH to 239', Circulate well clean. Auger plugged. Unplug same. Directional drill f/ 239' to 379'. Auger loaded up w/ gravel, belt broken. Replace Belt / unplug auger. Directional drill f/ 379' to 411'. Auger loaded up again. Noticed grinding in the gear box, begin changing out gear box on auger. Continue to reciprocate and circulate pipe at 1 BPM.
04/10/2011	Cont. to work on auger system, finished installing new gear box. Driller looked down hole and noticed no flow. Increased pump strokes to 2 BPM and pump pressure spiked to 2500 psi. Shut down pumps and bled off. Top drive frozen. Set pipe in slips, installed TIW valve and 2" circulation hose, confirmed circulation. Lowered top drive to rig floor. Disconnected kelly hose, began flushing ice chunks from kelly hose w/ steam. Clear ice from top drive w/ steam. Continue steaming ice from kelly hose. Attached 2nd steam hose to pump manifold and applied steam to standpipe. Used infrared temperature sensor to check standpipe temperature. Standpipe temperature 20' off rig floor @ 120°F, 40' off rig floor 100°F, then immediately above belly board @ 40' dropped to 20°F. Hoisted rig hand on man-rider to put hands on standpipe and verify frozen. Confirmed. Finished thawing out Kelly hose & standpipe. Circulate down HWDP @ 3 BPM / 150 psi. Pressure test kelly hose to 2500 psi. Directional drill f/ 411' to 1087', backreaming full stand prior to every connection. ADT: 9.26 hrs @ midnight.

04/11/2011	Cont. directional drilling f/ 1087' to TD at 1482'. Circulate bottoms up. Blow down top drive, monitor well. Static. POOH f/ 1482' to 300' on elevators, slight hangup at 1020 ft, worked through. RBIH to TD at 1482'. Circulate at 15.5 BPM, raise pump rate to 16.1 BPM, rotate & reciprocate. Continue to circulate at 16 BPM. Pump a 10.9 ppg sweep. Chase sweep with 9.4 ppg mud. Rotate & reciprocate at 45 RPM's. Blow down top drive, monitor well. Static. POOH f/ 1482' to 975'. RBIH f/ 975' to 1477'. Circulate new 9.1 ppg mud. Blow down top drive. POOH f/ 1477' to 220'. PJSM on radioactive sources. Continue POOH laying down 8" MWD tools. Remove nukes, dowload MWD data. Continue to lay down BHA #2.
04/12/2011	Ran 10 3/4" Surface Casing Down to 1,473' MD. Circulated 100 bbls of 10.0 ppg Mud Push follow by 299 bbls of 11.2 ppg Arctic Lite Crete, pumped addition 65.2 bbls of 12.0 ppg Deep Crete, chased with 128 bbls of 8.8 ppg OBM, bump plug and pressure up to 1010 psi and held pressure for 5 mins. RDMO Cementing Crew and Equipment.
04/13/2011	Rigged down and Shipped out Diverter. Installed FMC Gen 5 Wellhead System. NU 11" 5M BOP's and Crossover flow nipple with Annular. Started BOP testing.
04/14/2011	Finish Initial BOP Test. RIH With Production Drilling Assembly and Drilled out the wiper plug, float colllar, landing collar and shoe. Drilled addition 30' ft of new hole from bottom of shoe at 1,473' to 1,502' and preform LOT/FIT test. Continue drilling new production hole from 1,502' ft with 8.8 ppg OBM.
04/15/2011	Drilled a Total of 647' ft of New 9 7/8" Production Hole. Had problems keeping 8.8 ppg OBM chilled during drilling operation. TOOH to remove mud motor, found cone drag on Bit, replace with new bit with 1 (14) and 3 (20) nozzle jets. Lay down SperryDrill motor. TIH and continue with Drilling operation until midnight with very little cooling issue. 24 hour Drilled Section 1,530' ft to 2,220' ft.
04/16/2011	Drilled a Total of 377' of new 9 7/8" hole f/ 2220' to 2597' .Called TD of well at 2,597 ft after dealing with fluid cooling condition for most of the day while Drilling.Made Several Attempts to keep fluid cool with drill cool unit to proper temp with little success. CBU until clean, while conditioning well bore. Monitor well for flow, well static. Wiper trip to 10-3/4" shoe, no hole problems. POOH f/ 2,597 to BHA at 92.80' and Downloaded recorded data from LWD tools. Break down and lay down Drilling assembly.
04/17/2011	MIRU Schlumberger Wireline Equipment. MU and RIH logging BHA #1 to 2600', Made main pass log from 2600' to surface, found 10-3/4" CSG on depth at 1,473'. . MU and RIH BHA #2 to 2450'. Perform rad check in CSG, and log correction pass. Measure pressure and mobility with pressure express tool.
04/18/2011	Finish Logging operation with logging assembly #2. Log CMR/PEX/HNGS and 17 pressures with XPT to obtain mobilities in hydrate zone. POOH and lay down logging assembly #2. MU TLC-MDT logging assembly #3 and rih 2,259', SLB adjusted tool setting and logged hole to 1,977', x2. RIH and set packer on depth at 2071-2074 feet, start first stage of Mini-Frac. Release packer and rih and correlated for next packer depth. Stop & parked DP with center of packer at 2202 feet..
04/19/2011	Finished the second stage of the Mini-Frac and Obtain in-situ measurement.MU Schlumberger TLC-MDT logging assembly #4 and RIH to 2,235' dpmd and started Modular Dynamics Testing with tools setting at 2260'-2263'. After several hours, downhole modular pump not working properly, functioning very slowly. TOOH to swap out with downhole modular pump from logging assembly #3.
04/20/2011	POOH with MDT testing assembly. Remove modular pump from MDT assembly #4 and Replace with modular pump from MDT assembly #3. RIH to 1546' and installed side entry port and pump e-line cable and wet connection head & latched into logging assembly. Correlate depth and position center packer at 2261' ft and start MDT testing. Stage test area 2260'-2263', Unable obtain sample at stage. Release packer and RIH to next stage area, and place center of packer at 2303 ft.Start MDT testing at stage area 2302-2304 ft.
04/21/2011	Finished Modular Dynamics Testing on desired zone. Rig down and Release SLB logging Crew and Logging Equipment. Started Weekly BOP test and safety alarm system testing.
04/22/2011	Continue with testing BOP's. Observed upper rams and annular failed. Change out Upper rams and annular bag. Resume testing BOP's. Test Annular Upper pipe rams with 2 7/8", 4 1/2", 5" test joints. 250 / 3500 PSI. Perform Koomey test. Initial 200 PSI in 18 seconds, with full 3000 PSI in 85 seconds. 4 Nitrogen bottle with and avg PSI of 2075. Witness of test waived by AOGCC rep John Crisp @ 1645 HRS 4/21/11. Make up 9 7/8" Cleanout BHA with bit #2RR1, and trip in hole with no issues in open hole, proper displacement. Circulate bottoms up,mix and pump Hi Visc sweep @ 500 GPM's - 950 PSI. Reciprocate & rotate drill string. POOH laying down drill pipe and pigging every joint to remove oil base mud before laying DP to storage area.
04/23/2011	Continue POOH laying down 5" DP. Utilize Vac system to clean OBM from joints before removing from pipe shed. Install & test 7 5/8" Upper rams. Rig up to run 4 1/2" x 7 5/8" casing assembly. Held PJSM with all personnel. Make up shoe track assembly, fill pipe & check floats. Good. Continue RIH picking up 4 1/2" casing installing protector clamps as per detail Make up Pinnacle gauge carriers,and splice TEC wire as needed. Operation at midnight. Just finish the 4 1/2" Completion section of the production string, all three stages of the Pinnacle Gauge assembly is complete and secured. Start making up the 7 5/8" section.

04/24/2011	Continue run 4 1/2" x 7 5/8" casing string with TEC & DTS wires, attaching protector clamps as per detail. MU Casing hanger and landing joint. Terminate lines for hanger penetration. Secure & test same to 5000 PSI. RIH land casing hanger. UP / DN WT = 98K. Verify landed hanger as per FMC. RILDS. RU Schlumberger wireliners, and run GR-CCL log to correlate PIP tag and blank pipe depths. Observed 1/2' foot difference than pipe tally with wireline measurement. WLOH rig down Schlumberger. Nipple down, splitting the spools. . Nipple up, and test void on spools as per FMC to 5000 PSI. Utilize crane to off load all spools from rig floor, and load Flatpak spool with spool & cage. Load Upper 4.5" completion string and jewelry.
04/25/2011	Pull DTS & TEC wires through casing spool side ports as planned. Attach same. Terminate lines, and connect to there monitors to check for communication to the downhole gauges. Loaded and tallied 4.5" Upper completion. Removed 7 5/8" ram's and installed 2 7/8" x 5' vbr's and tested 250/3500 psi. Pickup and run in hole with 2 7/8" fox cementing work string with a baker 2.38" slick stinger down to top of baker packoff bushing at 2370 ft and string into packoff bushing and no-go 10 ft deeper. Establish circulation @ 3-4 bpm and condition chilled mud. Sting into packoff bushing, and establish circulation to 3 BPM for full circulation. Batch mis Mud Push & cement. Pump a total of 75 BBLS of mud push and 153 BBLS of Litecrete cement, observing 10 BBLS of 11.0 PPG cement to surface. CIP at 15:37 HRS. Floats held. Pull stinger, and reverse circulate with no cementg returns. Lay down tbg back to 1800' MD. Circulate 90 Deg OBM as per rig engineer. Blow down & RD DrillCool units.
04/26/2011	Circulated 90 deg heated OBM for a total of 10 hours. RIH w/ 2 7/8" work string down to 2364 ft. Displacement fluid after mixing surfactant was 57 deg, bring out more fluid, circulate pits to cool to 52 degree. Mix and circulate 40 bbls spacer of safe-surf, circulate 250 bbls of 52 deg. fresh water, displacing OBM until clean returns observed. Displace 7 5/8" to brine, spotting 15 bbls of brine with corrosion inhibitor in the 4.5" casing section. POOH, laying down 2 7/8" work string. Ready rig floor and 4.5" equipment. Make up 4.5" pipe handling equipment. Make up Baker seal assembly and lower completion jewelry as per Baker rep.
04/27/2011	Land 4.5" completion with Chemical injection mandrel, and FlatPak assembly. Install clamps at mid joint as per procedure. Terminate lines to hanger and test lines to 5, 000 psi. Pump down each Flatpak line @ 30 GPM - 2,150 psi, pump total of 6.2 bbls. RILDS. Test tubing to 3,000 psi for 30 mins, good test, bleed to 2,000 psi. Test IA to 3,000 psi for same, good test. Bleed tubing to zero and shear SOV. ND BOP stack. NU tree and test to 5,000 psi. Start freeze protect of well with diesel.
04/28/2011	Complete freeze protect of well TBG/ Casing with diesel. Secure wellhead and test below BPV to 3,000 psi. RDMO Nordic rig.

Appendix 4: Schlumberger "Interpretation of Iġnik Sikumi #1 MDT Micro-fracturing Tests," by Richard Birchwood, Vasudev Singh, and Osman Hamid

Interpretation of MDT Micro-fracturing Tests in the Well Ignik Sikumi #1, Prudhoe Bay, North Slope, Alaska

prepared for

ConocoPhillips

Houston, TX

Richard Birchwood
Senior Geomechanics Specialist
Project Leader

Vasudev Singh
Geomechanics Engineer

Osman Hamid
Geomechanics Engineer

May 2011

Schlumberger

TABLE OF CONTENTS

Schlumberger

Disclaimer

The following disclaimer applies to this report and any interpretation provided by Schlumberger DCS Geomechanics:

ANY INTERPRETATION, RESEARCH, ANALYSIS, DATA, RESULTS, ESTIMATES, OR RECOMMENDATION FURNISHED WITH THE SERVICES OR OTHERWISE COMMUNICATED BY SCHLUMBERGER TO CUSTOMER AT ANY TIME IN CONNECTION WITH THE SERVICES ARE OPINIONS BASED ON INFERENCES FROM MEASUREMENTS, EMPIRICAL RELATIONSHIPS AND/OR ASSUMPTIONS, WHICH INFERENCES, EMPIRICAL RELATIONSHIPS AND/OR ASSUMPTIONS ARE NOT INFALLIBLE, AND WITH RESPECT TO WHICH PROFESSIONALS IN THE INDUSTRY MAY DIFFER. ACCORDINGLY, SCHLUMBERGER CANNOT AND DOES NOT WARRANT THE ACCURACY, CORRECTNESS OR COMPLETENESS OF ANY SUCH INTERPRETATION, RESEARCH, ANALYSIS, DATA, RESULTS, ESTIMATES OR RECOMMENDATION.

CUSTOMER ACKNOWLEDGES THAT IT IS ACCEPTING THE SERVICES "AS IS", THAT SCHLUMBERGER MAKES NO REPRESENTATION OR WARRANTY, EXPRESS OR IMPLIED, OF ANY KIND OR DESCRIPTION IN RESPECT THERETO. SPECIFICALLY, CUSTOMER ACKNOWLEDGES THAT SCHLUMBERGER DOES NOT WARRANT THAT ANY INTERPRETATION, RESEARCH, ANALYSIS, DATA, RESULTS, ESTIMATES, OR RECOMMENDATION IS FIT FOR A PARTICULAR PURPOSE, INCLUDING BUT NOT LIMITED TO COMPLIANCE WITH ANY GOVERNMENT REQUEST OR REGULATORY REQUIREMENT. CUSTOMER FURTHER ACKNOWLEDGES THAT SUCH SERVICES ARE DELIVERED WITH THE EXPLICIT UNDERSTANDING AND AGREEMENT THAT ANY ACTION TAKEN BASED ON THE SERVICES RECEIVED SHALL BE AT ITS OWN RISK AND RESPONSIBILITY AND NO CLAIM SHALL BE MADE AGAINST SCHLUMBERGER AS A CONSEQUENCE THEREOF.

CUSTOMER CONFIRMS THAT SCHLUMBERGER DCS GEOMECHANICS HAS MADE NO PROMISE OR STATEMENT REGARDING THE SERVICES THAT IS INCONSISTENT WITH THESE TERMS OR THE SERVICE ORDER, OR THAT HAS CREATED, OR AMOUNTED TO A WARRANTY THAT THE SERVICES WOULD CONFORM TO ANY SUCH PROMISE OR STATEMENT, AND SCHLUMBERGER DCS DISCLAIMS ANY AND ALL WARRANTIES REGARDING THE SAME.

Schlumberger DCS Geomechanics is an industry leader in working jointly with clients to solve reservoir and production problems associated with oil and gas field development in a fully integrated manner that provides process controlled innovative, practical and cost-effective solutions.

LIST OF TABLES

Schlumberger

List of Figures

Schlumberger

1   SUMMARY

This report describes the results of micro-fracturing tests carried out on April 18-19, 2011 in the vertical well Ignik Sikumi #1 for purposes of measuring the minimum horizontal stress. The well was drilled with oil-based mud in the Prudhoe Bay Unit of the North Slope, Alaska and attained a total depth of 2600 ft RKB. Fractures were generated by pressurizing an interval approximately 3 ft in length isolated between the dual packers of the MDT tool. The nominal diameter of the borehole was 9.88 in. Micro-fracturing tests were carried out at two stations located at 2071.95 and 2202.58 ft RKB in order of chronology (the rig kelly bushing was 30.7 ft above ground level). The tool string used in both tests is shown in Appendix B.

Both tests were performed in open-hole conditions. The formation at the first test station was a gas hydrate bearing D-sand. A siltstone resided at the second test location. Because the tests were performed in soft sediments, problems with seal integrity, fracture initiation, and sticking were anticipated. Sealing problems did occur, but they were of limited duration and had minimal impact on the test. The other two problems did not occur. However irregular flow due to half-stroking of pumps was a frequent occurrence. This problem was probably caused by interaction of solids in the mud with pump check valves. Half-stroking complicated interpretation of corroborative parameters such as the leak-off pressure. However this problem did not affect the inference of the most crucial parameter, i.e., the closure stress. Therefore the main objective of these tests was satisfied. The tests yielded minimum horizontal stress estimates of 1364 psi (12.7 ppg) and 1625 psi (14.2 ppg) at the first and second test stations respectively.

2   NOMENCLATURE

C0, C1,C2,.. – Cycle 0, Cycle 1, Cycle2, etc.

CloseG – Closure pressure determined from Nolte (G-function) plot

CloseSq – Closure pressure determined from plot of pressure versus square root of shut-in time

E1 – Event 1

ISIP - Instantaneous shut-in pressure

LOP - interval pressure at start of fracture propagation (leak-off pressure)

LOV - volume of fluid pumped prior to fracture propagation

MRFC – Flow control module

MRPA - Dual packer module

MRPOUD/MRPOUD2/MRPOUD3 - Pump-out unit

PAFP - Packer valve status

PAHP - Dual Packer Inflate Pressure

PAQP - MRPA Quartz guage interval pressure

PAVP - Interval valve status

P_Close - Closure pressure determined from plot of pressure versus square root of shut-in time

P_Close_G-function - Closure pressure determined from Nolte (G-function) plot

Peak, Peak_P - Maximum pressure attained prior to unstable fracture propagation.

P_HYD - Hydrostatic pressure

POTFR – Total flow rate

POUDHP/POUDHP2 – MRPOUD/MRPOUD2 hydraulic pressure

POUDMS/POUDMS2 – MRPOUD/MRPOUD2 motor speed

P_Reb - Rebound pressure

Prop, Prop_P – Fracture propagation pressure

Reb – Rebound pressure

Stiff,Stiffness – Measure of wellbore stiffness equal to the gradient of the pressure vs. volume curve prior to fracture initiation

Vfrac, VL_Frac – Volume of fluid pumped into fracture

3   BRIEF DESCRIPTION OF MICRO-FRACTURING TESTS

In this section a brief description of the test procedures employed in Ignik Sikumi #1 is provided. For more details of micro-fracturing test procedures and apparatus, please consult Appendix A. The micro-fracturing test at each station commenced with inflation of the packers for the purpose of sealing an interval approximately 3 ft long. This was followed by a sequence of operations in which pressure in the *test interval*[1] between the packers was manipulated using three dual pump-out modules (MRPOUD, MRPOUD2, MRPOUD3). The operations were as follows:

1. *Filtration tests* in which the interval pressure was raised to a value less than that required to break down the formation followed by shutting in of the interval. This test is conducted in order to allow the packers to seat themselves properly against the formation, verify the integrity of the packer seal, and establish a baseline rate of pressure decline through the wellbore wall prior to fracturing.
2. Injection into the interval until initiation or propagation of a fracture occurred.
3. Propagation of the fracture for a designated period.
4. Cessation of pumping, isolation of the test interval, and observation of pressure decline.
5. Extension of the fracture by repeated execution of steps 2, 3, and 4.

In addition to these operations, a *rebound test* was conducted at the second station (2202.58 ft) whereby a fracture was propagated, fluid was suddenly withdrawn from the interval and the interval was shut-in. The interval pressure initially decreased rapidly and then rebounded. The final pressure approached during the shut-in period represents a lower bound on the closure stress.

In the proceeding discussion we adopt the convention that all episodes consisting of pressurization of the interval followed by shut-in and pressure decline are referred to as *cycles*. All other episodes, such as those involving packer inflation or withdrawal of fluid from the interval are referred to as *events*.

---

[1] Hereafter the test interval will be referred to simply as the *interval*.

4   FLOW RATE CORRECTIONS

Special care was taken to ensure that flow rates generated by the dual pump-out modules were accurately computed. Corrections were introduced to remove irregularities in computed flow rates due to disruption of flow by shutting of valves while the pump was running. For example, the flow delivered to the interval was set to zero whenever the interval valve was shut. Additional corrections to the flow rate were made to account for half-stroking of the pump piston. Half-stroking occurs when mud-check valves in the pump do not seal properly. As a result, fluid is not delivered by the pump. This problem occurred frequently, and may have been caused by exposure of mud check valves to solids in the mud. Half-stroking can be diagnosed be examining the pump hydraulic pressure. This pressure is unusually low when half-stroking occurs. In order to correct for this problem, the flow rate was set to zero whenever the hydraulic pressure fell below a designated cutoff.

.

5 TEST RESULTS

5.1 Test Results at 2071.95 ft

5.1.1 Overview

This test was carried out in a gas hydrate bearing sand. Figure 5.1 shows the location of the test interval. The borehole is slightly under-gauged, possibly due to mudcake build-up or creep. A small amount of separation between resistivity curves at the test location indicates mud invasion and possibly, some gas hydrate dissociation near the wellbore. The dynamic Young's modulus of the formation is approximately 7.6 GPa, which is typical of weakly consolidated sediments.
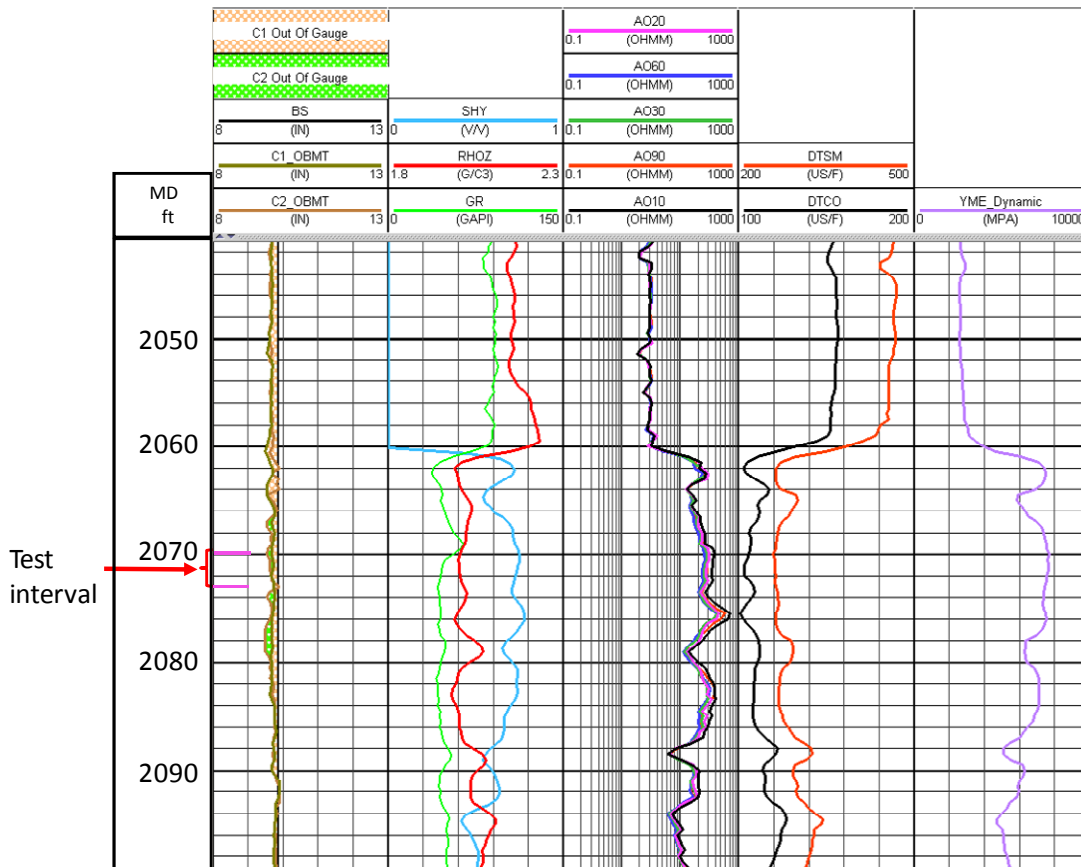
Figure 5.1: Logs in vicinity of Station 1.

The test interval was located in a gas hydrate bearing interval between 2069.9 and 2073.1 ft. TRACK 1: Measured Depth with respect to KB. TRACK 2: Dual caliper measurements C1_OBMT, C2_OBMT and bit size, BS. Shading reflects difference between each caliper measurement and the bit size. TRACK 3: Gas hydrate saturation, SHY, density, RHOZ, and gamma ray, GR. TRACK 4: Resistivities measured at various depths of investigation from shallow (A010) to deep (AO90) TRACK 5: Compressional (DTCO) and shear (DTSM) wave slownesses. TRACK 6: Dynamic Young's modulus.
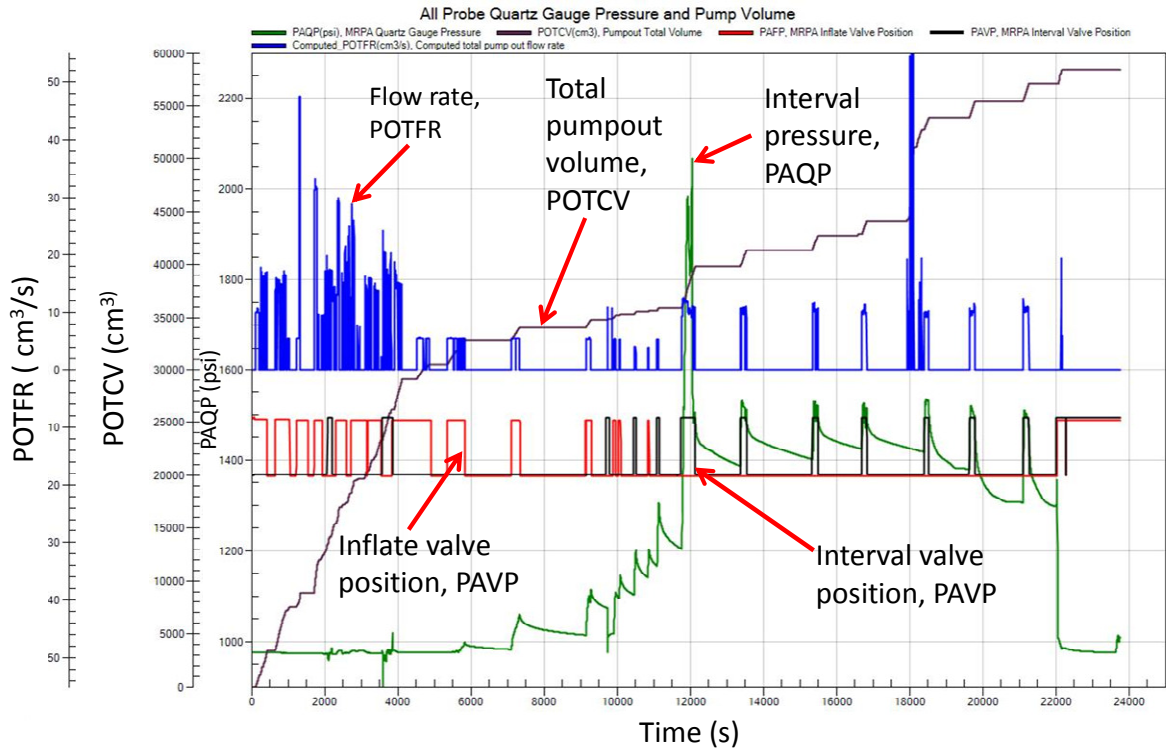
Figure 5.2: Overview of data acquired at Test Station 1 located at 2071.95 ft MD.

Figure 5.2 presents an overview of the most important data acquired during the test. The time corresponding to the peak interval pressure (green curve) roughly divides the test into two equal parts. The earlier part consisted of packer inflation and filtration tests. The later part consisted of fracture propagation/shut-in cycles. A total of seven fracture propagation /shut-in cycles were performed during the test. The static pressure of the mud column at the start of the test was 975.4 psi.

Figure 5.3 provides an overview of the packer pressure, interval pressure, and the difference between them. The packer pressure is generally higher than the interval pressure. This indicates that the packer is functioning as designed and provides some assurance that a proper seal is being maintained. However Figure 5.3 also shows a brief episode during the first injection cycle in which the packer pressure dropped below the interval pressure. This was most likely due to a temporary loss of seal. This problem will be highlighted later.

5.1.2 Packer Inflation

Figure 5.4 shows the packer inflation event. The packer was inflated over a period of more than 6000 s. A primary objective of this procedure was to avoid over-inflation of the packer that could cause it to stick or make poor contact with the borehole wall due to excessive yielding of the formation. Satisfying this objective involved determining the minimum packer pressure required to maintain adequate contact with the borehole wall. The initial pressure of the mud column was 975.65 psi. The packer was inflated in stages to 1250 psi. Whenever the pump was switched off,

the packer pressure declined gradually. This is because the interval pressure declines due to leakoff to the formation and the packer pressure follows the interval pressure.
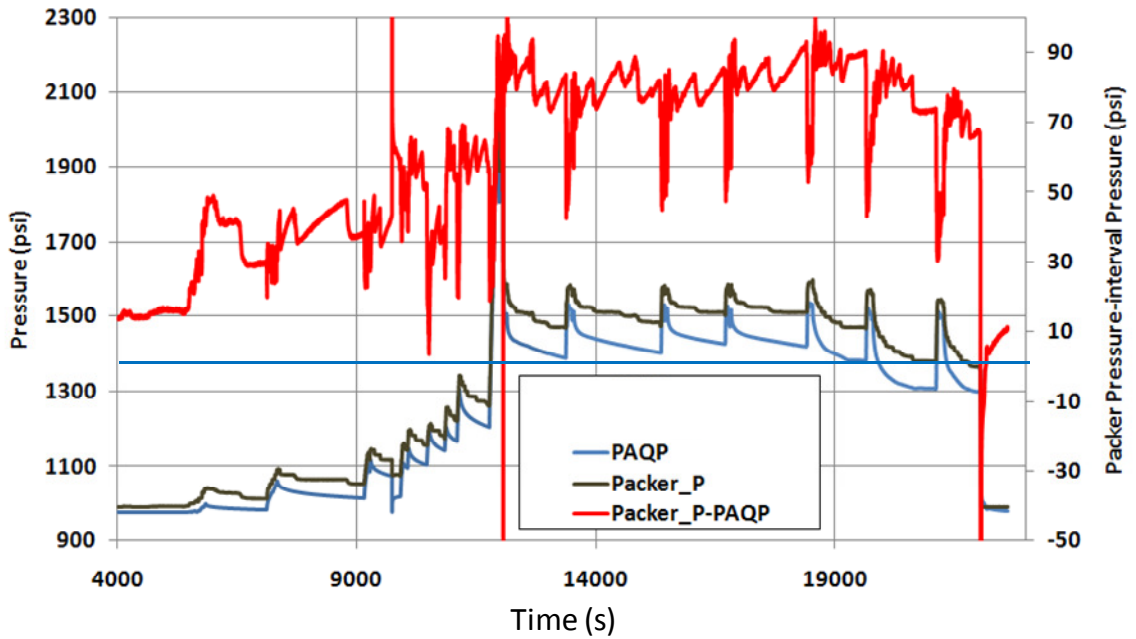
Figure 5.3: Packer and interval pressures versus time. Difference between packer pressure and interval pressure also shown.
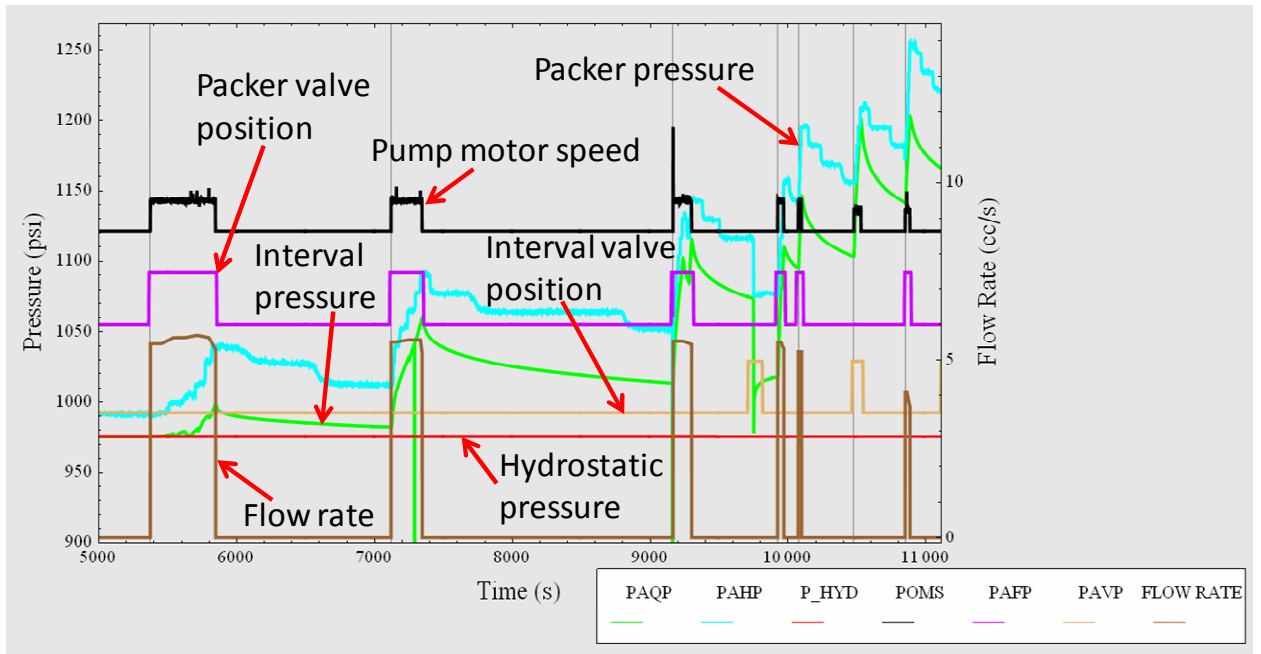
Figure 5.4:Packer Inflation (Event 0)

After the final inflation step, the packer pressure remained above the interval pressure and the seal was judged to be adequate for the next stage of the test.

5.1.3 Filtration test (Cycle 0)

Figure 5.5 presents the results of a filtration test conducted prior to breaking down the formation. Fluid was pumped into the interval at a rate of 5.5 cc/s for about 50 s and then the interval was shut in. Figure 5.6 plots the interval pressure versus the volume of fluid pumped into the interval. The curve is nonlinear indicating that the formation might be yielding or that the rate of fluid loss through the formation is high relative to the pump rate. Figure 5.7 shows the pressure during the shut in phase versus the square root of shut-in time. The derivative of the pressure with respect to the square root of shut-in time is also shown. Table 5.1 summarizes the results of this cycle.
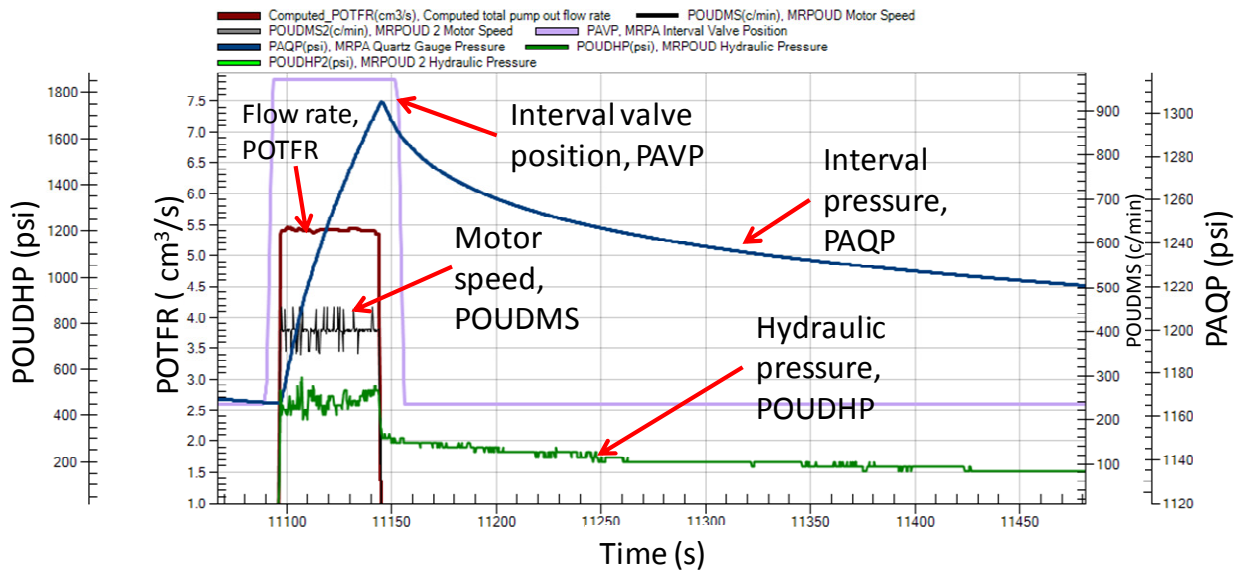
Figure 5.5: Cycle 0. Final filtration test.

Table 5.1: Cycle 0 Results

Stiff (psi/cc)	LOP (psi)	LOV (cc)	VL_frac (cc)	Peak_P (psi)	Prop_P (psi)	ISIP (psi)	P_close (psi)	P_clos_G-function (psi)
0.8405	1210	54	N/A	N/A	N/A	N/A	N/A	N/A
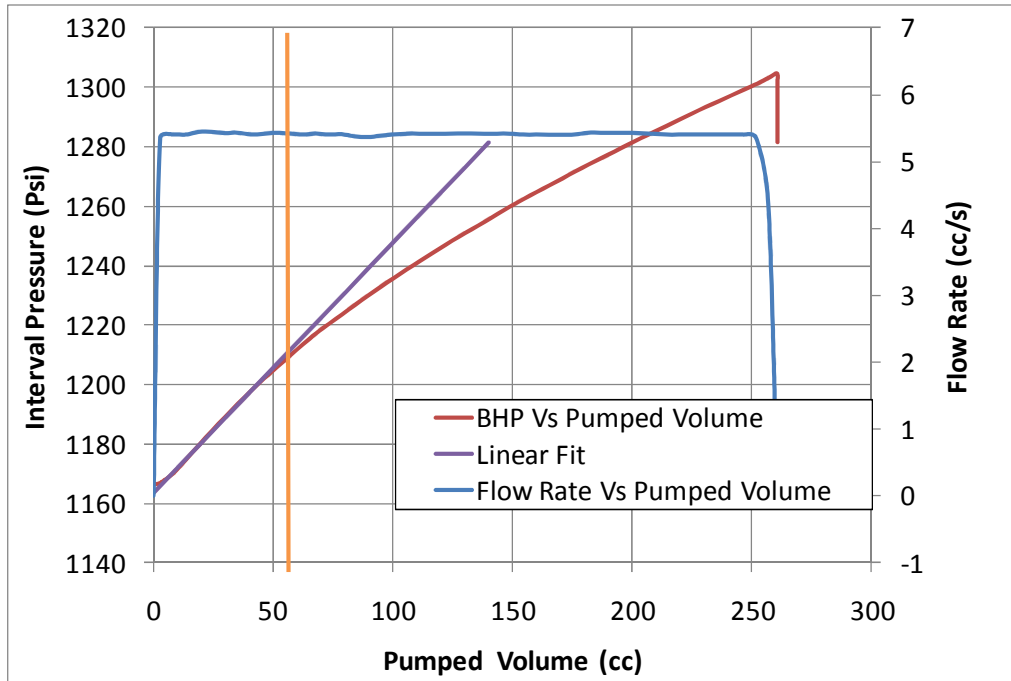
Figure 5.6: Plot of interval pressure vs. pumped volume during the filtration phase (red curve). A linear fit to this curve is shown in purple. Orange line shows location of departure of curve from linearity. The flow rate into the interval (blue curve) is also shown referenced to the right hand vertical axis.
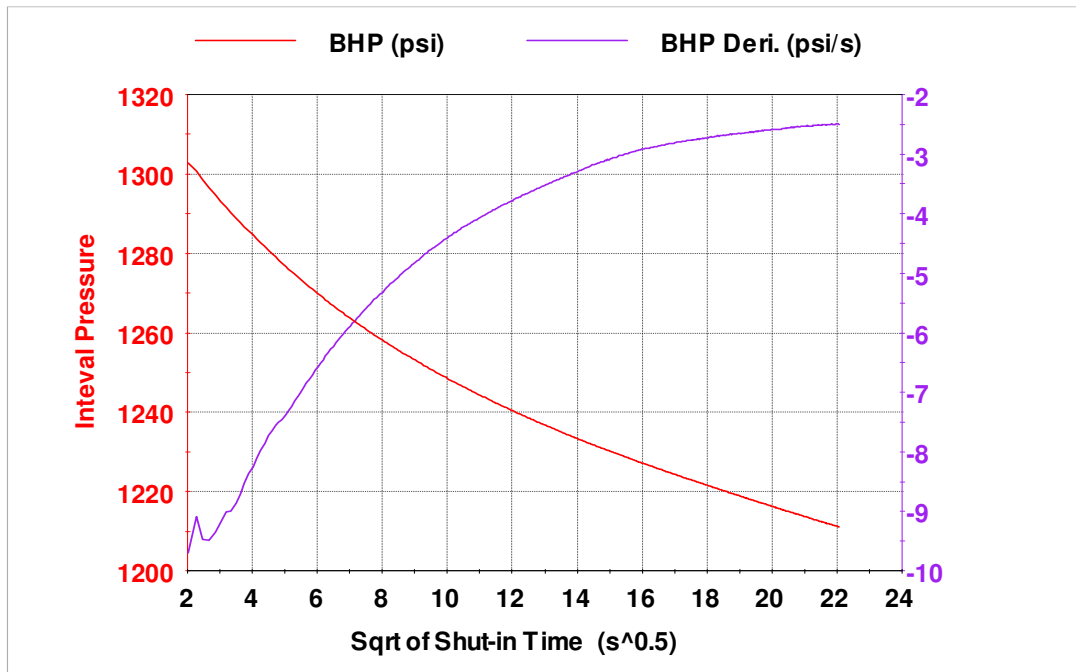
Figure 5.7: Plots of interval pressure (red curve) and its derivative (purple curve) versus square root of shut-in time.

5.1.4 Cycle 1

Figure 5.8 shows the results from Cycle 1. The interval pressure was raised until the formation appeared to break down at 11931 s at a peak pressure of 1985 psi. However as pumping continued, the pressure subsequently attained a much higher peak value of 2068 psi at 12064 s. There are three possible reasons for this:

1. The pump sputtered at the first peak leading to a premature decline in the pressure.
2. The packer seal was breached at the first peak leading to a premature decline in the pressure.
3. A fracture was formed at the first peak, but was bridged off from the interval by solids in the mud making it difficult to propagate.

The first explanation is ruled out on the basis that the pump maintained a hydraulic pressure well above the threshold for a malfunction (the threshold is typically ~ 100-300 psi). Figure 5.8 shows that the pump hydraulic pressure was above 1500 psi when the first peak pressure was attained.

The second explanation, a breach in the packer seal, can occur as a result of the packer fracturing the formation (a so-called "sleeve fracture"), or due to a loss of contact pressure between the packer and the formation caused by plastic yielding of the formation. However in both these cases, the pressure in the packer should drop before the pressure in the interval. Figure 5.9(a) shows that the pressure in the packer continued to rise for about 5 seconds after the interval pressure began to level off. Hence the second scenario seems unlikely.

The third explanation is the most likely one. It is also consistent with evidence of filtercake formation discussed in relation to later cycles. A filtercake probably formed either inside the fracture or at the mouth of the fracture soon after it was created. This process of bridging would have been encouraged by the drop in pressure that occurred right after breakdown. The filtercake sealed off the tip of the fracture from the wellbore. A higher wellbore pressure was thus required to further propagate the fracture.
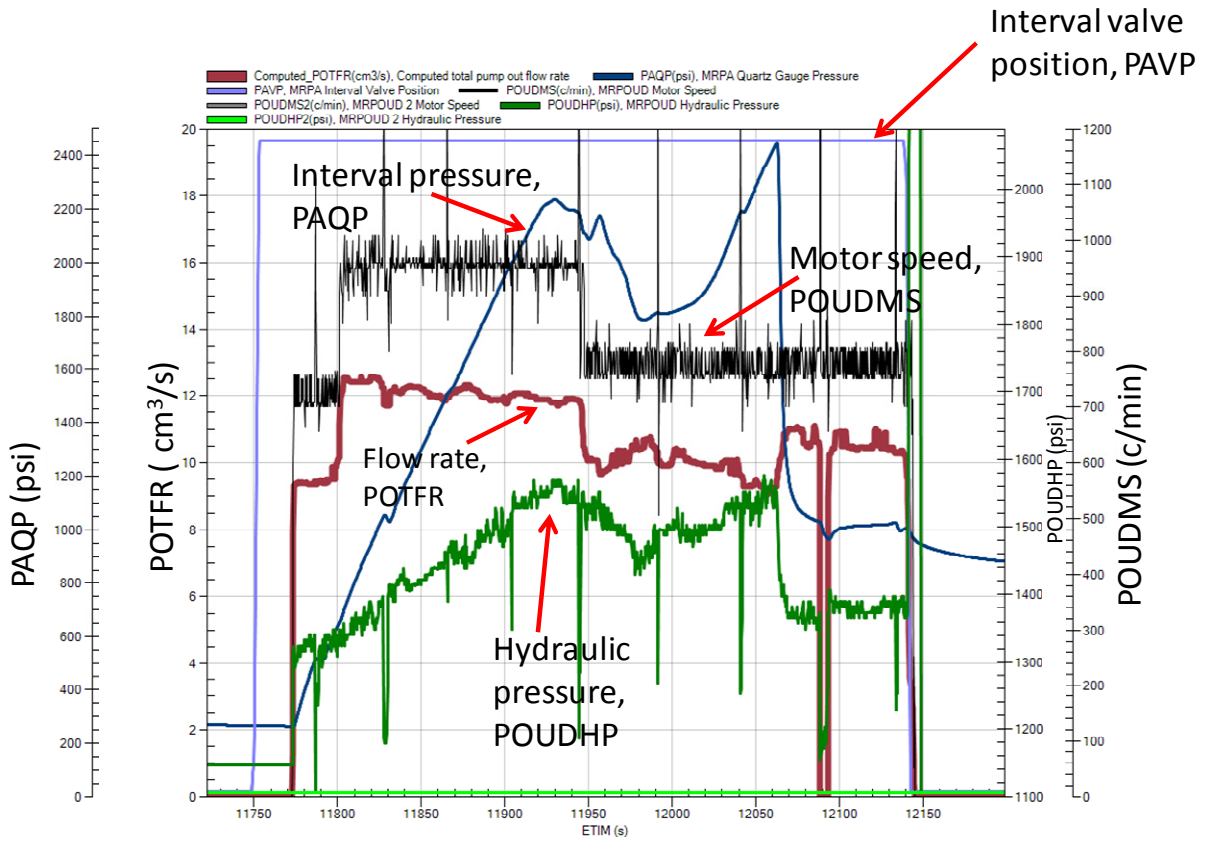
Figure 5.8: Cycle 1. Breakdown of the formation.
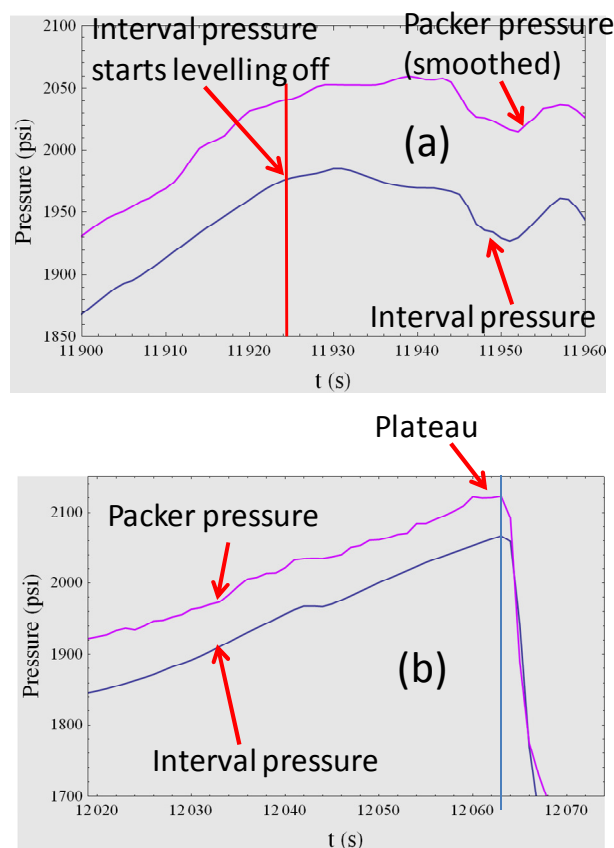
Figure 5.9: Packer and interval pressures versus time during Cycle 1. (a) Pressures in vicinity of first peak. (b) Pressures in vicinity of second peak.

Figure 5.9(b) shows the packer and interval pressures in the vicinity of the second peak pressure shown in Figure 5.8. A rapid decline in both pressures occurred at 12063 s. In this case, the packer pressure reached a plateau while the interval pressure was rising, indicating that events at the packer level were responsible for the sudden decline in pressure. It is probable that a temporary breach of seal occurred at the second peak. Additional evidence for a loss of seal can be found in the fact that the packer pressure momentarily dropped below the interval pressure (Figure 5.10). This is frequently an indication that the seal has been broken. This loss of seal may have been caused by the packer reseating itself against the formation or fracturing of the formation by the packer.

Figure 5.11 shows the interval pressure plotted against the volume of fluid pumped into the interval. The formation response is quite linear until the breakdown pressure is attained. Figure Figure 5.12 plots the shut-in phase of the cycle. An inflection point associated with closure of the fracture is identified at 1444 psi. An alternative construction using the G-function yields a closure pressure of 1442 psi (Figure 5.13). Table 5.2 summarizes the results of this cycle.

Table 5.2: Cycle 1 Results

Stiff (psi/cc)	LOP (psi)	LOV (cc)	VL_frac (cc)	Peak_P (psi)	Prop_P (psi)	ISIP (psi)	P_clos (psi)	P_clos_G-function (psi)
0.4208	1970	1750	2211.9	1985.2	N/A	1476	1444.1	1442
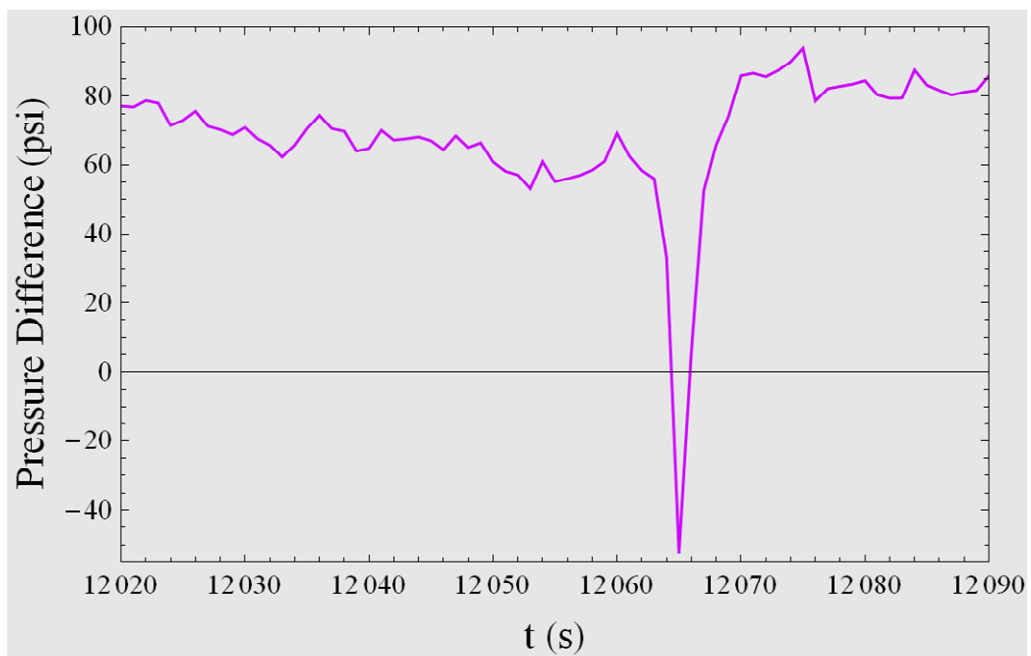
Figure 5.10: Packer pressure minus interval pressure during Cycle 1.
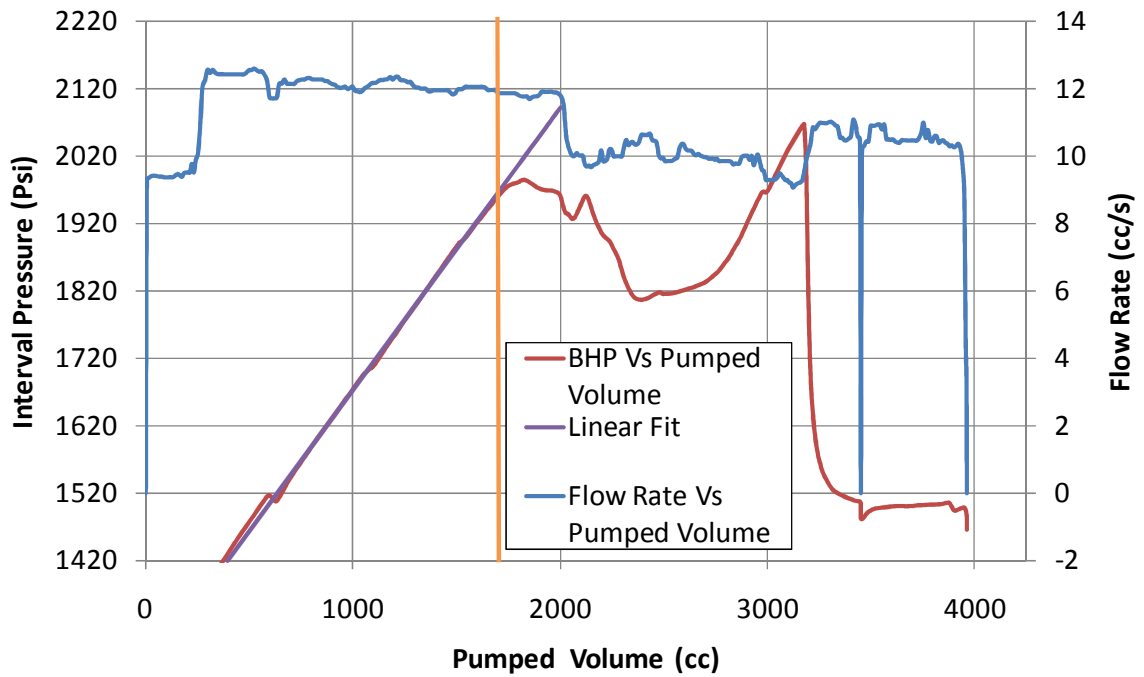
Figure 5.11: Plot of interval pressure vs. pumped volume during Cycle 1 (red curve). A linear fit to this curve shown in purple. The volume at which the curve departs from linearity shown by orange line. The flow rate into the interval (blue curve) is shown referenced to the right hand vertical axis.
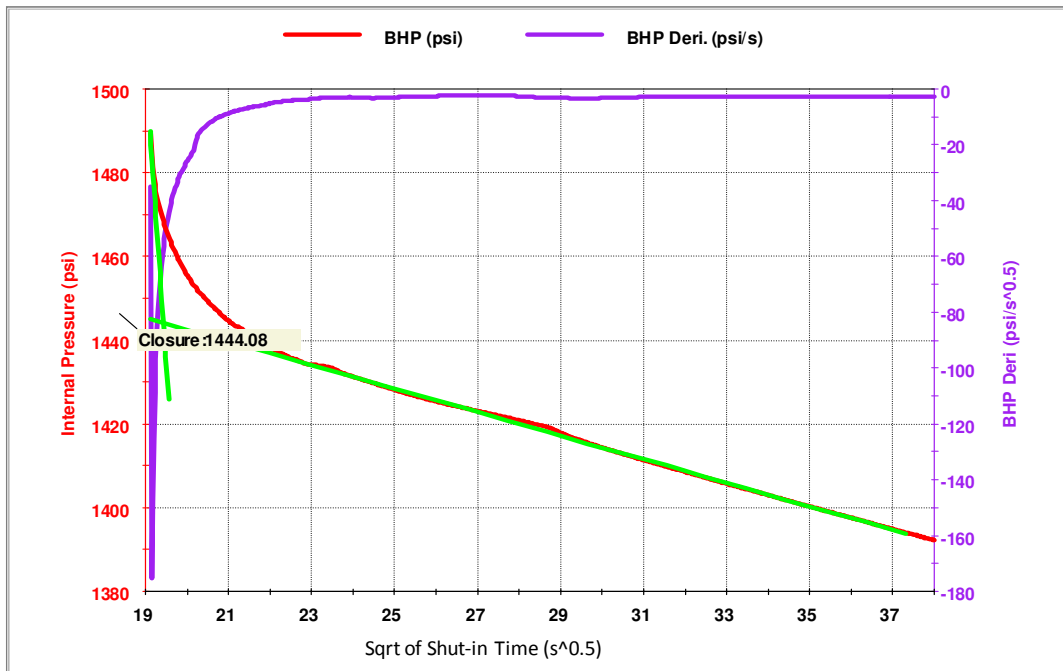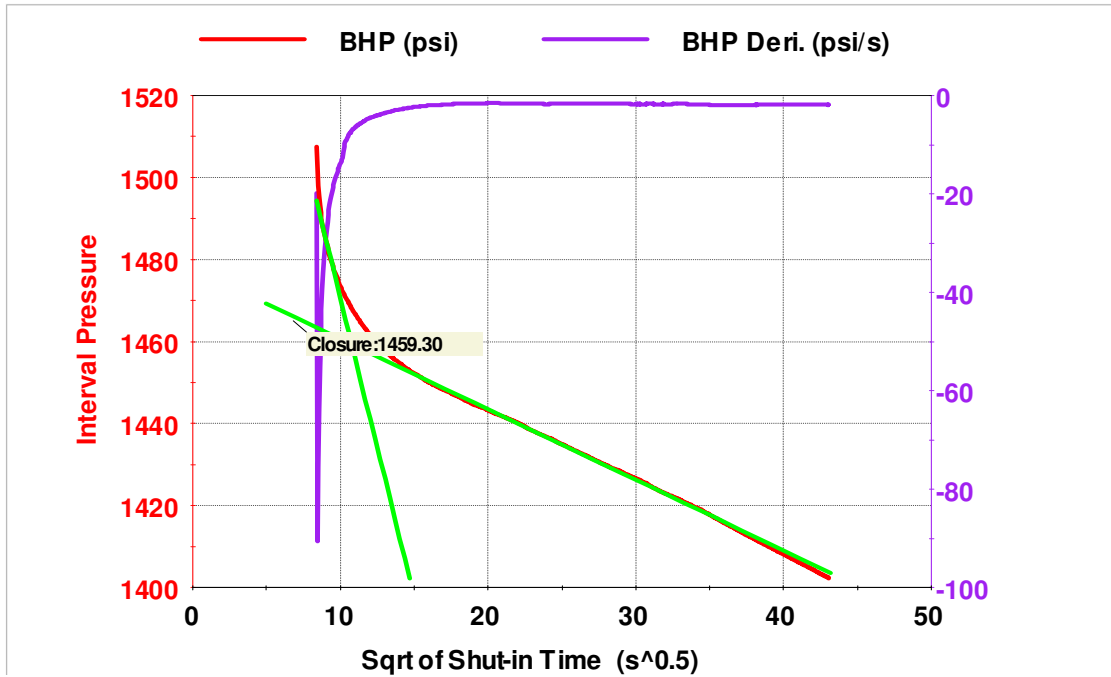

Figure 5.12: Pressure versus square root of time (red curve) during shut-in phase of Cycle 1. Pressure derivative is also shown (purple curve).
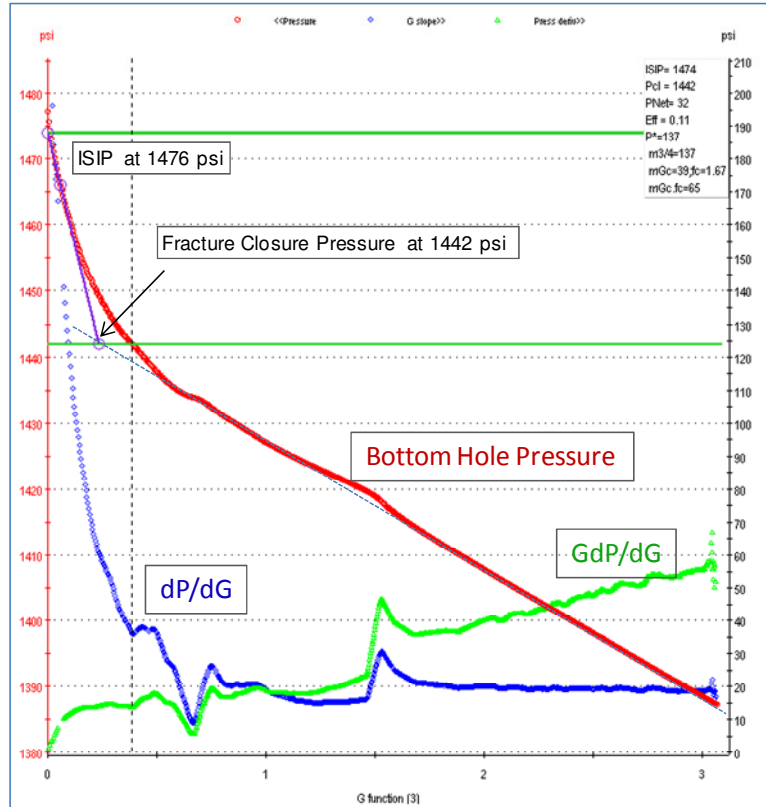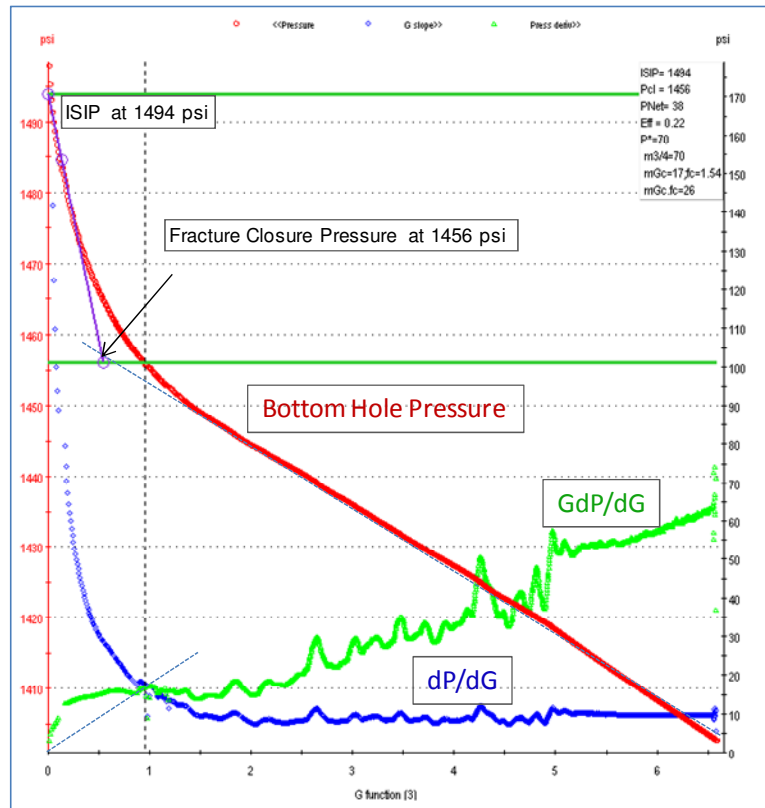
Figure 5.13: Cycle1-G-Function Interpretation.

5.1.5 Cycle 2

The interval was again pressurized and the fracture created in Cycle 1 was propagated for 130 s. Figure 5.14 shows key data from this test. During injection, the pump half-stroked twice as evidenced by sharp drops in the pump hydraulic pressure. During these episodes, the interval pressure to dipped and then recovered as pumping resumed. Figure 5.15 shows a plot of interval pressure versus pumped volume. In spite of the half-stroking of the pump, this curve maintains an almost constant gradient until the fracture reopens at 1511 psi. Figure 5.16 shows the plot of pressure versus square root of time for the shut-in phase. The fracture appears to close at 1459 psi. An alternative construction using the G-function yields a closure pressure of 1456 psi (Figure 5.17). Table 5.3 summarizes the principal results of this cycle.

Table 5.3: Cycle 2 Results

Stiff (psi/cc)	LOP (psi)	LOV (cc)	VL_frac (cc)	Peak_P (psi)	Prop_P (psi)	ISIP (psi)	P_clos (psi)	P_clos_G-function (psi)
0.677	1511.0	180.0	1265.0	1531.3	1518.7	1494	1459.3	1456
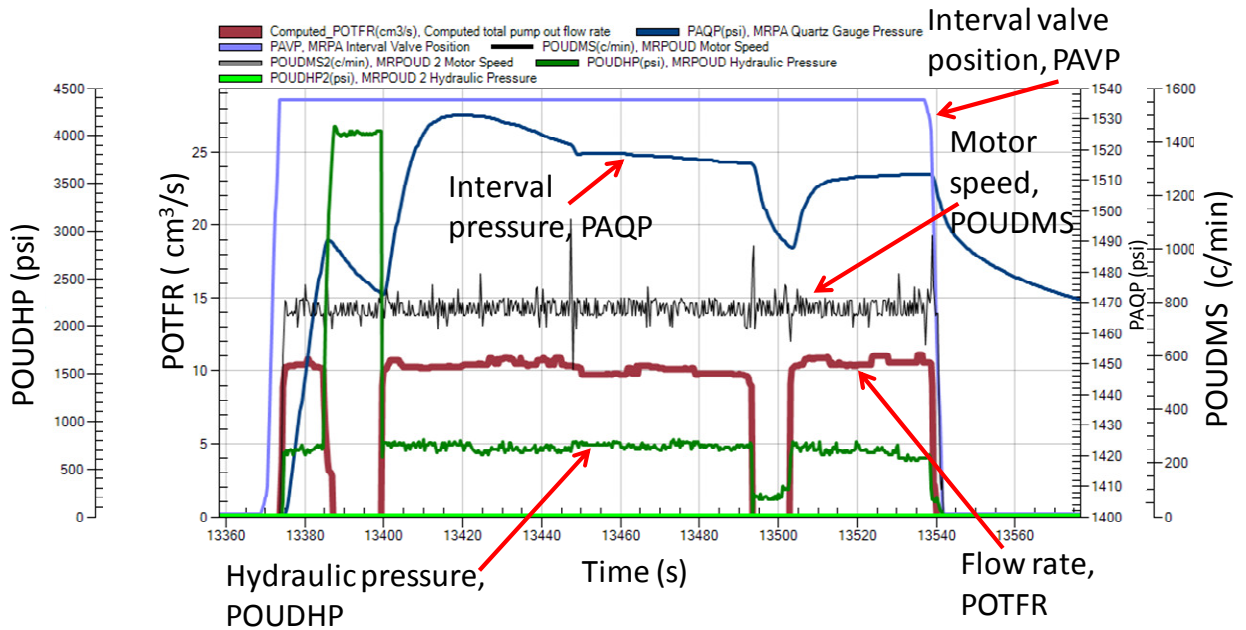
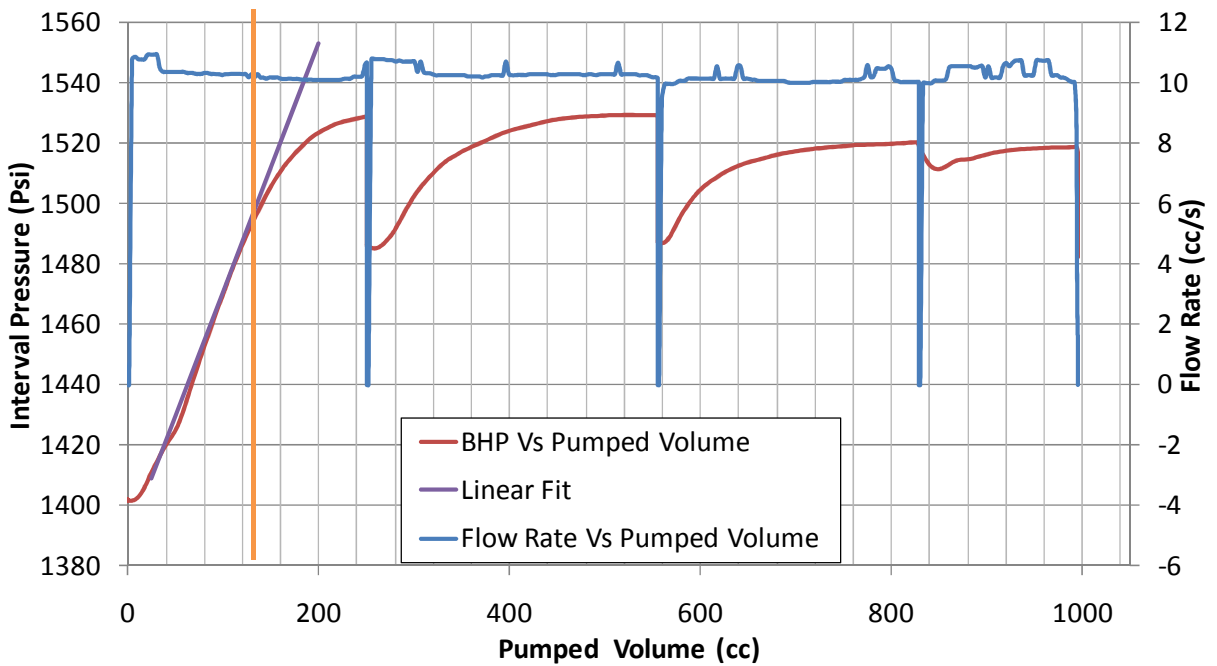**Figure 5.14: Cycle 1. Propagation of the fracture.**
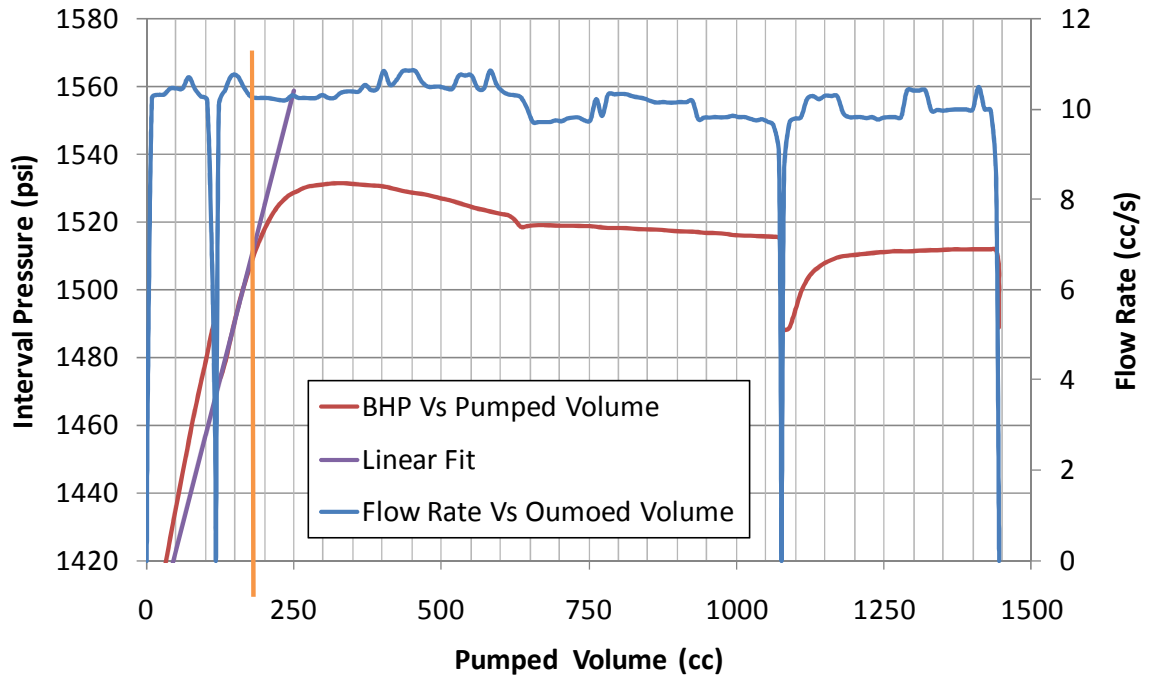
Figure 5.15: Plot of interval pressure vs. pumped volume during Cycle 2 (red curve). A linear fit to this curve shown in purple. The volume at which the curve departs from linearity shown by orange line. The flow rate into the interval (blue curve) is shown referenced to the right hand vertical axis.
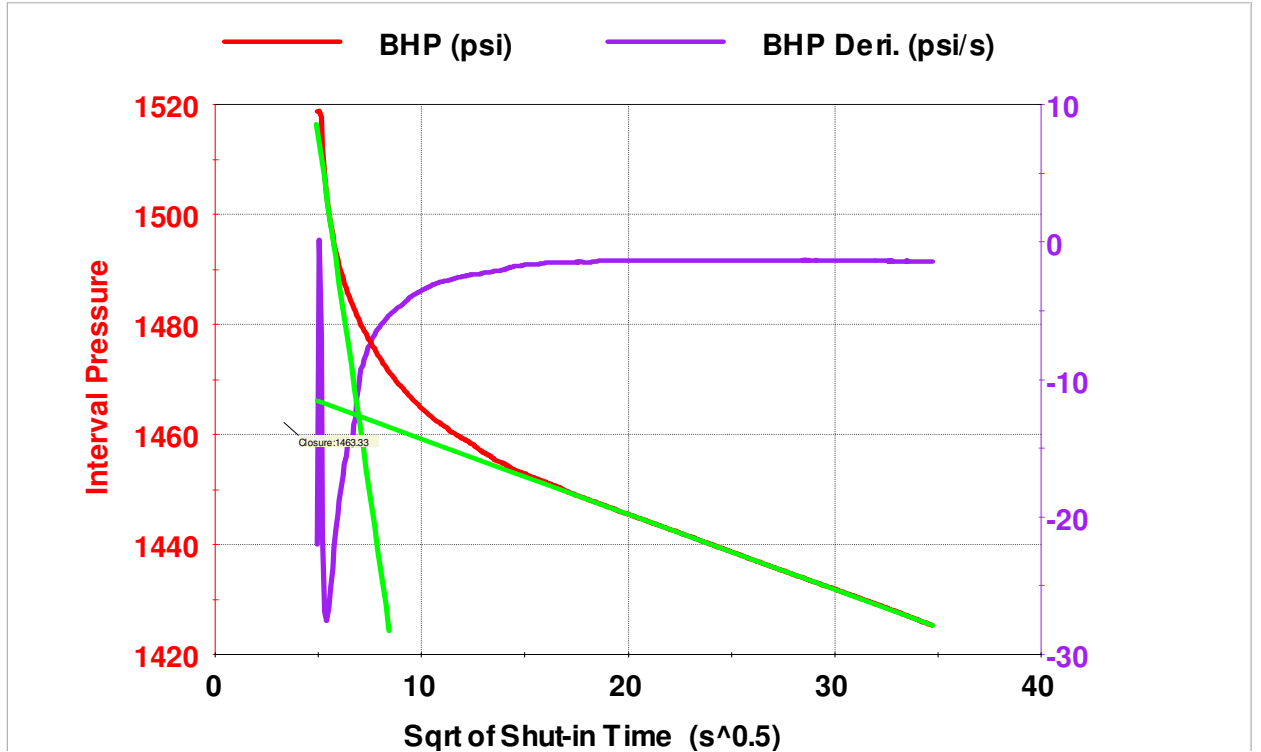
Figure 5.16: Pressure versus square root of time (red curve) during shut-in phase of Cycle 2. Pressure derivative is also shown (purple curve).
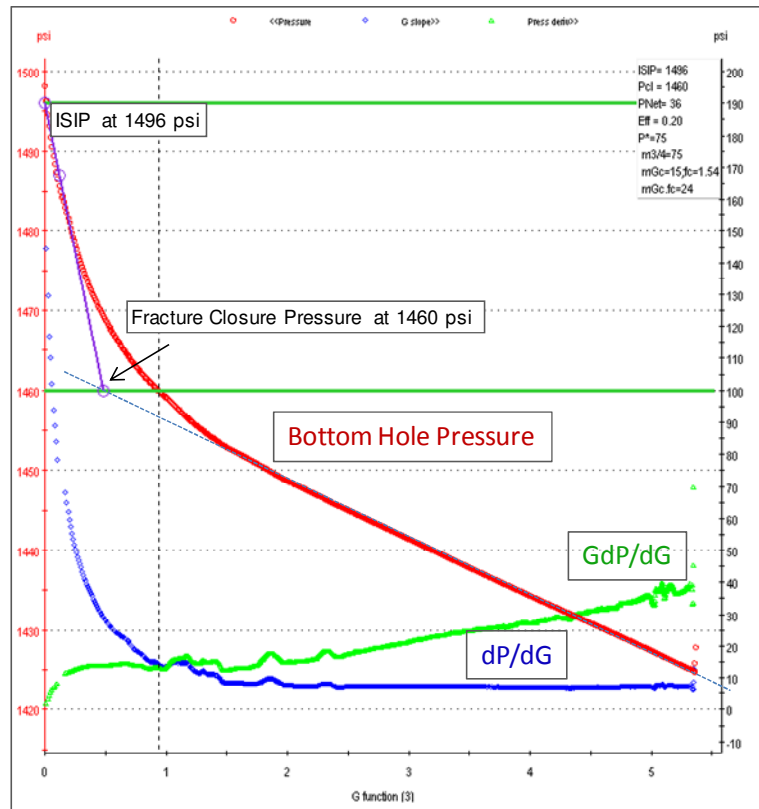

Figure 5.17: Cycle 2-G-Function Interpretation.

5.1.6 Cycle 3

Figures 5.18 and 5.19 show the raw data from the injection phase of Cycle 3. Injection occurred over a period of approximately 150 s. The pump half-stroked several times (Figure 5.18) causing the interval pressure to dip (Figure 5.19). Figure 5.20 shows the plot of interval pressure versus pumped volume. The fracture reopened at 1495 psi. Figure 5.21 shows pressure vs. square root of time. The fracture appeared to close at 1463 psi. An alternative construction using the G-function yielded a closure pressure of 1460 psi (Figure 5.22). Table 5.4 summarizes the results for this cycle.

Table 5.4: Cycle 3 Results.

| Stiff (psi/cc)	LOP (psi)	LOV (cc)	VL_frac (cc)	Peak_P (psi)	Prop_P (psi)	ISIP (psi)	P_clos (psi)	P_clos_G-function (psi)
0.8224	1495	130	866	1528.7	1519.7	1496	1463.3	1460
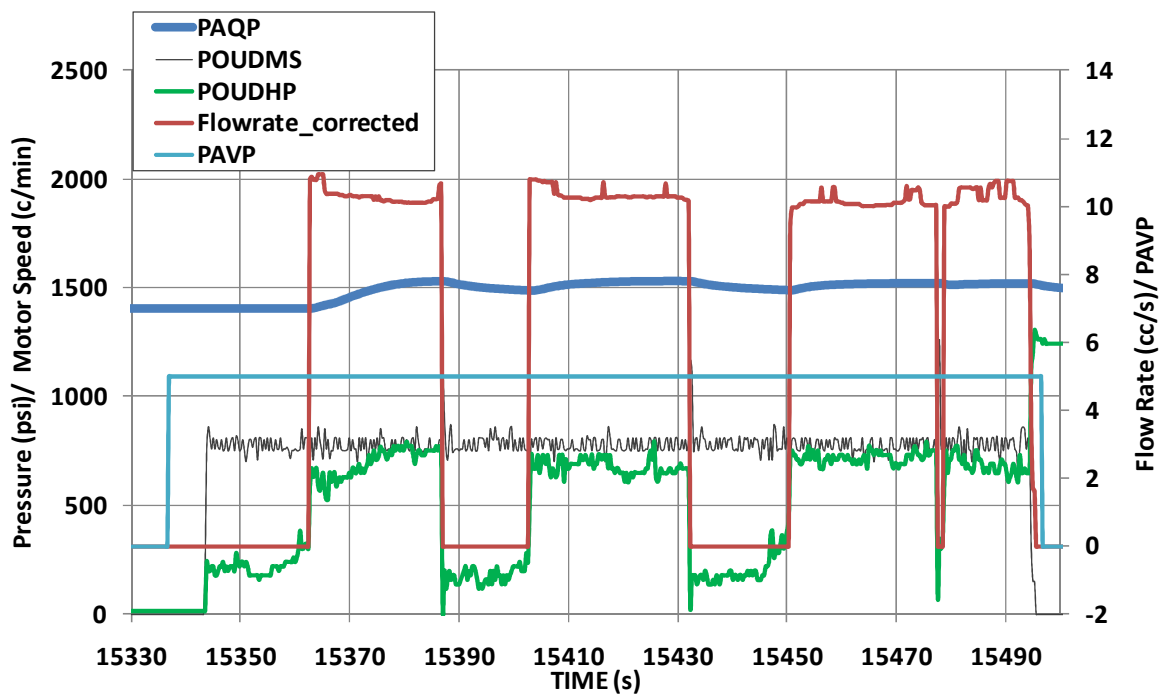
Figure 5.18: Cycle 3. Propagation of the fracture. Interval pressure (PAQP), pump motor speed (POUDMS), pump hydraulic pressure (POUDHP), flow rate (Flowrate_corrected), and interval valve position (PAVP) are shown.
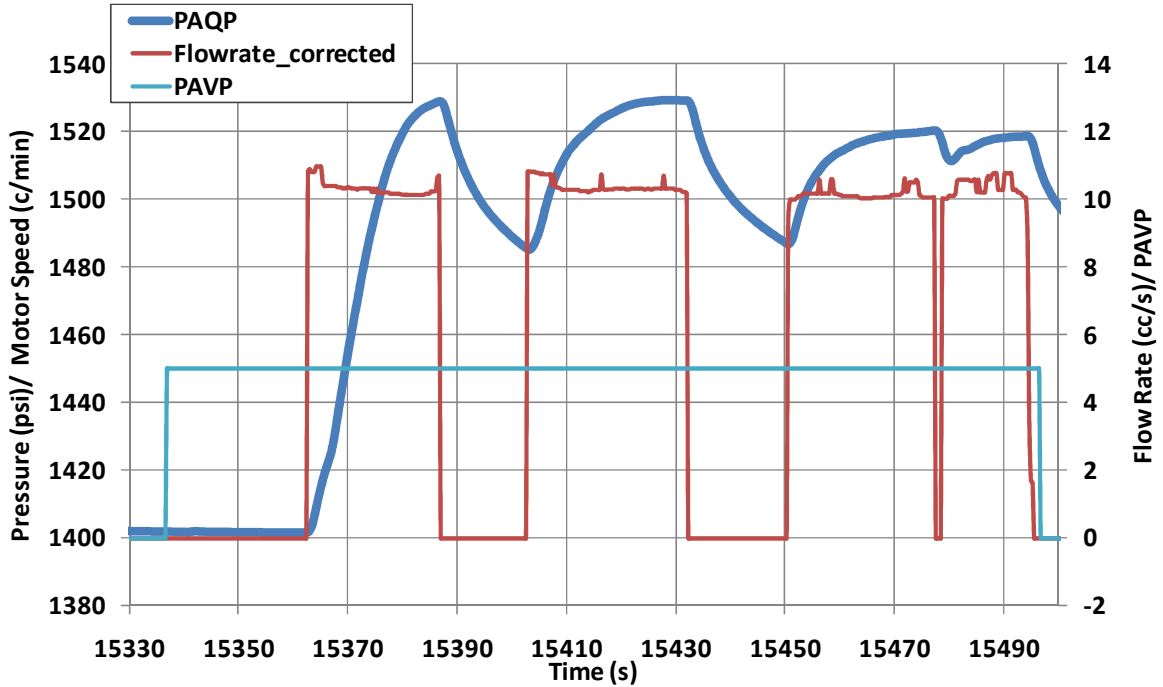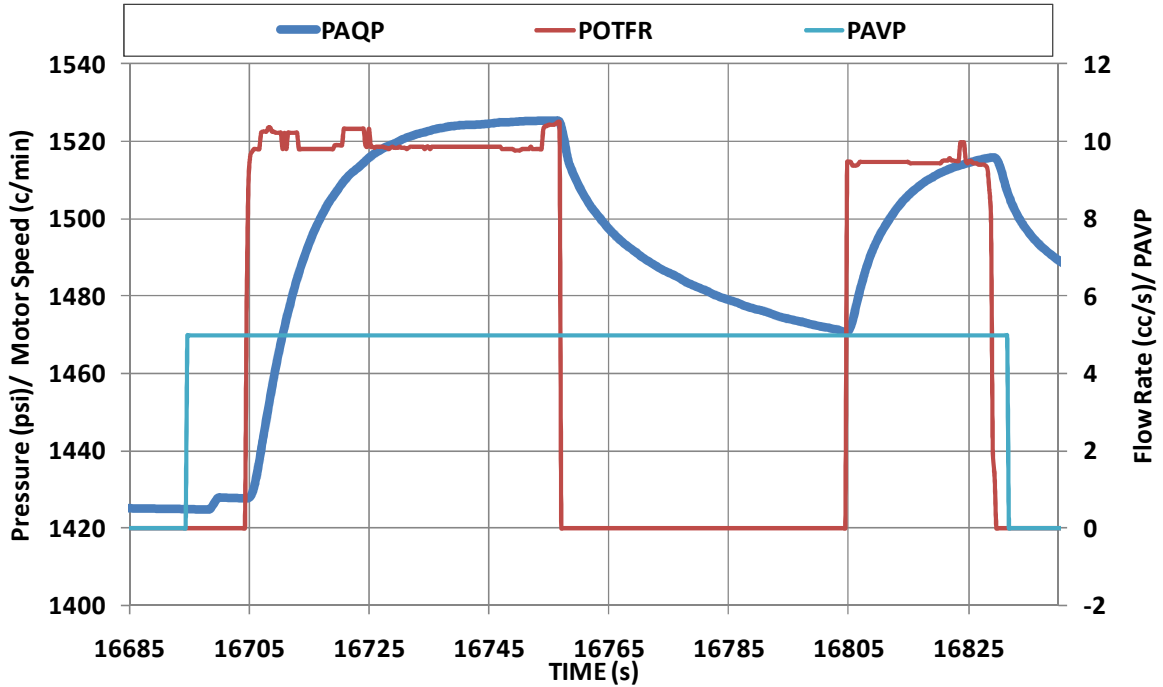
Figure 5.19: Interval pressure (PAQP), flow rate (Flowrate_corrected), and interval valve position (PAVP) during injection phase of Cycle 3.
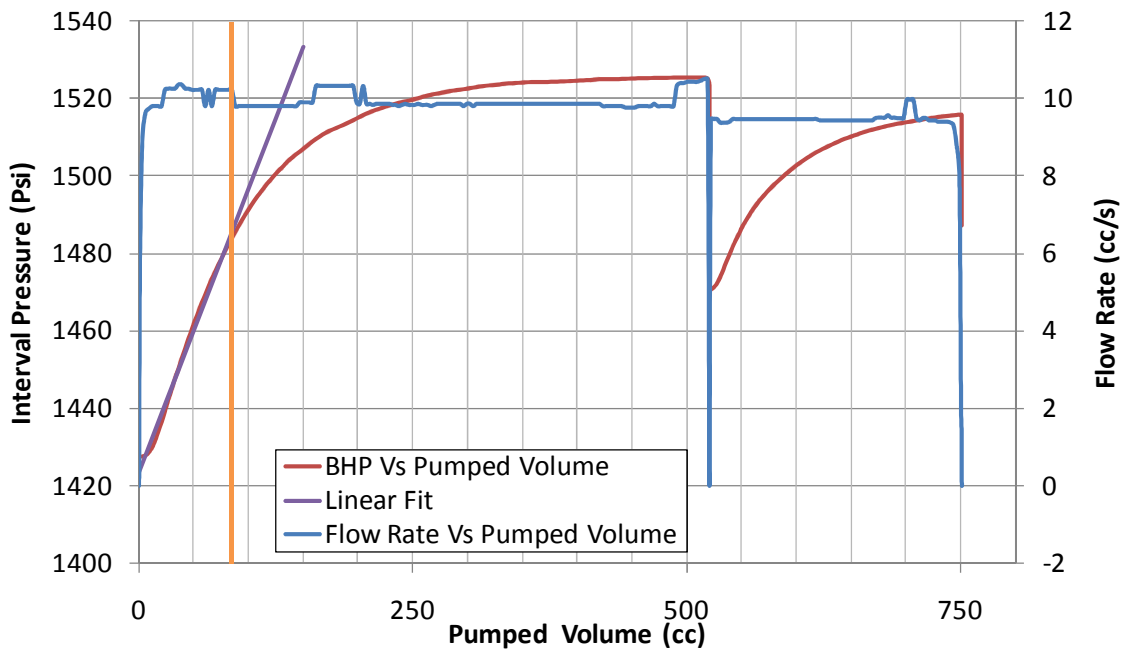

Figure 5.20: Plot of interval pressure vs. pumped volume during Cycle 3 (red curve). A linear fit to this curve shown in purple. The volume at which the curve departs from linearity shown by orange line. The flow rate into the interval (blue curve) is shown referenced to the right hand vertical axis.
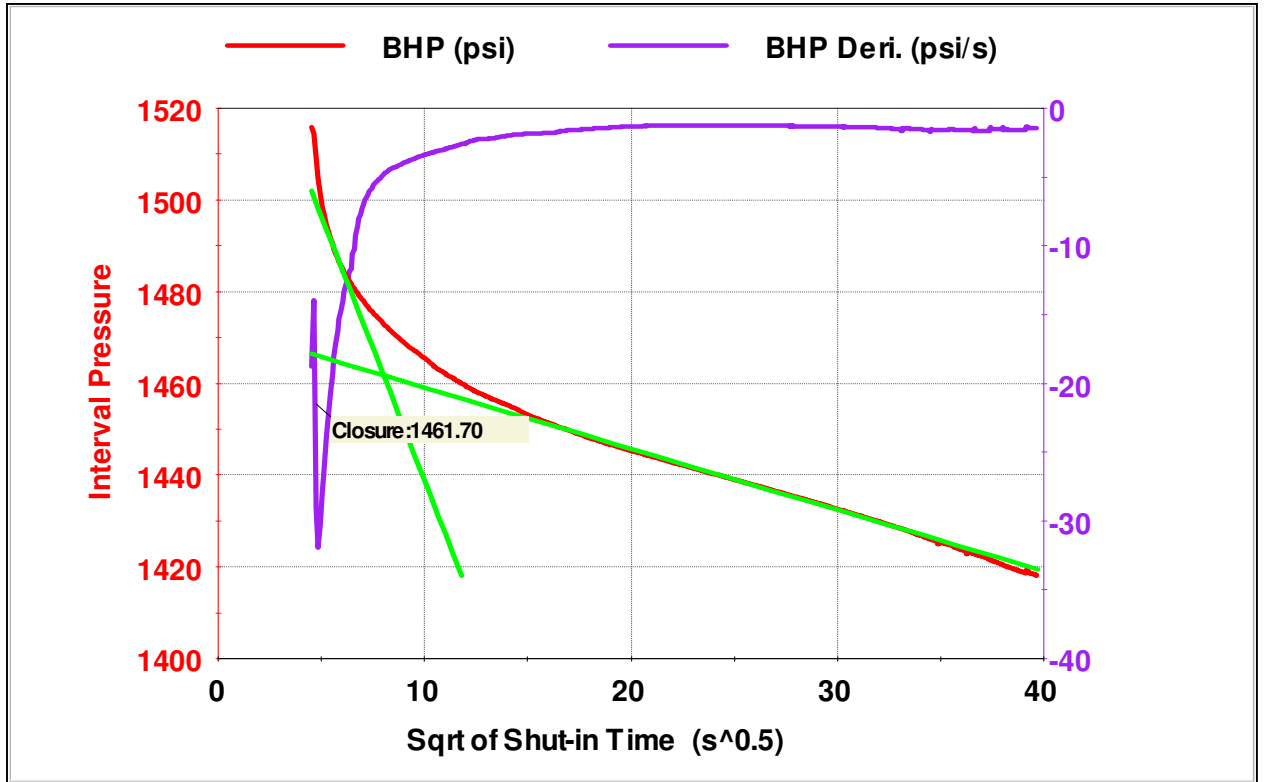
Figure 5.21: Pressure versus square root of time (red curve) during shut-in phase of Cycle 3. Pressure derivative is also shown (purple curve).
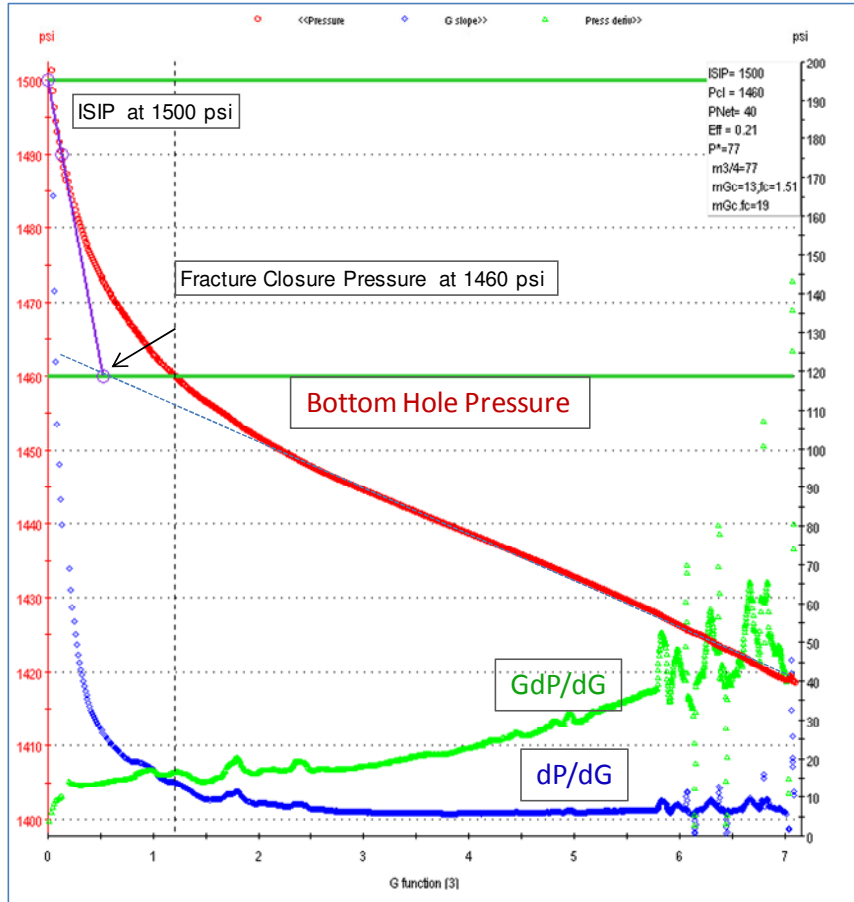

Figure 5.22: Cycle 3-G-Function Interpretation.

5.1.7 Cycle 4

Figures 5.23 and 5.24 show the raw data from Cycle 4. Injection occurred over a period of approximately 125 s and the pump half-stroked in the middle of this phase (Figure 5.23) causing the interval pressure to dip (Figure 5.24). Figure 5.25 shows the plot of interval pressure versus pumped volume. The fracture reopened at 1484 psi. Figure 5.26 shows pressure vs. square root of time. The fracture closed at 1462 psi. An alternative construction using the G-function yields a closure pressure of 1460 psi (Figure 5.27). Table 5.5 summarizes the results for this cycle.

Table 5.5: Cycle 4 Results

Stiff (psi/cc)	LOP (psi)	LOV (cc)	VL_frac (cc)	Peak_P (psi)	Prop_P (psi)	ISIP (psi)	P_clos (psi)	P_clos_G-function (psi)
0.7319	1484.1	84	666	1525.4	1525.2	1500	1461.7	1460
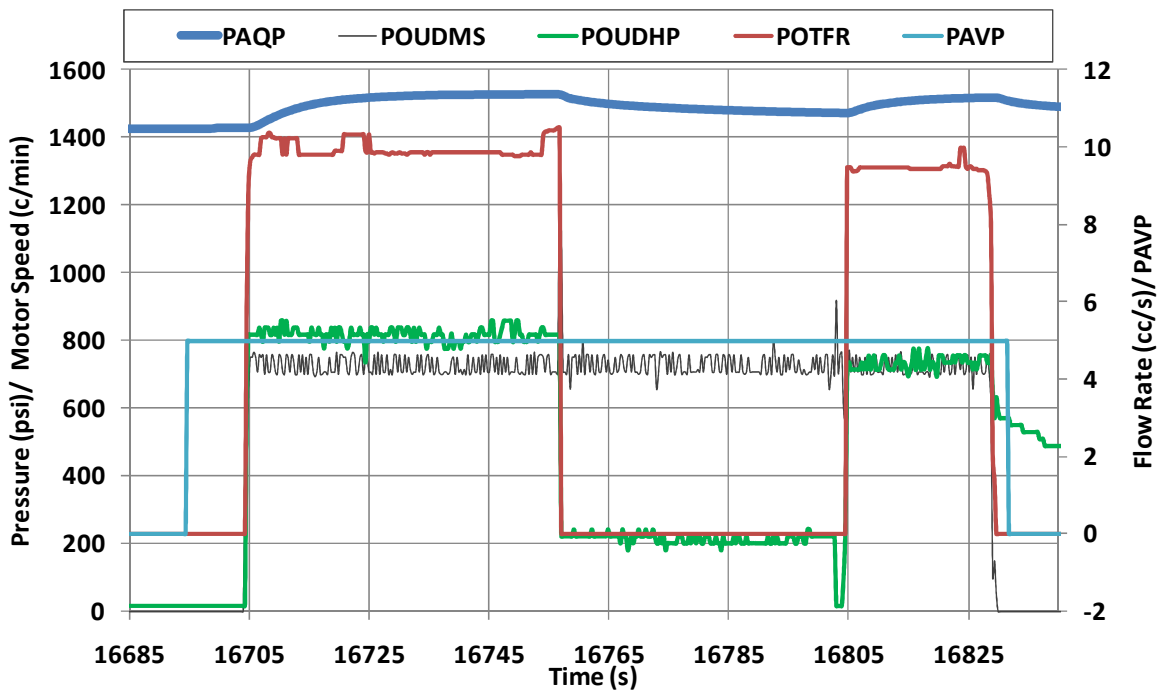
Figure 5.23: Cycle 4. Propagation of the fracture. Interval pressure (PAQP), pump motor speed (POUDMS), pump hydraulic pressure (POUDHP), flow rate (POTFR), and interval valve position (PAVP) are shown.

Figure 5.24: Interval pressure (PAQP), flow rate (POTFR), and interval valve position (PAVP) during injection phase of Cycle 4.

Figure 5.25: Plot of interval pressure vs. pumped volume during Cycle 4 (red curve). A linear fit to this curve shown in purple. The volume at which the curve departs from linearity shown by orange line. The flow rate into the interval (blue curve) is shown referenced to the right hand vertical axis.
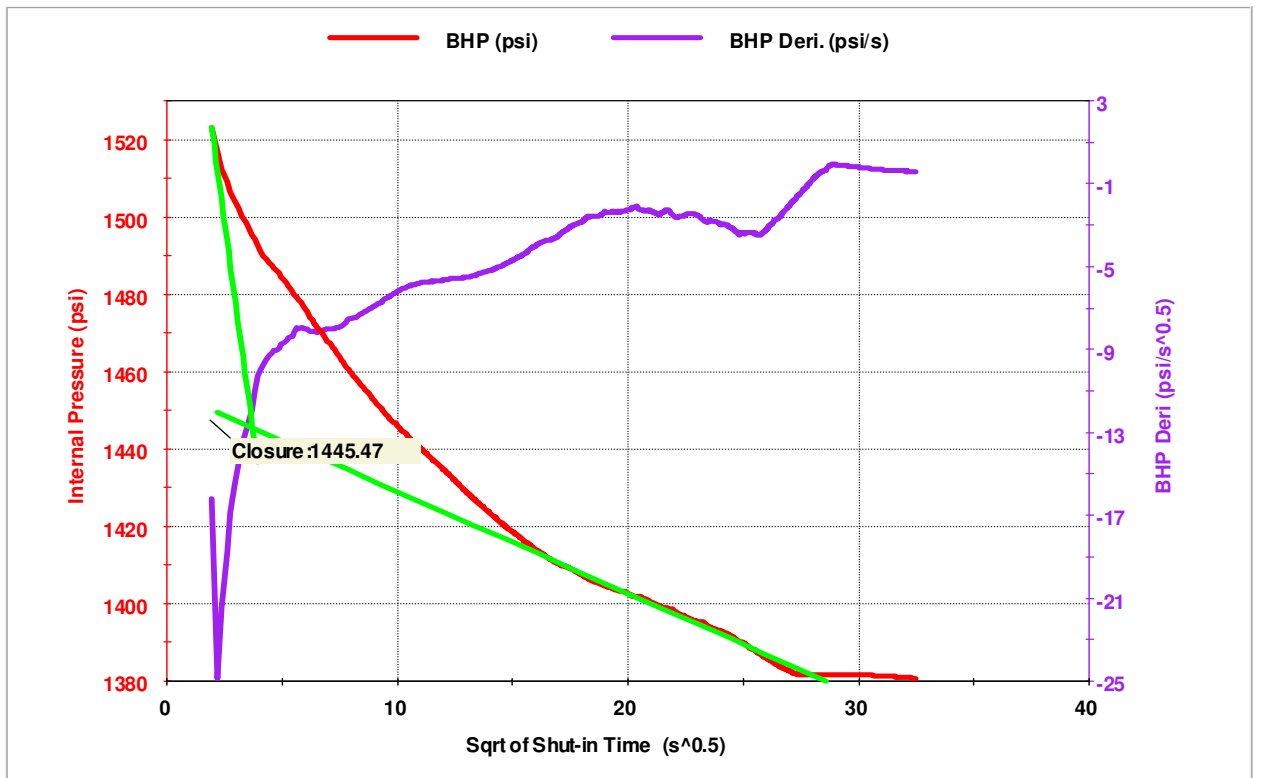
Figure 5.26: Pressure versus square root of time (red curve) during shut-in phase of Cycle 4. Pressure derivative is also shown (purple curve).
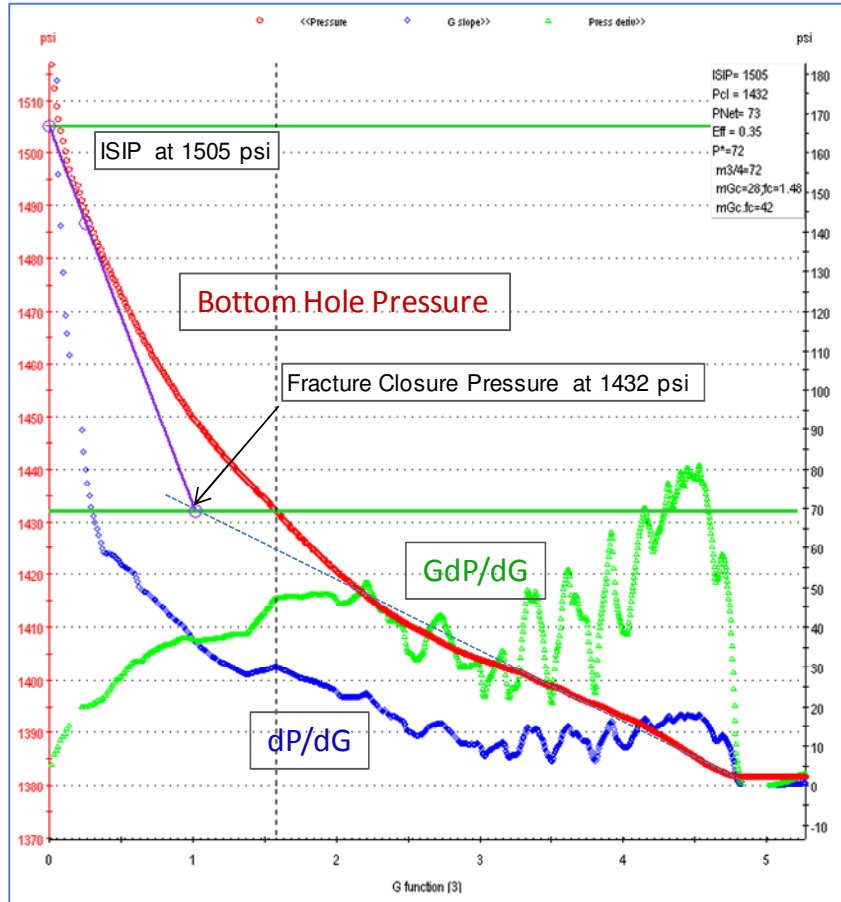
Figure 5.27: Cycle 4-G-Function Interpretation.

5.1.8 Cycle 5

Figure 5.28 shows the raw data from Cycle 5. Injection occurred over a period of approximately 120 s. The pump half-stroked briefly at 18450 s causing the interval pressure to dip slightly (Figure 5.28). Figure 5.29 shows a plot of interval pressure versus pumped volume. The fracture reopened at 1494 psi. Figure 5.30 shows pressure vs. square root of time. A peculiar feature appears at the end of this curve – the interval pressure suddenly stabilized at about 1380 psi.   Yet no such stabilization occurred during the filtration test carried out at much lower interval pressures (Figure 5.7). This suggests that a filtercake built up at the wellbore wall between the filtration test and the end of Cycle 5.

According to Figure 5.30, the fracture closed at 1446 psi. This value is significantly less than the closure pressure of 1462 psi recorded during the previous cycle. An alternative construction using the G-function yields an even lower closure pressure of 1432 psi (Figure 5.31). The fracture appears to be growing into a region with a lower stress. Table 5.6 summarizes the results of the current cycle.

Table 5.6: Cycle 5 Results

| Stiff (psi/cc)	LOP (psi)	LOV (cc)	VL_frac (cc)	Peak_P (psi)	Prop_P (psi)	ISIP (psi)	P_clos (psi)	P_clos_G-function (psi)
0.8511	1494	92	1063	1534.5	1532.7	1505	1445.5	1432
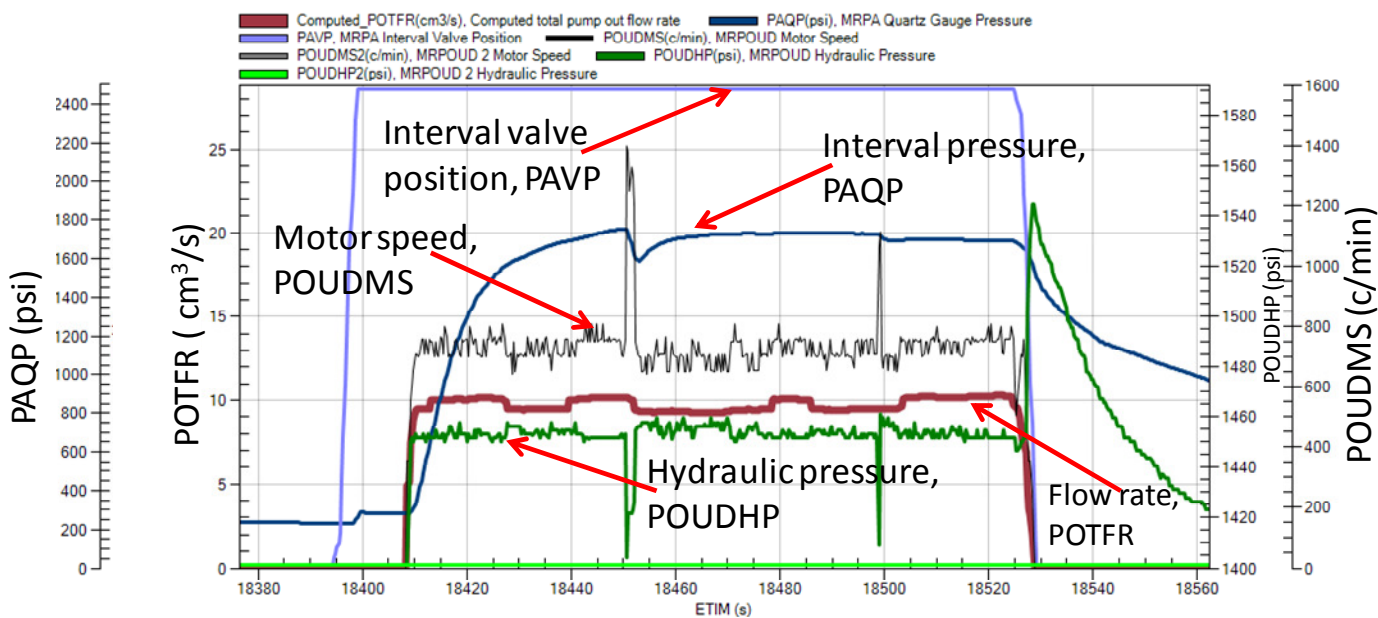
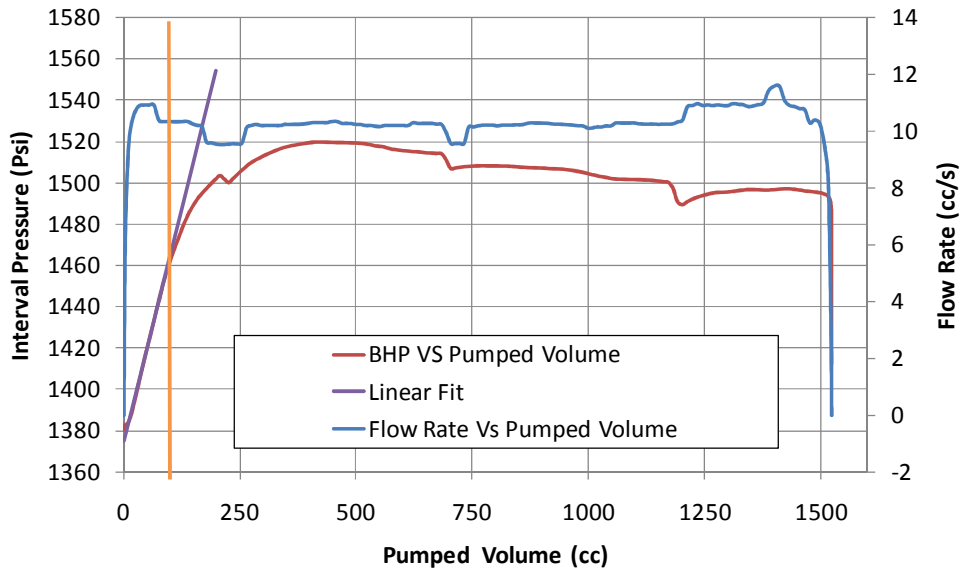**Figure 5.28: Cycle 5. Propagation of the fracture.**
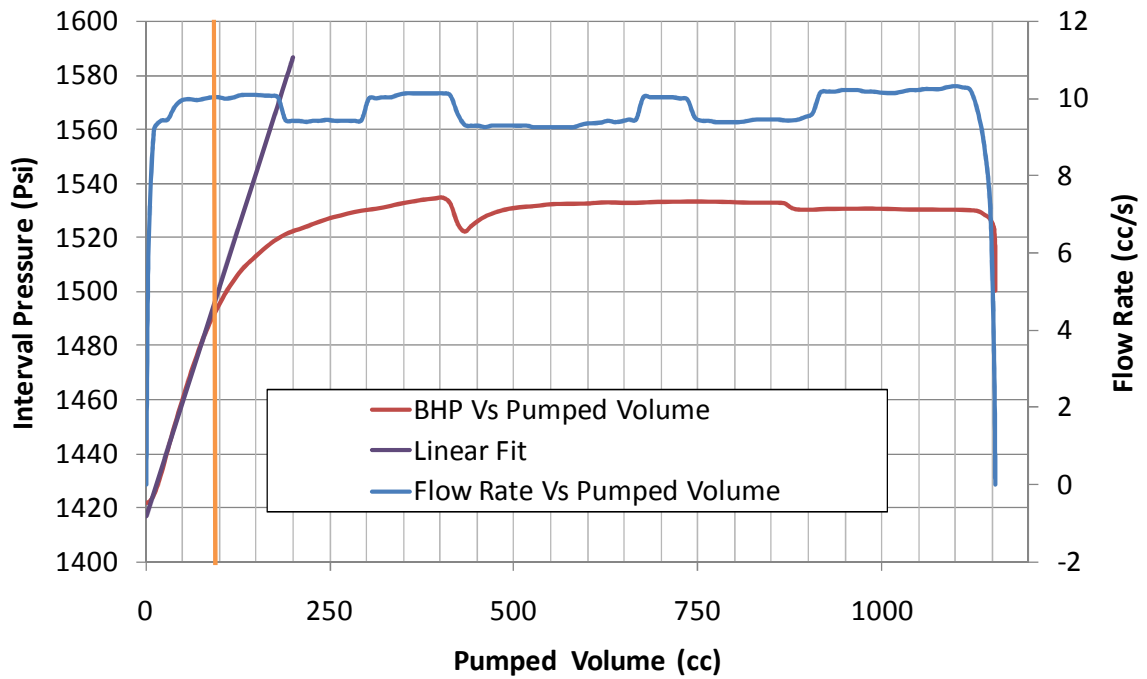
Figure 5.29: Plot of interval pressure vs. pumped volume during Cycle 5 (red curve). A linear fit to this curve shown in purple. The volume at which the curve departs from linearity shown by orange line. The flow rate into the interval (blue curve) is shown referenced to the right hand vertical axis.
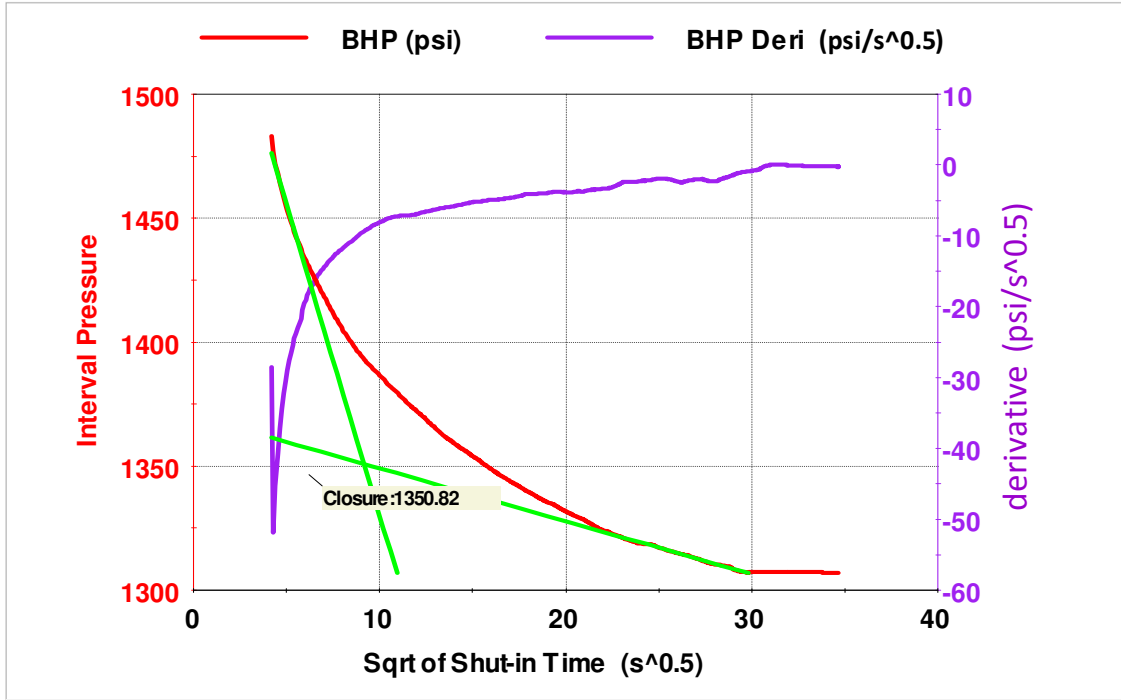

Figure 5.30: Pressure versus square root of time (red curve) during shut-in phase of Cycle 5. Pressure derivative is also shown (purple curve).
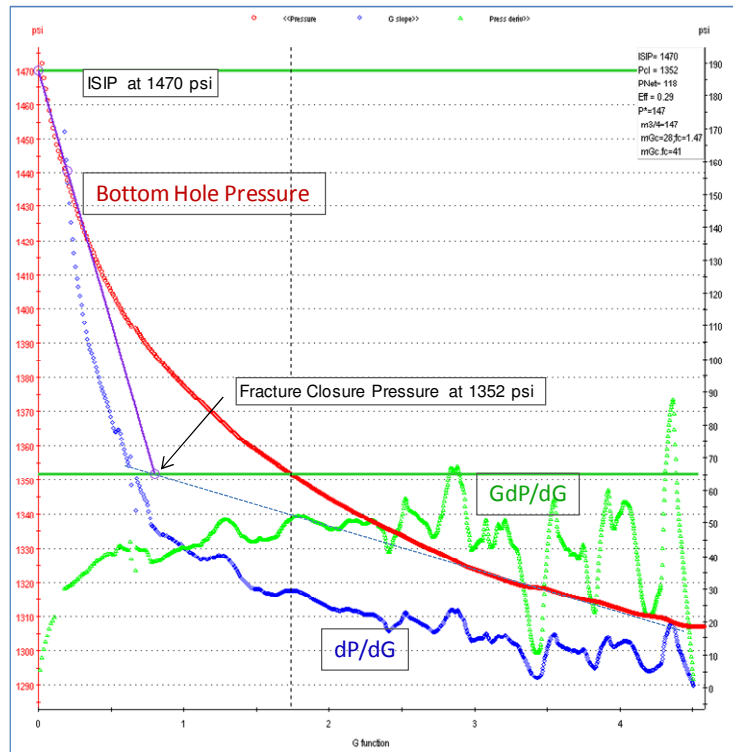
Schlumberger

Figure 5.31: Cycle 5-G-Function Interpretation.

5.1.9 Cycle 6

Figure 5.32 shows the raw data from Cycle 6. Injection occurred over a period of approximately 150 s. Some minor half-stroking occurred three times causing the interval pressure to dip temporarily (Figure 5.32). Figure 5.33 shows the plot of interval pressure versus pumped volume. The fracture reopened at 1460 psi. Figure 5.34 shows a plot of pressure vs. square root of time. Similar to the previous cycle, the interval pressure suddenly stabilized at about 1310 psi. The fracture closed at 1351 psi. This closure pressure is significantly less than the corresponding value of 1446 psi recorded during the previous cycle. An alternative construction using the G-function yields a comparable closure pressure of 1352 psi (Figure 5.35). Table 5.7 summarizes the results of the current cycle.

Table 5.7: Cycle 6 Results

| Stiff (psi/cc)	LOP (psi)	LOV (cc)	VL_frac (cc)	Peak_P (psi)	Prop_P (psi)	ISIP (psi)	P_clos (psi)	P_clos_G-function (psi)
0.8965	1459.8	95.92	1426.6	1520.0	1508.4	1470	1350.8	1352
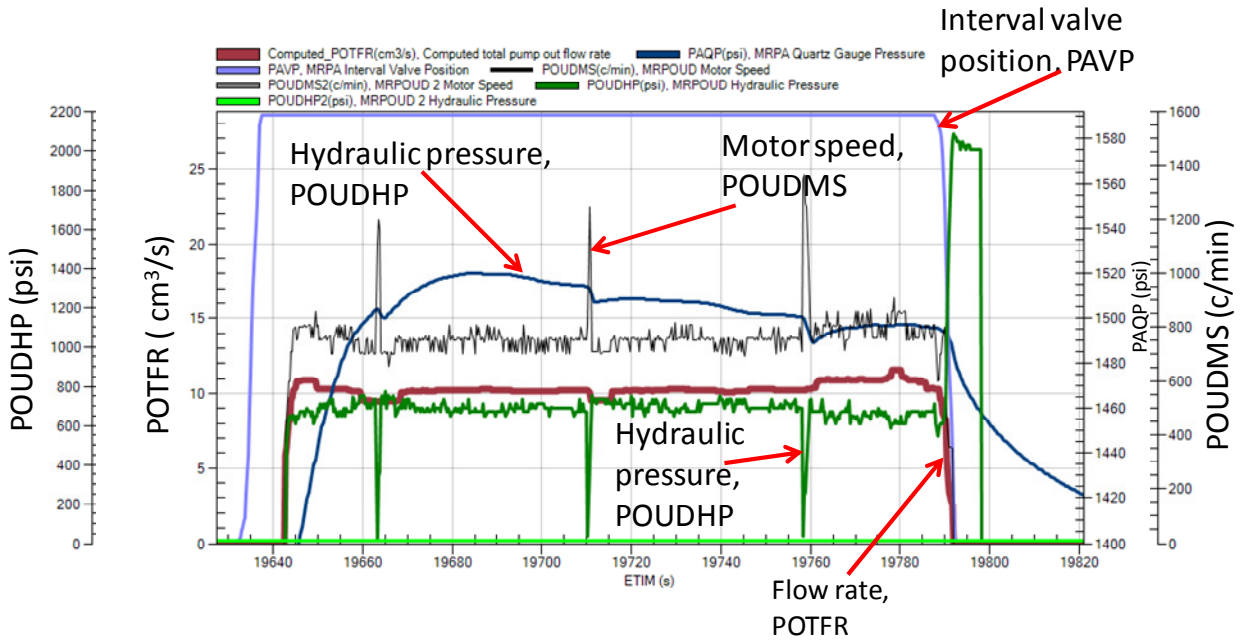
Figure 5.32: Cycle 6. Propagation of the fracture.

Figure 5.33: Plot of interval pressure vs. pumped volume during Cycle 6 (red curve). A linear fit to this curve shown in purple. The volume at which the curve departs from linearity shown by orange line. The flow rate into the interval (blue curve) is shown referenced to the right hand vertical axis.

Figure 5.34: Pressure versus square root of time (red curve) during shut-in phase of Cycle 6. Pressure derivative is also shown (purple curve).

Figure 5.35: Cycle 6. G-Function Interpretation.

5.1.10 Cycle 7

Figure 5.36 shows the raw data from Cycle 7. Injection occurred over a period of approximately 160 s. The pump half-stroked briefly four times causing the interval pressure to dip momentarily (Figure 5.36). Figure 5.37 shows a plot of interval pressure versus pumped volume. The fracture reopened at 1485 psi. Figure 5.38 shows pressure vs. square root of time. The fracture closed at 1382 psi. An alternative construction using the G-function yields a closure pressure of 1372 psi (Figure 5.39: Cycle 7-G-Function Interpretation. Unlike the previous cycles, the pressure in the interval did not stabilize during shut-in. Table 5.8 summarizes the results for this cycle.

Table 5.8: Cycle 7 Results

Stiff (psi/cc)	LOP (psi)	LOV (cc)	VL_frac (cc)	Peak_P (psi)	Prop_P (psi)	ISIP (psi)	P_clos (psi)	P_clos_G-function (psi)
0.7178	1485	243	1446	1510.6	1510.3	1459	1382.1	1372
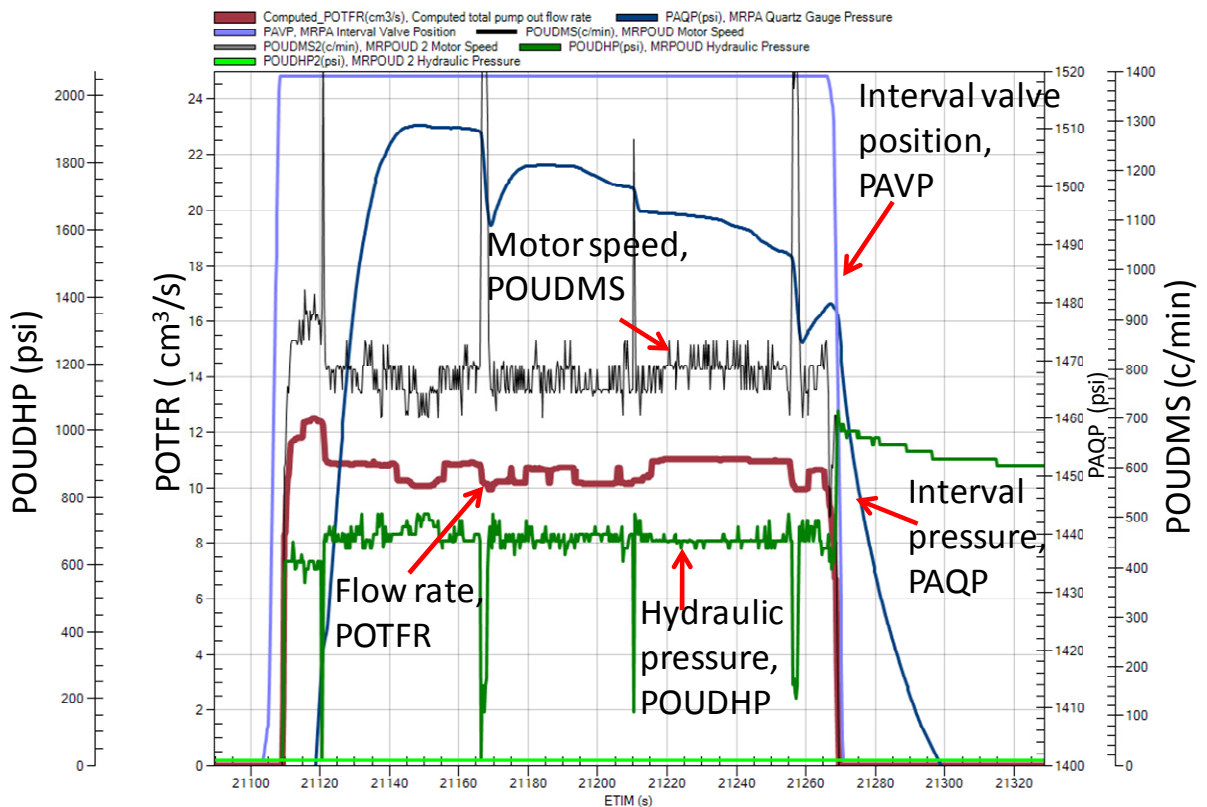
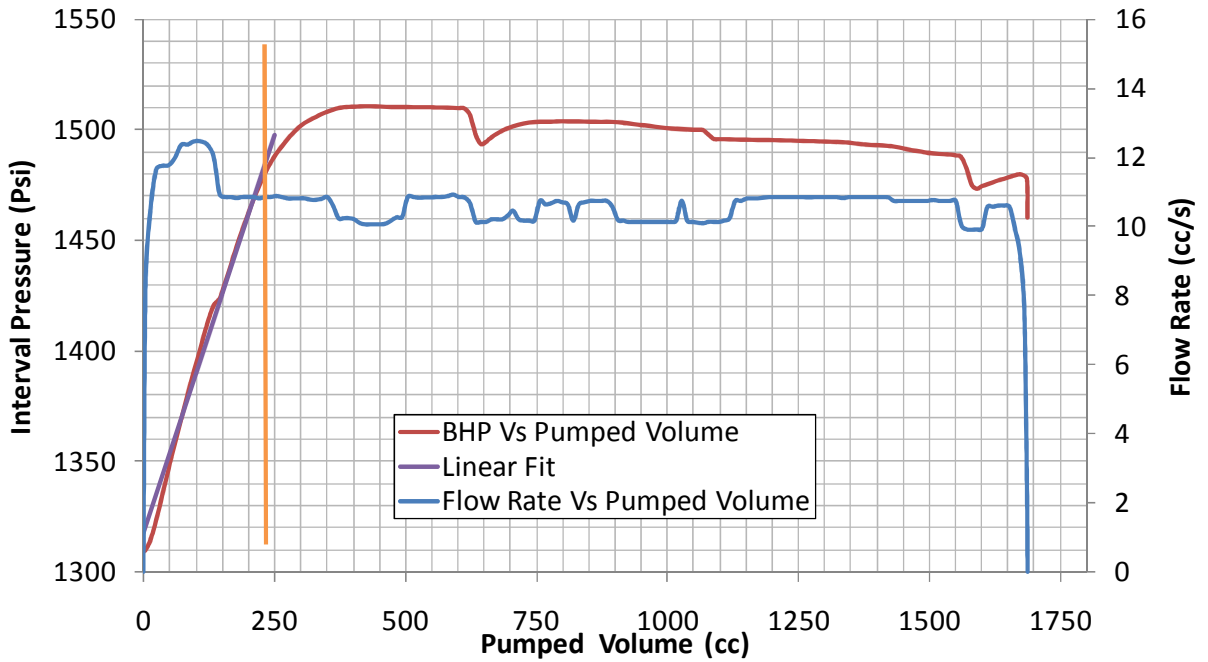**Figure 5.36: Cycle 7. Propagation of the fracture.**

Figure 5.37: Plot of interval pressure vs. pumped volume during Cycle 7 (red curve). A linear fit to this curve shown in purple. The volume at which the curve departs from linearity shown by orange line. The flow rate into the interval (blue curve) is shown referenced to the right hand vertical axis.
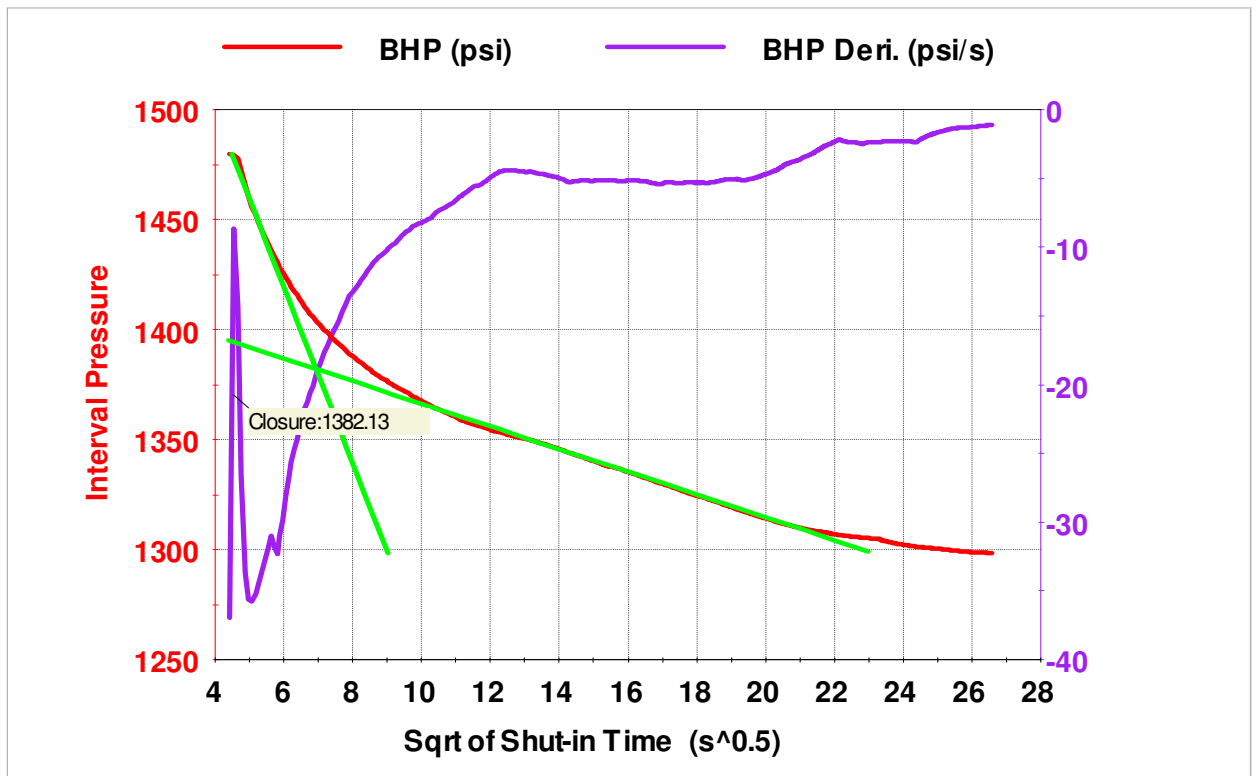

Figure 5.38: Pressure versus square root of time (red curve) during shut-in phase of Cycle 7. Pressure derivative is also shown (purple curve).

Figure 5.40 shows a reconciliation plot summarizing key diagnostic information from all 8 cycles. The closure pressures ascertained using square root of time plots (magenta triangles) and G-plots (brown triangles) are generally bounded above by the peak pressures (green triangles), leak-off pressures (orange triangles), ISIP's (black triangles), and propagation pressures (blue triangles). The system stiffness (yellow triangles) varied between 0.421 psi/cc and 0.896 psi/cc and did not exhibit any particular pattern (Figure 5.40a) .

It is seen that during injection cycles, the amount of fluid injected into the fracture ranged between 666 cc and 2212 cc (red triangles, Figure 5.40a). A total of 8.94 liters was pumped into the fracture in order to propagate it away from the near-wellbore stress concentration. However for the first four cycles the leak-off, peak, propagation, instantaneous shut-in, and closure pressures appear to be fairly constant (Figure 5.40b). This suggests that the fracture was growing away from the wellbore very slowly. This slow growth may be due to high rates of leak-off through the wellbore wall and the fracture faces. However as was discussed in relation to Cycle 5 (Section 5.1.8), during later cycles leak-off was reduced by the action of filtercake. This allowed more of the injected fluid volume to be utilized in growing the fracture. Between Cycles 4 and 6 the fracture appeared to move quickly away from the wellbore and the closure pressure decreased rapidly. By Cycle 6 the fracture appears to be sensing the far-field condition. Figure 5.40(b) shows a horizontal line corresponding to 1364 psi, the average of the closure pressures determined in Cycles 6 and 7. This is the best estimate of the closure stress in the far-field.
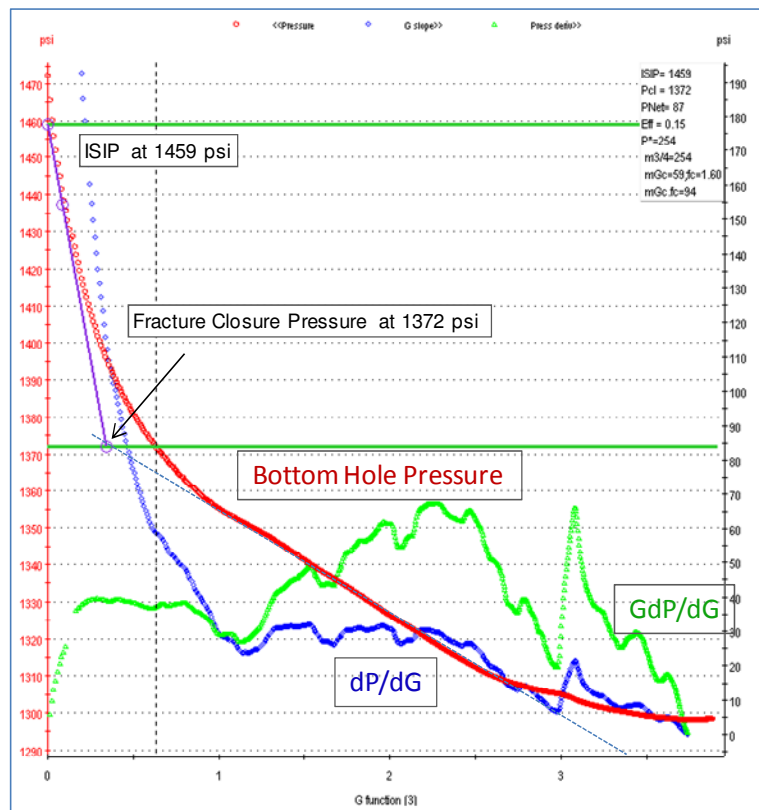

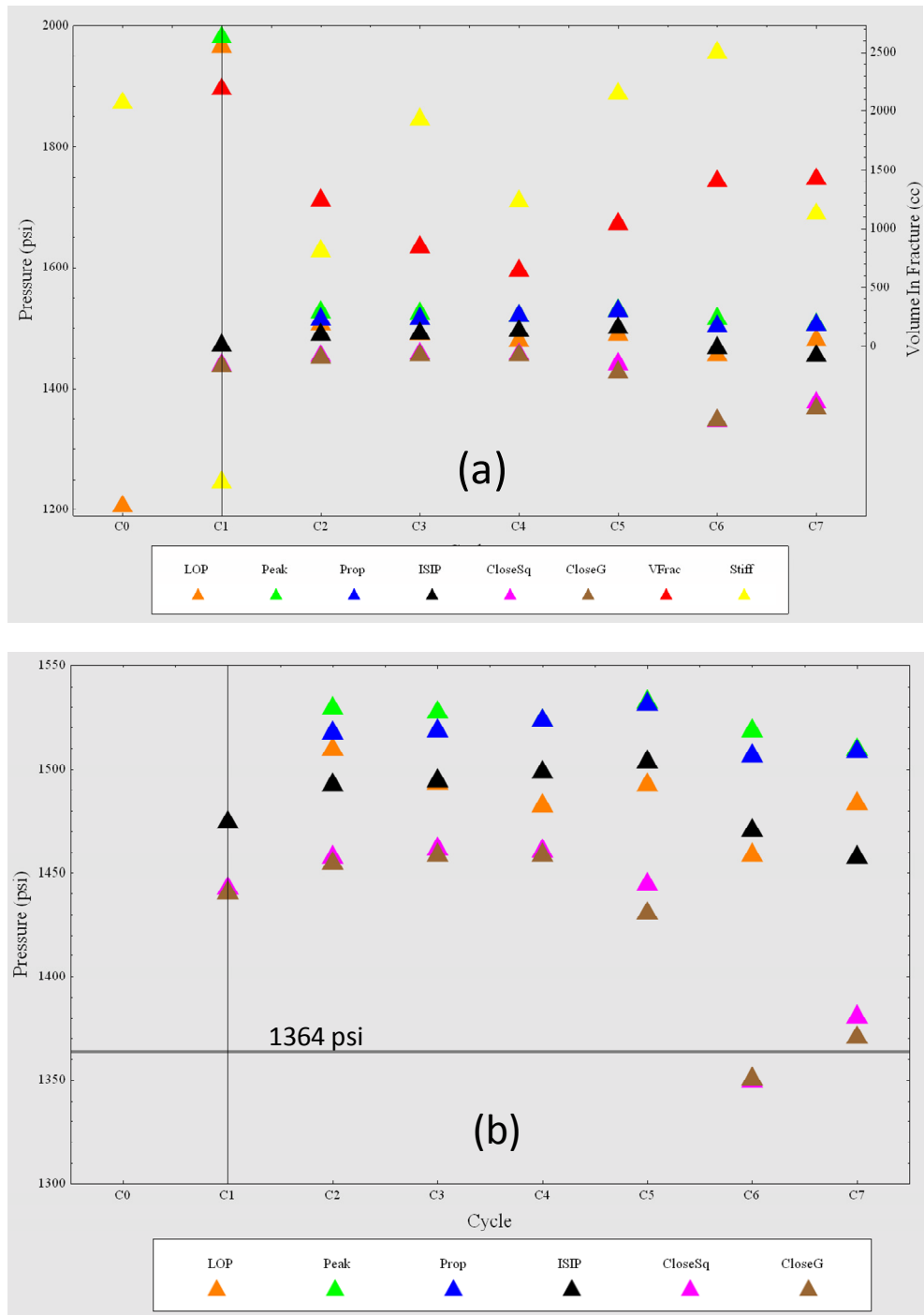**Figure 5.39: Cycle 7-G-Function Interpretation**

Figure 5.40: Reconciliation plot for Test Station 1. (a) All parameters. (b) Pressures only.

5.2 Test Results at 2,202.58 ft

5.2.1 Overview

This test was carried out in a silty formation. No gas hydrate was present. Figure 5.41 shows the location of the test interval. The borehole is in-gauge at the test location, but slighty undergauged at several locations above and below the test site. This may be due to mudcake build-up or creep. The resistivity curves at the test location exhibit negligible separation indicating little or no mud invasion. The dynamic Young's modulus is 4 GPa, which is typical of unconsolidated sediments.
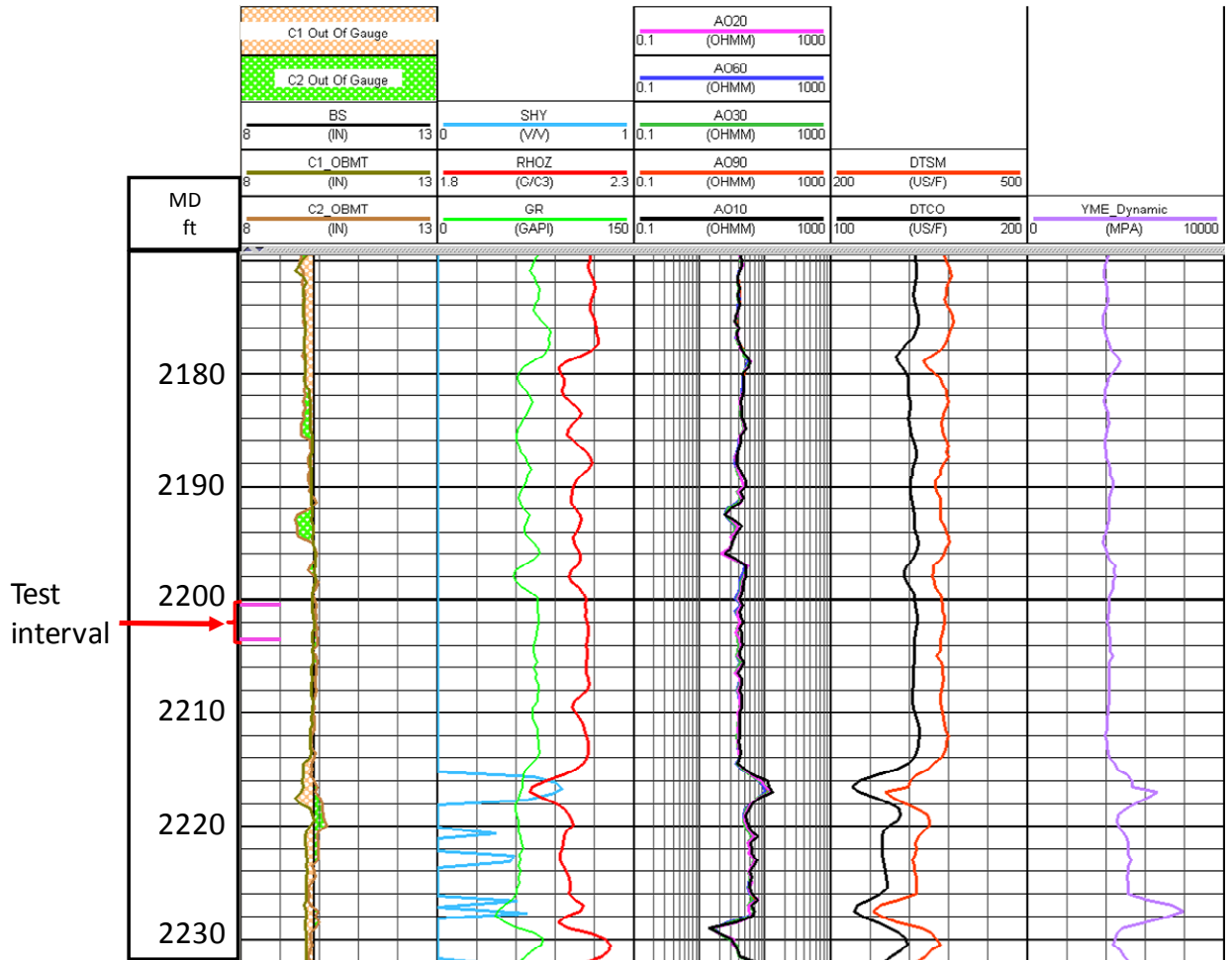
Figure 5.41: Logs in vicinity of Test Station 2.

The test interval was located between 2200.5 and 2203.8 ft. TRACK 1: Measured Depth with respect to KB. TRACK 2: Dual caliper measurements C1_OBMT, C2_OBMT and bit size, BS. Shading reflects difference between each caliper measurement and the bit size. TRACK 3: Gas hydrate saturation, SHY, density, RHOZ, and gamma ray, GR. TRACK 4: Resistivities measured at various depths of investigation from shallow (A010) to deep (AO90) TRACK 5: Compressional (DTCO) and shear (DTSM) wave slownesses. TRACK 6: Dynamic Young's modulus.
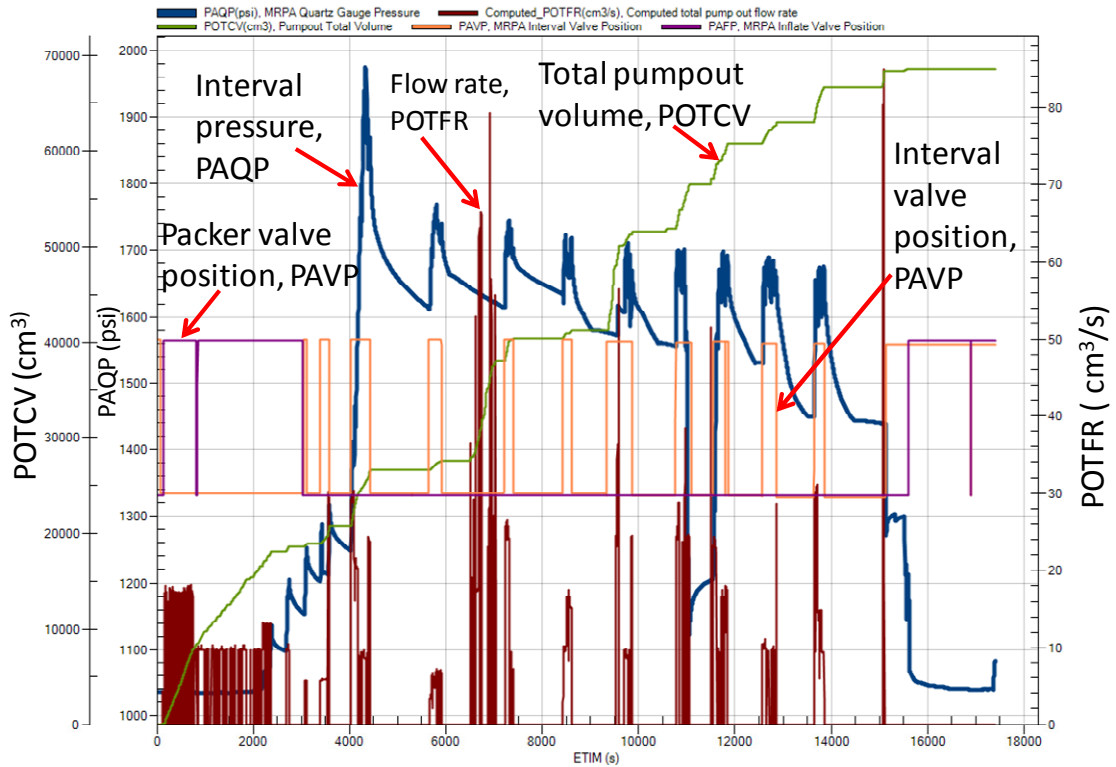
Figure 5.42: Overview of data acquired at Test Station 2 located at 2202.58 ft MD.

Figure 5.42 presents an overview of the most important data acquired during the test. The time corresponding to the peak interval pressure (blue curve) divides the test into two parts. The earlier part consisted of packer inflation and filtration tests. The later part consisted of fracture propagation/shut-in cycles and a rebound test. A total of nine fracture propagation /shut-in cycles were performed during the test. Pressures in the interval tended to decrease with each new injection cycle. This decrease is probably caused by propagation of the fracture away from the near-wellbore stress concentration.
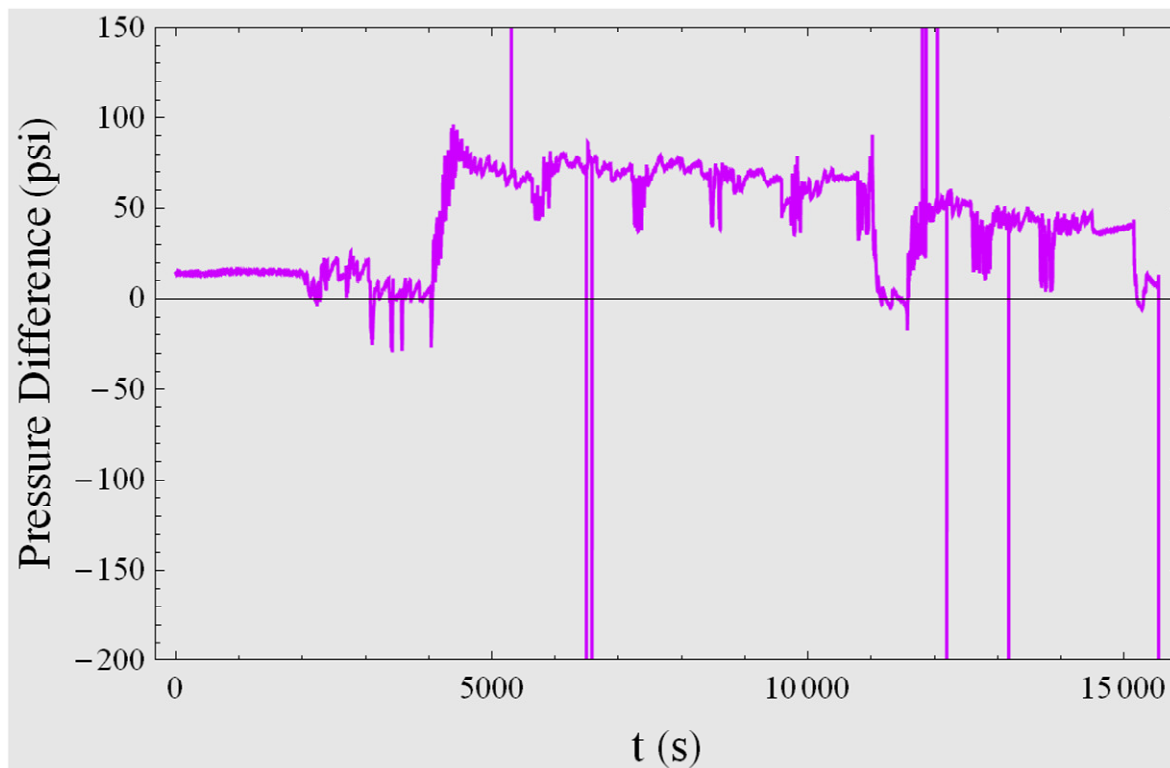
Figure 5.43: Packer pressure minus interval pressure vs. time.

Figure 5.43 shows the difference between the packer pressure and the interval pressure. After the commencement of the first fracture propagation cycle at 4030 s, the packer pressure is generally higher than the interval pressure. This indicates that the packer is functioning as designed and provides some assurance that a proper seal is being maintained. However Figure 5.43 also shows some episodes during which the packer pressure dropped below the interval pressure. These episodes are shown in Figure 5.44. For three of the cases shown in Figures 5.44 (a), (c), and (d) the decrease in the packer pressure had no impact on the interval pressure suggesting that no leak occurred. These occurrences may have been caused by temporary reseating of the packers. However some leakage may have occurred during the rebound test (Figure 44(b)) and also very briefly at 12044 s during the shut-in period of Cycle 7 (Figure 5.44(c)).
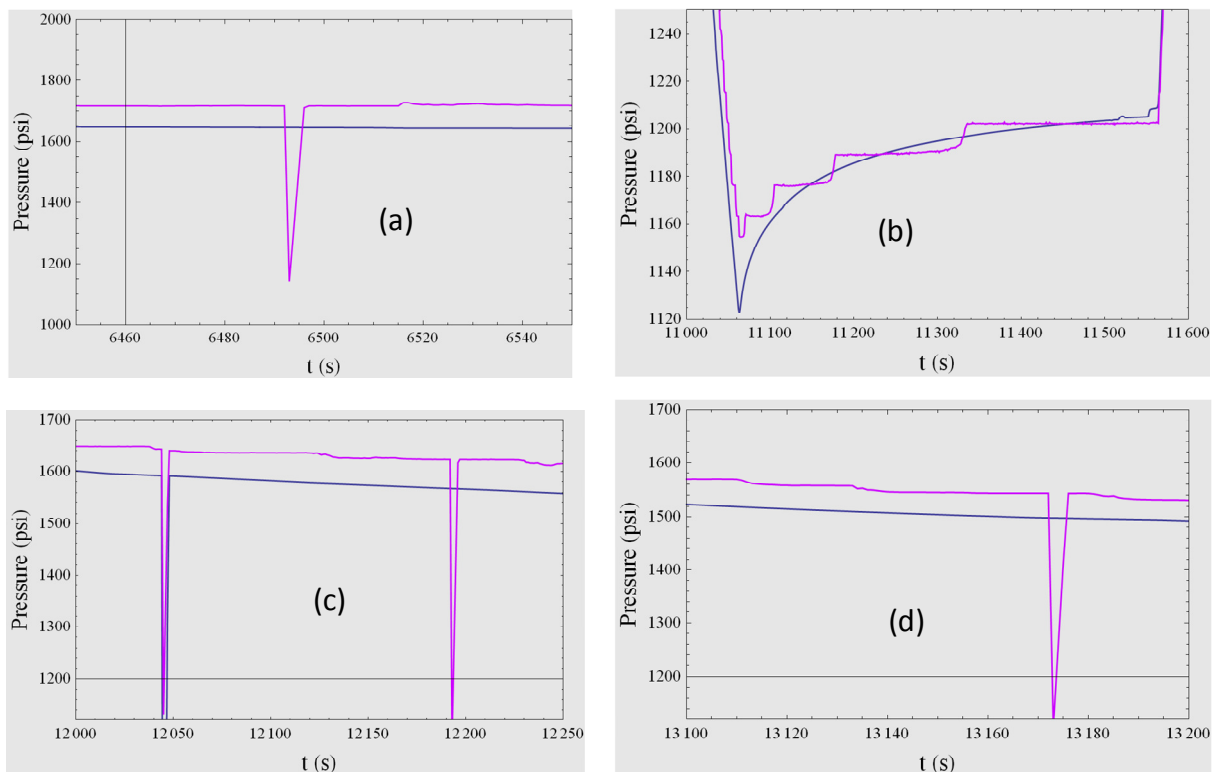
Figure 5.44: Interval (blue) and packer (purple) pressures during instances when the packer pressure fell below the interval pressure. (a) During Cycle 2 shut-in period. (b) During rebound test following Cycle 6 (c) During Cycle 7 shut-in period. (d) During Cycle 8 shut-in period.

5.2.2 Packer Inflation (Event 0)

Figure 5.45 shows the packer inflation event. A primary objective of this procedure was to avoid over-inflation of the packer that could cause it to stick in the unconsolidated silt or make poor contact with the borehole wall due to excessive yielding of the formation. The low Young's modulus of the formation (Section 5.2.1) made it imperative to maintain the packer pressure at the minimum value required to seal the interval. The initial pressure of the mud column was 1035 psi. The packer was inflated in stages to 1220 psi. During inflation the pump half-stroked several times, as evidenced by the flow rate going to zero while the pump motor was running. The interval pressure rose with the packer pressure and declined quickly due to leak-off when the pump was switched off. The packer pressure also declined during pumps off periods in response to the decrease in interval pressure. After the final inflation step, the packer pressure was judged to be stable enough to begin pumping into the interval.
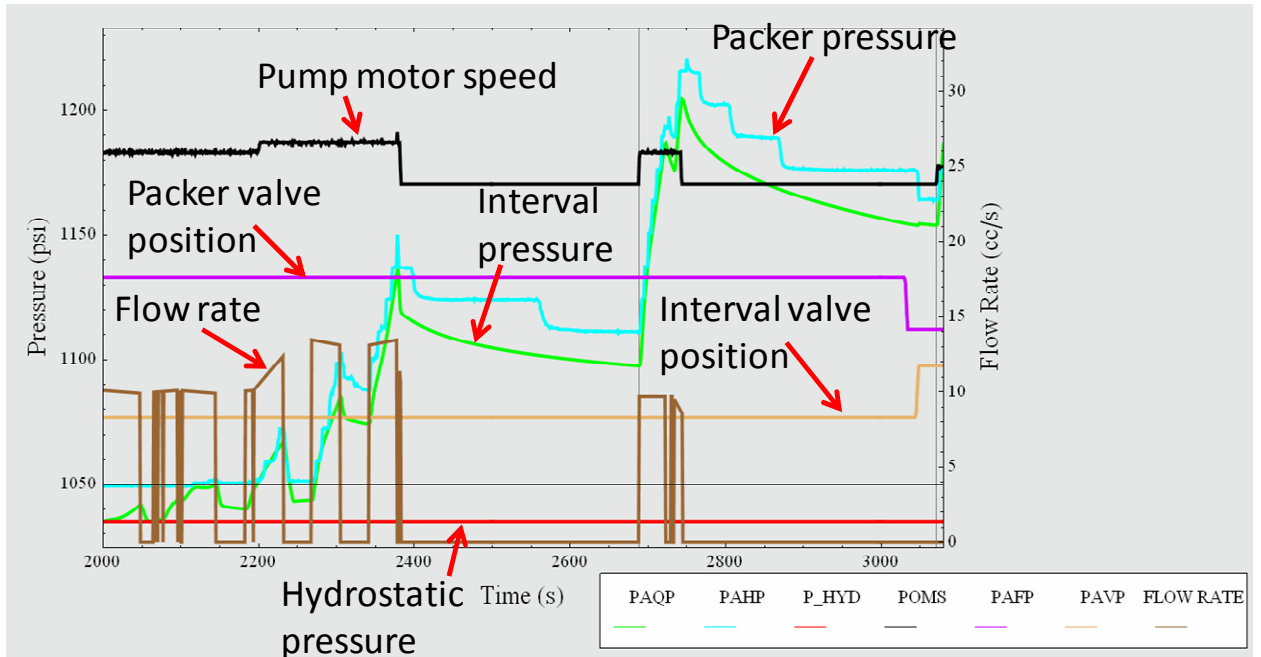
Figure 5.45: Packer Inflation.

5.2.3 Filtration tests (Cycle 0)

Figure 5.46 shows the two filtration tests performed prior to breaking down the formation. The pump half-stroked during the second test, so a total of three pressure build-up phases can be observed. During all three pressure build-ups, the packer pressure lagged slightly below the interval pressure. However the packer pressure caught up with the interval pressure during pressure relaxation periods. This made it possible for a seal to be maintained during the first and third relaxation periods. However a rapid drop in pressure indicates that the seal broke during the second relaxation period. This occurred because the packer pressure was too close to the interval pressure to maintain a seal. However by the final filtration test, the pressure appeared to bleed off normally. Figure 5.47 shows a plot of interval pressure vs. volume. The curve is initially linear but departs from linearity when the pressure is 1265 psi. Since the interval pressure is far below the fracture breakdown pressure, the departure from linearity is probably due to yielding of the formation against the packers, rather than fracture initiation. Figure 5.48 shows the bleed-off phase after the final pressure build-up. From the derivative plot it is possible to show that the rate of pressure decline ranged between 2.5 psi/ft and 0.05 psi/ft. Table 5.9 summarizes the results for this cycle.

Table 5.9: Cycle 0 Results.

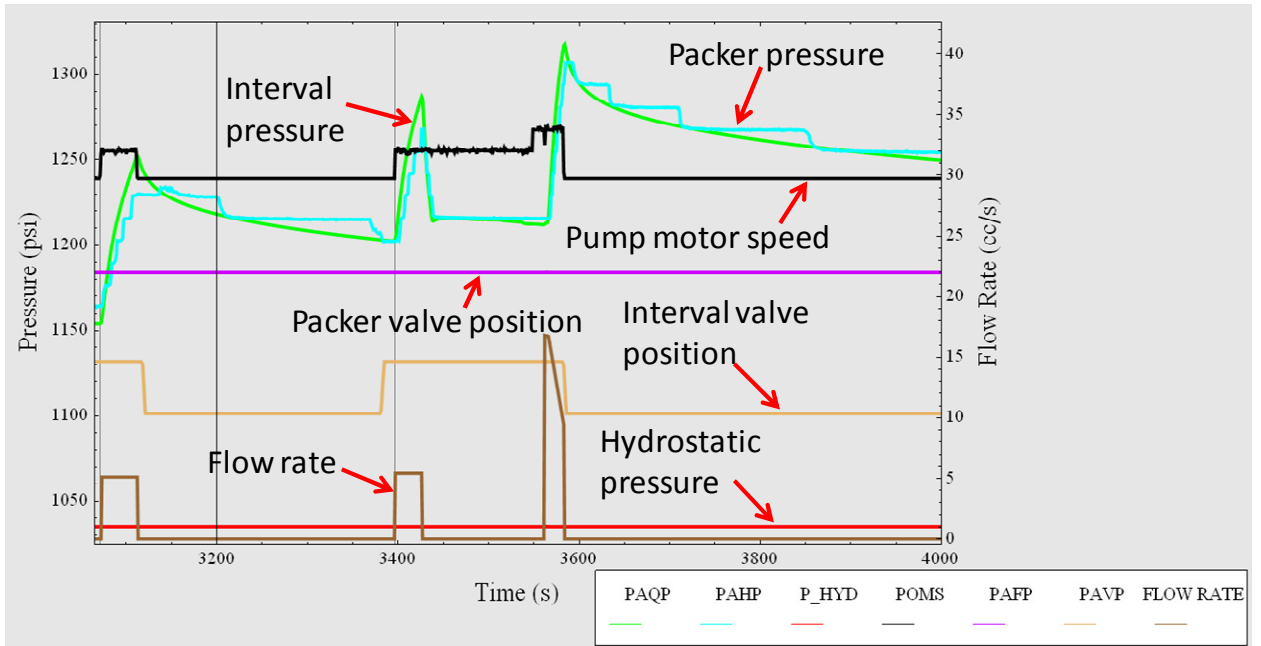| Stiff (psi/cc)	LOP (psi)	LOV (cc)	VL_frac (cc)	Peak_P (psi)	Prop_P (psi)	ISIP (psi)	P_clos (psi)	P_clos_G-function (psi)
0.9409	1265	54	N/A	N/A	N/A	N/A	N/A	N/A

Figure 5.46: Filtration tests (Cycle 0). The first filtration test started at 3071 s and the second started at 3397 s.
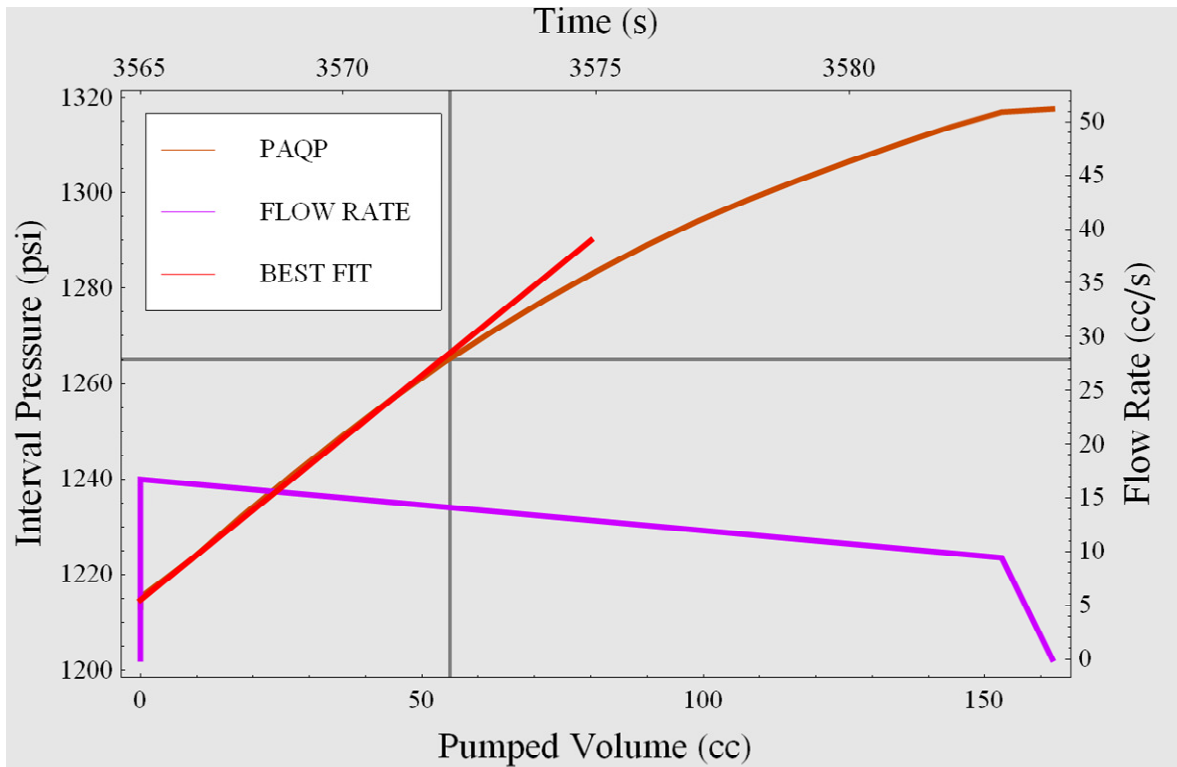

Figure 5.47: Plot of interval pressure vs. pumped volume (brown curve) during the filtration test (Cycle 0). A linear fit to this curve shown in red. The volume at which the curve departs from linearity shown by grey cross-hairs. The flow rate into the interval (purple curve) is shown referenced to the right hand vertical axis.
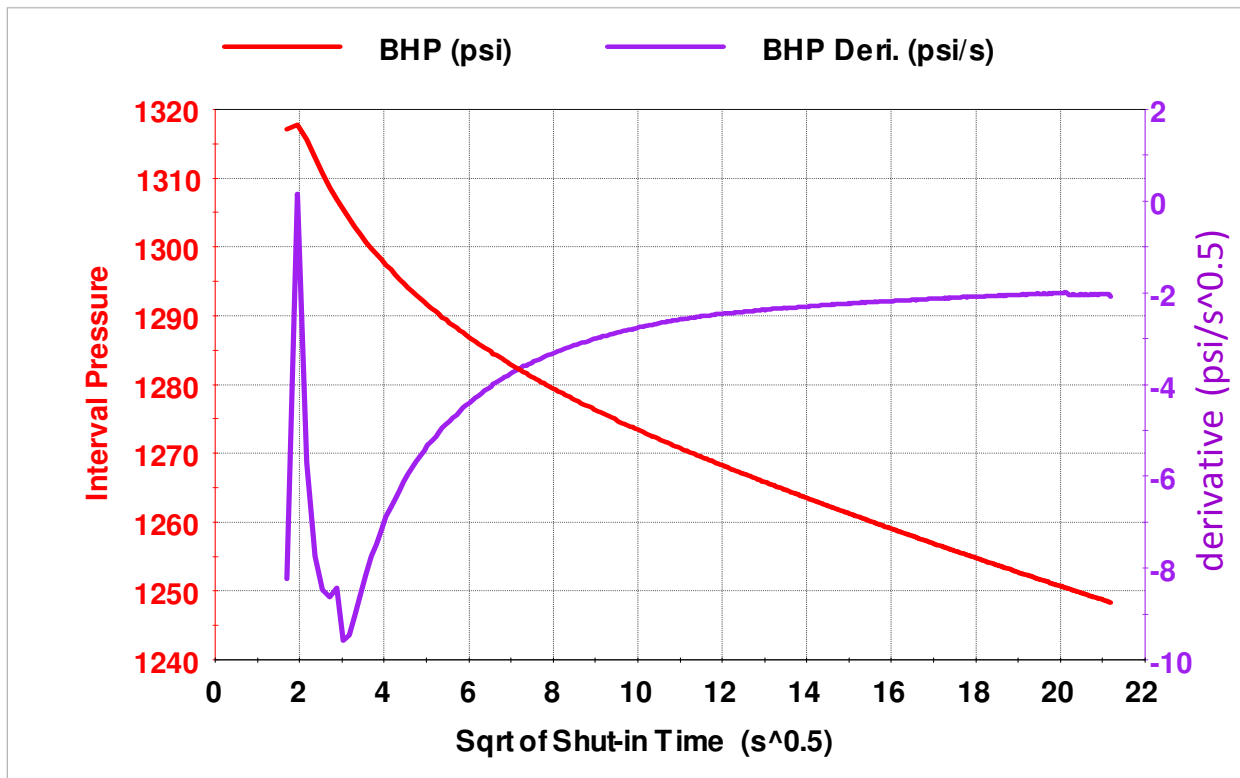
Figure 5.48: Plots of interval pressure (red curve) and its derivative (purple curve) versus square root of shut-in time.

5.2.4 Cycle 1

Figure 5.49 shows the raw data from the injection phase of Cycle 1. Injection occurred over a period of approximately 400 s however the flow into the interval during this period was intermittent due to half-stroking of the pump (Figure 5.49). Half-stroking caused the interval pressure to dip several times. Figure 5.50 shows the plot of interval pressure versus pumped volume. The formation broke down at 1970 psi. Figure 5.51 shows pressure vs. square root of time during pressure decline. According to this construction, the fracture closed at 1726 psi. An alternative construction using the G-function yields a closure pressure of 1723 psi (Figure 5.52). Table 5.10 summarizes the results for this cycle.

Table 5.10: Cycle 1 Results

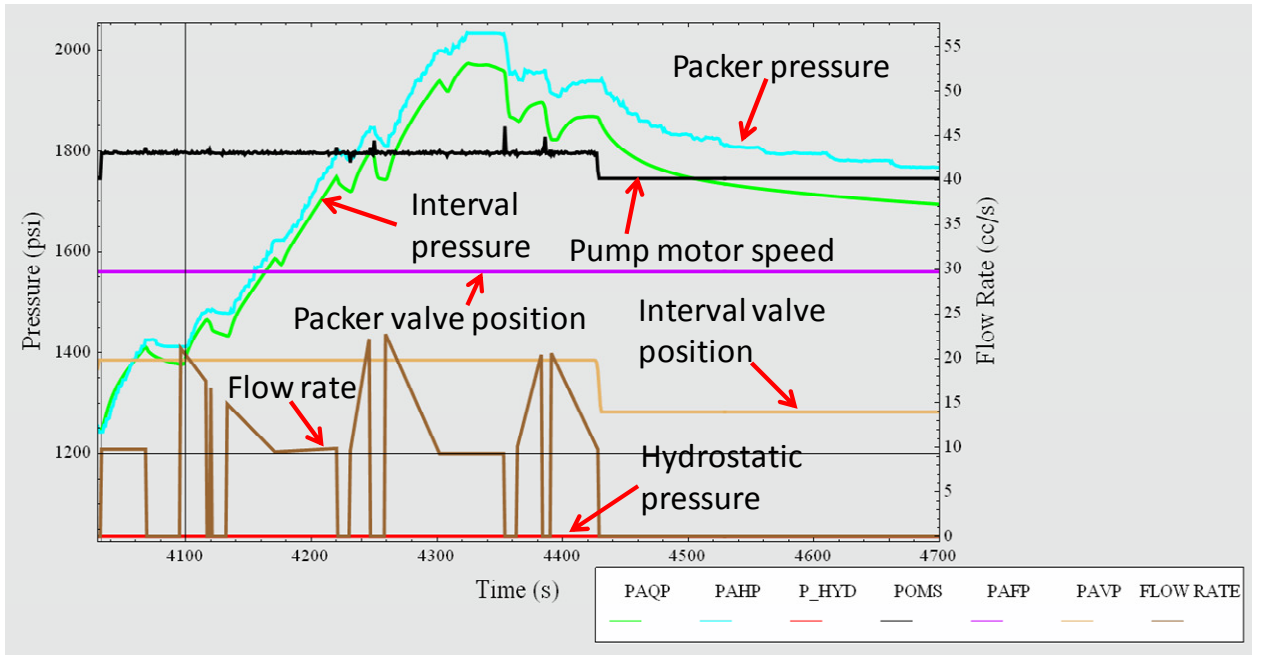| Stiff (psi/cc)	LOP (psi)	LOV (cc)	VL_frac (cc)	Peak_P (psi)	Prop_P (psi)	ISIP (psi)	P_clos (psi)	P_clos_G-function (psi)
0.2602	1970	2600	1066	1970.0	1867.1	1864	1725.9	1723

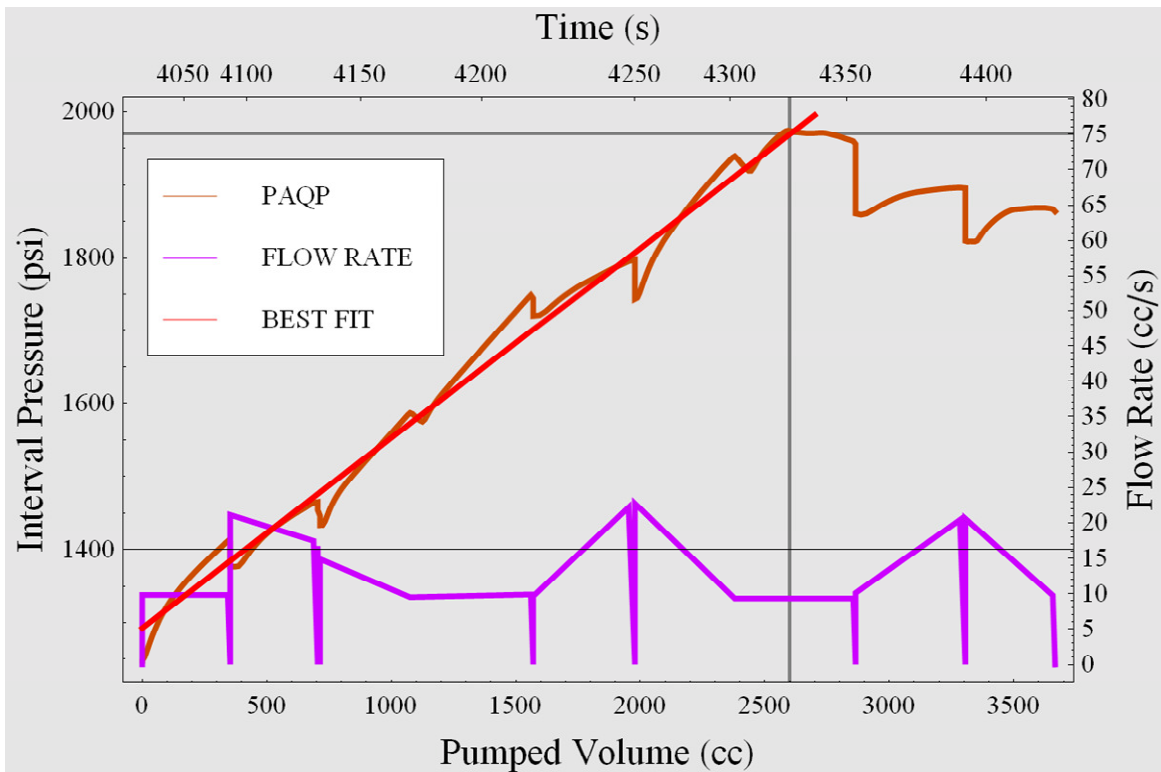**Figure 5.49: Cycle 1. Breakdown of the formation.**

Figure 5.50: Plot of interval pressure vs. pumped volume (brown curve) during Cycle 1. A linear fit to this curve shown in red. The volume at which the curve departs from linearity shown by grey cross-hairs. The flow rate into the interval (purple curve) is shown referenced to the right hand vertical axis.
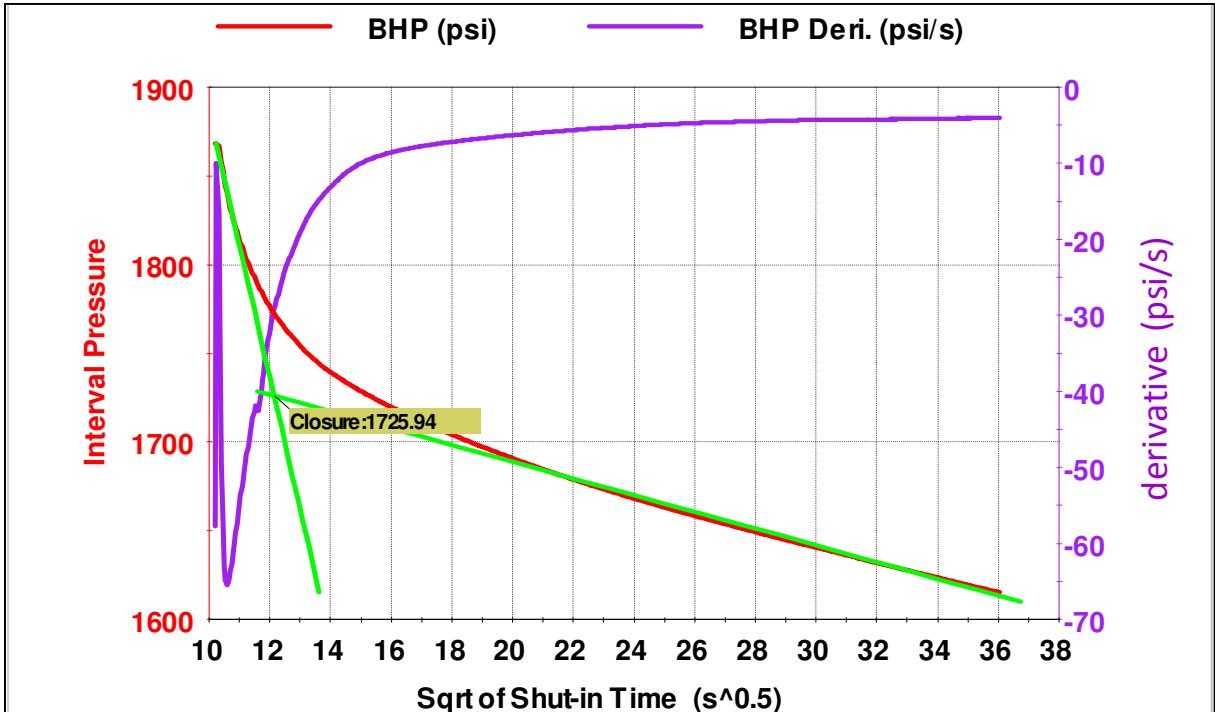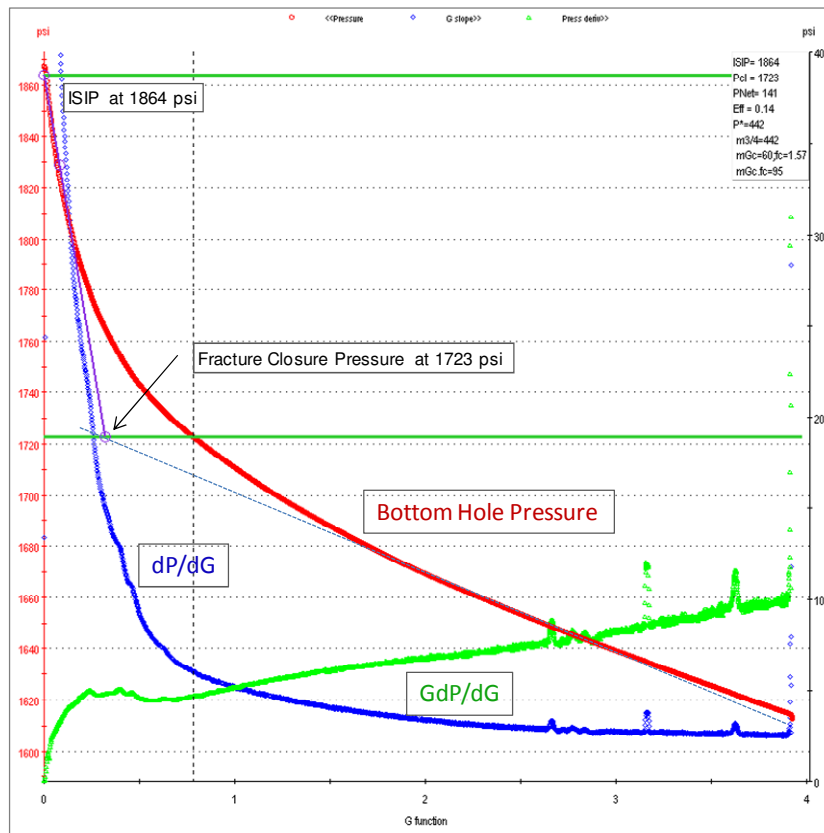
Figure 5.51: Plots of interval pressure (red curve) and its derivative (purple curve) versus square root of shut-in time.

Figure 5.52: Interpretation of fracture closure during Cycle 1 using the G-function.

5.2.5 Cycle 2

The interval was again pressurized and the fracture created in Cycle 1 was propagated for approximately 240 s. Figure 5.53 shows key data from this test. During injection, the pump half-stroked several times, particularly in the latter half of the injection phase. Figure 5.54 shows a plot of interval pressure versus pumped volume. The fracture appears to reopen at 1655 psi. This figure is much lower than the previous closure pressure. Figure 5.55 shows q plot of pressure versus square root of time for the shut-in phase. The fracture appears to close at 1683 psi. An alternative construction using the G-function yields a closure pressure of 1675 psi (Figure 5.56). Table 5.11 summarizes the principal results of this cycle.

Table 5.11: Cycle 2 Results

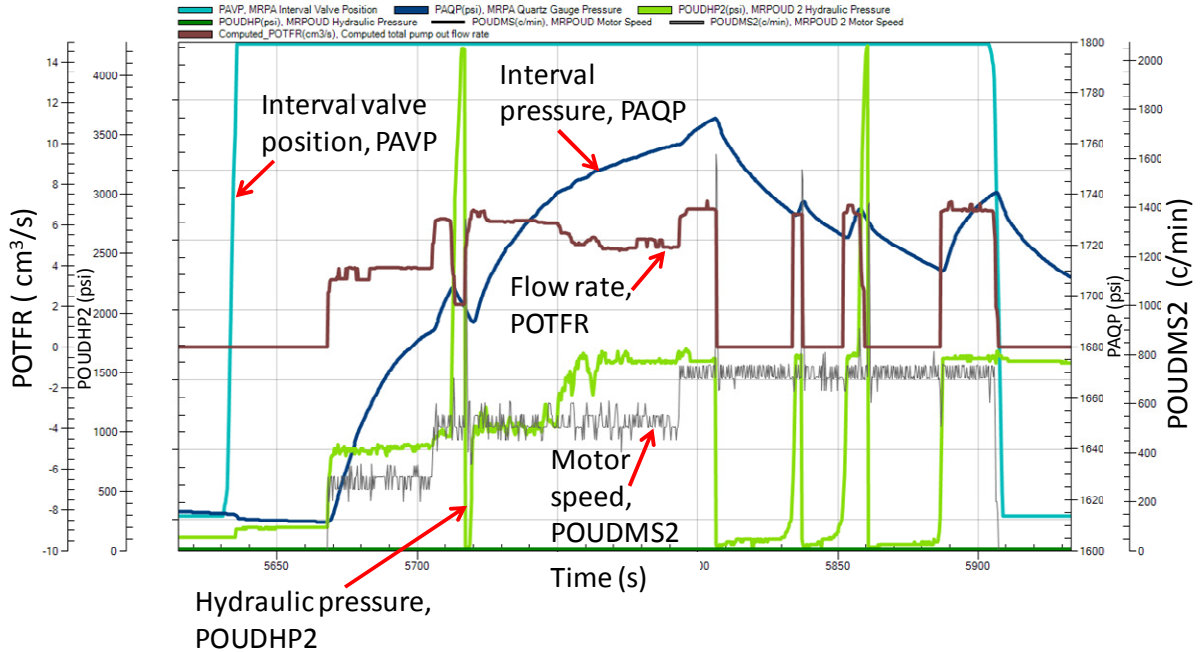| Stiff (psi/cc)	LOP (psi)	LOV (cc)	VL_frac (cc)	Peak_P (psi)	Prop_P (psi)	ISIP (psi)	P_clos (psi)	P_clos_G-function (psi)
0.914	1654.5	48.3	858.58	1769.14	N/A	1732	1683.3	1675

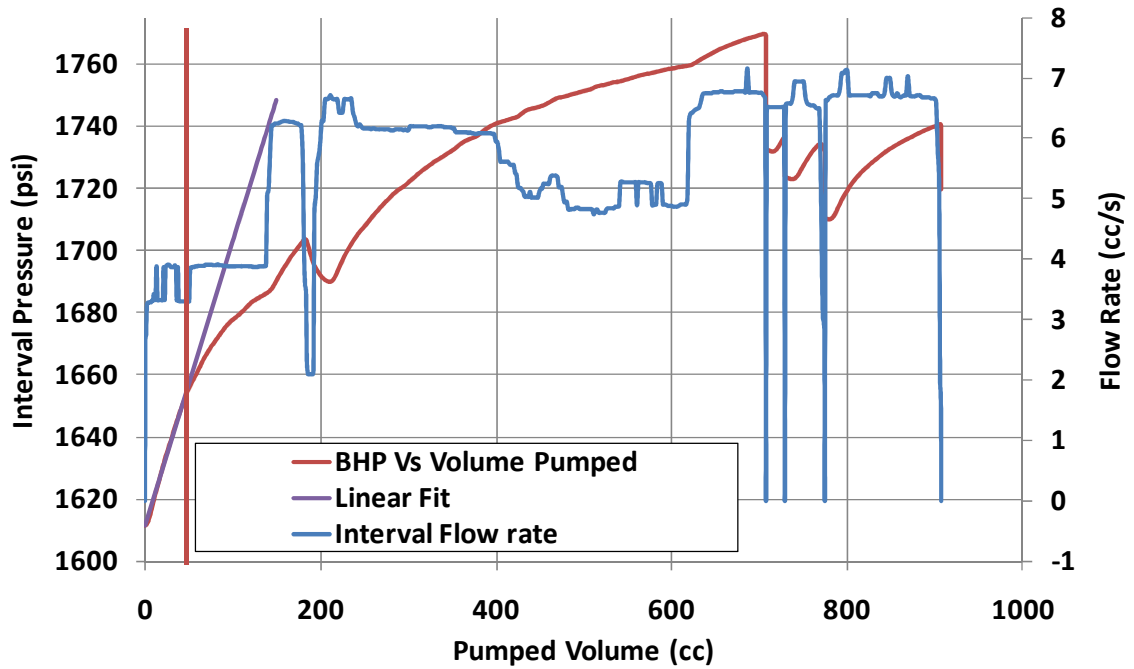**Figure 5.53: Cycle 2. Propagation of the fracture.**

Figure 5.54: Plot of interval pressure vs. pumped volume during Cycle 2 (red curve). A linear fit to this curve shown in purple. The volume at which the curve departs from linearity shown by orange vertical line. The flow rate into the interval (blue curve) is shown referenced to the right hand vertical axis.
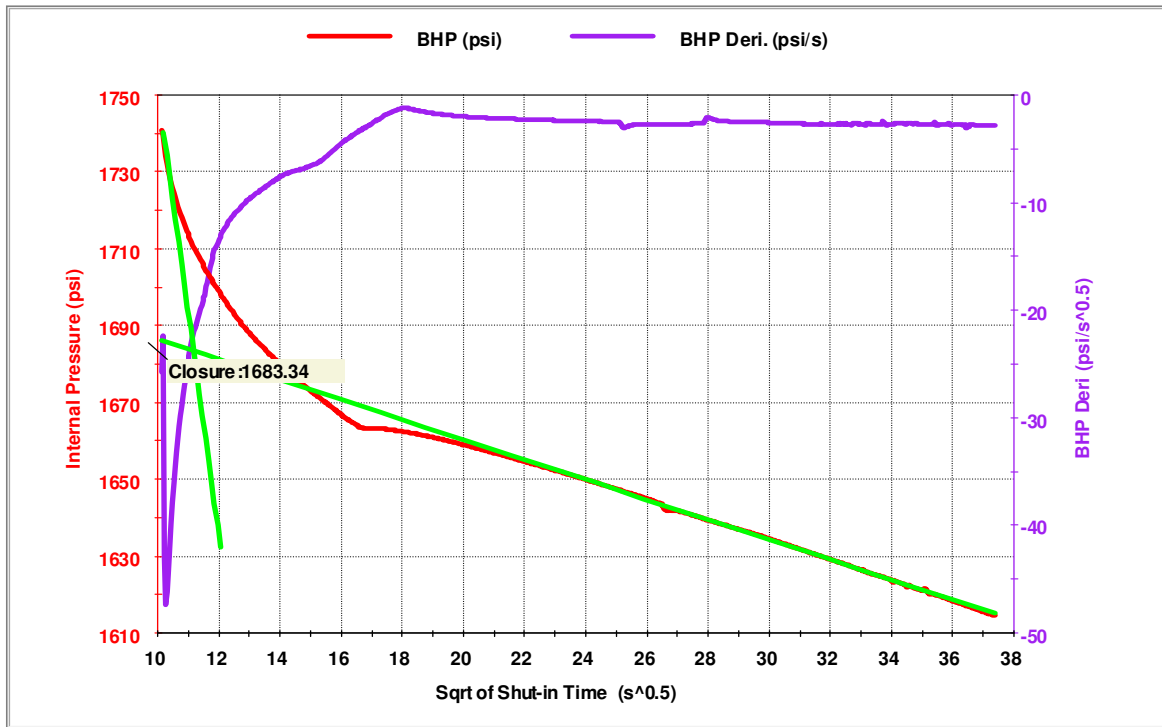

Figure 5.55: Plots of interval pressure (red curve) and its derivative (purple curve) versus square root of shut-in time.
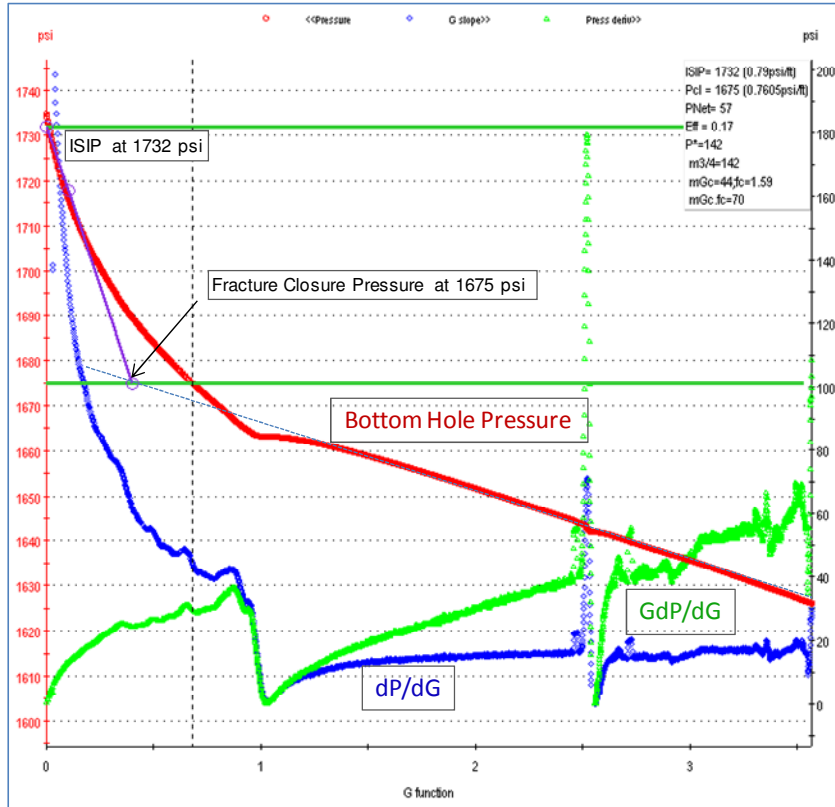
Figure 5.56: Cycle 2-Depth 2-G-Function Interpretation.

5.2.6 Cycle 3

Figures 5.57 and 5.58 show the raw data from the injection phase of Cycle 3. Injection occurred over a period of approximately 175 s. The pump half-stroked several times (Figure 5.57) causing the interval pressure to dip (Figure 5.58). Figure 5.59 shows a plot of interval pressure versus pumped volume. The fracture reopened at 1679 psi. Figure 5.60 shows pressure vs. square root of time. The fracture appears to close at 1682 psi. An alternative construction using the G-function yields a closure pressure of 1680 psi (Figure 5.61). Table 12 summarizes the principal results of this cycle.

Table 5.12: Cycle 3 Results

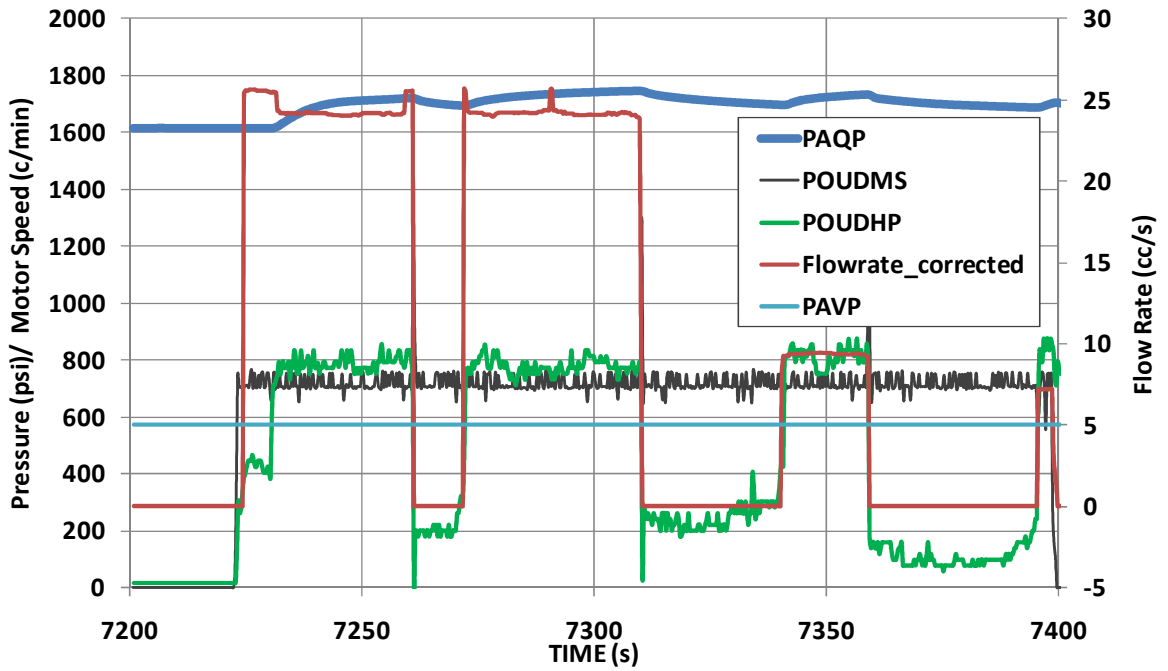| Stiff (psi/cc)	LOP (psi)	LOV (cc)	VL_frac (cc)	Peak_P (psi)	Prop_P (psi)	ISIP (psi)	Piccolos (psi)	P_clos_G-function (psi)
0.375	1678.66	347.84	1680.05	1744.89	N/A	1700	1681.7	1680

Figure 5.57: Raw data from Cycle 3. Interval pressure (PAQP), pump motor speed (POUDMS), pump hydraulic pressure (POUDHP), flow rate (POTFR), and interval valve position (PAVP) are shown.
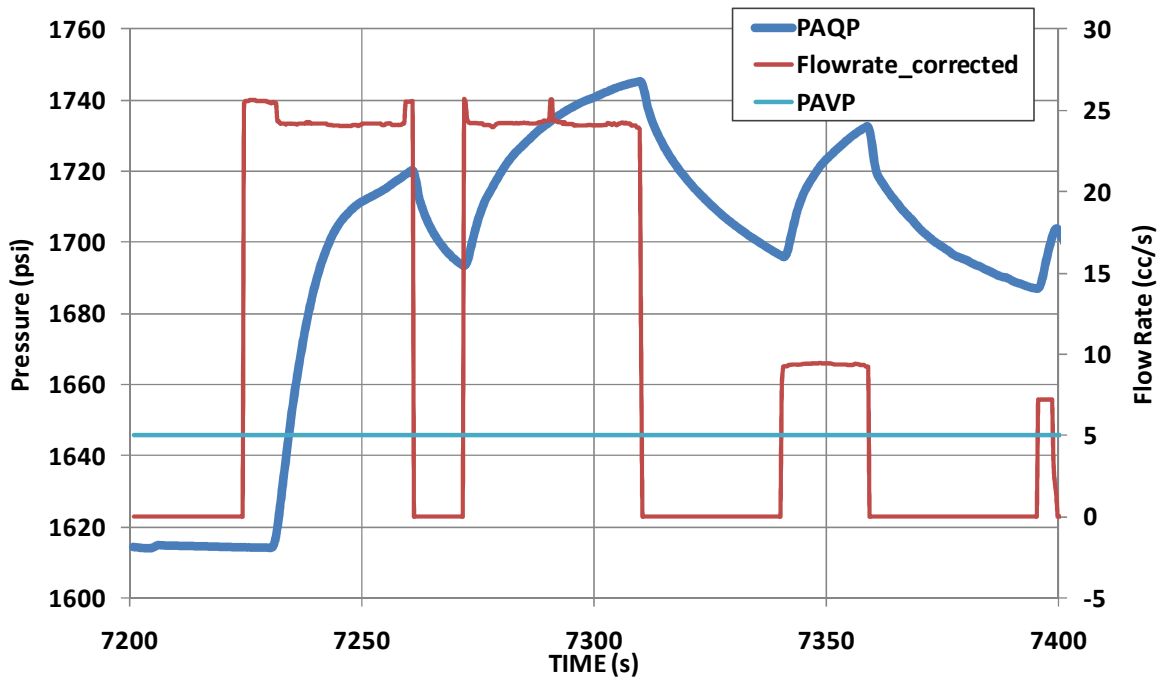

Figure 5.58: Interval pressure (PAQP), flow rate (Flowrate_corrected), and interval valve position (PAVP) during injection phase of Cycle 3.
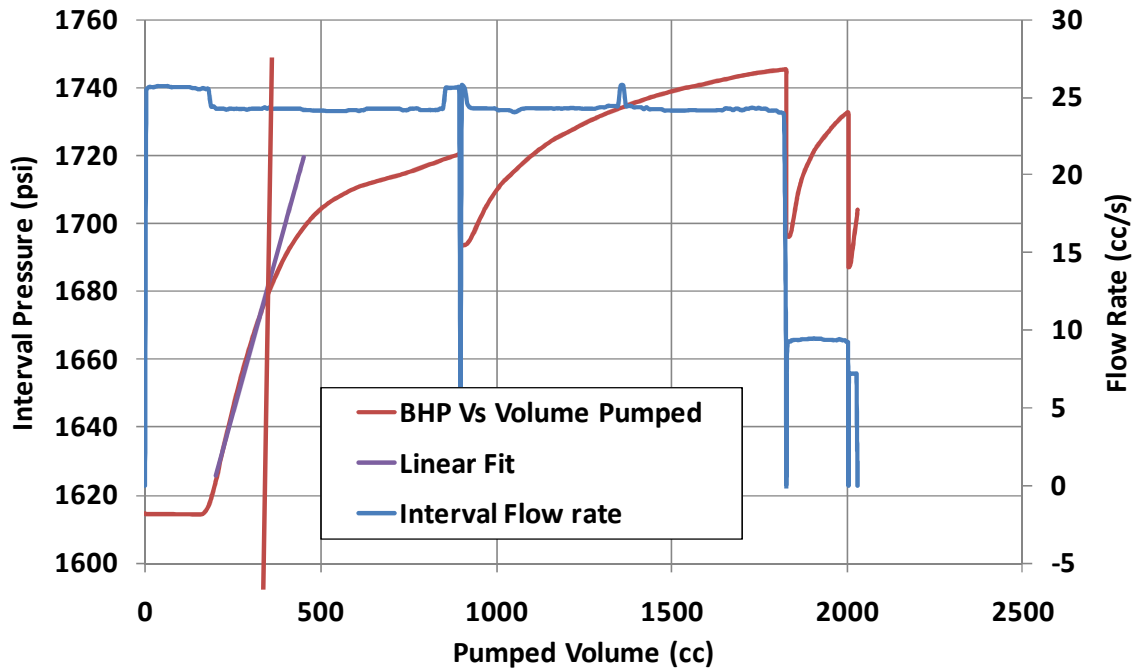
Figure 5.59: Plot of interval pressure vs. pumped volume during Cycle 3 (red curve). A linear fit to this curve shown in purple. The volume at which the curve departs from linearity shown by orange vertical line. The flow rate into the interval (blue curve) is shown referenced to the right hand vertical axis.
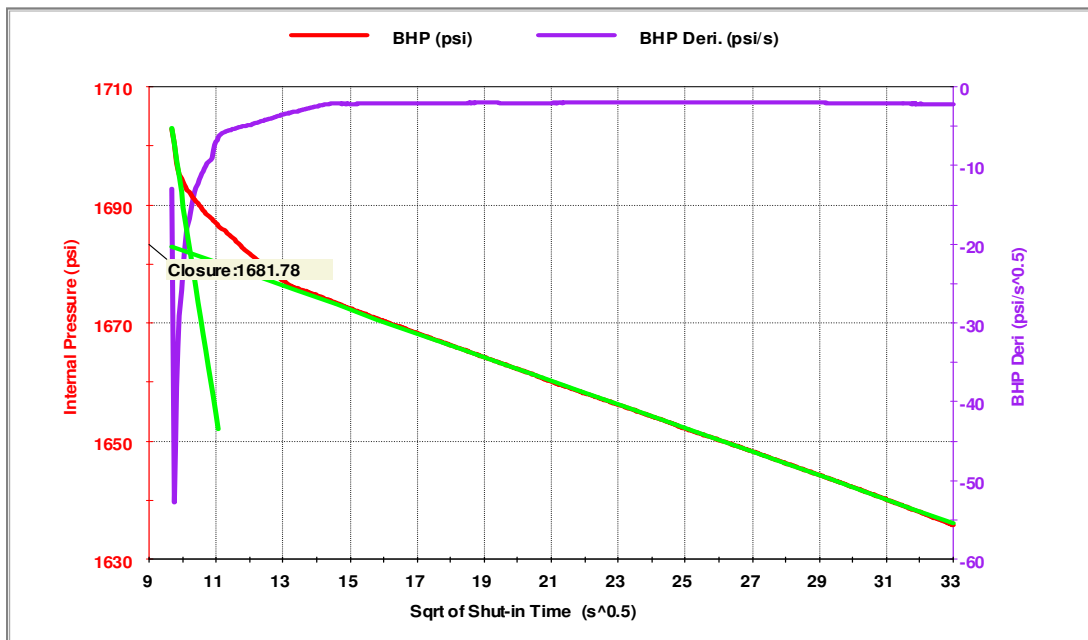

Figure 5.60: Plots of interval pressure (red curve) and its derivative (purple curve) versus square root of shut-in time.
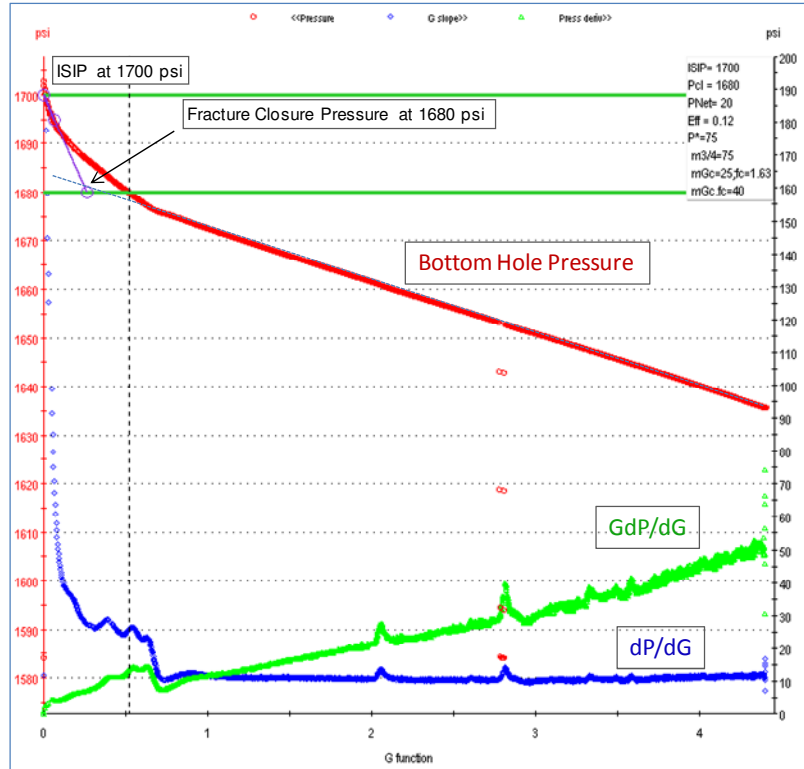
Figure 5.61: Cycle 3-Depth 2-G-Function Interpretation.

5.2.7 Cycle 4

Figures 5.62 and 5.63 show the raw data from the injection phase of Cycle 4. Injection occurred over a period of approximately 175 s and the pump half-stroked in the middle of this operation (Figure 5.62) causing the interval pressure to dip (Figure 5.63). Figure 5.64 shows the plot of interval pressure versus pumped volume. The fracture reopened at 1673 psi. Figure 5.65 shows pressure vs. square root of time during the shut-in period. The fracture appears to close at 1630 psi. An alternative construction using the G-function yields a closure pressure of 1631 psi (Figure 5.66). Table 13 summarizes the principal results of this cycle.

Table 5.13: Cycle 4 Results

Stiff (psi/cc)	LOP (psi)	LOV (cc)	VL_frac (cc)	Peak_P (psi)	Prop_P (psi)	ISIP (psi)	P_clos (psi)	P_clos_G-function (psi)
1.0199	1672.9	185.55	810.38	1724.12	1715.1	1698	1630.35	1631

A peculiar feature appears at the end of the pressure decline curves in Figure 5.65 and 5.66. The interval pressure suddenly stabilized at about 1580 psi. Yet no such stabilization occurred during the filtration test at much lower interval pressures (Figure 5.48). This suggests that a filtercake built up at the wellbore wall between the filtration test and the end of Cycle 4.
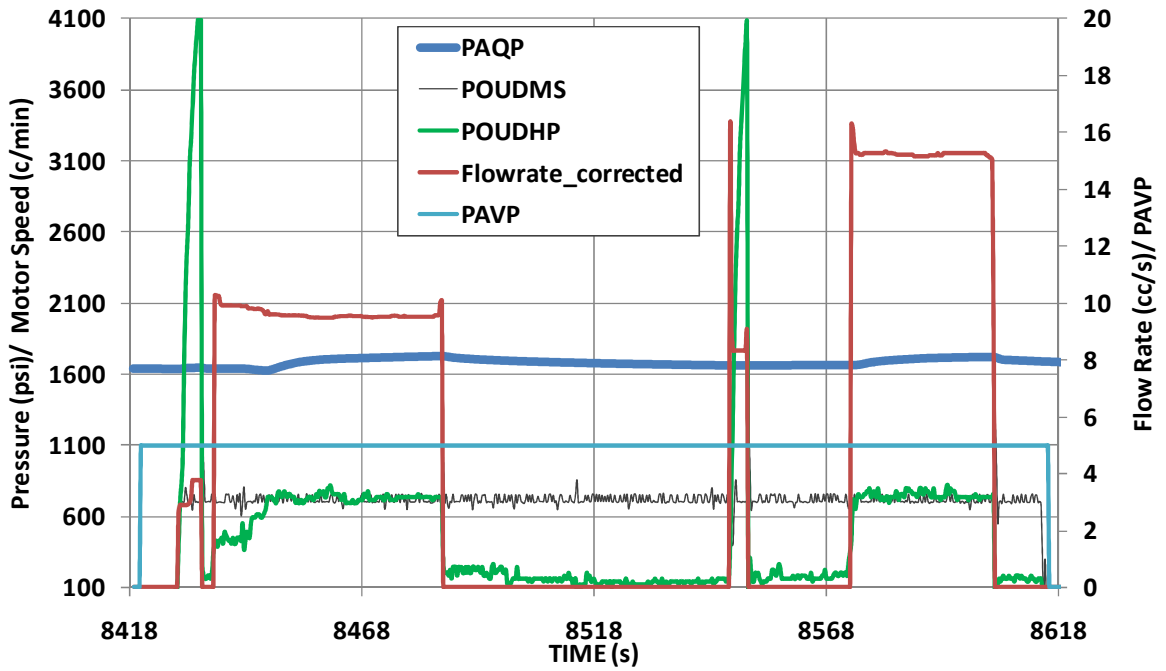
Figure 5.62: Raw data from Cycle 4. Interval pressure (PAQP), pump motor speed (POUDMS), pump hydraulic pressure (POUDHP), flow rate (Flowrate_corrected), and interval valve position (PAVP) are shown.
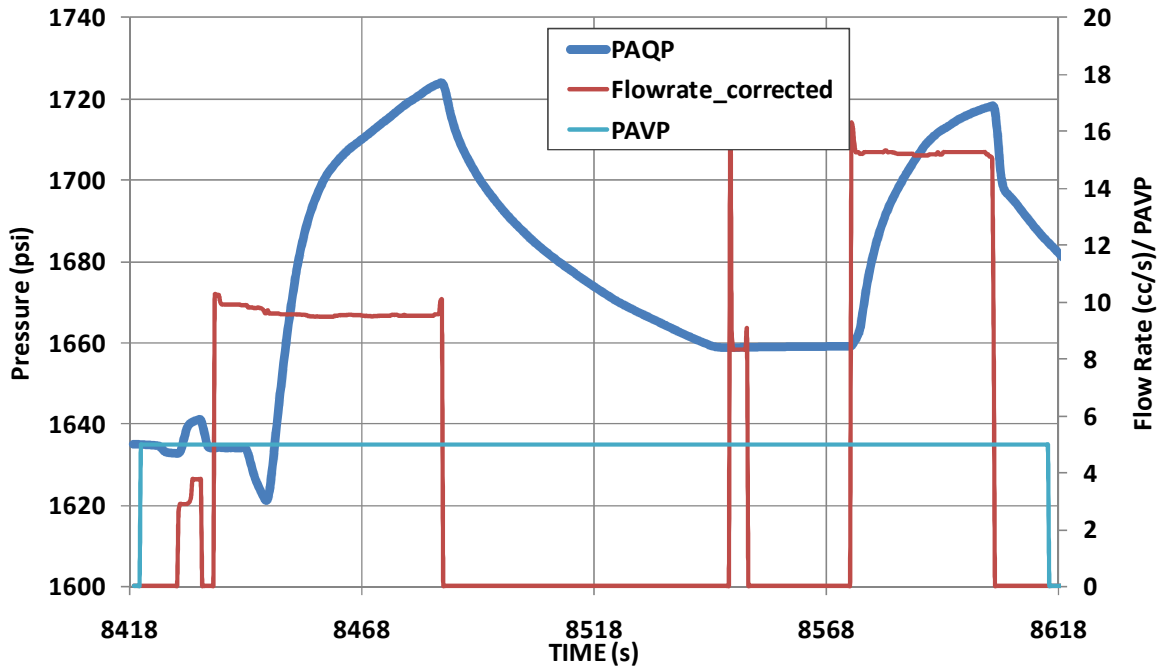

Figure 5.63: Interval pressure (PAQP), flow rate (Flowrate_corrected), and interval valve position (PAVP) during injection phase of Cycle 4.
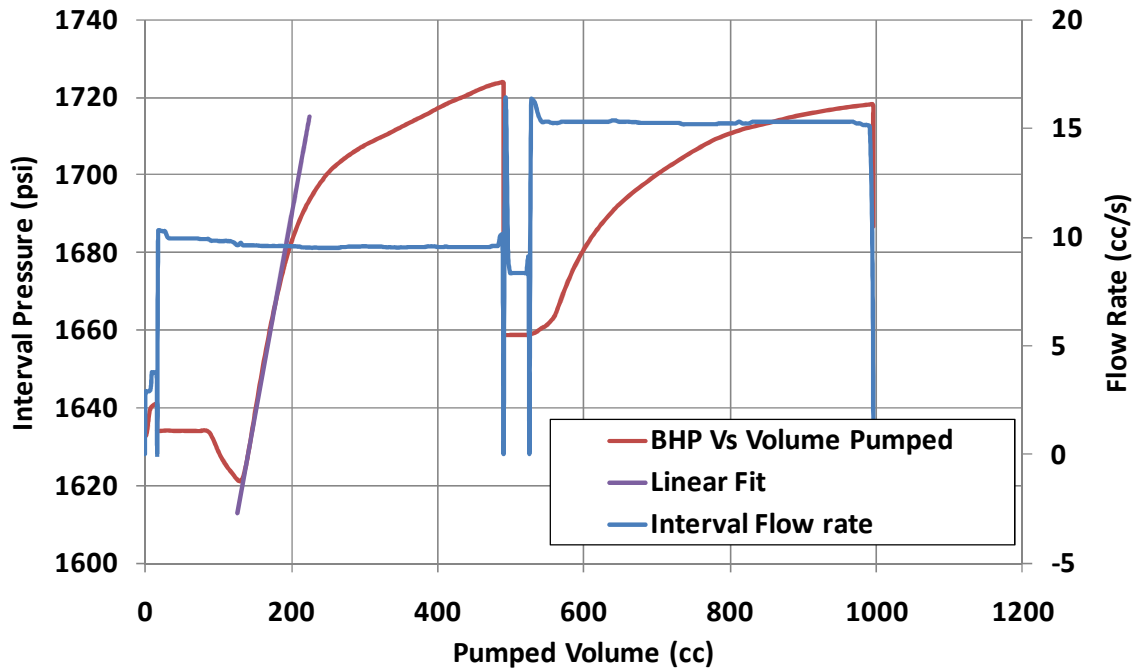
Figure 5.64: Plot of interval pressure vs. pumped volume during Cycle 4 (red curve). A linear fit to this curve shown in purple. The volume at which the curve departs from linearity shown by orange vertical line. The flow rate into the interval (blue curve) is shown referenced to the right hand vertical axis.
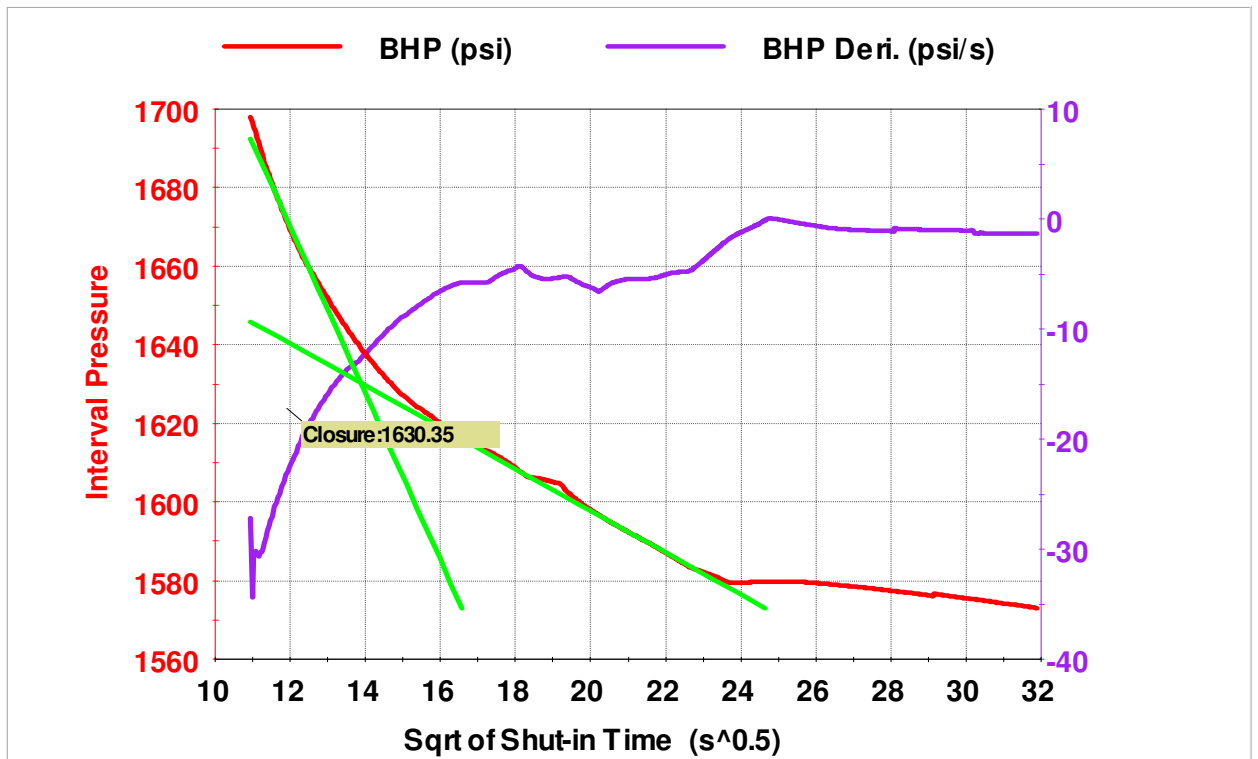

Figure 5.65: Plots of interval pressure (red curve) and its derivative (purple curve) versus square root of shut-in time.
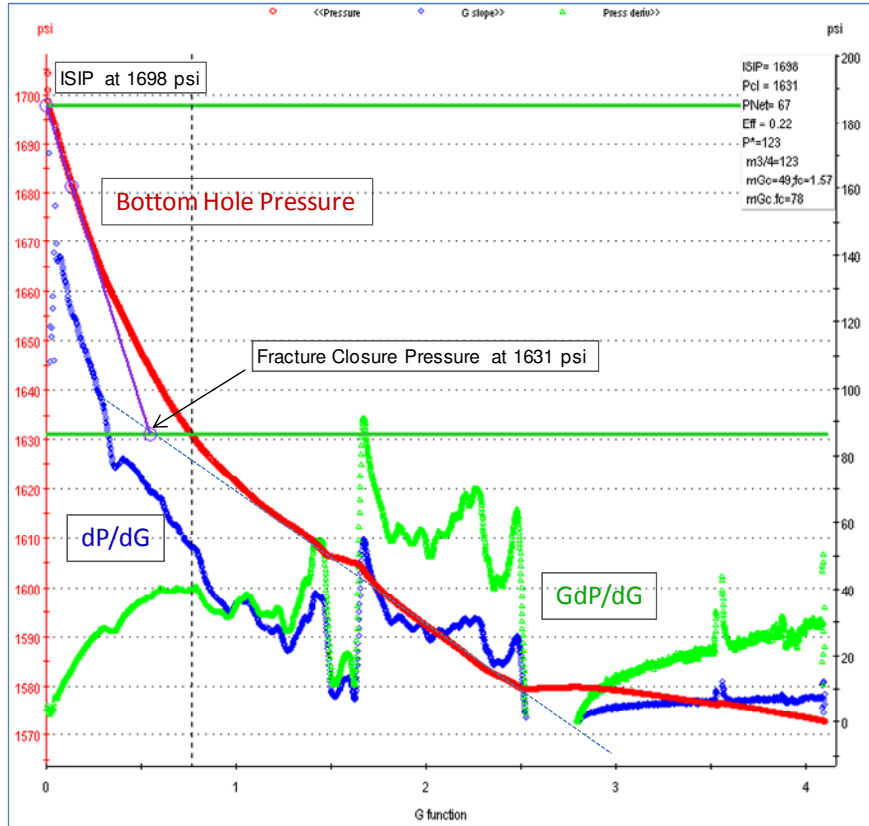
Figure 5.66: Cycle 4-Depth 2-G-Function Interpretation.

5.2.8 Cycle 5

Figures 5.67 and 5.68 show the raw data from the injection phase of Cycle 5. Injection occurred over a period of approximately 170 s. The pump half-stroked a few times (Figure 5.67) causing the interval pressure to dip slightly (Figure 5.68). Figure 5.69 shows a plot of interval pressure versus pumped volume. The fracture reopened at 1684 psi. Figure 5.70 shows pressure vs. square root of time during the shut-in phase.   The same stabilization of pressure seen in the previous cycle appears at the end of this cycle.   Before this happens the fracture appears to close at 1629 psi. An alternative construction using the G-function yields a closure pressure of 1625 psi (Figure 5.71). Table 14 summarizes the principal results of this cycle.

Table 5.14: Cycle 5 Results

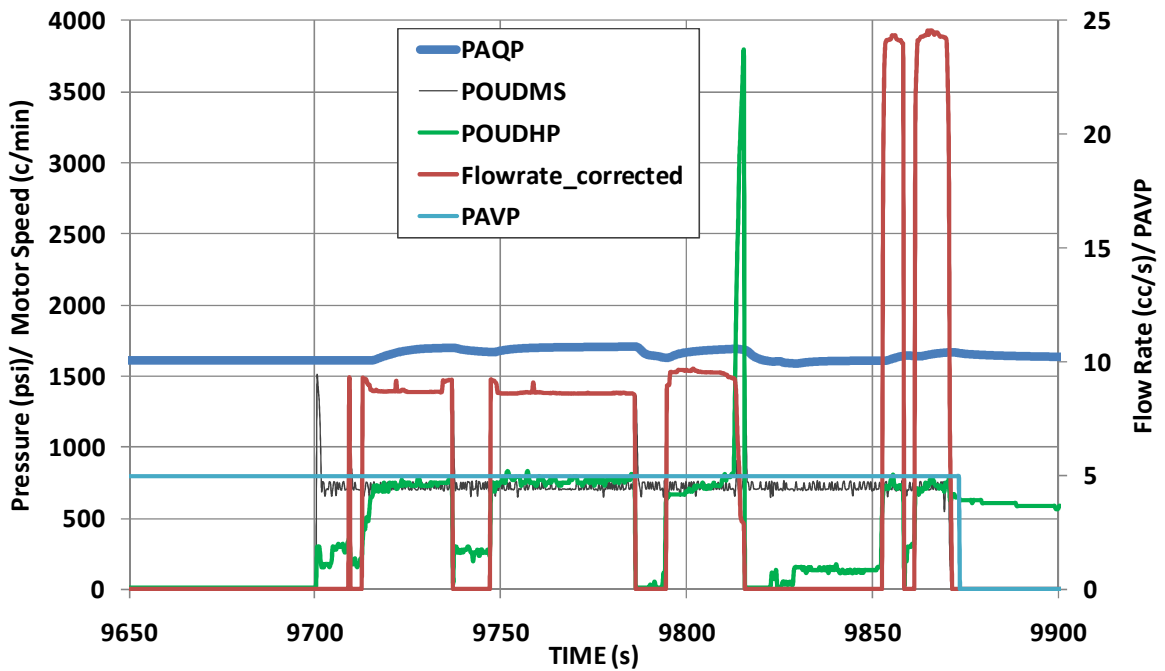| Stiff (psi/cc)	LOP (psi)	LOV (cc)	VL_frac (cc)	Peak_P (psi)	Prop_P (psi)	ISIP (psi)	P_clos (psi)	P_clos_G-function (psi)
0.8525	1683.5	112.32	991.37	1710.87	1707.7	1656	1629.0	1625

Figure 5.67: Raw data from Cycle 5. Interval pressure (PAQP), pump motor speed (POUDMS), pump hydraulic pressure (POUDHP), flow rate (POTFR), and interval valve position (PAVP) are shown.
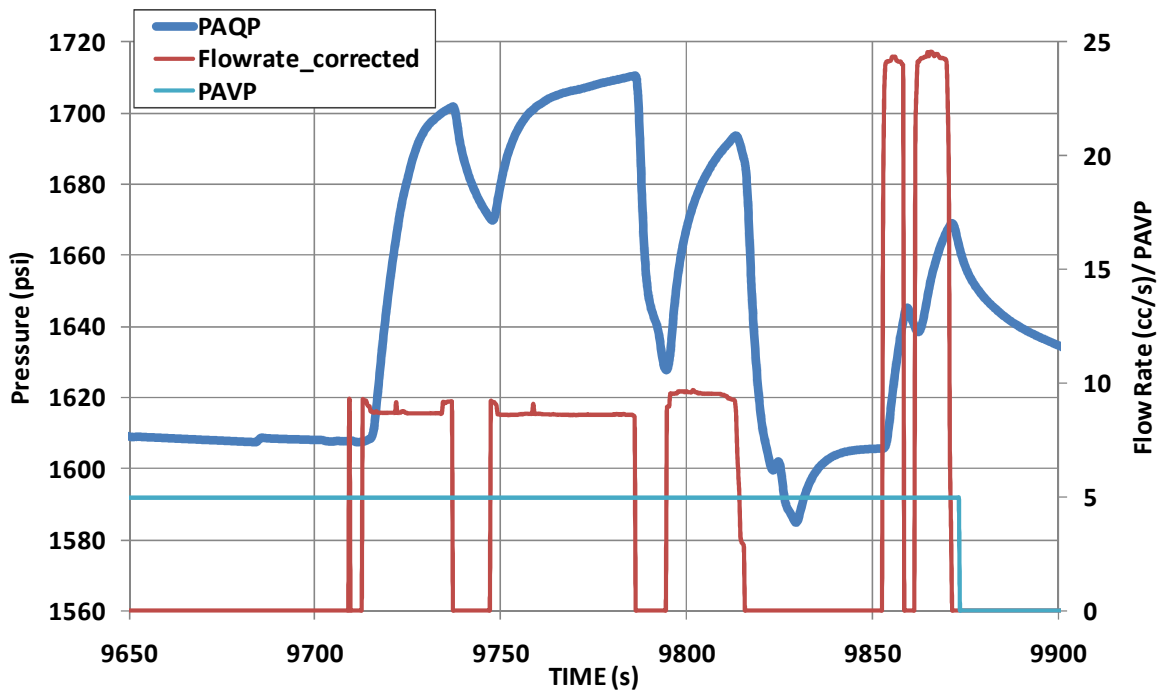

Figure 5.68: Interval pressure (PAQP), flow rate (Flowrate_corrected), and interval valve position (PAVP) during injection phase of Cycle 5.
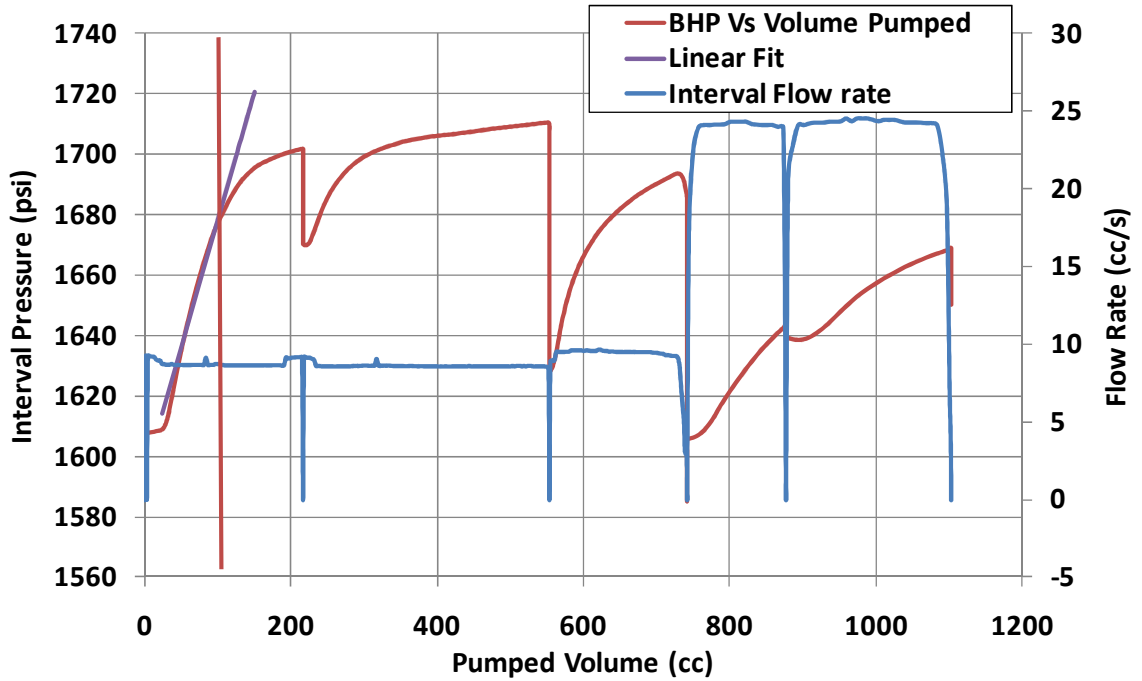
Figure 5.69: Plot of interval pressure vs. pumped volume during Cycle 5 (red curve). A linear fit to this curve shown in purple. The volume at which the curve departs from linearity shown by orange vertical line. The flow rate into the interval (blue curve) is shown referenced to the right hand vertical axis.
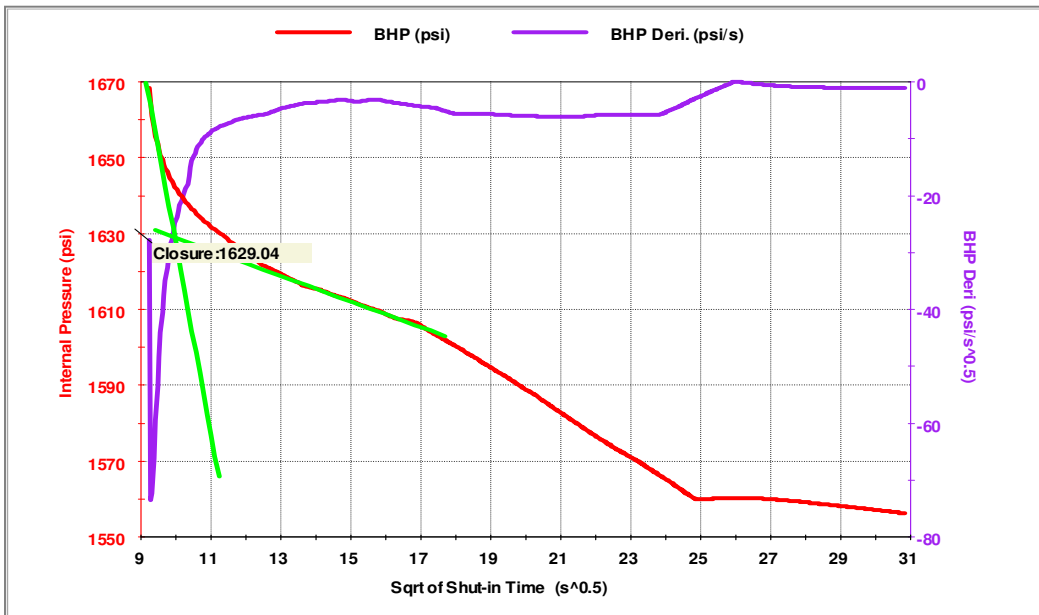

Figure 5.70: Plots of interval pressure (red curve) and its derivative (purple curve) versus square root of shut-in time.
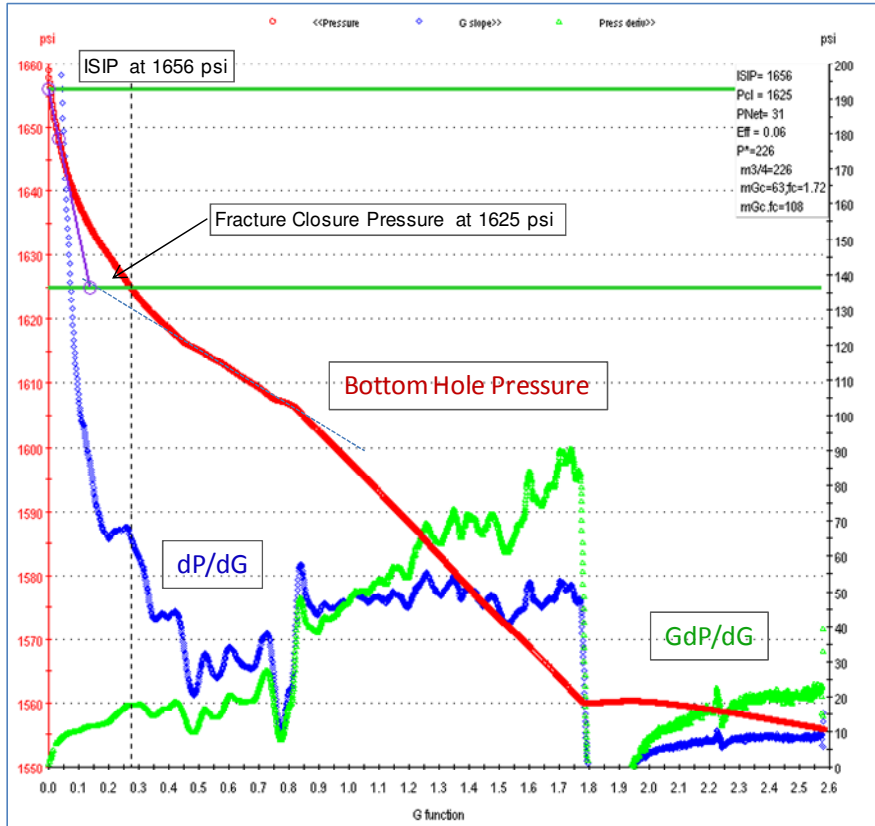
Figure 5.71: Cycle 5-Depth 2-G-Function Interpretation.

5.2.9 Cycle 6

Figures 5.72 and 5.73 show the raw data from Cycle 6. Injection occurred over a period of approximately 230 s. The pump was then reversed and fluid was evacuated from the interval causing the pressure to decrease sharply (Figure 5.73). This rebound test will be discussed in the next section. Half-stroking occurred several times during the injection phase (Figure 5.72). Figure 5.74 shows the plot of interval pressure versus pumped volume. The fracture reopened at 1660 psi. Table 15 summarizes the principal results of this cycle.

Table 5.15: Cycle 6 Results

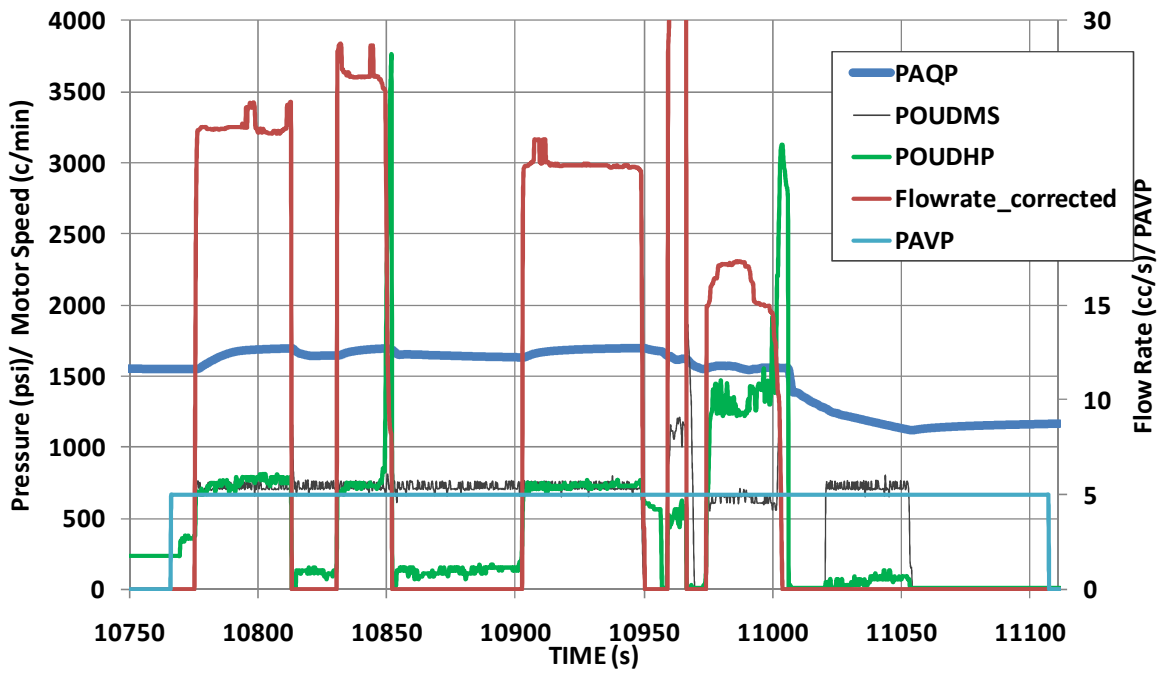| Stiff (psi/cc)	LOP (psi)	LOV (cc)	VL_frac (cc)	Peak_P (psi)	Prop_P (psi)	ISIP (psi)	P_clos (psi)	P_clos_G-function (psi)
0.394	1660.3	288.9	2928.5	1702.1	1698.88	N/A	N/A	N/A

Figure 5.72: Raw data from Cycle . Interval pressure (PAQP), pump motor speed (POUDMS), pump hydraulic pressure (POUDHP), flow rate (Flowrate_corrected), and interval valve position (PAVP) are shown.
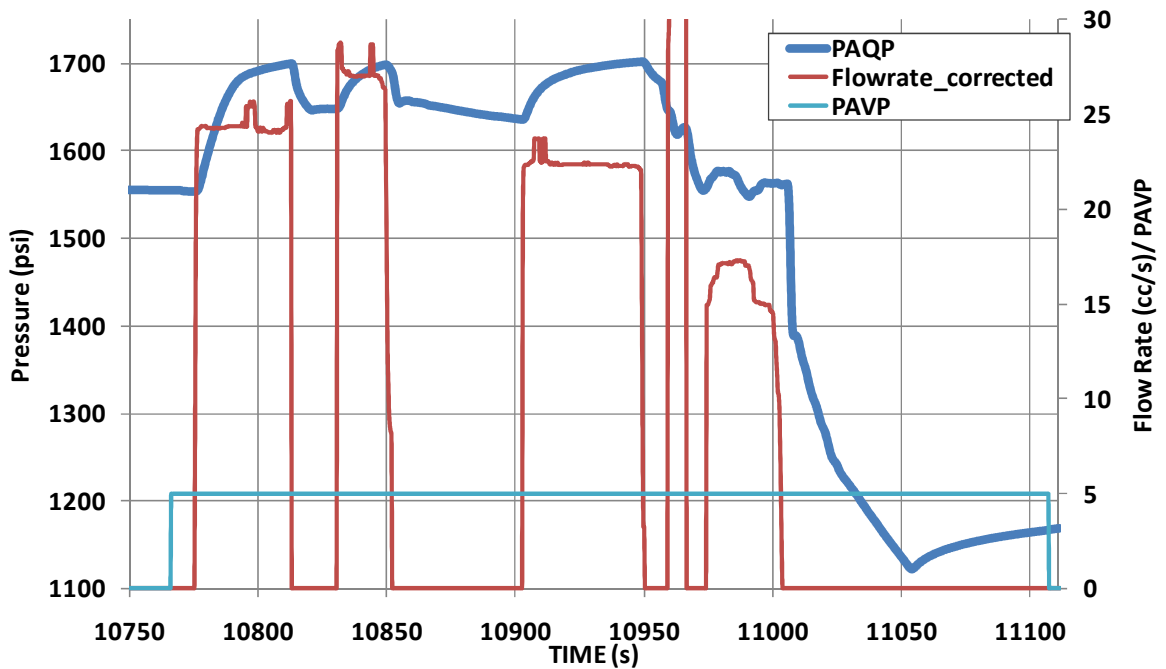

Figure 5.73: Interval pressure (PAQP), flow rate (Flowrate_corrected), and interval valve position (PAVP) during injection phase of Cycle 6.
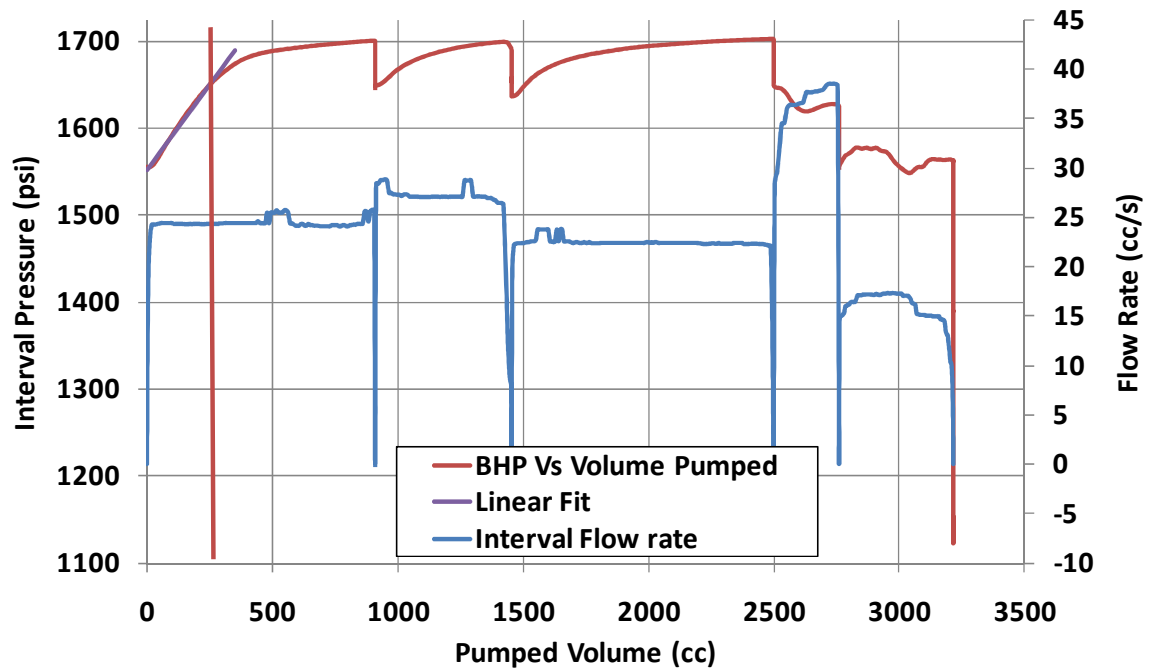
Figure 5.74: Plot of interval pressure vs. pumped volume during Cycle 6 (red curve). A linear fit to this curve shown in purple. The volume at which the curve departs from linearity shown by orange vertical line. The flow rate into the interval (blue curve) is shown referenced to the right hand vertical axis.

5.2.10 Rebound Test (Event 1)

Figure 5.75 shows data from the rebound test and the preceding cycle (Cycle 6). During evacuation of the fluid from the interval, the pressure dropped to a minimum value of 1123 psi at which point the pump was stopped. This minimum value is well above the initial pressure of the mud column (1035 psi). After pumping ceased the pressure climbed quickly at first and then more slowly towards the end of the shut-in period. The pressure can only climb in this manner as a result of fluid supplied to the wellbore by the fracture. Moreover if the packers were not sealing properly, the pressure would tend to fall to the hydrostatic pressure in the mud column rather than rise. Thus the rebound phenomenon provides confidence that a fracture exists and that the packers are sealing properly. At the end of the shut-in period the pressure was still climbing slowly. A rough estimate of the asymptotic value approached by the interval pressure is 1210 psi. This constitutes a lower bound on the closure pressure.
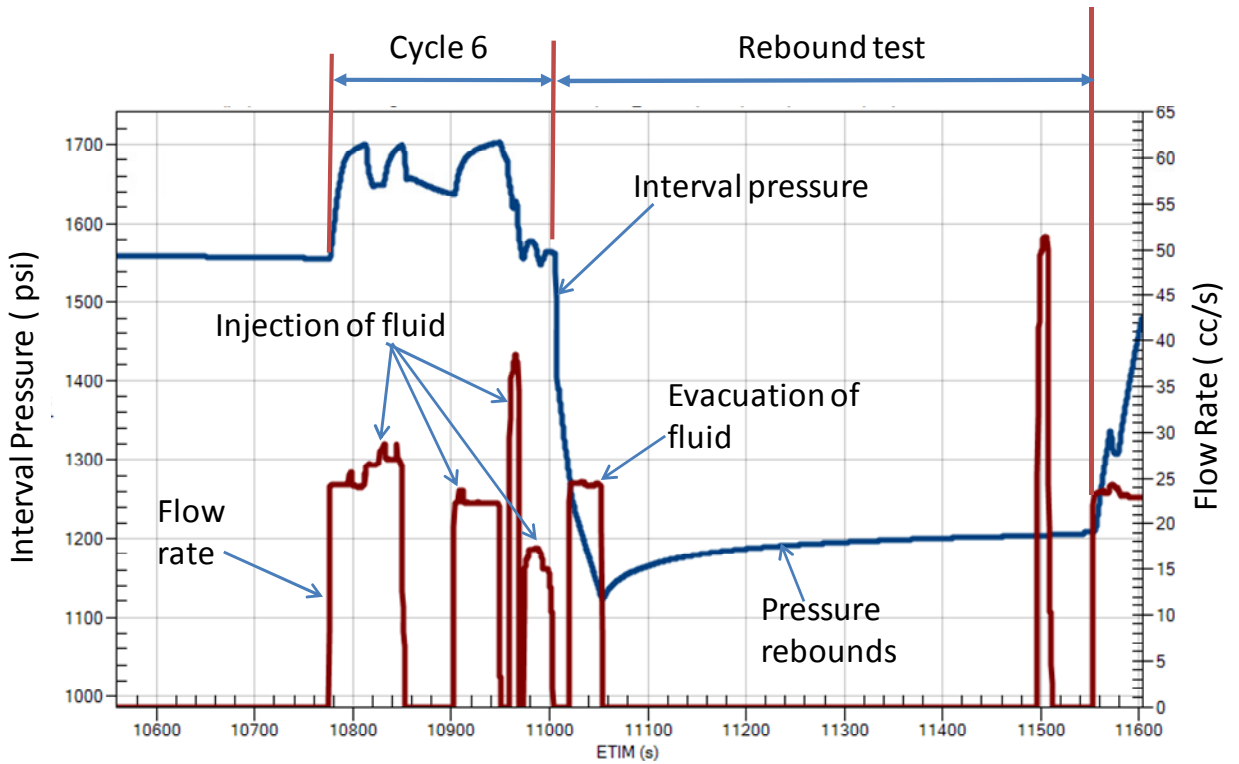
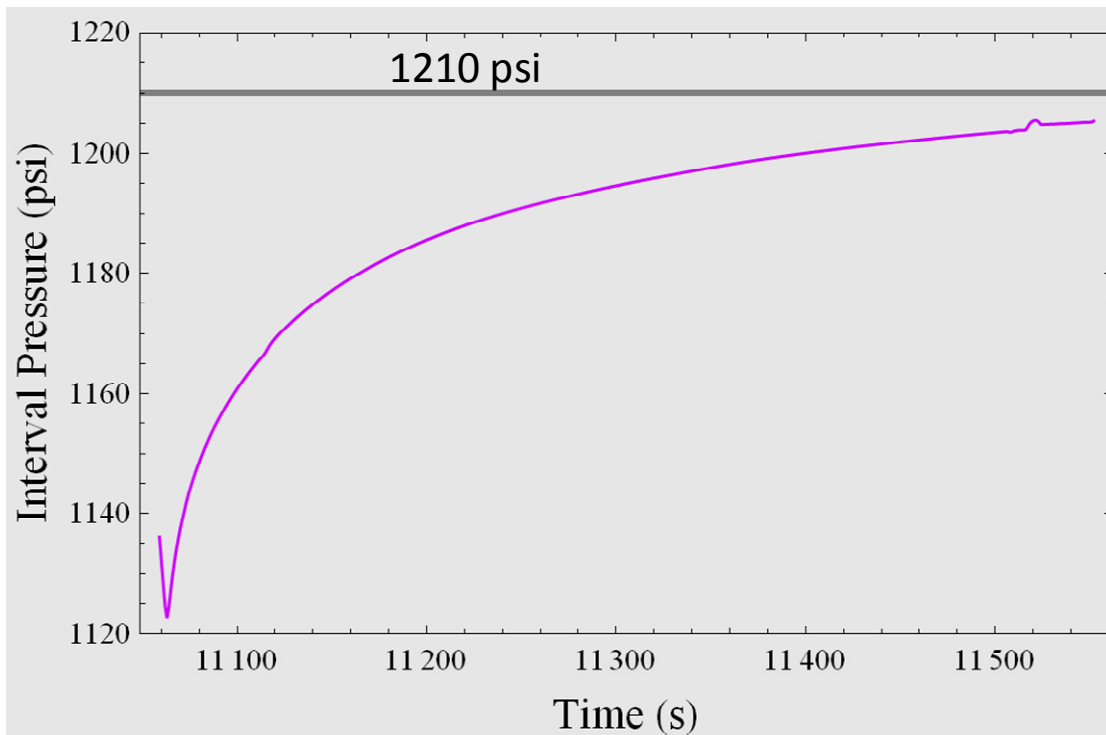**Figure 5.75: Cycle 6 followed by Rebound Test.**

Figure 5.76: Plot of interval pressure (red curve) versus time during rebound test (Event 1). Grey horizontal line represents approximate asymptotic value of the pressure (1210 psi).

Schlumberger

5.2.11 Cycle 7

Figures 5.77 and 5.78 show the raw data from Cycle 7. Injection occurred over a period of approximately 300 s and the pump half-stroked several times (Figure 5.77) causing the interval pressure to dip (Figure 5.78). Figure 5.79 shows a plot of interval pressure versus pumped volume. A subtle change of slope occurs at 1552 psi, however this value is much lower than the fracture reopening pressure recorded in preceding and subsequent cycles. Consequently, fracture reopening was interpreted to occur at a much higher pressure of 1680 psi. Figure 5.80 shows pressure vs. square root of time during the shut-in phase. The fracture appears to close at 1632 psi. An alternative construction using the G-function yields a closure pressure of 1627 psi (Figure 5.81). Table 5.16 summarizes the principal results of this cycle.

Table 5.16: Cycle 7 Results

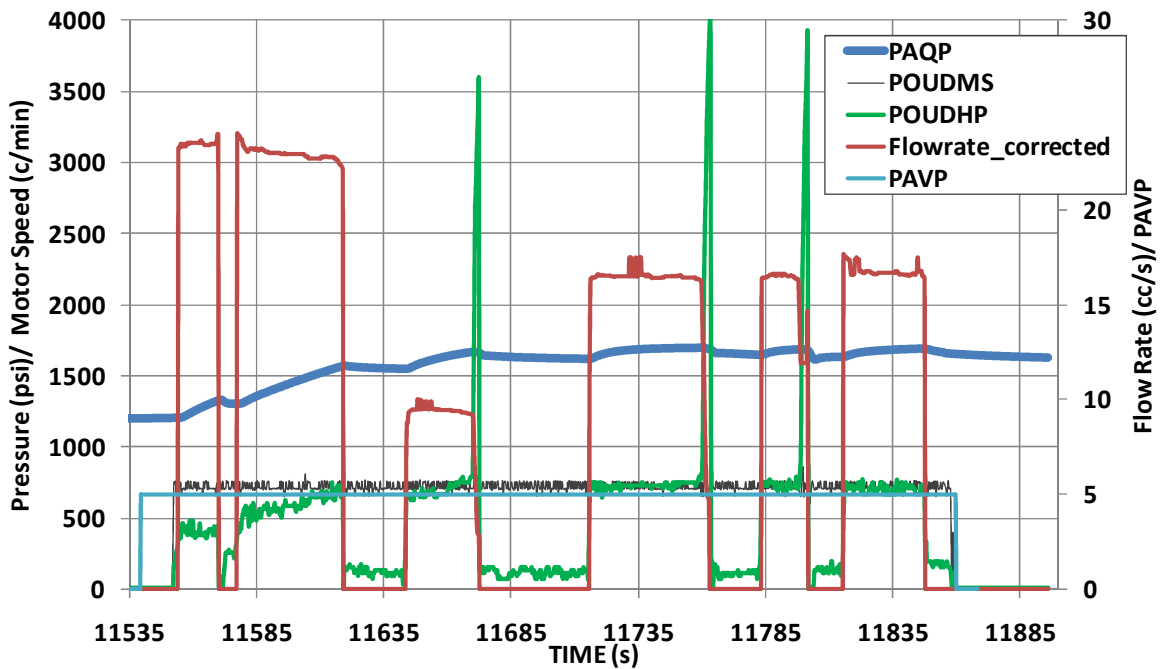| Stiff (psi/cc)	LOP (psi)	LOV (cc)	VL_frac (cc)	Peak_P (psi)	Prop_P (psi)	ISIP (psi)	P_clos (psi)	P_clos_G-function (psi)
0.2795	1680	1710	1490	1699.34	1695.2	1693	1631.9	1627

Figure 5.77: Raw data from Cycle 7. Interval pressure (PAQP), pump motor speed (POUDMS), pump hydraulic pressure (POUDHP), flow rate (Flowrate_corrected), and interval valve position (PAVP) are shown.

Figure 5.78: Interval pressure (PAQP), flow rate (Flowrate_corrected), and interval valve position (PAVP) during injection phase of Cycle 3.

Figure 5.79: Plot of interval pressure vs. pumped volume during Cycle 7 (red curve). A linear fit to this curve shown in purple. The volume at which the curve departs from linearity shown by orange vertical line. The flow rate into the interval (blue curve) is shown referenced to the right hand vertical axis.

Figure 5.80: Plots of interval pressure (red curve) and its derivative (purple curve) versus square root of shut-in time.
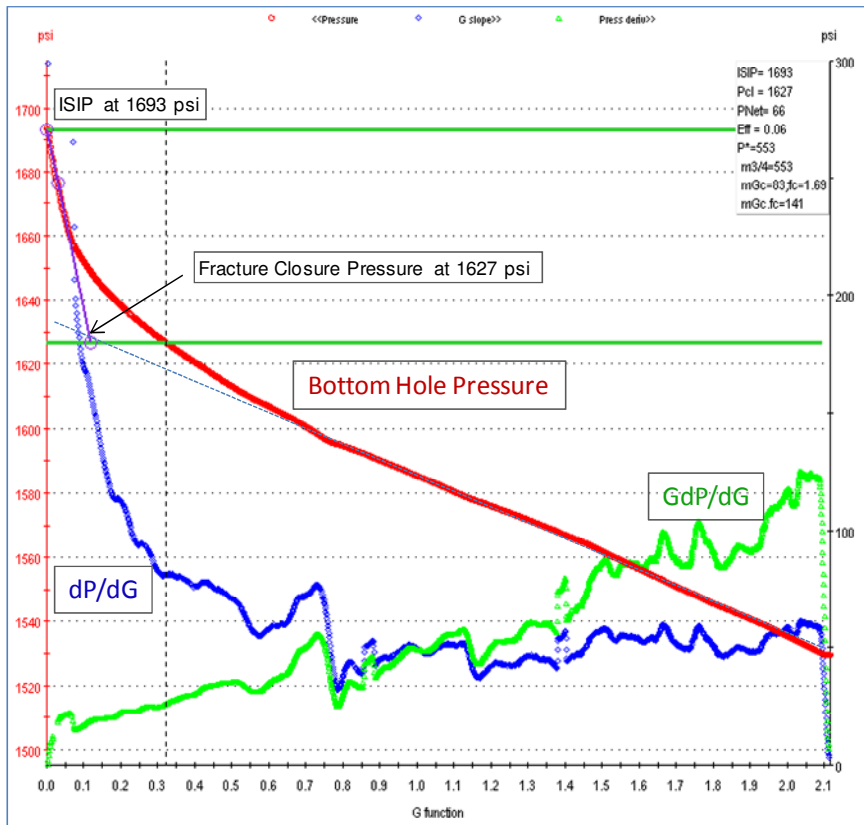
Figure 5.81: Cycle 7-Depth 2-G-Function Interpretation.

5.2.12 Cycle 8

Figures 5.82 and 5.83 show the raw data for Cycle 8. Injection occurred over a period of approximately 280 s and the pump half-stroked several times (Figure 5.82) causing the interval pressure to dip (Figure 5.83). Figure 5.84 shows a plot of interval pressure versus pumped volume. The fracture reopened at 1641 psi. Figure 5.80 shows pressure vs. square root of time during pressure relaxation. The fracture appears to close at 1622 psi. An alternative construction using the G-function yields a closure pressure of 1640 psi (Figure 5.86). Table 5.17 summarizes the principal results of this cycle.

Table 5.17: Cycle 8 Results

Stiff (psi/cc)	LOP (psi)	LOV (cc)	VL_frac (cc)	Peak_P (psi)	Prop_P (psi)	ISIP (psi)	P_clos (psi)	P_clos_G-function (psi)
0.8349	1640.7	163.21	1672.9	1689.5	1687.58	1696	1622.4	1640
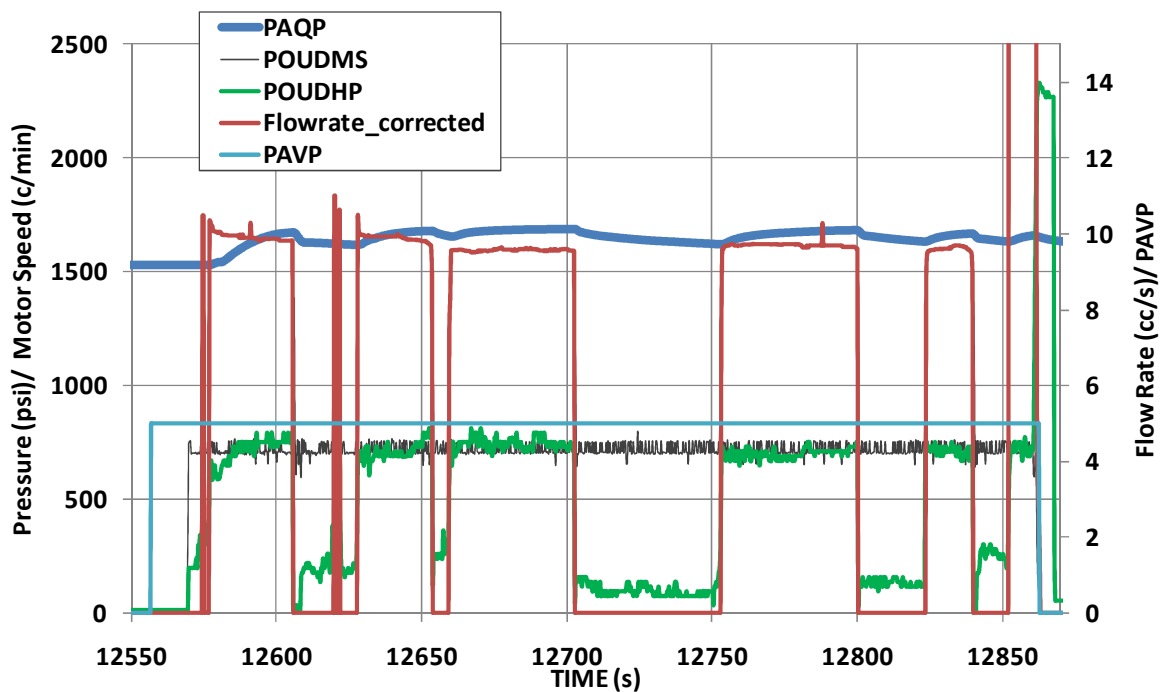
Figure 5.82: Raw data from Cycle 8. Interval pressure (PAQP), pump motor speed (POUDMS), pump hydraulic pressure (POUDHP), flow rate (Flowrate_corrected), and interval valve position (PAVP) are shown.
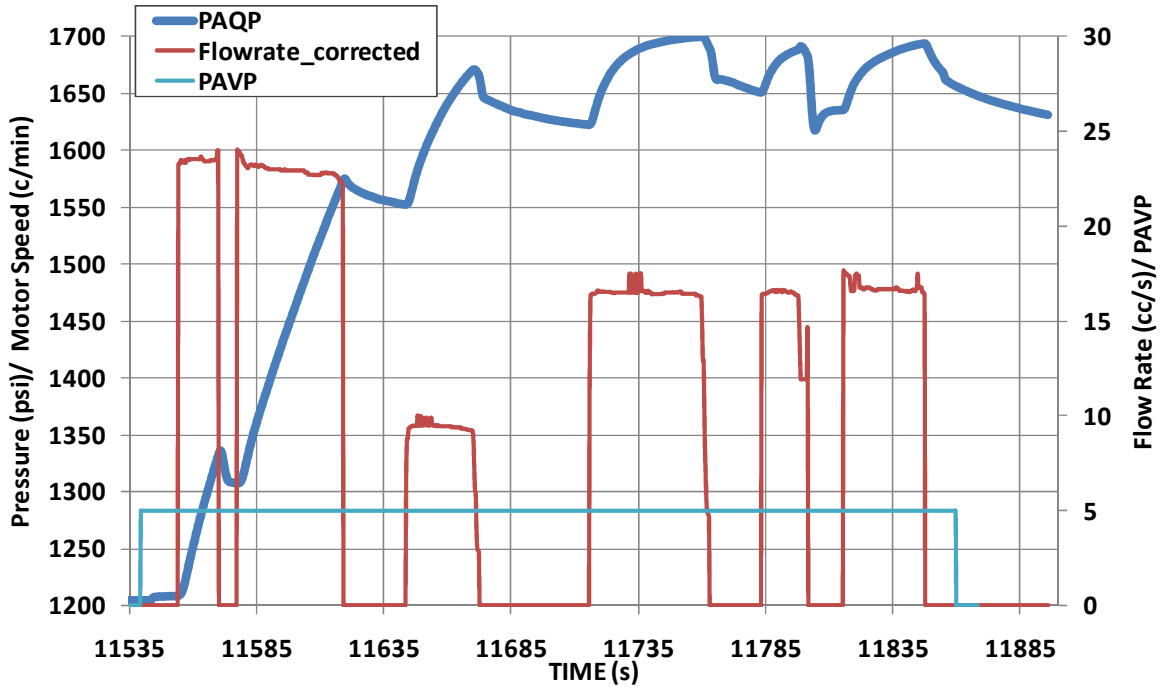
Figure 5.83: Interval pressure (PAQP), flow rate (Flowrate_corrected), and interval valve position (PAVP) during injection phase of Cycle 8.
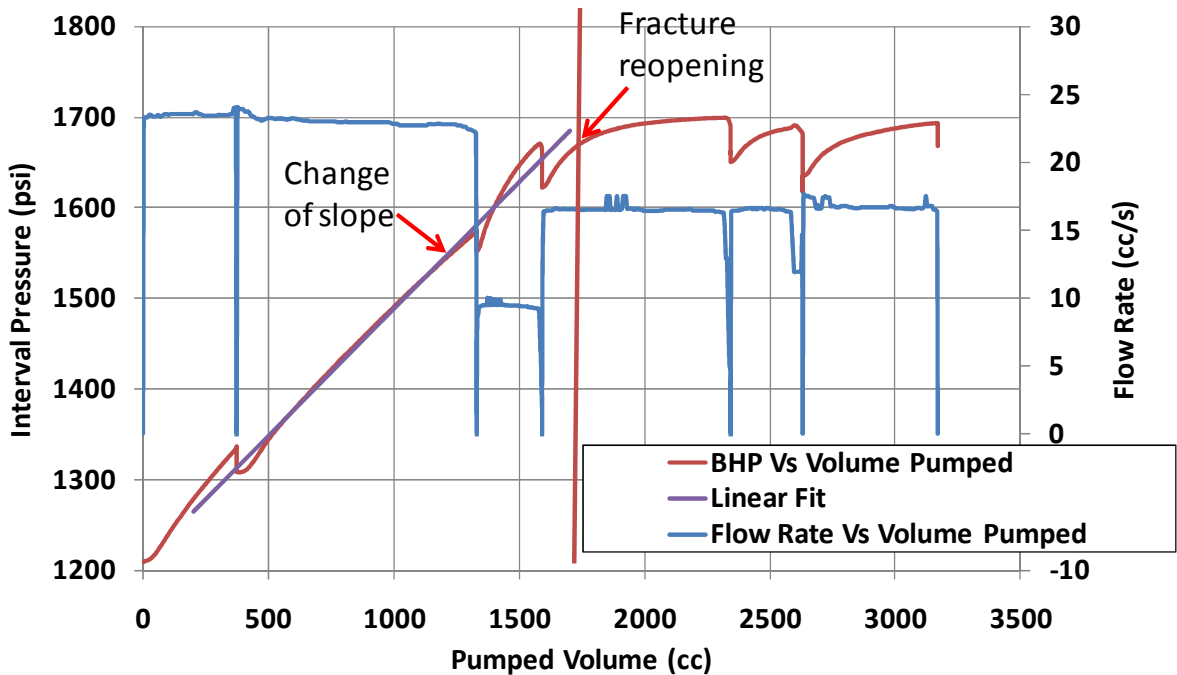

Figure 5.84: Plot of interval pressure vs. pumped volume during Cycle 8 (red curve). A linear fit to this curve shown in purple. The volume at which the curve departs from linearity shown by orange vertical line. The flow rate into the interval (blue curve) is shown referenced to the right hand vertical axis.
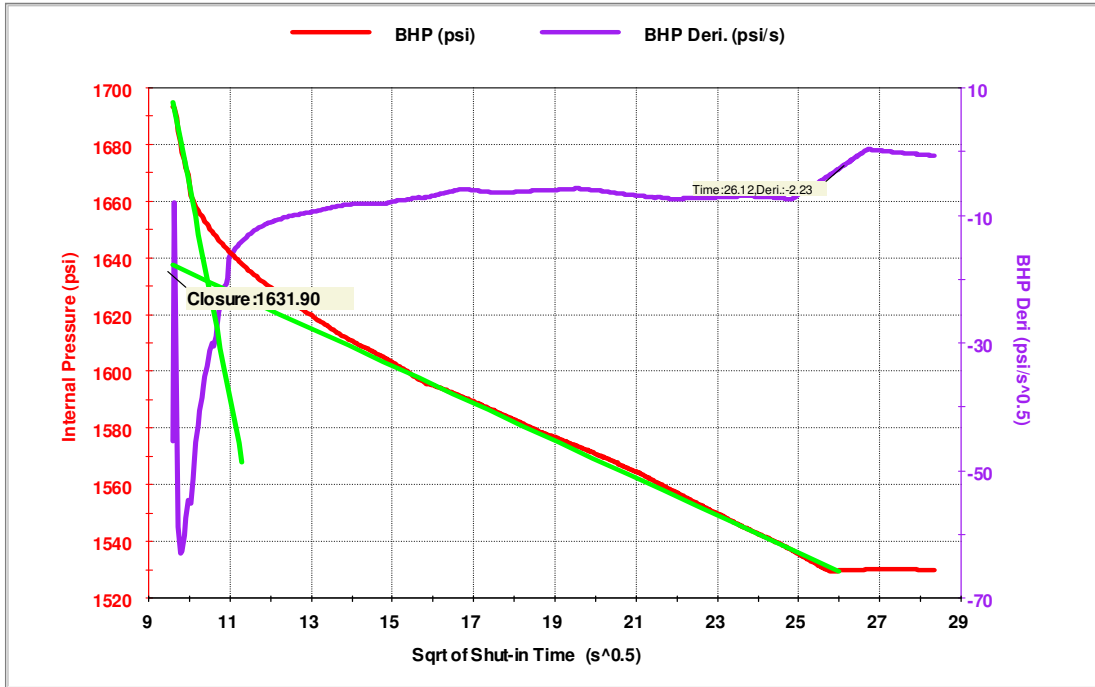
Figure 5.85: Plots of interval pressure (red curve) and its derivative (purple curve) versus square root of shut-in time.

Figure 5.86: Cycle 8-Depth 2-G-Function Interpretation.

5.2.13 Cycle 9

Figures 5.87 and 5.88 show the raw data for Cycle 9. Injection occurred over a period of approximately 230 s and the pump half-stroked twice (Figure 5.87) causing the interval pressure to dip (Figure 5.88). Figure 5.89 shows the plot of interval pressure versus pumped volume. The fracture reopened at 1580 psi. Figure 5.90 shows pressure vs. square root of time during the shut-in phase. The fracture appears to close at 1608 psi. The G-function however did not yield a definitive closure pressure (Figure 5.91). Table 5.18 summarizes the principal results of this cycle.

Table 5.18: Cycle 9 Results

| Stiff (psi/cc)	LOP (psi)	LOV (cc)	VL_frac (cc)	Peak_P (psi)	Prop_P (psi)	ISIP (psi)	P_clos (psi)	P_clos_G-function (psi)
0.3112	1580	508.25	1261	1675.8	1674.3	1655	1608.1	N/A
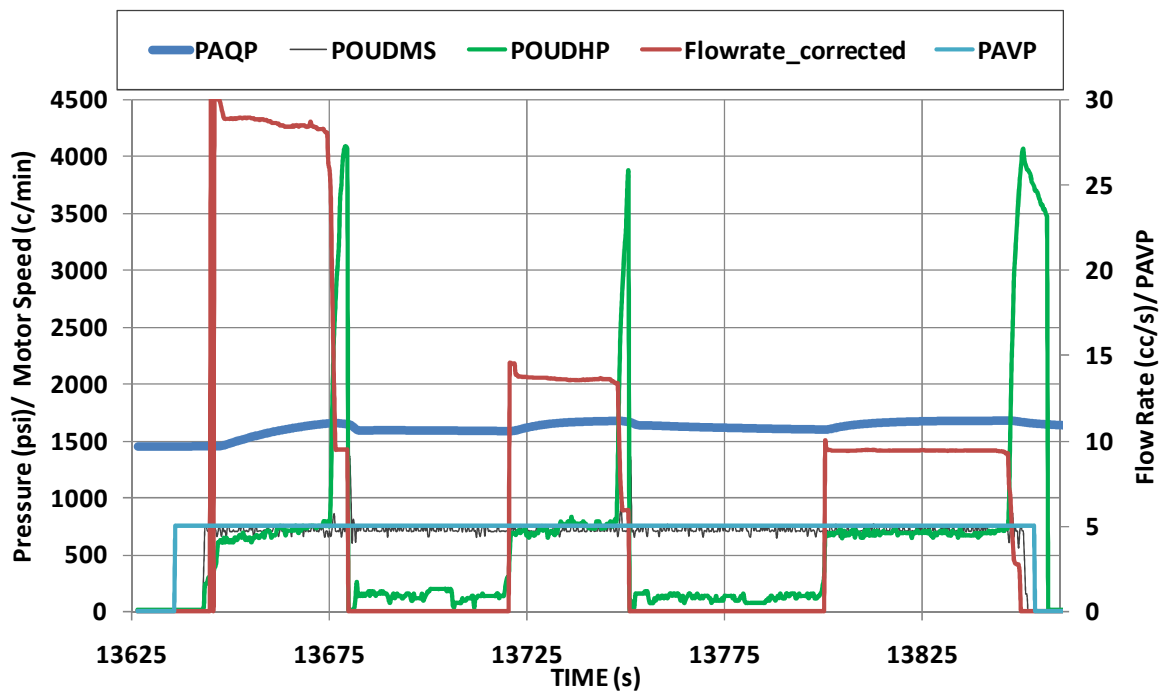
Figure 5.87: Raw data from Cycle 9. Interval pressure (PAQP), pump motor speed (POUDMS), pump hydraulic pressure (POUDHP), flow rate (Flowrate_corrected), and interval valve position (PAVP) are shown.
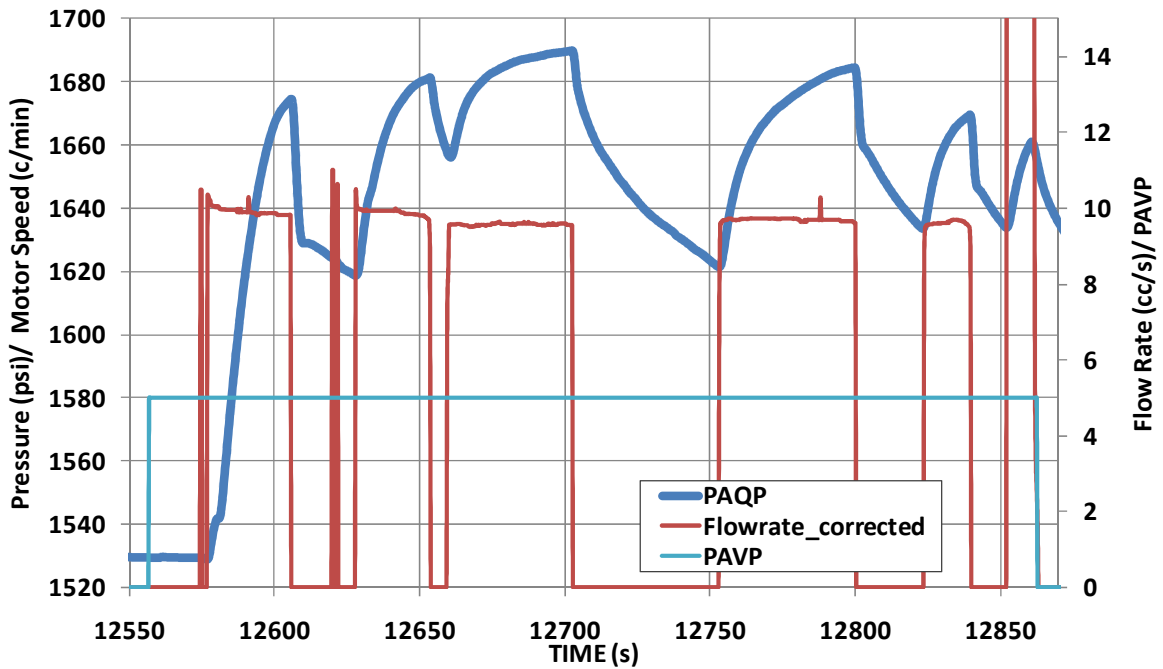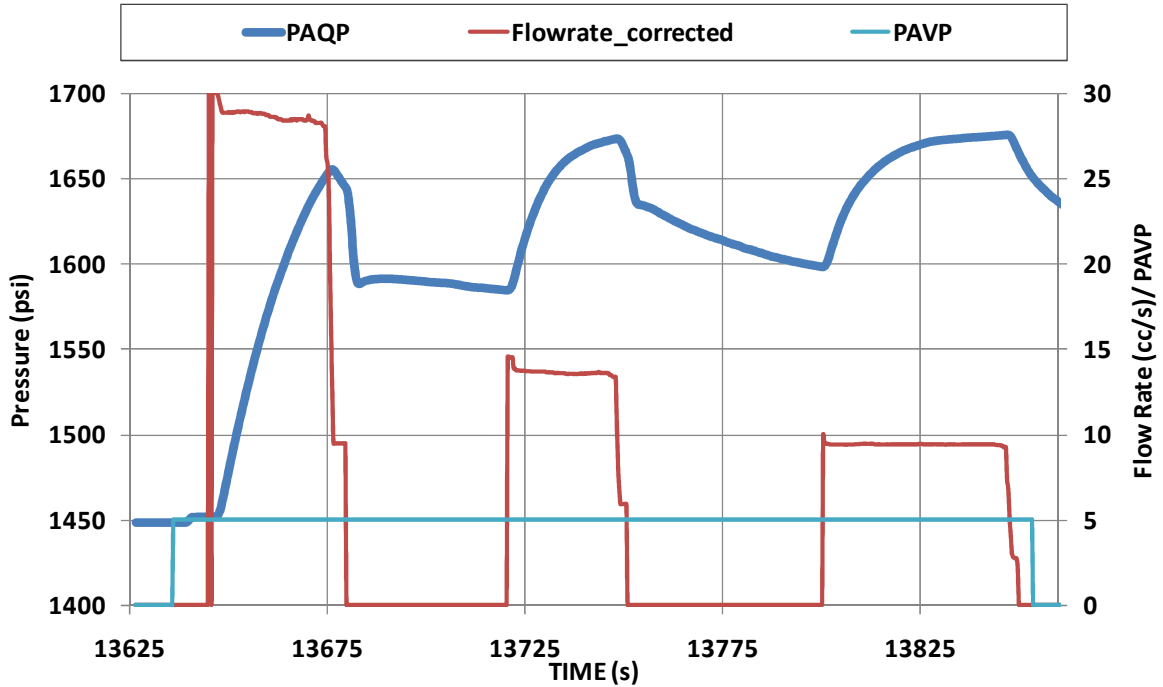
Figure 5.88: Interval pressure (PAQP), flow rate (Flowrate_corrected), and interval valve position (PAVP) during injection phase of Cycle 9.
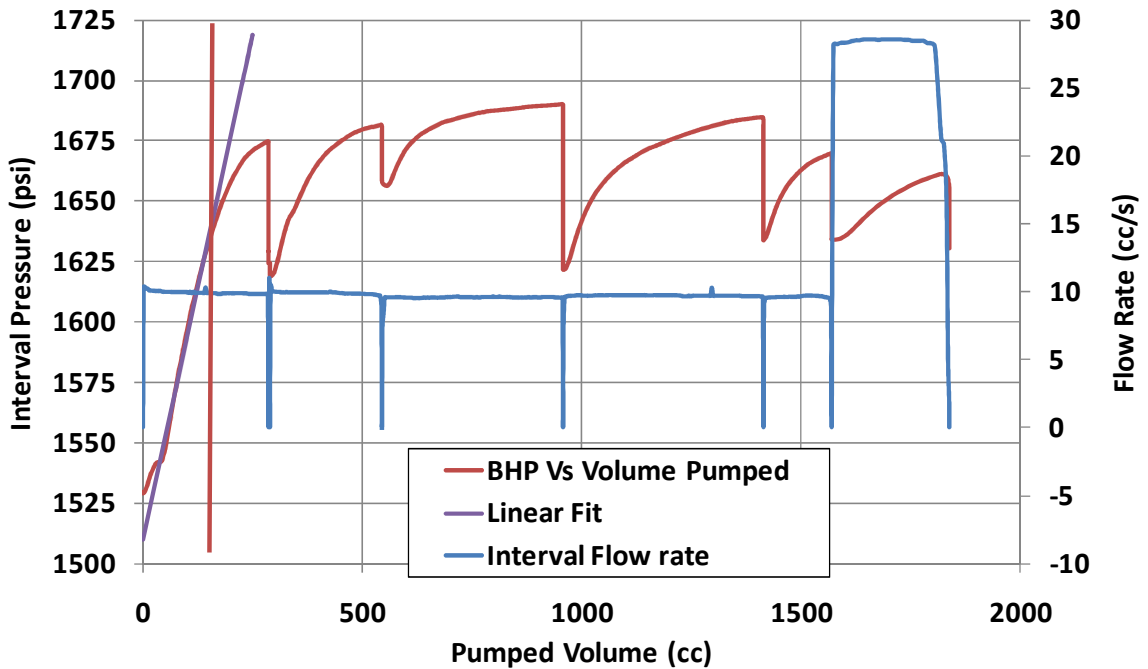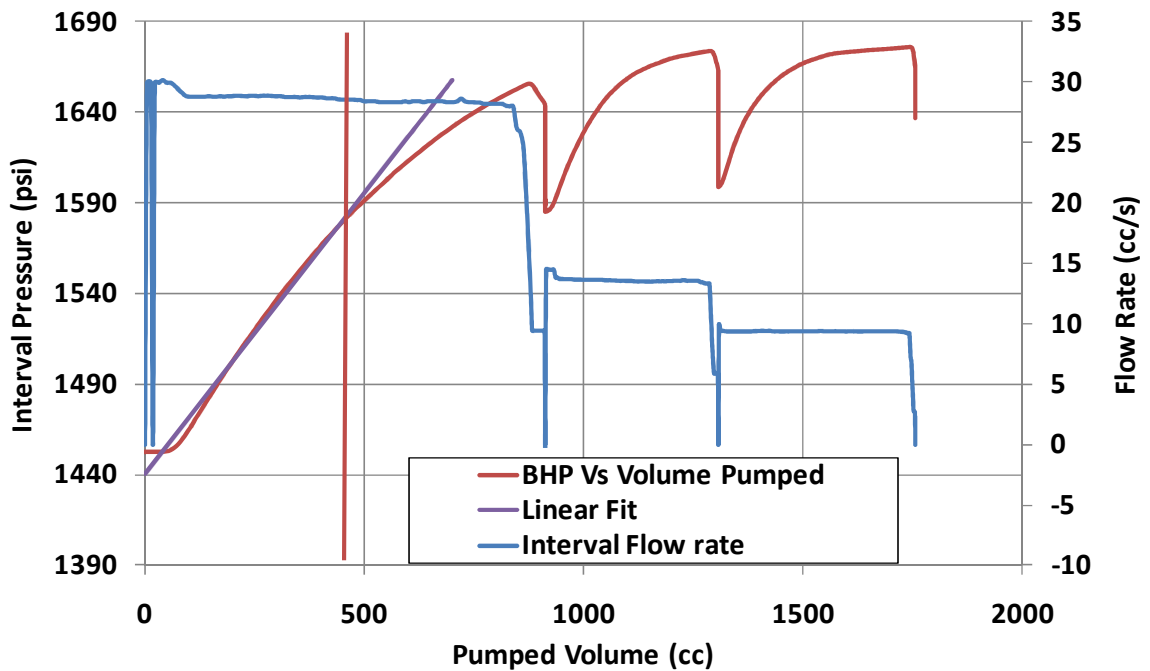

Figure 5.89: Plot of interval pressure vs. pumped volume during Cycle 3 (red curve). A linear fit to this curve shown in purple. The volume at which the curve departs from linearity shown by orange vertical line. The flow rate into the interval (blue curve) is shown referenced to the right hand vertical axis.
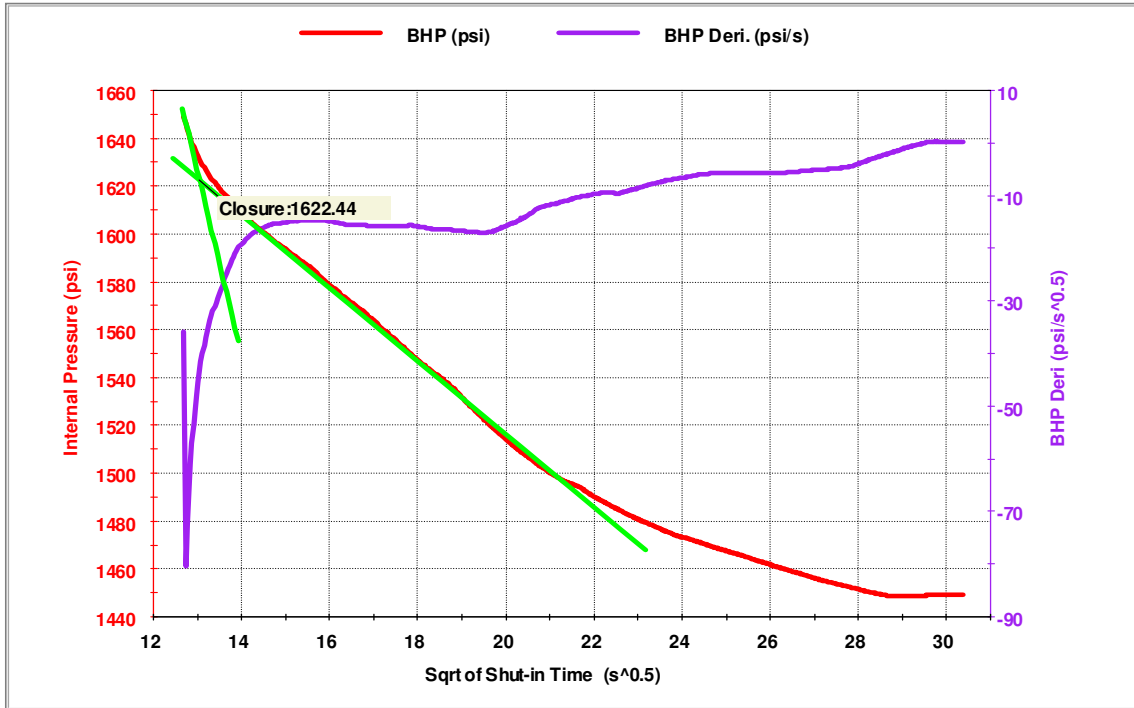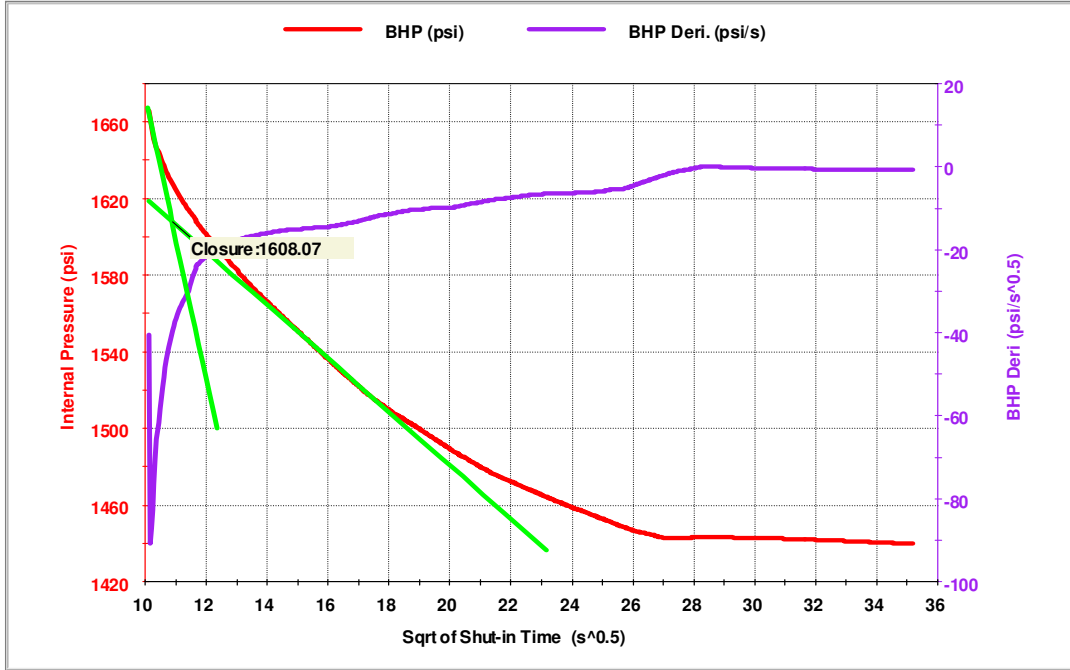
Figure 5.90: Plots of interval pressure (red curve) and its derivative (purple curve) versus square root of shut-in time.
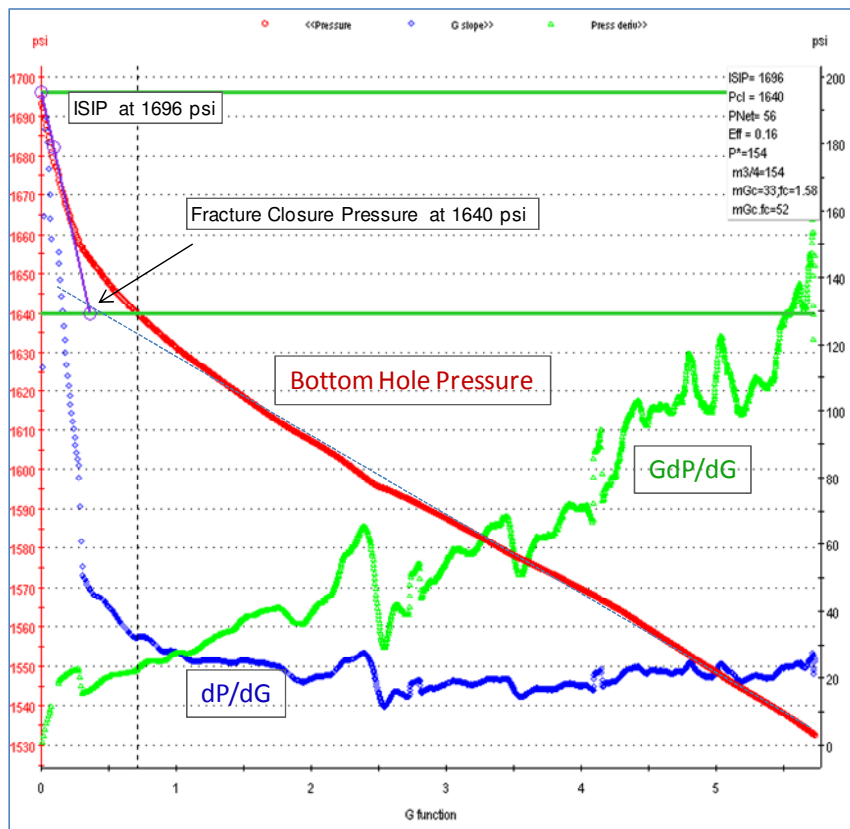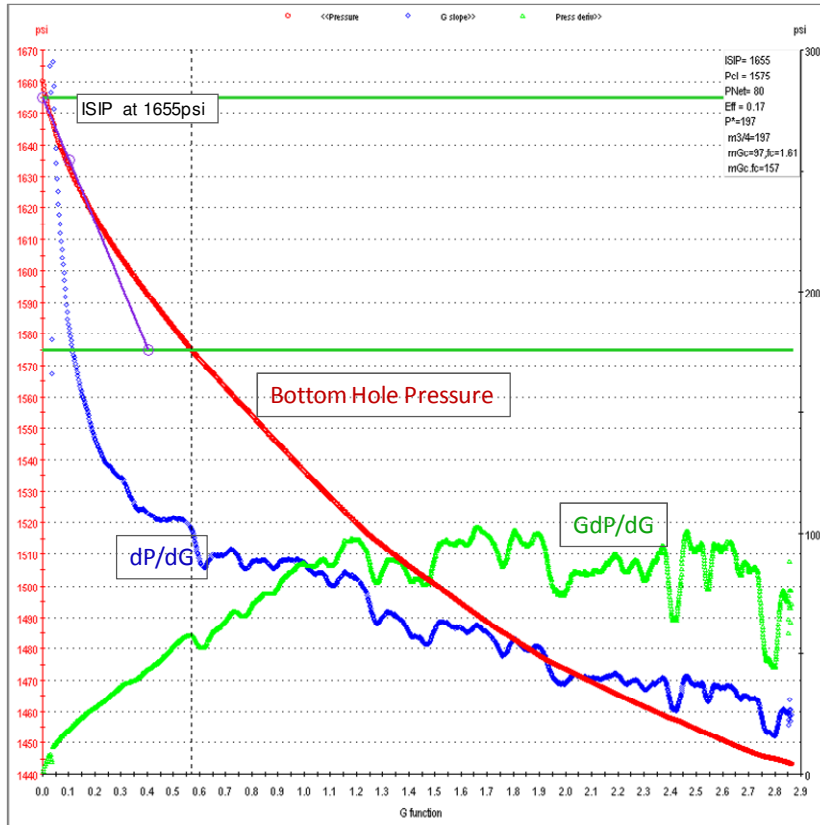

Figure 5.91: Cycle 9-Depth 2-G-Function Interpretation.

Figure 5.92 shows a reconciliation plot summarizing key diagnostic information from all Events and Cycles. The closure pressures ascertained using square root of time plots (magenta triangles) and G-plots (brown triangles) are generally bounded above by the peak pressures (green triangles), leak-off pressures (orange triangles), ISIP's (black triangles) and propagation pressures (blue triangles). The sole rebound pressure obtained at the second test station is also shown on the plot. As expected, it provides a lower bound on the closure stress, albeit a wide one. The system stiffness (yellow triangles) varied between 0.26 psi/cc and 1.02 psi/cc and did not exhibit any particular pattern.

It is seen that during injection cycles, the amount of fluid injected into the fracture ranged between 810 cc and 2928 cc (red triangles). A total of 12.8 liters was pumped into the fracture in order to propagate it away from the near-wellbore stress concentration. The objective of escaping the near-well stress concentration appears to have been achieved by Cycle 4. Figure 5.93 shows that from Cycles 4 through Cycle 8, the closure pressures fluctuated around 1625 psi. The leak-off pressure, ISIP and peak stress are also fairly constant over this range of cycles while the propagation pressure appears to decline slowly with cycle. However Cycle 9 departs from the general trend. Pressures extracted during this cycle were somewhat lower than those obtained during preceding cycles. The closure pressure for this cycle identified using a square root of time plot was 1608 psi, but the fact that the G-function did not show any closure throws this interpretation into doubt. The reopening pressure for this cycle was also well below the trend established during previous cycles. It is possible that the fracture may have penetrated into a lower stress region. Whatever the reason, the results of Cycle 9 will be treated as outliers from the main trend. A value of 1625 psi is the best estimate of the closure pressure away from the near-wellbore stress concentration.
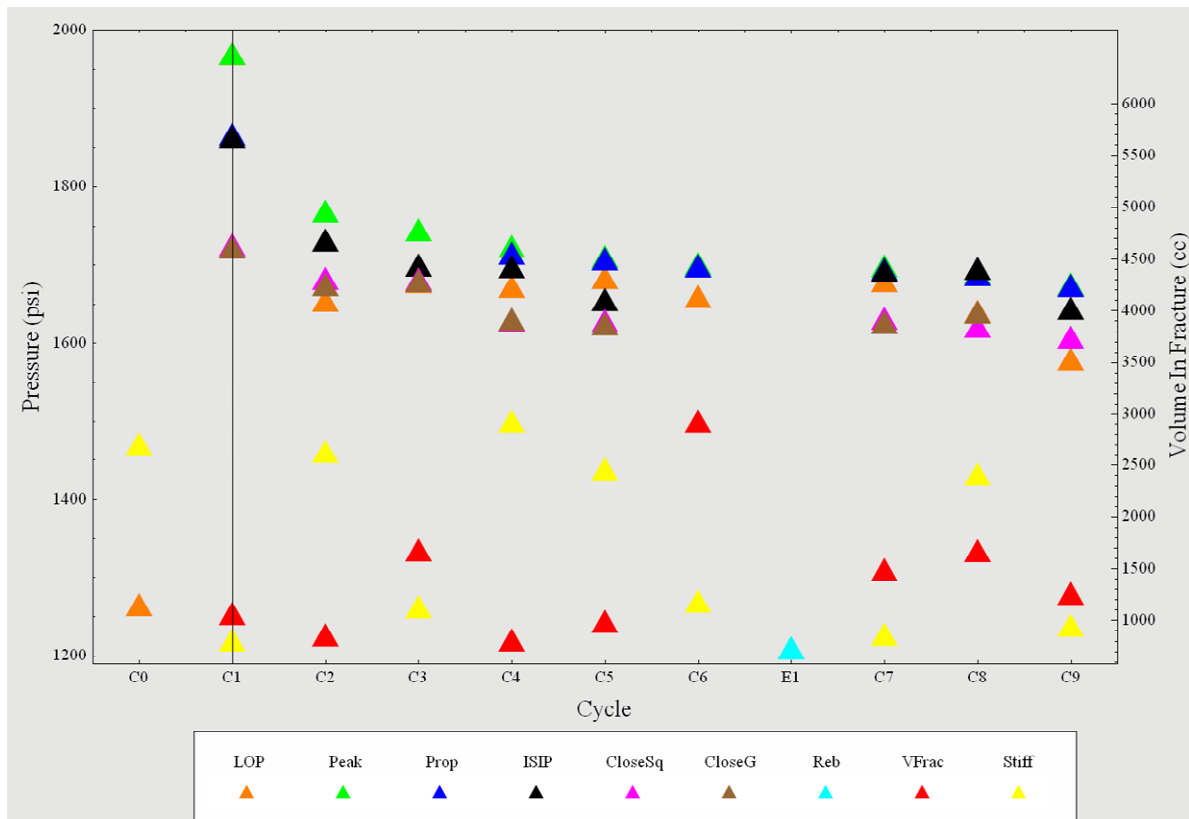
Figure 5.92: Reconciliation Plot at Test Station 2.
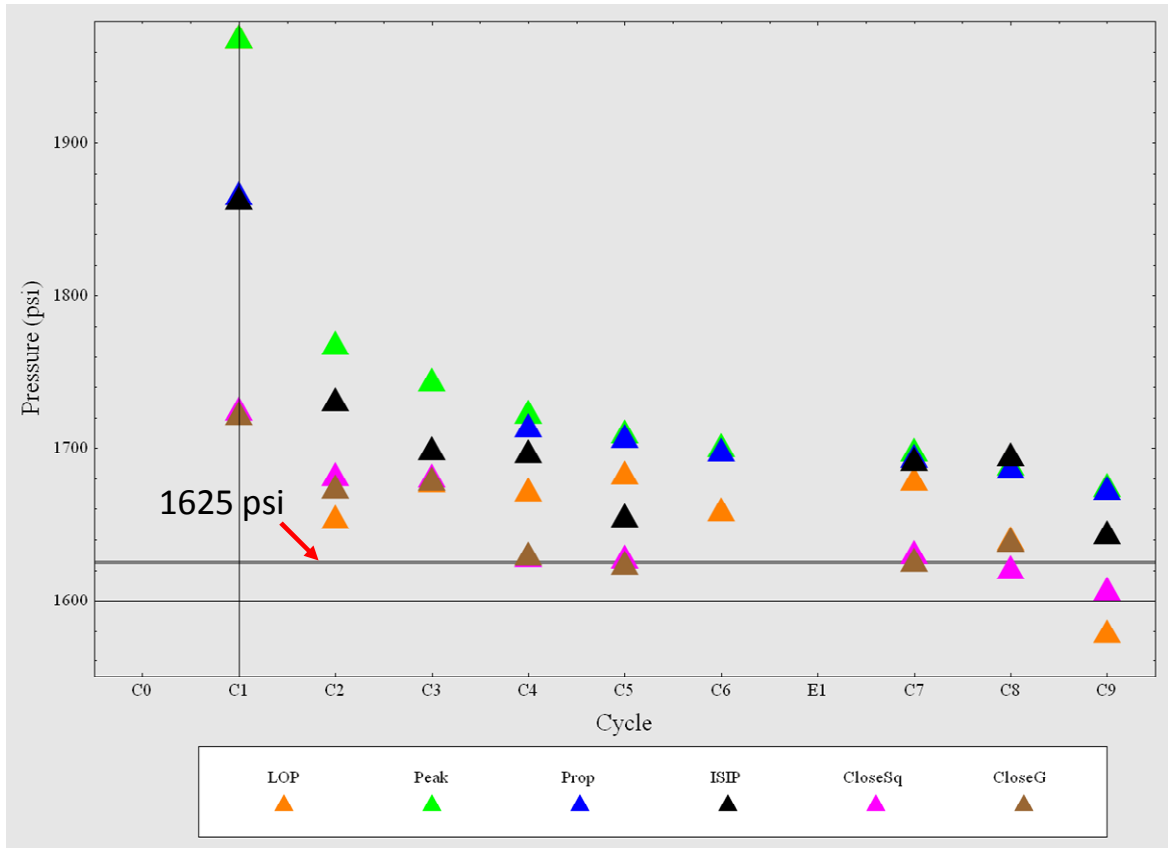
Figure 5.93: Reconciliation Plot at Test Station 2. Pressures only.

6 CONCLUSIONS

❑ The best estimate of the minimum principal stress at 2071.95 ft MD is 1364 psi, equivalent to 12.7 ppg.

❑ The best estimate of the minimum principal stress at 2202.58 ft MD is 1625 psi, equivalent to 14.2 ppg.

❑ Since the inferred minimum principal stresses are much less than typical estimates of overburden pressure, these stresses are most likely equal to the minimum far-field horizontal stresses at their respective depths.

❑ Half-stroking of the pumps complicated the interpretation of fracture reopening and propagation pressures. However it did not affect interpretation of the closure stress.

❑ Some leakage through the packers did occur at both stations. However this leakage was of very limited duration and did not have a detectable impact on the most decisive, latter stages of these tests.

❑ Significant leak-off rates were observed at both test stations suggesting that permeability was not negligible.

❑ Evidence of filtercake formation was seen in the form of below gauge caliper measurements, twin breakdown peaks, and a marked decrease in leak-off rates with time.

Schlumberger

7 APPENDIX A

7.1 MDT micro-fracturing operational procedure

MDT micro-fracturing configuration

The MDT (Modular Dynamics Tester) represents the latest generation of wireline formation testers and it consists of a series of modules, each designed to perform specific functions, which can be configured for the desired objectives. The MDT tool is controlled in real time by software commands from the logging unit during the entire test sequence.

Basic MDT micro-frac configuration is with Dual Packer and Pumpout modules:

- Dual Packer Module: The Dual Packer Module has two rubber straddle packers that allow one meter section of wellbore to be isolated. The Dual Packer Module is equipped with a dual system of sensors (Strain Gauge and CQG* Crystal Quartz Gauge) to measure pressure in the tested interval in real time. The pressure in the packers is also monitored for quality control. When the test is complete the packers can be deflated and the tool string can be moved to another test interval.
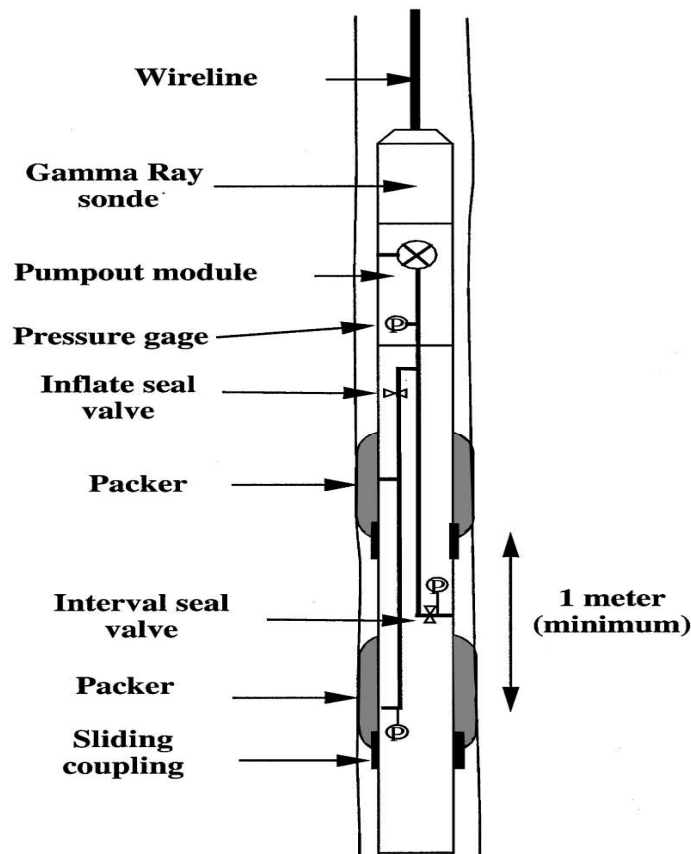
Basic MDT micro-frac configuration schematic

- Pumpout Module: The Pump-out Module is used to inflate the rubber elements of the Dual Packer Module and to pressurise the test interval to create the hydraulic fracture. Due to the fact that the pump is downhole, wellbore storage effects are limited.

Standard MDT micro-fracturing procedure

Packer Inflation: once the tool has been properly positioned, the interval to be tested is isolated by inflating the straddle packer arrangement until the pressure in the interval starts to rise. The subsequent pressure decline is then observed to check the quality of the packer seal. Packers are further pressurized if the seal is not satisfactory.

Leak-Off Cycles: a series of increasing pressure steps to a level well below the formation breakdown is performed, in order to test that the packer seal is holding and also to test the fluid leak off into the formation.
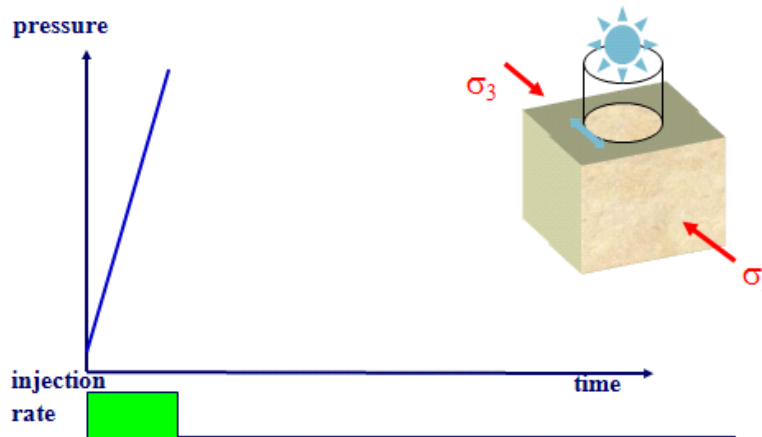
Hydraulic Fracturing: fluid is again injected into the interval at a constant flow rate and up to the initiation of a tensile fracture. Fracture initiation is recognized either by a breakdown or by a pressure plateau. The fracture is then extended for 1 to 5 minutes before the interval is isolated and the pump stopped.
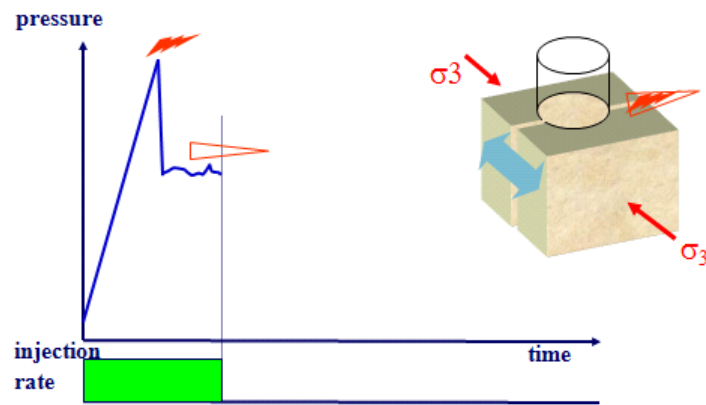
Fall-off: When the pump is stopped the pressure is allowed to fall-off to a pressure level that ensures that the fracture is closed. In low permeability formations, fracture closure may take a long time due to low fluid filtration, and as contingency, a Flow Control Module can be used to withdraw the fluid at a low, constant rate in order to close the fracture and obtain a fall off curve that can be analyzed.
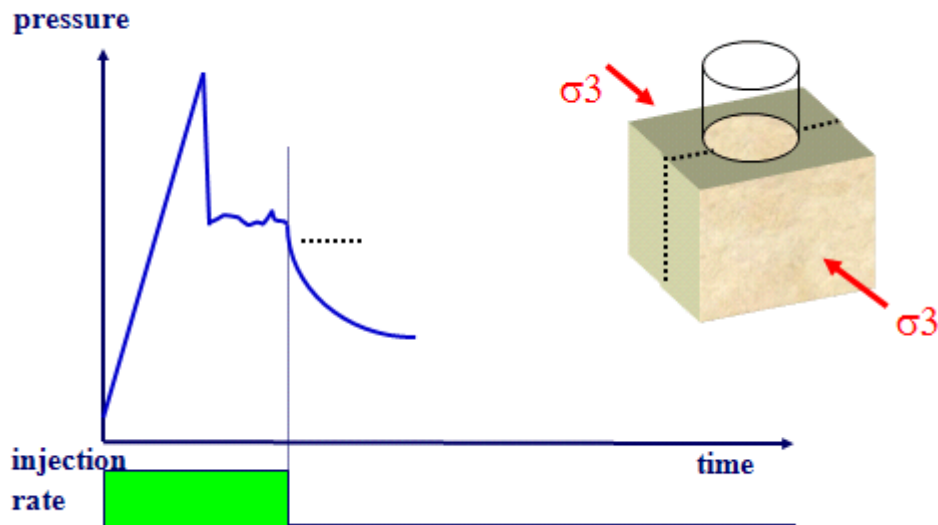
Fracture Reopening, Propagation, Fall-off Cycles: A series of such injection/falloff cycles followed by reopening, further propagation, and closure of the fracture are instigated to check that the test is repeatable and possibly change the injection parameters (flow rate and injected volume).
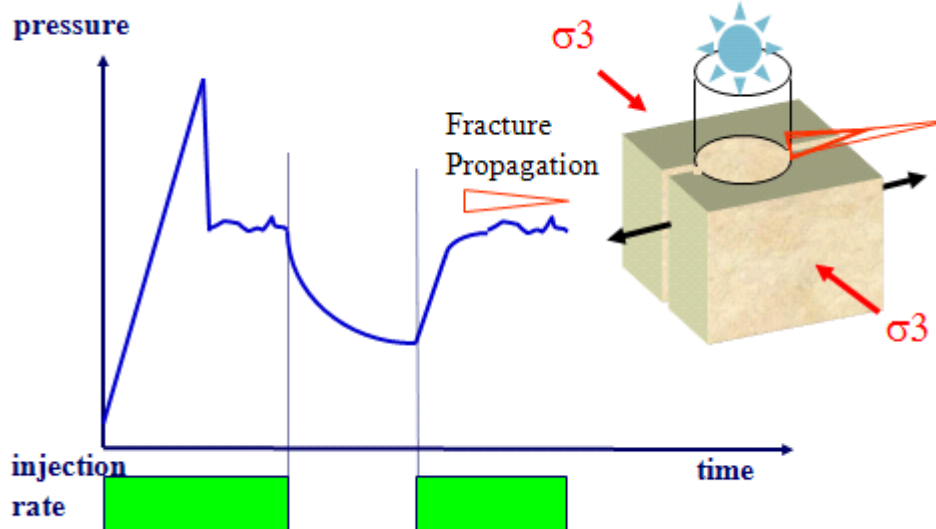
Packer Deflation: Once the operator and reservoir domain expert is satisfied that good quality data were acquired, packers are deflated and the tool is moved to the next interval.

A typical micro-frac test comprises of 2 to 5 injection/propagation/fall-off cycles, and it can usually take from 1 to 3 hours.

Alternate MDT micro-frac procedures

Sleeve Fracturing: if the mud cake is nearly impermeable, or if the formation itself is nearly impermeable, the classic procedure may lead to fracture initiation under the packer elements and premature failure of the test. This situation can be easily recognized during the leak-off cycles, with no pressure decline observed. Experience shows that a mud with an API leak-off parameter of less than 2.5 ml/30 min will form a mudcake that is impermeable for MDT stress test purposes.

In such cases a sleeve fracturing procedure can be followed: fluid is pumped at a constant rate into one of the packers up to the maximum allowable inflatable pressure. This may result in initiation of a stable fracture. The packer can then be deflated and the tool positioned so that the interval is at the level of the created fracture. This procedure ensures that fracture extension will start at the interval level. The traditional procedure can then be applied: packer inflation, leak-off cycles, and hydraulic fracturing cycles.

Flowback/Pressure Rebound: when injection is stopped, fluid can be quickly withdrawn from the fracture to close it in the vicinity of the wellbore only (the remainder of the fracture stays pressurized above the closure stress, and hence, remains open). Fluid withdrawal is then stopped so that the fracture produces back to the wellbore, resulting in a pressure rebound. A rebound to a pressure level much higher than the mud pressure is a good indicator that a hydraulic fracture has indeed been created and it can provide a lower bound on the minimum stress, if the rebound procedure has been correctly followed.

MDT micro-fracturing interpretation methodology

Stress test interpretation is carried out analyzing each hydraulic fracturing cycle and determining, if possible, the following parameters: breakdown pressure, propagation pressure, instantaneous shut-in pressure (ISIP), closure pressure, reopening pressure and rebound pressure. This is followed by a "reconciliation phase" where all quantities for all cycles are considered together, to determine the consistency of the data and the magnitude of minimum stress.

The *Breakdown pressure* is the pressure at which the fracture is created. It is characterized by a sharp pressure drop while fluid is flowing into the interval.

If fluid injection is maintained after breakdown the wellbore pressure should stabilize and the fracture propagates continuously. A *Propagation Pressure* can be determined.

Once injection has stopped, the pressure in the wellbore will quickly stabilize to a value called the *Instantaneous Shut-In Pressure* or *ISIP*. The *Closure Pressure* is the pressure at which the fracture closes after injection has stopped. Fluid leak off in the formation or drawdown with a Flow Control will deplete the fluid contained into the fracture. At some point, the fluid pressure in the fracture will equal the opposing *in situ* stress acting on the fracture and the fracture will close. The wellbore pressure at this point is called the *Closure Pressure* and is assumed to be a reliable estimate of the average stress acting on the fracture surface.

To determine closure pressure, the square root plot method is used. Other methods can be found in the literature but this method is quite robust for determining the closure pressure. Plotting interval pressure against the square root of the time since shut-in, the interval pressure will follow a straight line until the fracture is closed. Departure from this linear behavior is taken as the point at which the fracture mechanically closes for the first time, and the pressure value at that point is chosen as an estimate for the closure stress.

The *Reopening Pressure* is the pressure at which a pre-existing fracture opens. This corresponds to a change in the stiffness of the tested interval. Normally it is identified as the point at which the pressure during injection deviates from linearity with respect to the injected volume.

Reconciliation Plot

No single parameter (inferred closure pressure, ISIP, etc.) determined from a single hydraulic fracturing cycle provides a reliable estimate of the actual closure stress. Once each cycle has been analyzed separately, the stress test record should be interpreted in its entirety to determine the best possible estimate of the closure stress. All estimates are plotted for every event along the time axis in a reconciliation plot. A reconciliation plot summarizing events during the test is included below. It makes it possible to check that the fracture has grown away from the influence of the near-wellbore stress. Once the fracture is mostly sensing the far field stresses, estimates of the closure pressure stop varying from one cycle to the next. If no consistency (repeating of the values for a certain parameter like closure stress within a certain range) is found on the reconciliation plot, the data cannot be considered representative and are discarded.
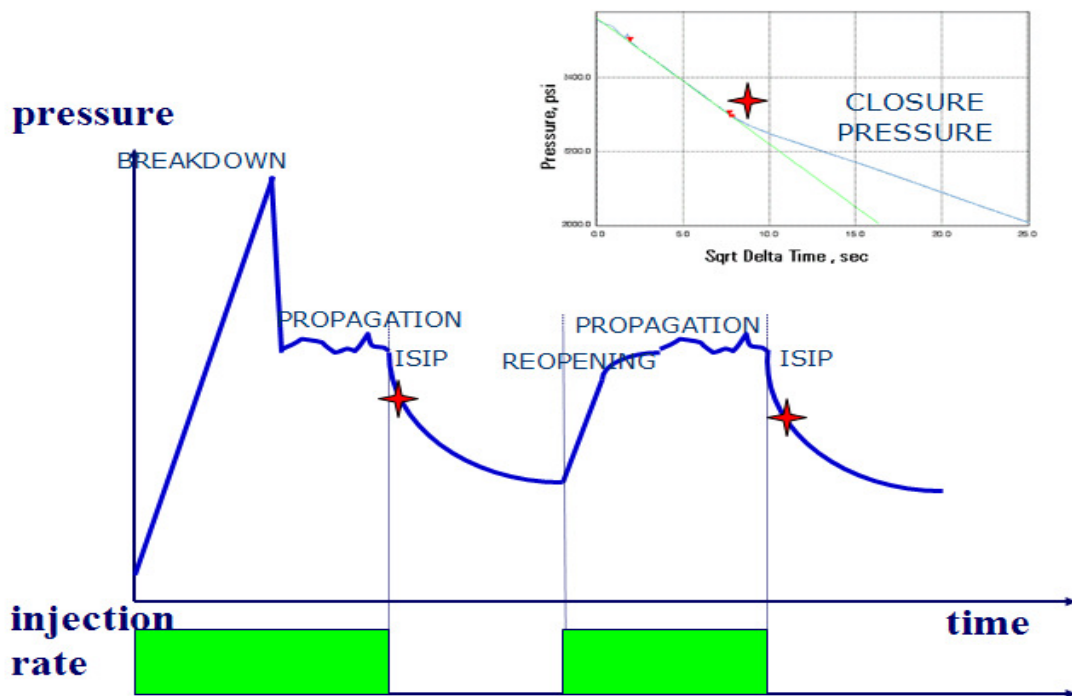
Determination of breakdown pressure, propagation pressure, instantaneous shut-in pressure (ISIP), closure pressure, reopening pressure in MDT micro-frac tests cycles
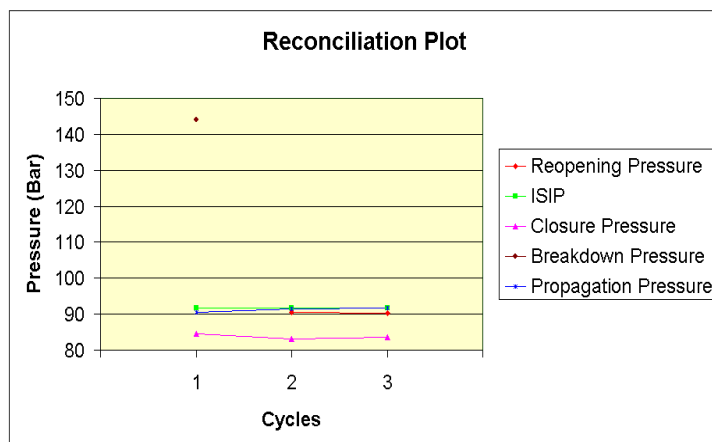
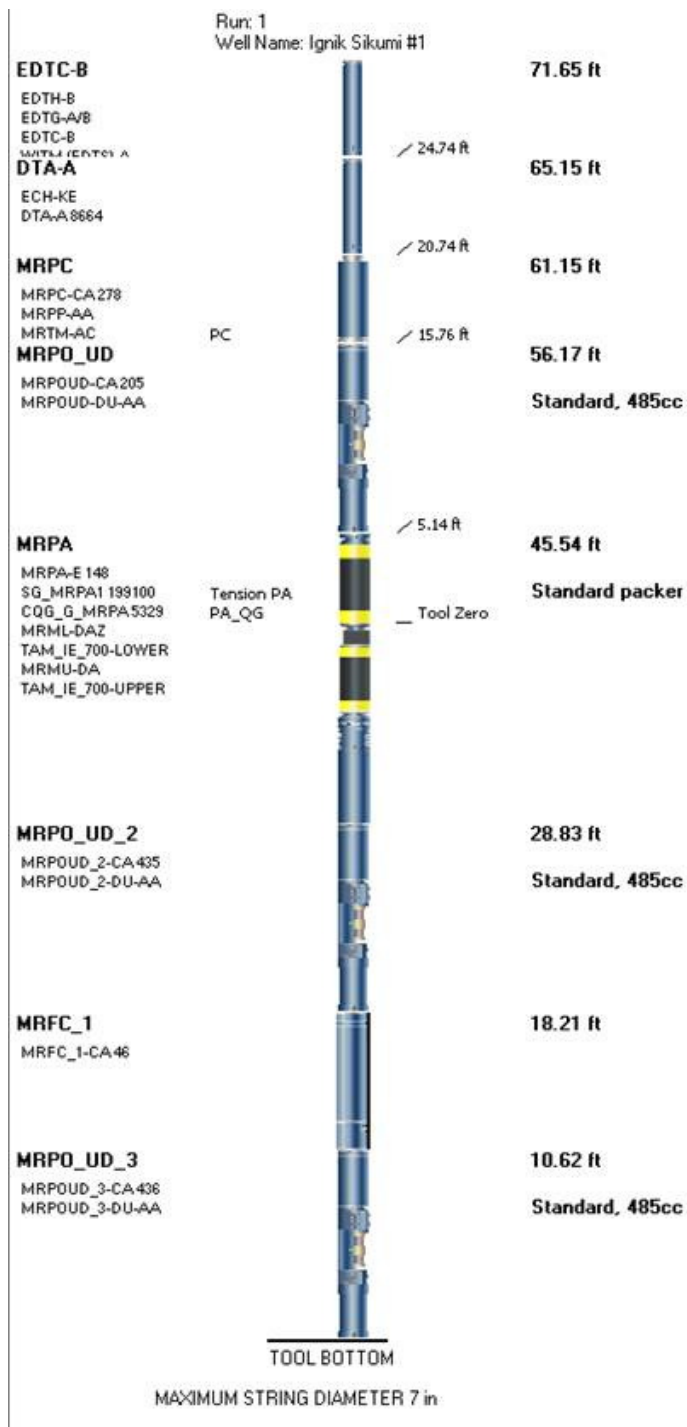**Example of reconciliation plot for three cycles**

8 APPENDIX B – Toolstring Used for Micro-fracturing Tests

Appendix 5: Schlumberger "Iġnik Sikumi #1 XPT/MDT Pretest and Sampling Report," by Ahmad Latifzai

ConocoPhillips Alaska, Inc.

Ignik Sikumi #1

Logging Date: April, 17th 2011

Pretest and Sampling Report

Pressure Measurement

The objectives of formation testing in this well were divided into three categories:

- Stress testing
- Formation pressure
- Formation permeability
- Formation fluid sampling both above and below hydrate dissociation pressure

Modular dynamics tester (MDT) and pressure express (XPT) tools were employed to meet these objectives. The XPT tool was employed to measure formation pressure above the hydrate dissociation pressure, this process also allowed for the evaluation of formation mobility. The formation was expected to have low permeability above hydrate dissociation pressure. The operation requirements called for making the pressure and mobility measurement above the hydrate dissociation pressure. In the past inflatable packers were used to perform this task due inflatable packers ability to the expose large area of the formation. The XPT allows for very low fluid flow rate which is controlled from surface by the user. In addition the large area packer modification (Figure 1) increased the formation area exposed to the probe barrel. Both lower flow rate and larger area allowed for smaller drawdown pressure as shown by D'Arcy's equation.

$$\Delta P = \frac{Q * \mu}{A * k}$$

Equation 1: *D'Arcy's equation where: ΔP is pressure drawdown, Q is flowrate, μ is fluid viscosity, A is area, and k is formation permeability.*
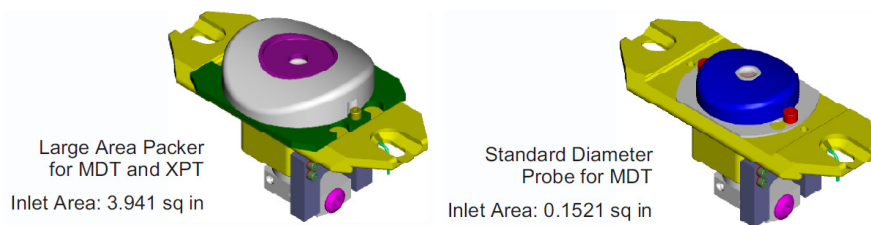

Figure 1: *Probe comparison. Note the area exposed by the large area packer is significantly more than that of the conventional probe.*

Mobility of the formation is defined as the permeability divided by the viscosity of fluid withdrawn from the formation during the pretest period. Since the viscosity of fluid withdrawn during the pretest period is unknown it's not possible to calculate formation permeability using the mobility data. The viscosity of an immiscible fluid mixture in most cases can be higher than the viscosity of each individual fluid component. The depth of investigation (DOI) of each pretest is within one to two wellbore diameters, which is relatively shallow when compared to drill stem testing (DST) or miniDST performed using the MDT toolstring. The DOI of pretest mobility data is near that of the permeability measured by the nuclear magnetic resonance (NMR) tools. A comparison of these two measurements has been shown in Figure 2 below keeping in mind the differences in measurement techniques. In the top sand (2065 to 2130 ft) the pretest mobility and NMR permeability are in good agreement. In the lower sand (2235 ft to 2370 ft) these two measurement techniques display a difference on one order of magnitude while they are in agreement at other depths.

During a number of pretests the formation pressure stabilized at a value very close to hydrostatic pressure. These pressures were assumed to be lost seals due to possible fluid flow from the wellbore around the packer and into the probe barrel where the pressure gauge is located. Examples of these tests will be shown during the detailed pretest section of this report. One possible explanation for this phenomenon is lack of mud cake. All lost seals are indicated by the red pips in the pressure track (Figure 2). Note the CMR permeability is measured to be less the 0.2 mD. In low permeability formations since little or no filtrate invasion takes place it's also not possible to form competent mud cake.
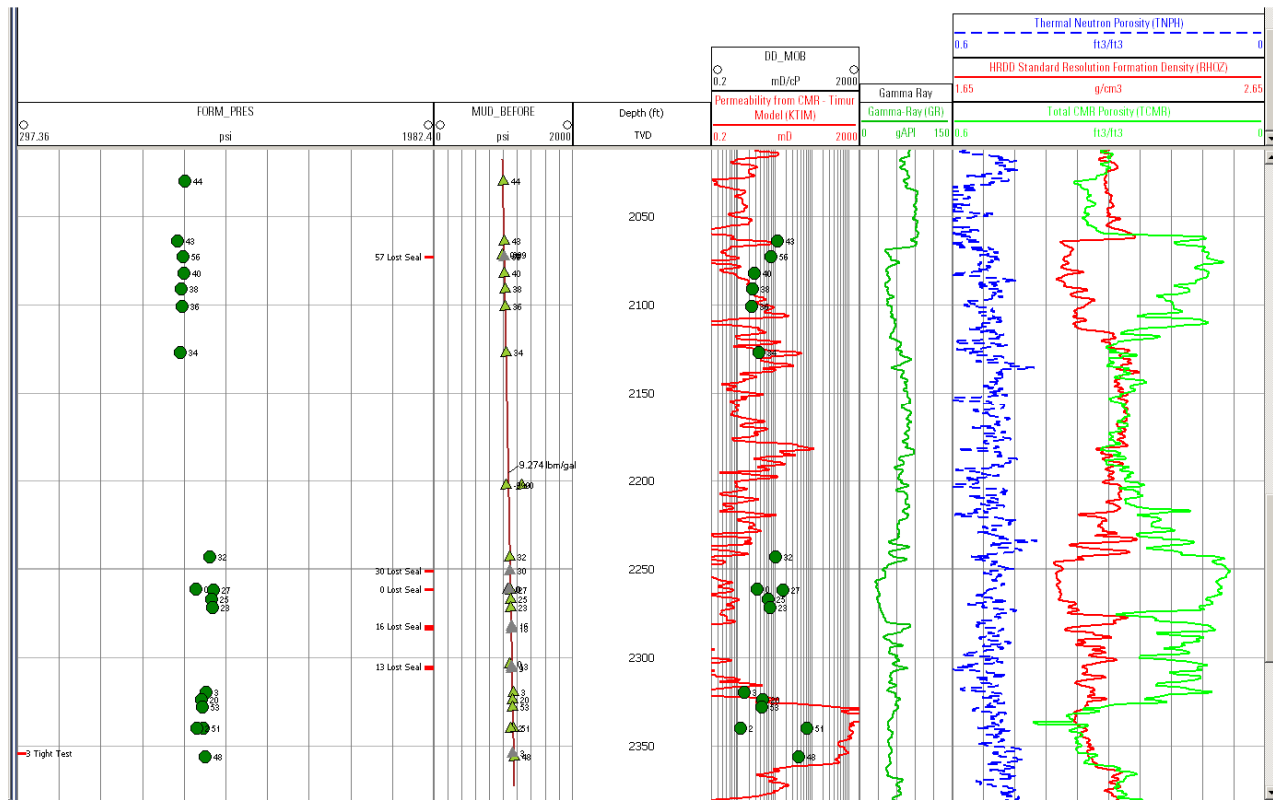

Figure 2: *Pressure, mobility and NMR data plotted for comparison. Note the agreement of mobility and NMR permeability in the top sand. The majority of the data in the lower sand differ by an order of magnitude.*

The mobility data were used when changes to the toolstring became necessary when flow back tests became impossible due to the failure of the flow control module. Since the mobility of the formation was determined to be higher than expected, flowback tests were unnecessary during the stress test operation. As a precaution the toolstring was reconfigured to allow flowback tests. A separate report showing the analysis of the stress test data will be submitted. The mobility data were also used to select sampling station depths.

Individual pretest stations of the XPT

The XPT tool was installed in the same toolstring as the CMR and HNGS (Figure 3).
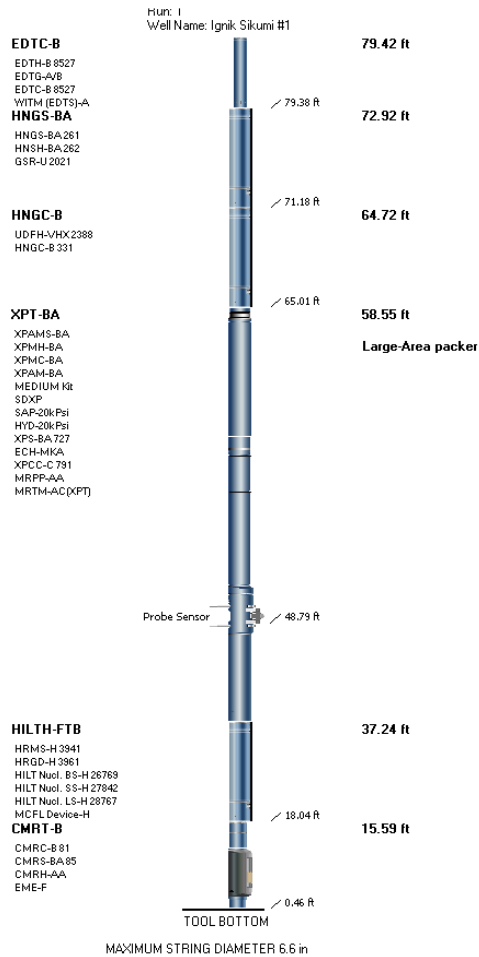
Figure 3: *Toolstring containing the XPT, CMR and HNGS*

The XPT packer and flowline was tested in the casing show to check for leaks in the flowline. Figure 4 (file 33) shows that the sealing system of the XPT was intact before proceeding with the operation. Note that the flowline pressure was lowered to less than 120 psi to be certain all portions of the sealing system were capable of operating under the stress of large pressure differentials.
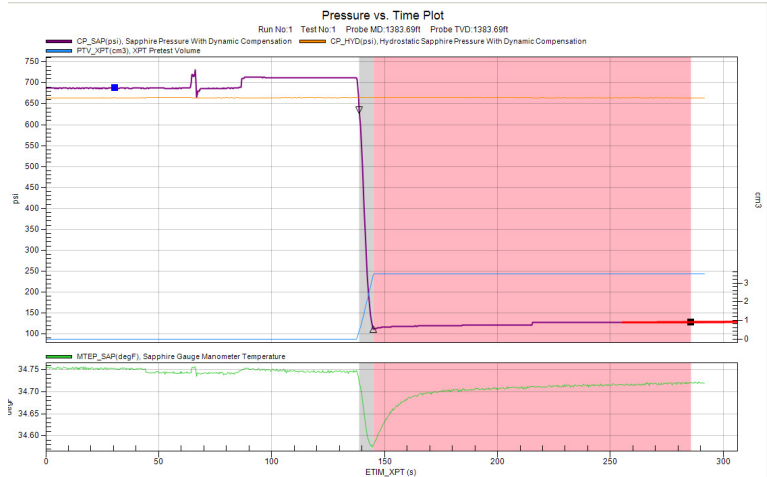
Figure 4: *Data from file 30 showing the sealing system of the XPT tool.*

2320 ft

The toolstring was conveyed to the lower sand and after correlation station depth at 2320 ft was chosen to test first. Initially the pressure in the flowline was drawn to 1060 psi and allowed to buildup and stabilize (figure 5). The flow rate of the pretest was set to 0.05 cc/s, which is the minimum flow rate achievable by the XPT tool. The tool also allows the user to set maximum pretest volume and minimum flowline pressure limits which either one of which could stop the pretest piston. In this case the volumetric limit was reached first. A second pretest with larger volumetric limit was performed. The last buildup pressure was 1061.43 psi. A final pretest was performed to confirm the last build up pressure value from the previous pretest. The final pressure value of this station was 1061.41 psi. The mobility values of the second and third pretest (1.54 and 1.06 mD/cP respectively) were on the same order of magnitude when compared to each other.
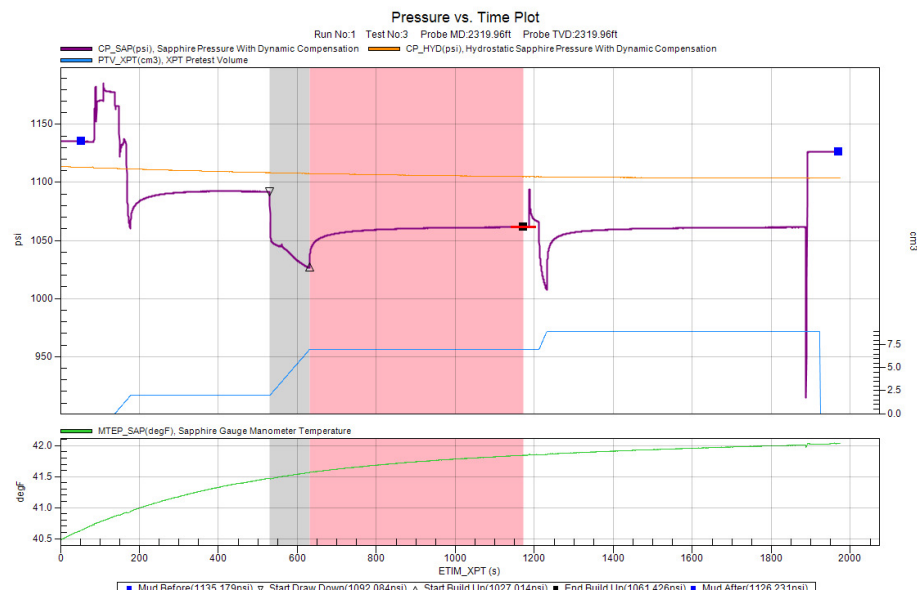
Figure 5: *Pretest station 2320ft, file 42*

2306 ft

The tool was then moved to 2306 ft, a number of pretests were performed at this depth (Figure 6) all of which stabilized at a pressure very close to hydrostatic pressure. While it's possible that the hydrostatic pressure and the formation pressure are very close it's more likely that the wellbore is not completely isolated from the formation. This results in wellbore fluids leaking through pore throats and possible fractures and vugs in the formation into probe barrel.
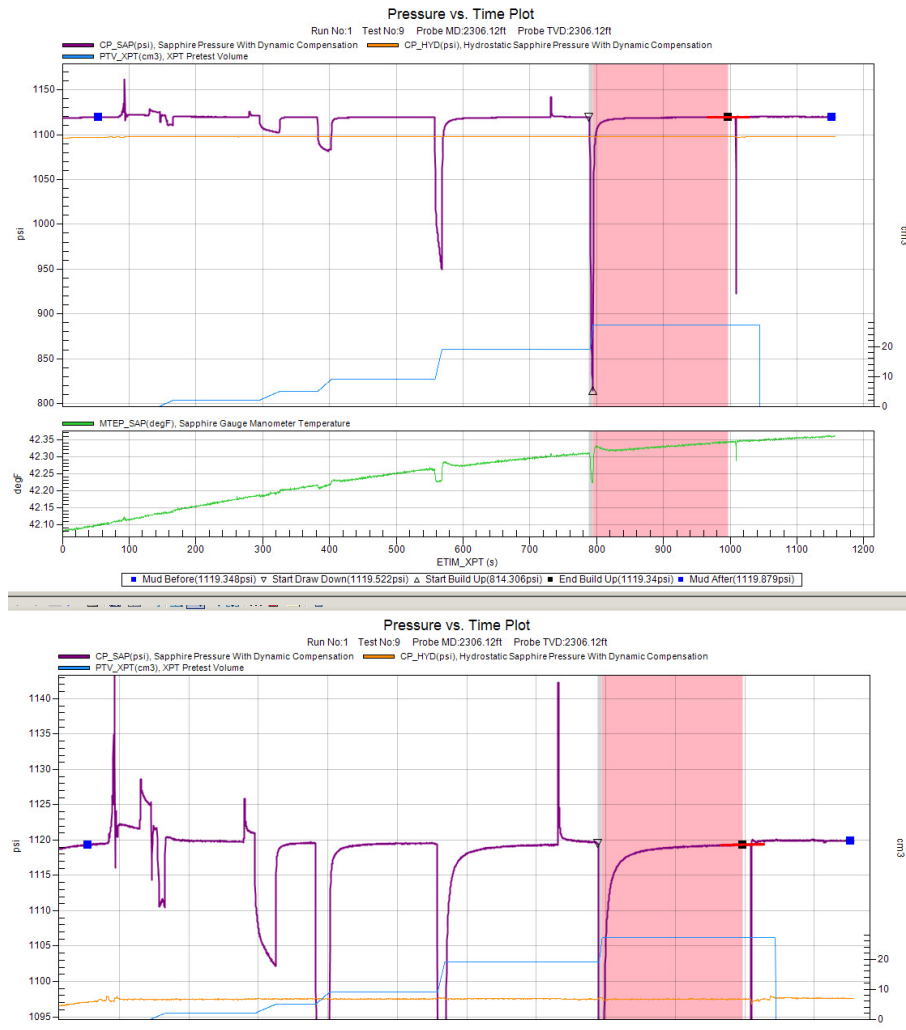
Figure 6: *Pretest station 2306ft, file 43*

2305 ft

The tool was moved to 2305 ft to perform a pretest and obtain formation pressure data. A number of pretests were performed at this station depth as well (Figure 7). Similar to station depth at 2306 ft, the last buildup pressure from each pretest stabilized near the hydrostatic pressure. This is also indicative of leaky mud cake seal.
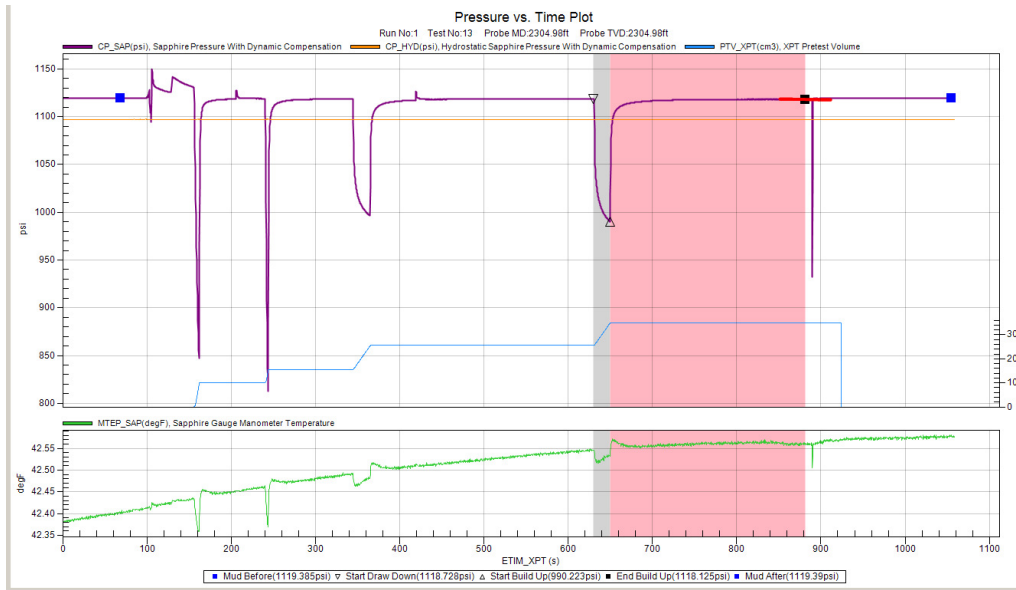
Figure 7: *Station depth 2305 ft, file 44.*

2282 ft

The tool was moved to 2282 ft where a number of pretests were performed. The last build up pressure is only 3 psi lower than the hydrostatic pressure. The data from this station depth must also be excluded due to possible leak in the mud cake.
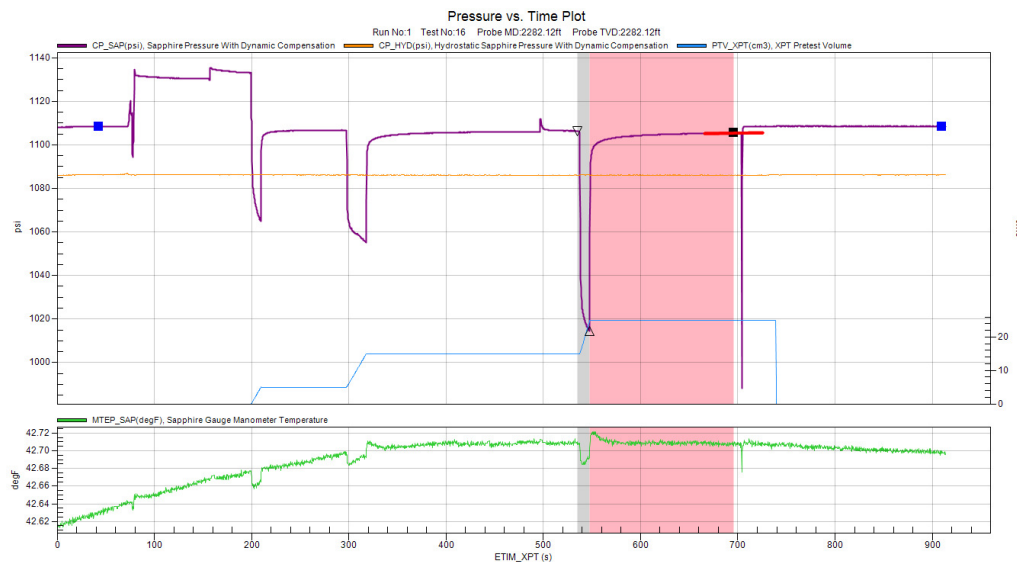
Figure 8: *Station depth 2282 ft, file 45*

2284 ft

The tool was moved to a nearby depth to the previous station depth. The volumetric limit was increased to 10cc, the buildup pressure was very close to the hydrostatic pressure (Figure 9). Therefore the data from this station depth must be excluded.
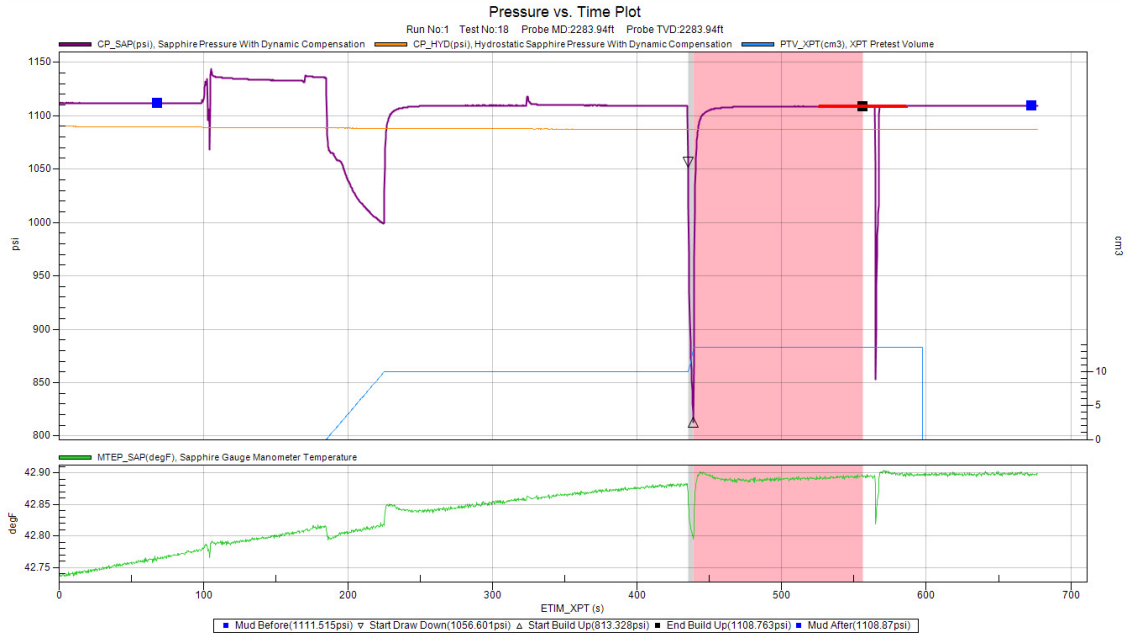
Figure 9: *Station depth 2284 ft, file 46*

2324 ft

The tool was lowered to 2324 ft which is very close the first station depth of the program. The purpose of this station was to test the seal system of the tool and mud cake. Two pretests were performed at this depth (Figure 10) to confirm the last build up pressure. The first pretest stabilized at 1044.44 psi while the second pretest stabilized at 1044.29 psi. P* was calculated to be 1044.27 psi. The drawdown mobility of the first and second pretest are 5 and 6 mD/cP respectively. Spherical and radial mobility was calculated 6.6 mD/cP and 6.2 mD ft/cP.
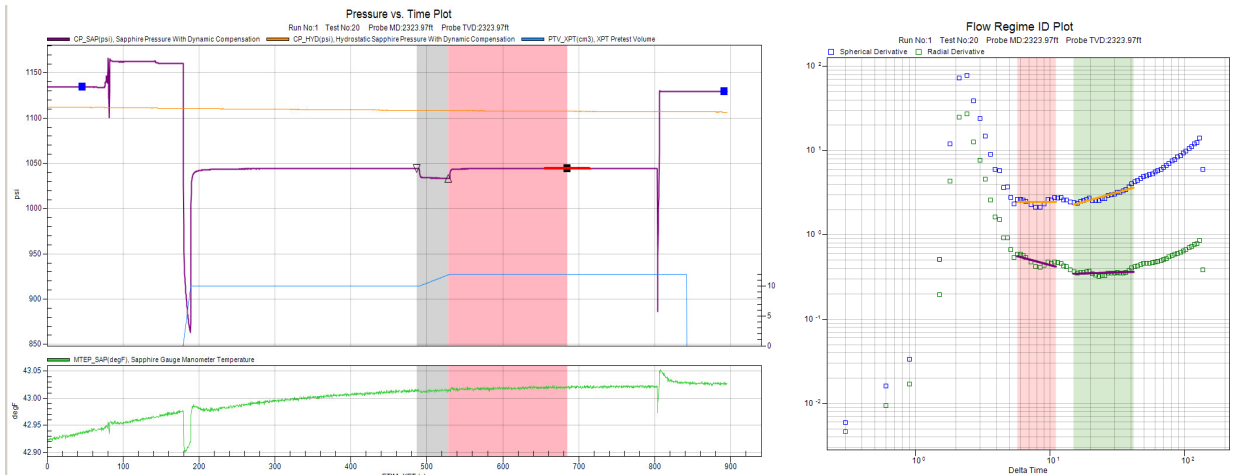
Figure 10: *Station depth 2324 ft, file 47. Derivative plot (right)*

2272 ft

The tool was conveyed to 2272 ft after confirming the seal system at the previous station depth. Multiple pretests were performed to confirm the pressure data (Figure 11). Last buildup pressures from the first two pretests did not stabilize at similar values therefore a third pretest was performed which confirmed the second pretest.
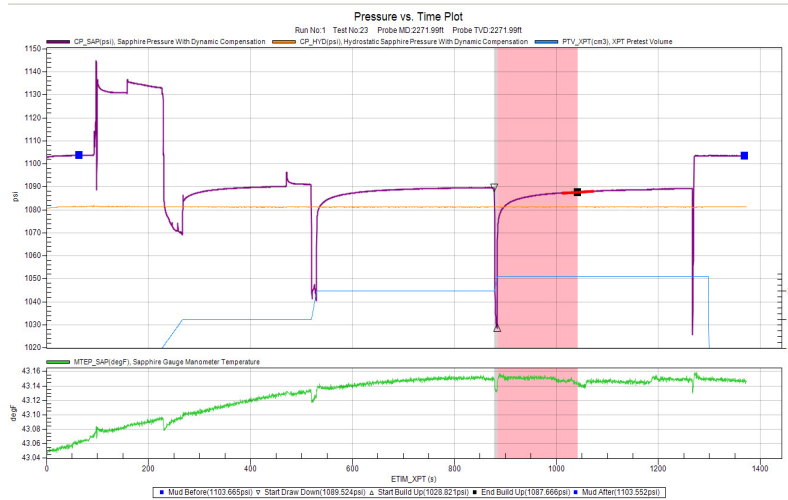
Figure 11: *Station depth 2272 ft, file 48.*

The formation pressure from this station is 1087.67 psi. The drawdown mobility was calculated to be 8 mD/cP.

2267 ft

The tool was moved to the next station depth at 2267ft where two pretests were performed. The drawdown period of the second pretest displayed steady state flow where the reservoir provided fluid as the rate which the pretest mechanism demanded (Figure 11). The derivative plot shows a long radial regime while the spherical regime is short of nonexistent. This could be due to a very thin section.
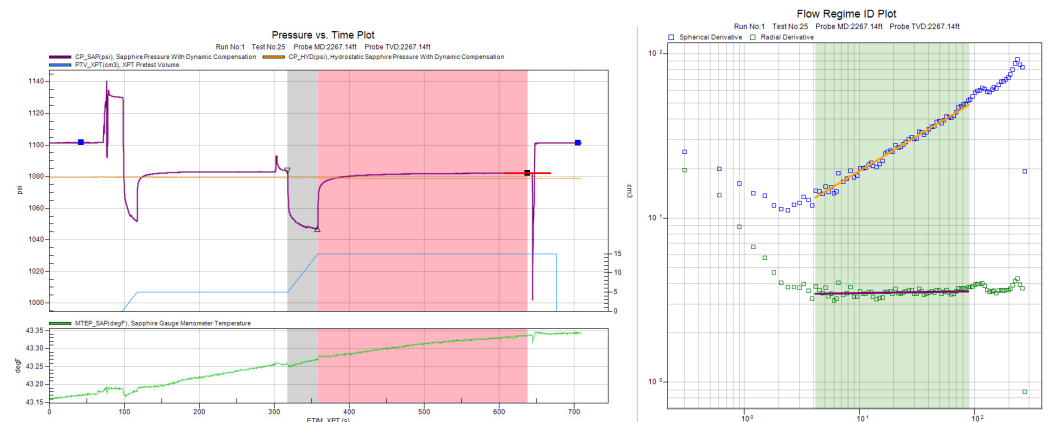
Figure 11: *Station depth 2267 ft, file 50. Derivative plot on the right.*

The final buildup pressure was 1082.23 psi, while the P* from the radial flow was 1082.63 psi. The drawdown mobility was calculated to be 6.9 mD/cP while the radial mobility is 2.7 mD ft/cP.

2262.1 ft

The tool was moved to the next station depth at 2262.1 ft slightly shallower than the previous station depth. Two pretests were performed at this depth as well, the last build pressure from both pretests stabilized at similar values (Figure 12).
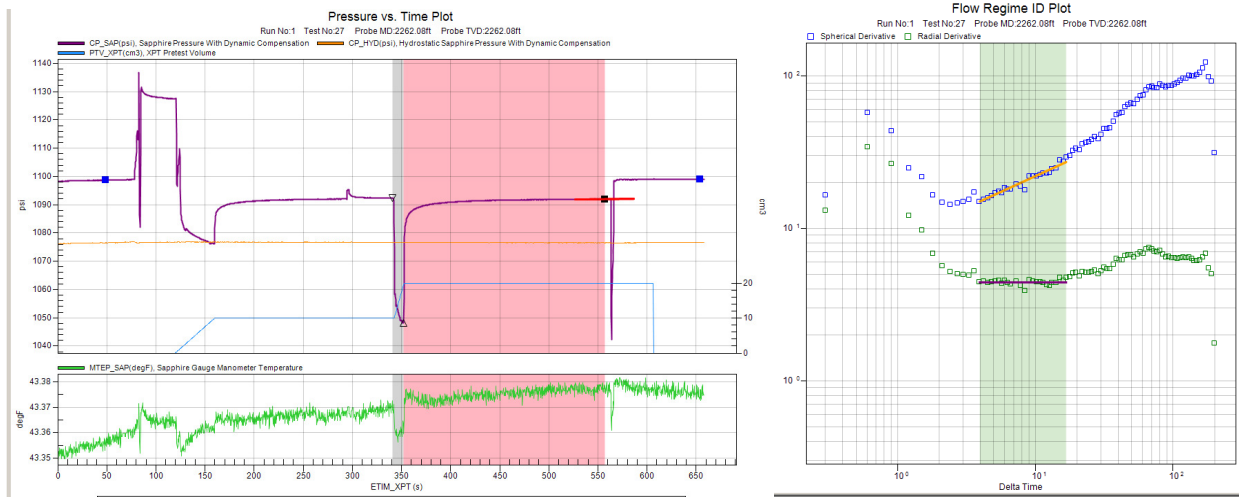
Figure 12: *Station depth 2262.1, file 51. Derivative plot on the right.*

The derivative plot shows a very short to nonexistent spherical flow regime while the radial flow regime is longer indicating a possible thin section. The last build up pressure was 1091.45 psi while the P* was calculated to be 1091.45 psi as well. The drawdown mobility was calculated to be 17 mD/cP while the radial mobility was calculated to be 7.2 mD ft/cP.

2251 ft

At 2251 multiple pretests were performed (Figure 13) all of which stabilized at similar pressure values, however these values were within 3 psi of the hydrostatic pressure. It's possible that fluid from the wellbore is leaking through the mud cake and into probe barrel. This results in a lost seal similar to the behavior seen at 2284 ft. The data from this station must be excluded.
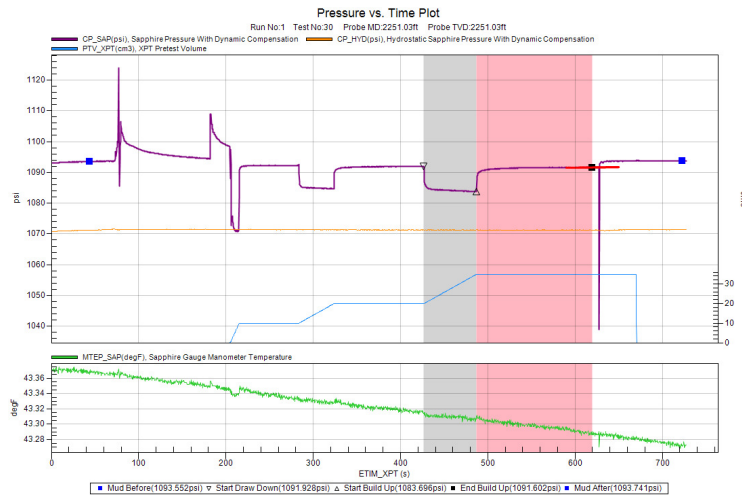
Figure 13: *Station depth 2251 ft, file 52.*

2243 ft

The tool was moved to the next station depth at 2243 ft where two subsequent pretests were performed. Both of the buildup periods stabilized at similar pressure values (Figure 14). The last buildup pressure stabilized at 1076.99 psi while the drawdown mobility was calculated to be 10.6 mD/cP. The derivative plot was inconclusive.
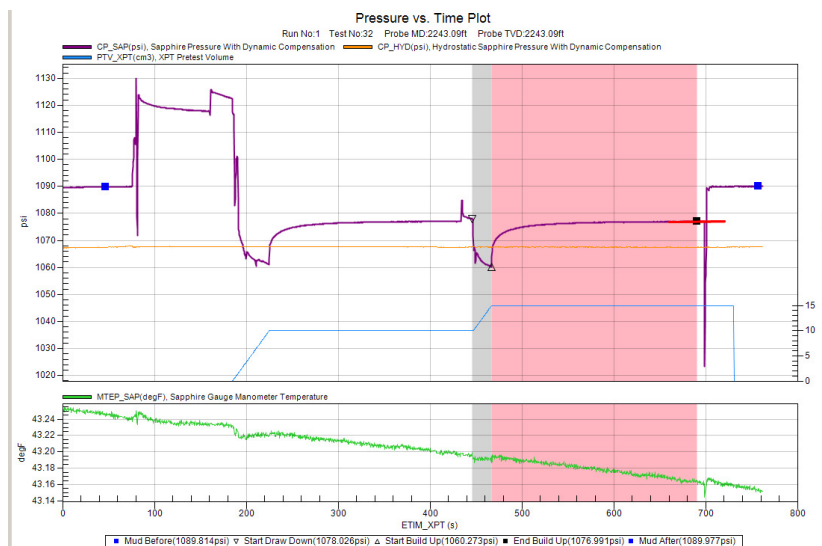
Figure 14: *Station depth 2243 ft, file 53.*

2127 ft

The tool was moved to the shallower sand where the first station depth was at 2127 ft. Two pretest stations were performed at this depth (Figure 15). Note in both cases the pressure stabilized at similar values indicating that the flowline pressure was decompressed below reservoir pressure. During the drawdown periods of both tests steady state flow behavior was seen. The derivative plots were

inconclusive. Last build up pressure was 958.37 psi while the drawdown mobility was calculated to be 4 mD/cP
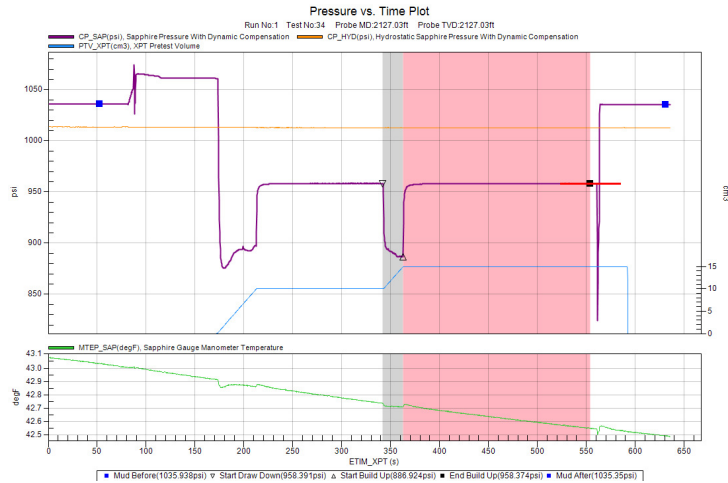
Figure 15: *Station depth 2127 ft, file 54.*

2101 ft

The tool was moved to the next station depth at 2101 ft and two subsequent pretests were performed at this depth. Both pretests stabilized at similar values (Figure 16). The derivative plot shows both spherical and radial flow regimes. The large difference between the spherical and radial regime occurrence could be an indication of this sand. The last buildup pressure was measured to be 965.41 psi while P* from the radial calculation was 963.98 psi. The drawdown mobility was calculated to be 2.5 mD/cP, spherical mobility was 2.3 mD/cP while the radial mobility was calculated to be 0.64 mD ft/cP.
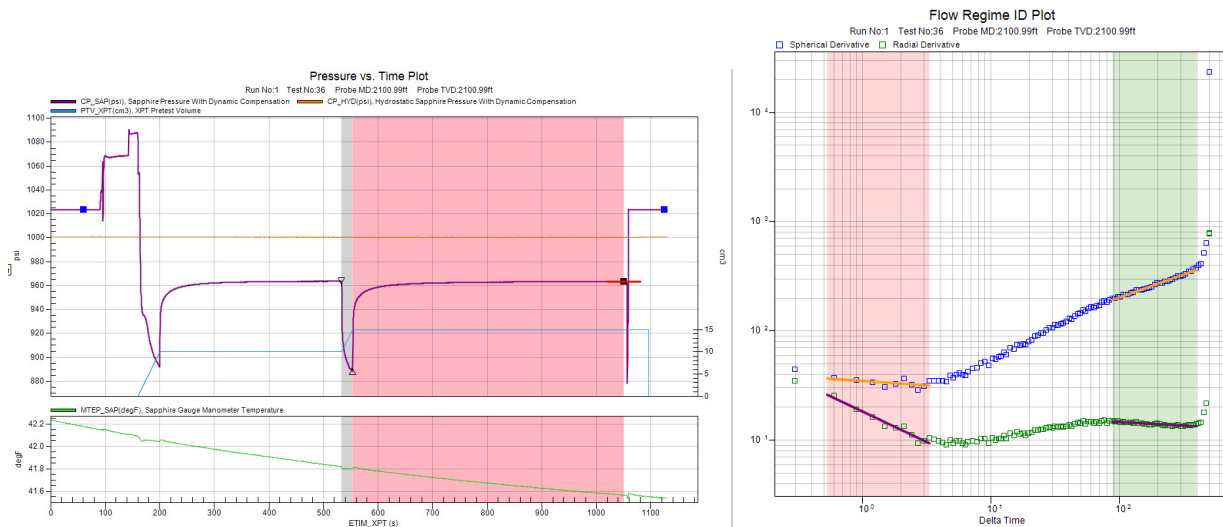
Figure 16: *Station depth 2101 ft, file 55. Derivative plot on the right.*

2091 ft

The probe was moved to the next station depth at 2091 ft and two subsequent pretests were performed at this depth. Buildup pressures from both pretests stabilized at similar values (Figure 17) 960.00 psi. The mobility was calculated to be 2.6 mD/ cP. The derivative plots were inconclusive.
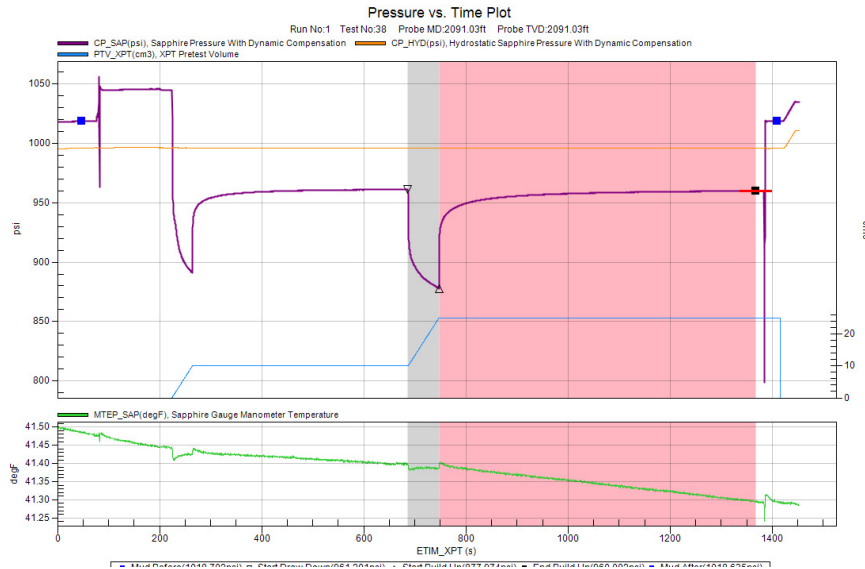
Figure 17: *Station depth 2091 ft, file 56.*

2082 ft

The probe was moved to the next station depth at 2082 ft where two subsequent pretests were performed. The buildup pressures from both pretests stabilized at similar values (Figure 18) 972.65 psi. The mobility was calculated to be 2.8 mD/cP. The derivative plots were inconclusive.
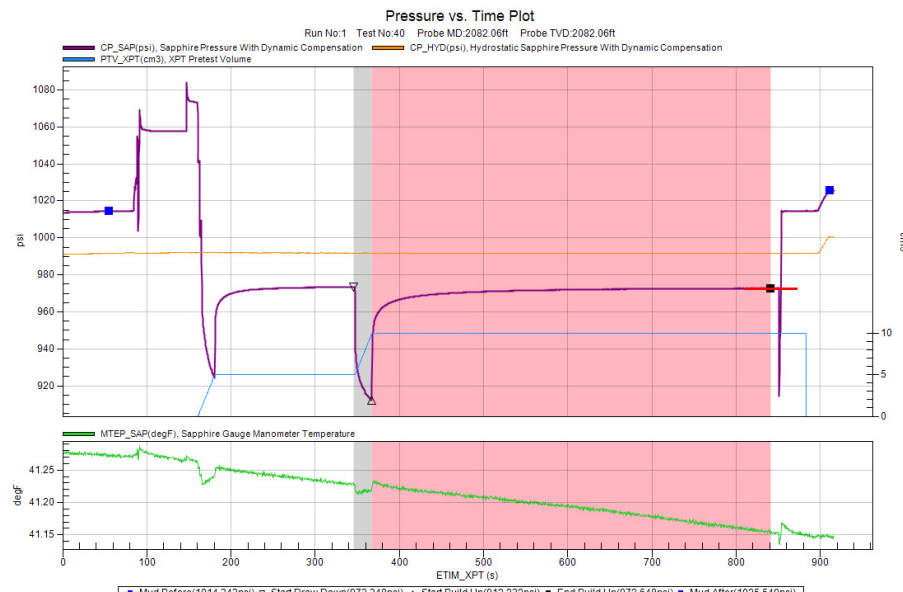
Figure 18: *Station depth 2082 ft, file 57.*

2064 ft

The probe was moved to the next station depth at 2064 ft where three subsequent pretests were performed. The buildup pressures from the final two pretests stabilized at similar pressure values (Figure 19) 945.77 psi. The mobility is was calculated to be 12 mD/cP. The derivative plots were inconclusive.
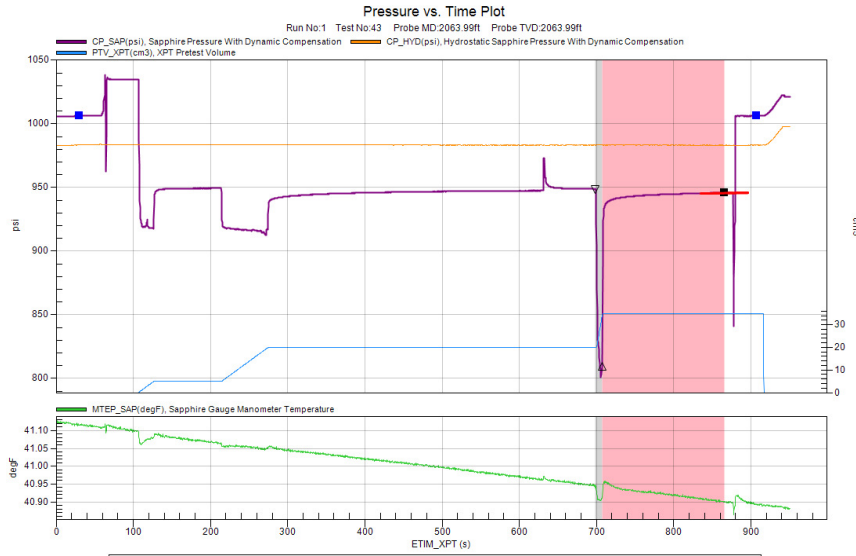
Figure 19: *Station depth 2064 ft, file 58.*

2029 ft

The probe was moved to the caprock at 2029 ft to determine the mobility of the formation. The pressure response indicated very low mobility formation.
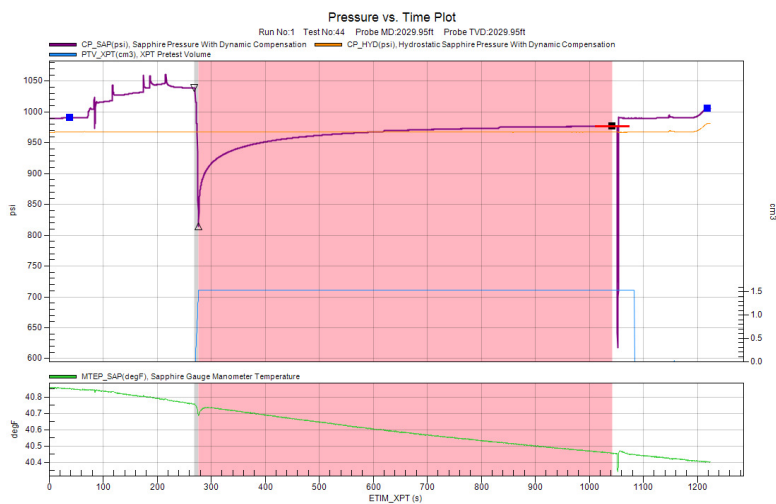
Figure 20: *Station depth 2029 ft, file 59.*

2356 ft

The probe was lowered to the lower most wet sand at 2356 ft. Multiple pretests were performed at this depth until two subsequent buildup pressures repeated (Figure 21) indicating that the flowline has been decompressed sufficiently. The final buildup pressure was 1057.48 psi while the drawdown mobility was calculated to be 45 mD/cP. The derivative plots were inconclusive.
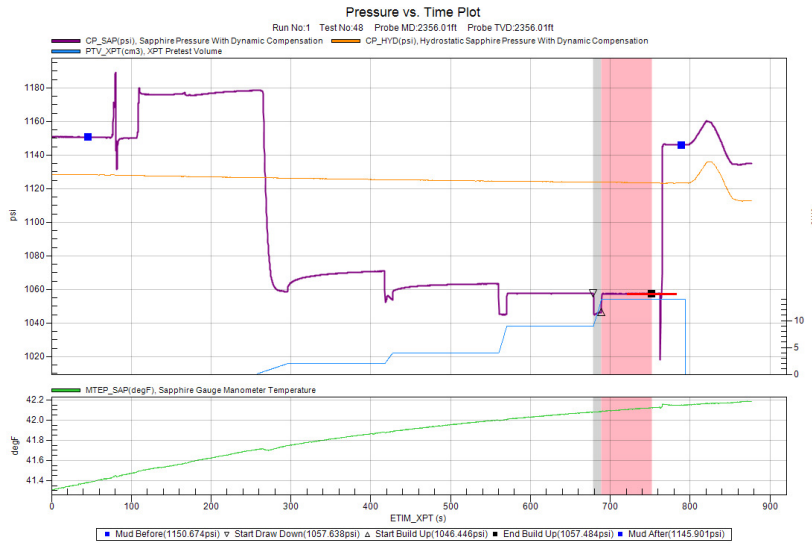
Figure 21: *Station depth 2356 ft, file 61.*

2340 ft

The probe was moved to the next station depth in the water sand at 2340 ft. Three pretests were performed at this depth (Figure 22). The final two buildup pressures were in agreement indicating the flowline had been decompressed below reservoir pressure. The final buildup pressure was measured to be 1050.12 psi while the mobility was calculated to be 75 mD/cP. The derivative plots were inconclusive.
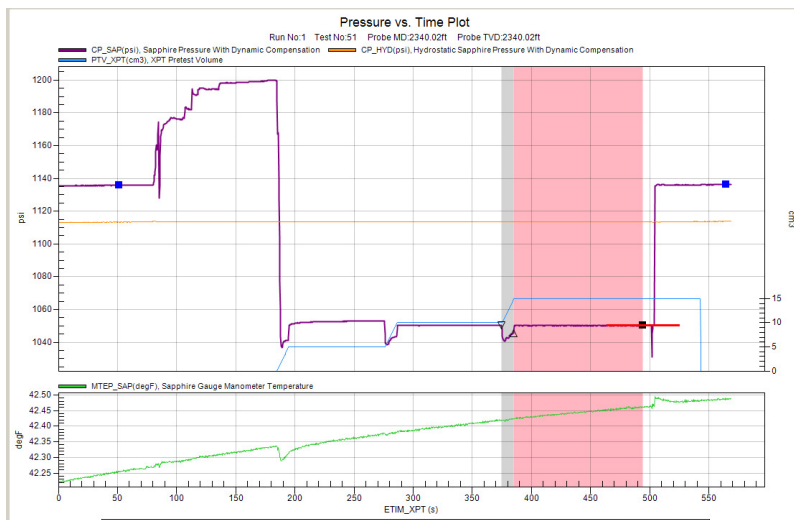
Figure 22: *Station depth 2340 ft, file 62.*

2328 ft

The probe was moved to the next station depth in the water sand at 2328 ft. Two subsequent pretests were performed both resulting similar final buildup pressures (Figure 23). The final buildup pressure was measured to be 1045.54 psi while the drawdown mobility was calculated to be 4.7 mD/cP. The derivative plots were inconclusive.
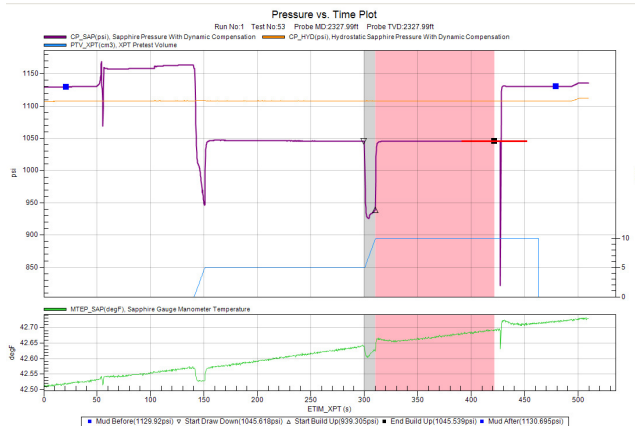
Figure 23: *Station depth 2328 ft, file 63.*

2073 ft

After the completion of the pressure survey, an attempt to determine the hydrate dissociation pressure was made using the XPT tool. Hydrate dissociation pressure requires lowering the flowline pressure below the dissociation pressure at which point gas flow may result in increase of mobility by an order of magnitude. Since the compressibility of gas is also significantly higher than liquid the flowing pressure curve is also expected to behave similar to steady state flow. This technique is only possible with the XPT due to its capacity to decompress the flowline slowly.

The probe was moved to 2073 ft in the hydrate zone, where the flowline decompressed using pretest mechanism to a pressure below 700 psi. The attempt was unsuccessful since multiple pretests at different rates were attempted (Figure 24) and the pretest volume was exhausted. The flowline pressure was not lowered below the expected dissociation pressure. The probe was retracted and set again at the same depth (Figure 25) and the flowline was decompressed at the maximum capacity of the XPT tool. There was a seal failure (Figure 25) resulting in the flowline pressure to stabilize at the hydrostatic pressure. Due to the sharp decrease in the hydraulic oil pressure coinciding with the sharp increase in flowline pressure it's possible that the formation near the probe collapsed resulting in the loss of seal.
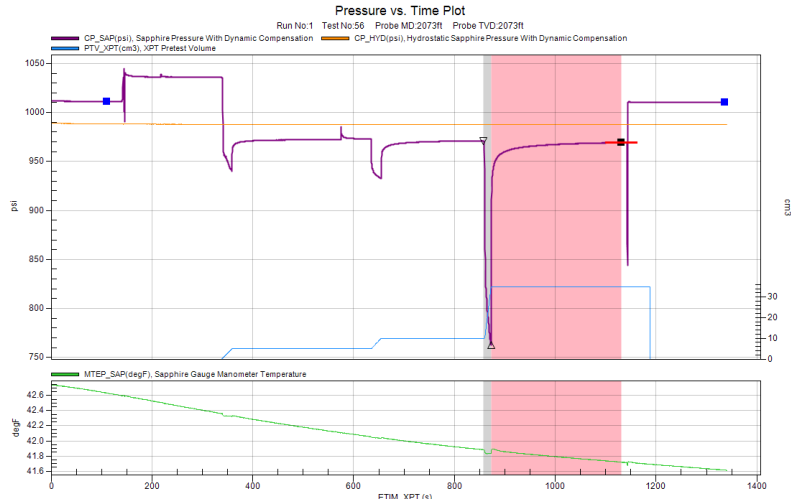
Figure 24: *Station depth 2073, file 64.*
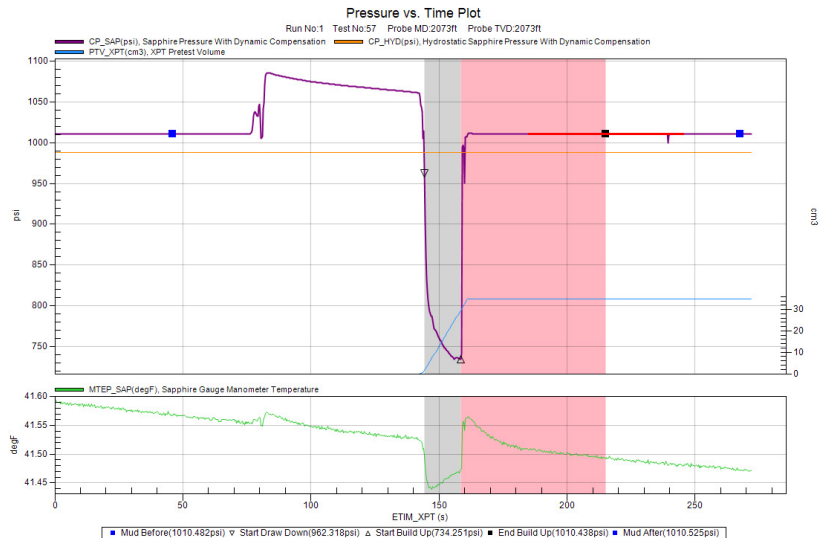
Figure 25: *Station depth at 2073, file 65.*

Fluid Sampling

The inflatable packers were used to obtain fluid samples from the formation. The objective was to obtain free water sample, and water sample below hydrate dissociation pressure. Due to the unconsolidated nature of the formation it was necessary to install redundant modules in the toolstring (Figure 26)
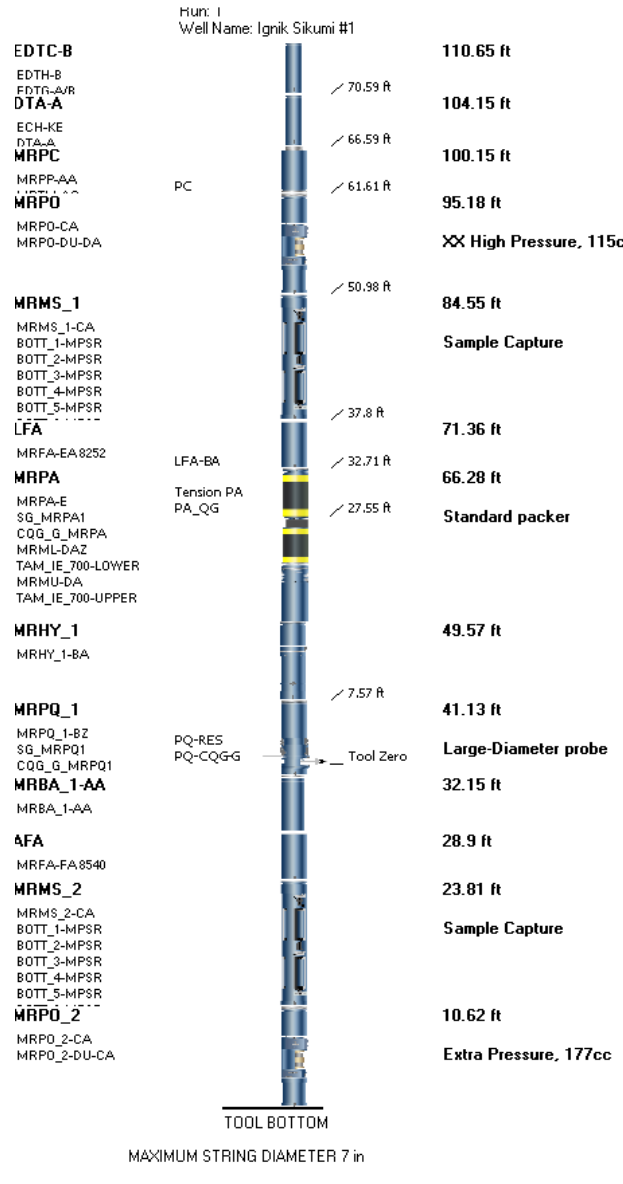
Figure 26: *Sampling toolstring*

Additional pump, multi-sample module and fluid analyzer were installed both above and below the inflatable packer module for redundancy. A probe was also installed in the toolstring for water sampling in case evacuation of the packer interval required significant pumping time. Seven inch TAM packer elements were installed on the inflatable packer module. Low flow pumps were used to minimize both drawdown and sand production.

Sampling Operation

2261.5 ft

Wellbore fluid was to be used to inflate the packer elements. The formation was expected to be unconsolidated and thought to produce sand once reservoir fluid was entered the flowline. Therefore low flow pumps were used to allow the fluid sufficient residence time in the packer element interval to trap solid particle before their entry into the flowline. Due to the low flow rate pump the time requirement for the inflation was significant. The operation was further complicated due to the existence of fines in the mud system. LCM was not present in the mud system therefore the pump issues must have been due to solid particles in the mud systems if the cuttings had not been circulated out. The pump had numerous issues during packer inflation process therefore it was decided to trip out of the well to clear the pumps. Due to the low flow rate pumps it was also not possible to clear the pumps using high flow rate fluids.

On surface a large amount of sand particles were discovered to have been trapped in the mud check valves (MCV) of the pump. The debris was cleared and a high flow rate pump was installed in the toolstring since the mobility was higher than expected. The packer elements were inflated successfully at 2303 ft and an attempt was made to drawdown fluid from the formation for drawdown and buildup test (Figure 27) near 10,000 seconds.
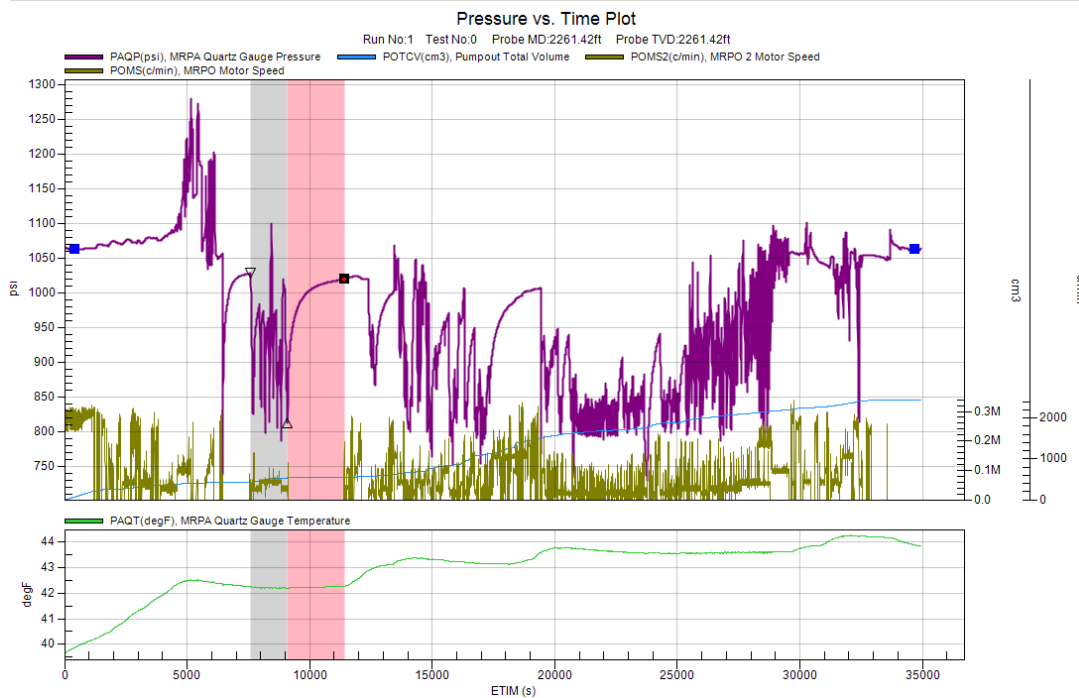
Figure 27: *Station depth 2261.4 ft, file 45.*

The buildup analysis from the inflatable packers calculated a mobility of 3.3 mD/cP and measured a last buildup pressure of 1020.01 psi. When compared to the XPT data from the same depth the overbalance when the inflatable packers were used is 43 psi while the same parameter is between 10 to 20 psi. The mobility on the other hand is comparable from both tools. It's advisable to use the pressure measured by the inflatable packers in the analysis of the reservoir.

After the buildup period fluid flow from the formation was attempted. The pumps during this period had a few issues due to sand production, however the pressure response fluctuated (Figure 27) due to pump half stroking and possible fluid leak from the wellbore through the formation and into the flowline. This could have been caused by poor mud cake or formation collapsing around the packer interval or both. After 25,000 seconds it was not possible to pumps were not longer able to displace fluid from the interval into the wellbore efficiently and finally at 28,000 seconds both pumps failed completely resulting in abandonment of this station.

2303.7 ft

The packers were conveyed to this depth and inflated. In this portion of the sand there were a number of issues with lost seals during the XPT run. Short buildup stations were attempted (Figure 28), however the packers were not able to maintain seal (10,000 seconds Figure 28).
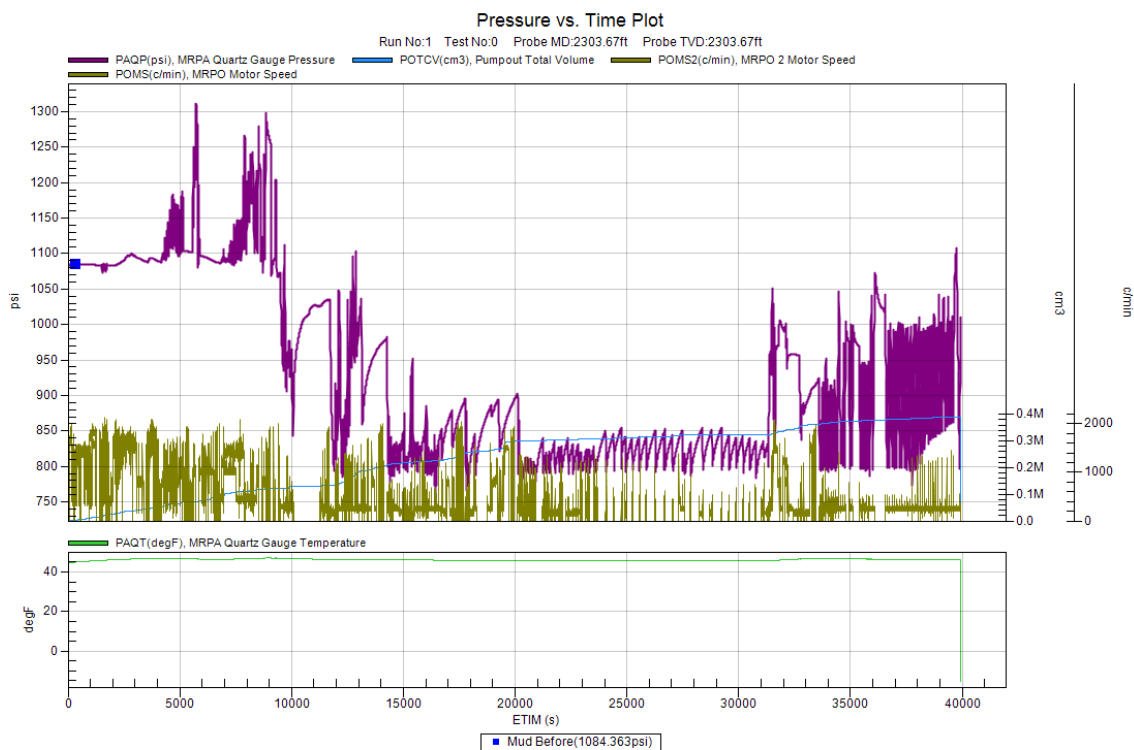
Figure 28: *Station depth 2303.7 ft, file 47*

For the remainder of the operation the pumps were half stroking however the interval was never cleared from wellbore fluids allowing the entry of formation fluids into the flowline. At 35,000 seconds the pumps were completely plugged and the station was abandoned after 40,000 seconds.

2340 ft

The probe was used to attempt obtaining formation water from the water zone. After the pretest period the pump was started (Figure 29) which resulted in sharp decline of pressure in the flowline. The probe was perhaps plugged. The station was abandoned. The fluid analyzer show a small amount of water mixed with hydrocarbons possible oil based mud (OBM) filtrate. Upon the arrival of the tools on surface

the pump displacement unit was checked for possible traces of water however only mud was discovered. If the displacement unit contained any water it might have leaked during the conveyance out of the well.
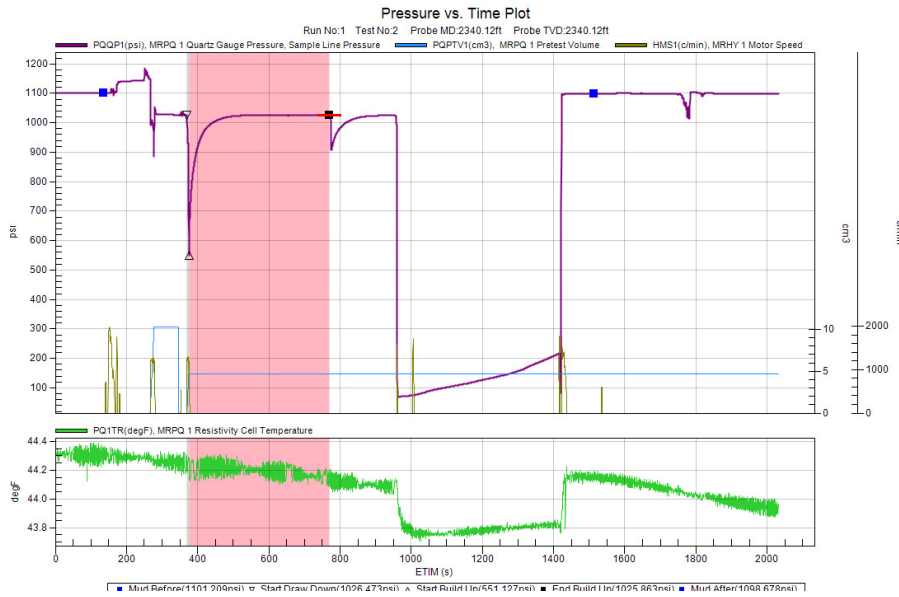
Figure 29: *Station depth 2340 ft, file 50.*

Conclusions and recommendations

- The XPT tool performed well when obtaining formation pressure and mobility.
- The formation mobilities were higher than expected.
- The possible capability of the XPT to detect hydrate dissociation pressure needs to be explored further.
- Continue the use of large area packers for the XPT.
- The mud system must be clear from all possible debris and LCM.
- The newly designed MCV needs to be installed in the toolstring on all future jobs.
- XPT mobility data must be reviewed before selecting displacement units for the downhole pumps.
- Mobility data from small scale (CMR) to intermediate scale (XPT) to larger scale (inflatable packers) must be reconciled to determine possible the amount of heterogeneity of the formation.

Appendix 6: Schlumberger "Iġnik Sikumi #1 Interpretation Report (OBMI, Rt Scanner, Sonic Scanner, & CMR)", by Jason Burt, Doug Hupp, Mai ElFouly, Ray Heath, and June Wu

Data & Consulting Services

Company: CPAI
Well: Ignik Sikumi #1
Field Prudhoe Bay
State: Alaska
Country: USA
Date: 27-May-2011

Schlumberger
Data and Consulting Services
2525 Gambell Street
Suite 400
Anchorage, Alaska
99503

Ignik Sikumi #1 Interpretation Report
(OBMI, Rt Scanner, Sonic Scanner, & CMR)

Jason Burt, Doug Hupp, Mai ElFouly,
Ray Heath, and June Wu

Schlumberger

Standard Disclaimer

The use of and reliance upon this recorded-data by the herein named company (and any of its affiliates, partners, representatives, agents, consultants and employees) is subject to the terms and conditions agreed upon between Schlumberger and the Company, including: (a) Restrictions on use of the recorded-data; (b) Disclaimers and waivers of warranties and representations regarding company's use and reliance upon the recorded-data; and (c) Customer's full and sole responsibility for any inference drawn or decision made in connection with the use of this recorded-data.

*Mark of Schlumberger

Table of Contents

FIGURES

TABLES

Table 1.1: Summary of acquisition details.

Table 1.2: Formation Tops in the Ignik Sikumi #1 well as provided from COP.

Table 2.1: Classification of the dips and their interpretation scheme.

Table 2.2: Zones defined by shale dip azimuth.

Table 2.3: Facies descriptions.

Table 5.1: Selected parameters.

Table 6.1: T2 Cutoffs for Bin Processing.

SUMMARY

The Oil Base MicroImager (OBMI*), Rt Scanner, Sonic Scanner, CMR*, and PEX was logged on April 17, 2011 in the well Ignik Sikumi over the interval 1490 to 2565 ft MD for ConocoPhillips.

Image processing, manual dip-picking, automatic dip picking and detailed structural interpretation were preformed over the interval. The overall image quality was good except for a small washed out section. Detailed structural interpretation included sedimentological and structural dip determination. Sedimentological dips were classified into sand, shale, and deformed sand, while structural dips were classified according to fractures (resistive and conductive) and possible micro-faults. The predominate shale and sand dip was to the north east with greater variations in the sand dips near the bottom of the borehole. The majorities of the fractures are striking either NE-SW or NW-SE and represent conjugate sets throughout the interval. Sedimentologically this interval represented a series of five coarsening upward sequences bound on top by shale of a flooding surface. A sand count was generated using a synthetic resistivity curve determined from the OBMI* and yielded a net sand count of 133.7 ft.

Formation Anisotropy and formation dip was examined within the interval from 1490 to 2565 ft MD from examination of the Sonic Scanner and Rt Scanner processed data. The Rt Scanner showed resistive anisotropy in the shales that was also confirmed from the Sonic Scanner. Additionally the Rt Scanner determined formation dips (NE dip direction) that highly correlate to manually picked dips from the OBMI* analysis.

A volumetric elemental analysis (ELAN*) and combinable magnetic resonance (CMR*) identified regions of gas hydrate, ice, and water. ELAN* determined the volumetric percentages of clay, quartz, ice, hydrate, water, bound water, and irreducible water. Porosity, permeability, and grain size are identified from the CMR*. The gas hydrates are identified by the low percentage of bin T2 distribution because the hydrogen index is zero over those intervals, while water sands have a large bin size percentage. Multiple gas hydrates, two water sands, and an ice region are identified.

1. INTRODUCTION

The Oil Based Micro Imager (OBMI*), Rt Scanner, Sonic Scanner, and CMR* have been logged in the Ignik Sikumi #1 well, Prudhoe Bay Alaska. The image data has been processed at the request of Conoco Phillips Alaska Inc. for the interval 1490-2565 ft MD.

The main objective of this study is to provide a detailed reservoir analysis over the logged interval, including:

- Structural dip zonation and interpretation
- Lithologic facies analysis
- Net Sand Count
- Rt Scanner Analysis
- Sonic Scanner Analysis
- ELAN*, volumetric analysis
- CMR* porosity and T2 analysis

The data has undergone quality control checks prior to processing, and manual dip analysis from OBMI* has been performed within the following framework:

- Identify the principle structural features and determine gross structural trends
- Identify the principle stratigraphic features with the available image data

1.1 Interval of Interest

The following table (Table 1.1) summarizes the main acquisition details for the well Ignik Sikumi #1. Formation tops supplied by the client are in Table 1.2

Well	Ignik Sikumi #1
Date Logged	17-Apr-11
Logging Interval	1490 - 2592 ft MD
Maximum deviation	9.95 deg
Bit Size	9.88 in
Mud Type	OBM

Table 1.1: Summary of acquisition details

Ignik Sikumi #1 Formation Tops	Depth (ft)	
	MD	TVD
Sagavanirktok	143	59
Mid-Eocene Shale Marker	1,473	1,389
Sagavanirktok "F"	1,572	1,488
Sagavanirktok "E"	1,920	1,836
Sagavanirktok "D"	2,060	1,976
Sagavanirktok "Upper C"	2,214	2,130
Sagavanirktok "Lower C"	2,278	2,194
Sagavanirktok "B" Sand	2,550	2,466

Table 1.2: Formation Tops in the Ignik Sikumi #1 well as provided from COP

2. OBMI* – OIL BASED MICRO-IMAGER

2.1 Tool overview and Introduction

The development of the Oil Base Micro-Imager (OBMI*) was a major advancement on the ability to acquire electrical borehole images in non-conductive mud systems and is a significant enhancement over its predecessor, the Oil-Base Dipmeter Tool (OBDT*). The OBMI* is a four-pad device with a five-button array on each pad providing a maximum resolution of 1.2 inches
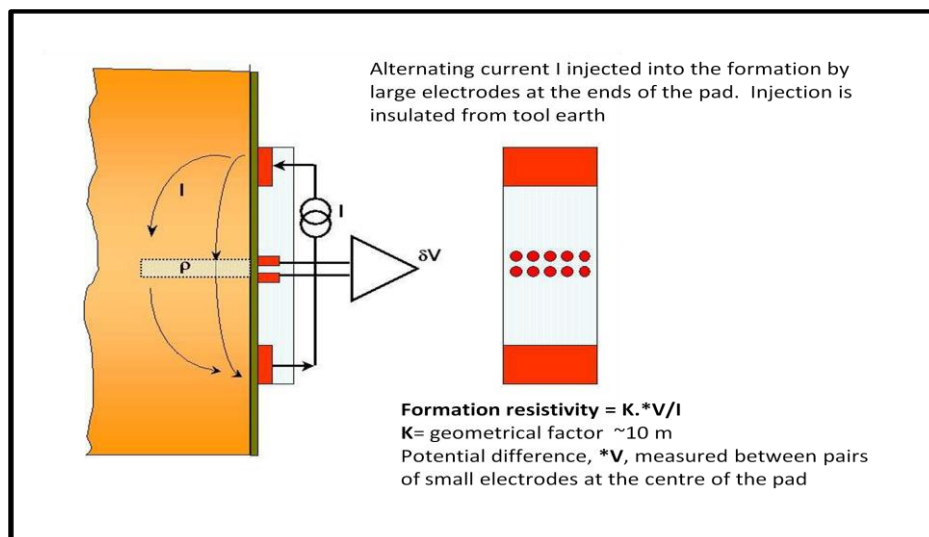
Fig 2.1: Profile of an OBMI* pad applied to the borehole wall, with current [I] passing between the current electrodes and measurement of the potential difference between the voltage electrodes.

Five pairs of voltage electrodes are present on each OBMI* pad providing the ability to identify sedimentary features with significantly greater confidence than previously. This ability is in contrast to the OBDT that possessed only a single button per pad and a maximum resolution of 2 inches. The other direct enhancement is the OBMI* is an imaging device whereas the OBDT is standard dipmeter.

The OBMI* follows the principle of laterolog resistivity logging. While logging, the four pads of the OBMI* tool are applied against the borehole wall, where a thin layer of nonconductive mud is between the pad face and the formation. In accordance with the four-terminal or short-normal method of measuring resistivity, an alternating current is injected into the formation between the two electrodes at opposing ends of each pad (see Figure 2.1).

The electronics within each OBMI* pad and the cartridge measure the potential difference between paired button electrodes at the centre of the pad. From this value, the resistivity of the invaded zone, R_{xo} opposite the sensors can be accurately and quantitatively determined using Ohm's law. Each of the four pads acquires five measurements and the data are displayed as a colored image, oriented with respect to the geometry of the tool and borehole. Structural and stratigraphic features as small as 0.4 in. (1 cm) can be resolved, yielding a wealth of high-resolution, azimuthal information unobtainable through conventional logging techniques in oil base mud.

In addition to the pad assembly, the tool incorporates a navigational module the GPIT (General Purpose Inclinometry Tool). The purpose of the GPIT is to measure three components of the earth's gravitational and magnetic field. From these six measurements, a number of parameters e.g. deviation, hole azimuth, geographic north, Pad-1 azimuth and tool acceleration are computed. These are necessary to produce an azimuthally oriented image and allow correct dip orientation. In addition, parameters such as tool acceleration are used to correct the image when the tool moves with a velocity higher or lower than the normal speed i.e. in cases of sticking and jerking.

2.2 OBMI* – Data Used

Data used for the interpretation of the dual OBMI* data of the well Ignik Sikumi #1 are as follows:

- High-resolution resistivity image data from OBMI* tool over the interval 1490 – 2567 ft (MD).
- Resistivity data from Array Induction Tool (AIT*) with various resolutions.
- Other open-hole logs including measurements of high resolution bulk Density (RHOZ) and Sandstone Corrected Porosity (NPHI) and Gamma Ray.

2.3 Data Quality – OBMI* LCQ flags

The OBMI* LQC Image is an indication of the data quality and is independent of formation signature or acquisition. The data quality deteriorates from green to yellow to red, as the standoff from the borehole wall increases and current saturation causes a blue flag (Figure 2.2). Where

8

pad contact is good the flag will be green. As standoff occurs, the flag will turn yellow. The flag turns red when there is no contact of the pad with the formation and the tool is no longer measuring formation. A blue flag indicates that the button signal has saturated.

The quality of the OBMI* flags for the interval between 1490 and 1565 ft MD is good except for a few intervals where the hole is washed out. The washed out sections occur between 1708 -1726 and 1732 – 1740 ft MD.
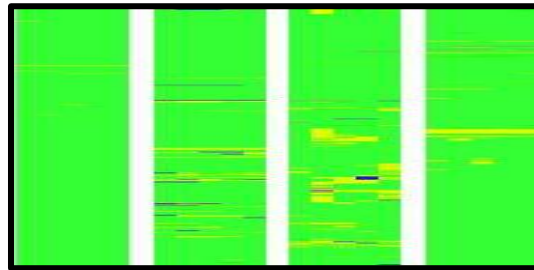
Figure 2.2: OBMI* LQC Image Flag

2.4. OBMI* PROCESSING TECHNIQUE AND DIP CLASSIFICATION

Processing of the OBMI* data for Ignik Sikumi was performed on the GeoFrame platform using the OBMI* workflow. The raw image data was first speed corrected and equalized using the GPIT Survey* and BorEID* modules. The speed corrected image was then statically normalized. This process assigns a color spectrum of a user defined bin set to the resistivity data to obtain an image pixel that is representative of a particular bin size. When all pixels are viewed together the normalized image is produced.
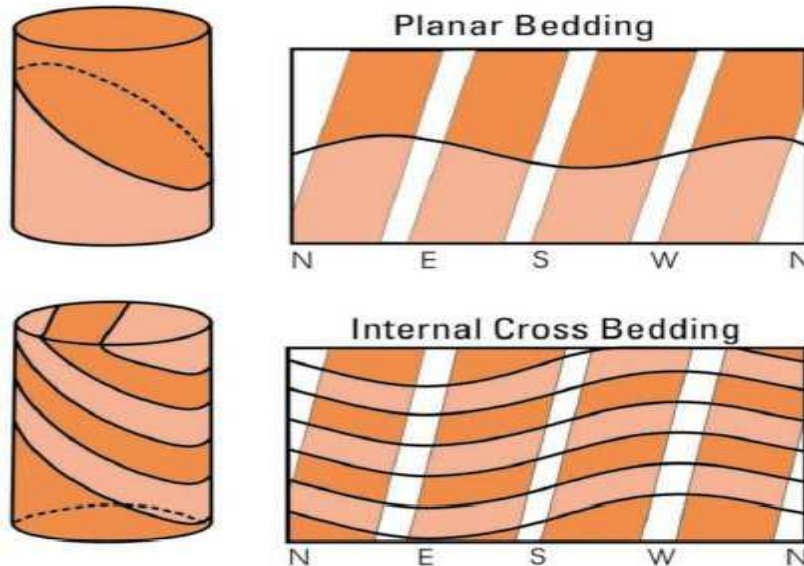
Figure 2.3: 2-D unwrapped presentation of OBMI-capture features with the help of sine waves.

Two types of normalization are performed; static and dynamic. In static normalization a preferred spectrum of colors (64) are distributed over the data interval. This technique provides a good overall representation of the data, highlighting major resistivity variations. Higher resolution normalization is achieved through the process of dynamic normalization, where a preferred spectrum of colors, up to 64, is distributed over a 2 ft-window length. A sliding window method is applied to the whole data interval. The calibrated and normalized images thus produce the optimized image of the resistivity data and are presented side by side on a processed plot at a 1/10 vertical scale.

All interpretations have been carried out using a combination of static and dynamic normalization. A resistivity contrast is represented by color variation on the images and therefore inferences that relate to the textural characteristics of the respective lithology are made based upon the resistivity contrast. The images are 2D, unwrapped representation of the 3D borehole and borehole crossing; planar features are represented by sine waves at abrupt resistivity contrasts, as illustrated in figure 2.3 above.

Sedimentary dips were defined as those resulting through depositional processes and include bed boundaries (e.g. planar bed tops and bases) and internal bedding features (e.g. internal sand deformation).

Feature Name	Description	Symbol
Sedimentary Dips:		
Sand	Internal sand bedding (e.g. Laminations, cross bedding)	
Shale	Internal shale bedding and lamination	
Deformed sand	Relatively high angle irregular bedding in sand beds	
Bed Top	Planar (non-erosional) upper sand bed lithological/facies contact	
Bed Base	Planar (non-erosional) lower sand bed lithological/facies contact	
Structural Dips:		
Conductive Fracture	Continuous / discontinuous planar feature cutting bedding. Conductive indicates open 9or shale fill). No sense of offset	
Resistive Fracture	Continuous / discontinuous planar feature cutting bedding. Resistive indicates cement. No sense of offset	
Possible Micro Fault	Continuous planar feature cutting bedding, minimal offset, minor drag features	

Table 2.1: Classification of the dips and their interpretation scheme

Structural features include those planes that cut across bedding (e.g. fractures, faults). Drilling induced fractures and breakouts were not observed on the image. The dip classification scheme is summarized in Table 2.1.

2.5 Manual Dip Analysis

Unlike dipmeter processing, which uses only 1 or 2 resistivity curves per pad, manual dip picking form and image can provide high quality dips to a significantly high level of confidence even when the image is degraded. The notable improvement, both in dip density and dip quality, is mainly due to the fact that manual picking takes full advantage of both the borehole coverage of the 4 image tracks and the accuracy of the human eye. Interactive dip picking is performed with a sliding sine wave of which both the amplitude and azimuth can be manually fitted to a planar feature on the image.

When the interpreter determines the fit between the sine wave and image feature is satisfactory the dip is computed. The interactive dips are then classified according to the type of interpretation being undertaken. The Dips are denoted in the graphics using tadpoles with the head circle being the magnitude of the dip and the tail indicating the azimuth of the same (figure 2.4).
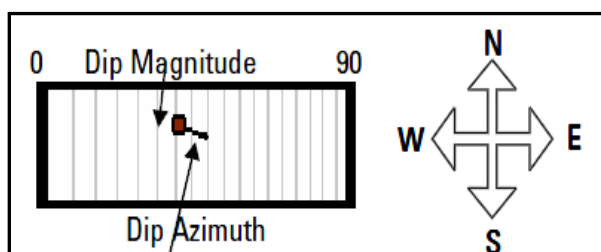
Figure 2.4: Dip tadpole plot denotations

Structural interpretation includes defining structural dip zones, magnitudes and azimuths; indentifying any angular unconformities; identifying and determining the orientation of features with tectonic origin including faults and fractures.

2.6 Structural Dip Zonation

Structural dip is generally defined from bedding in lithologies that are assumed to have been deposited with a horizontal or near-horizontal attitude. This includes bedded or laminated shale and thinly interlaminated lithologies. Over some intervals in the Ignik Sikumi #1 well structural dip can be determined with confidence from the shales (Appendix Figure A2.2).

Structural dip zones (Table 2.2) are separated based on the different Sagavanirktok formations (Table 1.2) and the dip orientation within the formations (Table 2.1).

Zone	Formation	Interval (ft)	Dips Used	Mean Dip	Mean Azimuth
Zone 1	Mid-Eocene Shale	1,504 - 1,572	Shale	10.02	359.70
Zone 2	Sagavanirktok F	1,572 - 1,920	Shale	7.40	32.40
Zone 3.1	Sagavanirktok E	1,920 - 1987	Shale	6.32	26.14
Zone 3.2	Sagavanirktok E	1,987 - 2,011	Shale	8.80	338.2
Zone 3.3	Sagavanirktok E	2,011 - 2,060	Shale	10.39	27.64
Zone 4	Sagavanirktok D	2,060 - 2,214	Shale	10.61	71.20
zone 5.1	Sagavanirktok C	2,214 - 2,483	Shale	7.98	18.50
zone 5.2	Sagavanirktok C	2,483 - 2,550	Shale	5.70	56.90

Table 2.2: Zones defined by shale dip azimuth
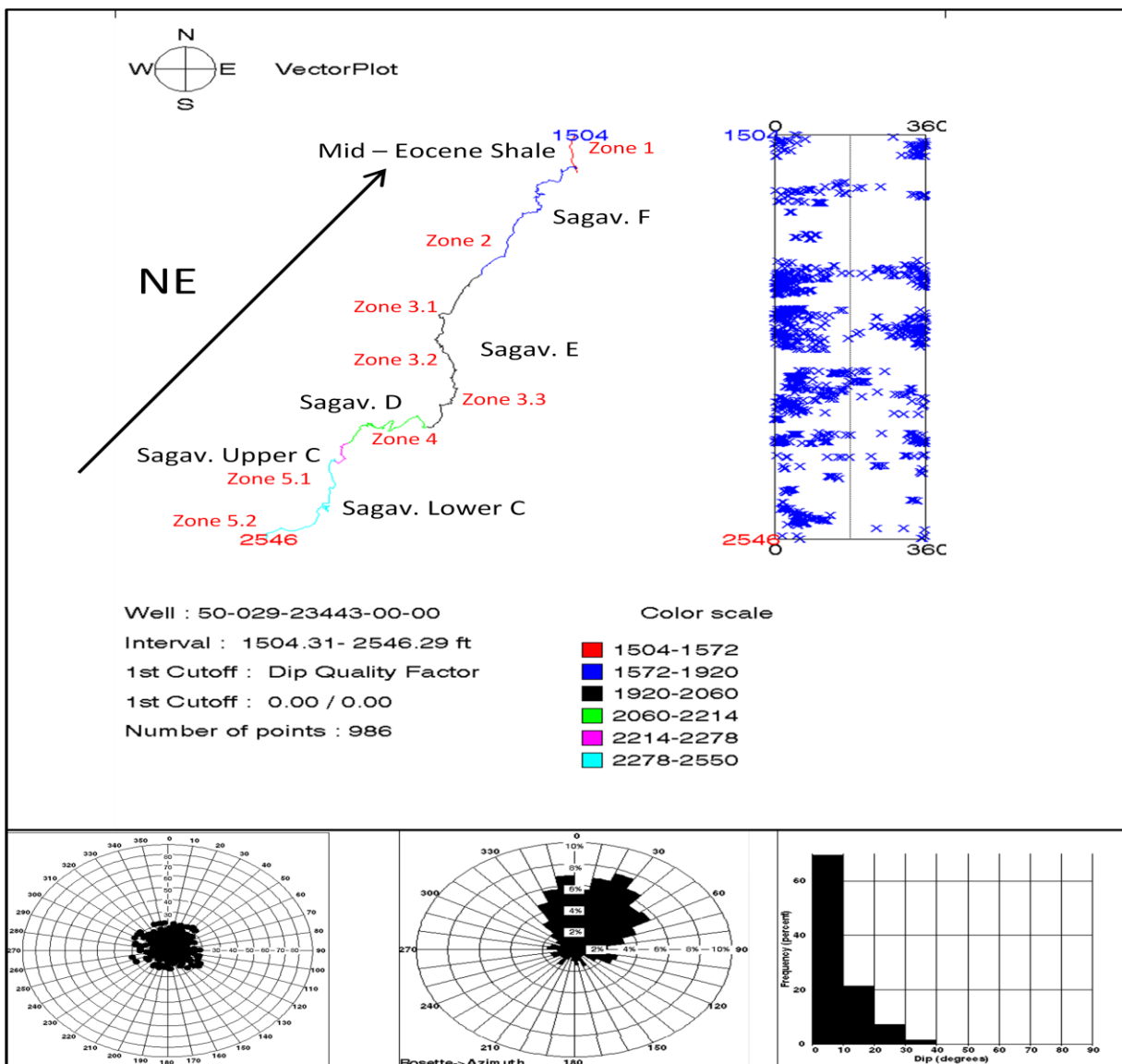
Figure 2.5: Vector Plot with the dips separated by formations and zones.

2.7 Sand Dips

Features picked within in the sands were differentiated into two categories, sand dips and deformed sand dips (Appendix Figure A2.2). A vector plot of the sand dips indicates the majority of the beds are dipping to the north and north-east and are dipping less than 10 degrees (figure 2.6).
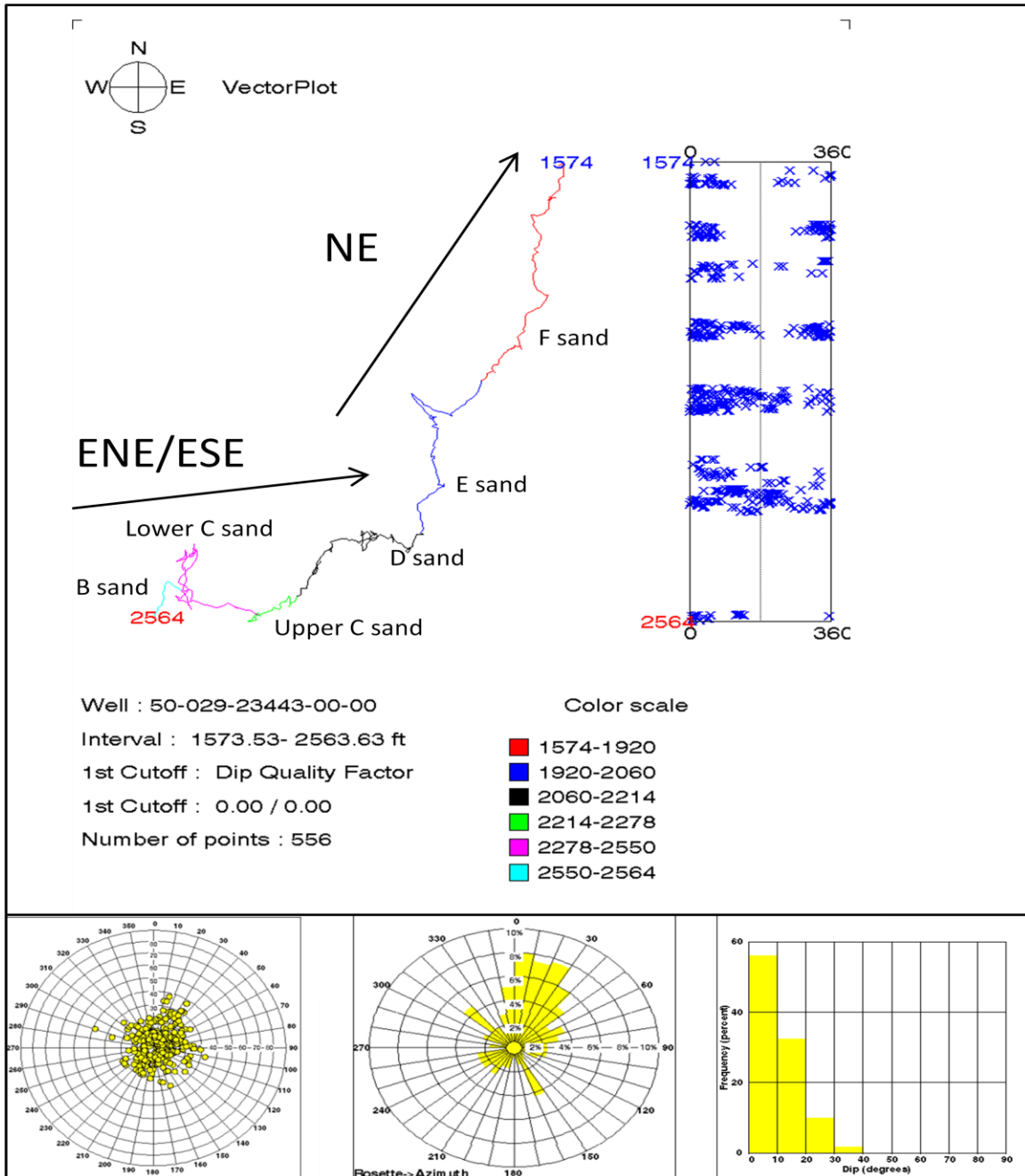
Figure 2.6: Vector plot, Schmidt plot, Rosette, and Histogram of the sand dip azimuths and orientations

2.8 Fractures and Faults

Thirty nine resistive fractures and thirty four conductive fractures were observed between 1,490 and 2,565 ft MD and examples are illustrated in appendix figures A2.2 & A2.5. The majorities of the fractures are striking either NE-SW or NW-SE (Figure 2.7) and represent conjugate sets throughout. The resistive fractures may be open or OBM filled, while conductive fractures may indicate clay filling.

Five possible micro-faults were identified and are illustrated in appendix figure A2.2 and have a NE-SW strike.

| Possible Micro Fault | Resistive Fracture | Conductive Fracture |
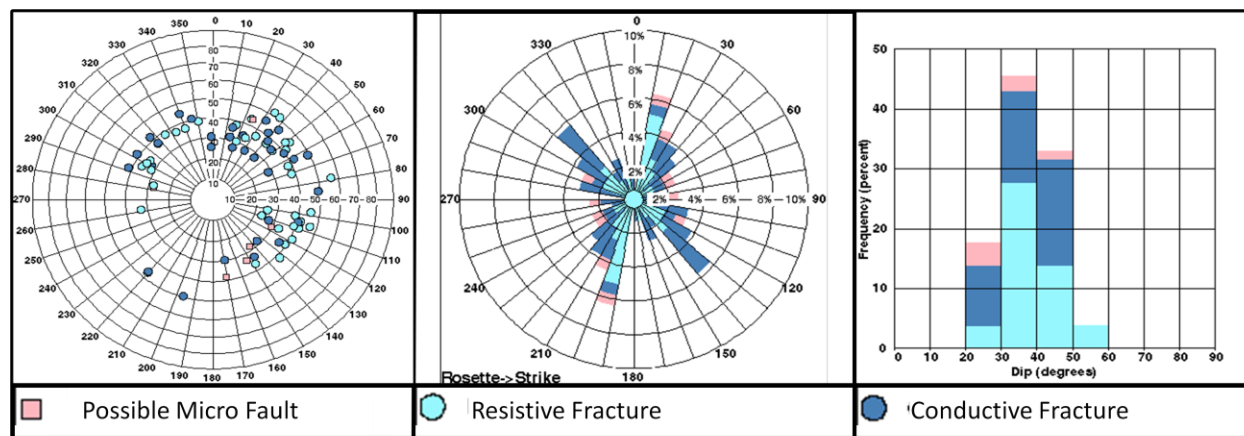
Figure 2.7: Schmidt plot, Rosette Strike, and Dip Magnitude Histogram for the possible micro faults, resistive fractures, and conductive fractures.

2.9 Net Sand-count

The net sand count is determined from the synthetic resistivity curve created from the OBMI*. A cutoff of 46 ohm.m was used over the logged section. The resistivity curve is then integrated and is defined as net sand. The total net sand count for the interval 1490 to 2565 ft MD is 133.7 ft of pay reservoir.

2.10 Sedimentology and Facies Identification

The interval between 1,490 and 1,565 ft MD is subdivided by formation zones (Table 1.2) and the lithology is classified from the log response and OBMI* analysis. Ten different facies are identified (Table 2.3) and examples are given in Figures A2.2, A2.3, A2.4, and A2.5. The interval examined from the OBMI* consists of a series of coarsening upward sequences. Each sequence is defined within a formation zone and a description of these zones is given below.
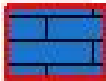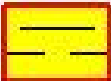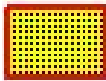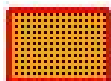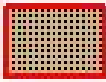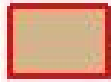
Facies	Color and Pattern	Image Description
Deformed Sandstone		Resistive sand with over-steepened / Contorted bedding
Concretion		Thin (2 in) high resistive layers or nodules
Cross-bedded Sandstone		Resistive formation with clean gamma ray, high sand count, and cross stratified features.
Shaly Sandstone		Resistive layers with thin layers or clusters of conductive mud
Laminated Sandstone		Resistive laminated layers with clean gamma ray and larger amounts of sand sized particles
Massive Sandstone		Thick resistive layers with clean gamma ray and larger amounts of sand sized particles
Laminated Silt		Laminated Conductive silt with moderate amounts of clay and sand particles
Massive Silt		Conductive thick silt with moderate amounts of clay and sand particles
Laminated Shale		Conductive laminated mudrock with high gamma ray values, low resistivity, and large amounts of clay
Massive Shale		Conductive mudrocks with large amount of clay, high gamma ray, and low resistivity values

Table 2.3: Facies descriptions

- **Sagavanirktok B (2550 – 2565 ft MD: Figure A1.2)** – Only the upper 15 ft of the B formation was logged and it consists of a wet sandstone mostly massive in structure with some faint laminations mainly tending towards the NE direction.

- **Sagavanirktok C (2215 – 2550 ft MD: Figures A1.2)** – The base of this formation consists of a shale that coarsens upward into two main sands sections. The lower sand section contains small layers of cross-bedding within sands intercalated with silt and shaly beds. The upper sand however is cleaner and contains some deformation towards the base. This unit fines upwards to a silt and shale interlaminated zone which is 2 to 5 ft thick. Both resistive and conductive fractures as well as micro-faults are seen through this section with main strike towards the NE-SW.

- **Sagavanirktok D (2060 – 2215 ft MD: Figures A1.2 and A1.3)** – The base of this formation consists of mostly laminated shale. At 2113 ft MD the formation quickly transforms from a shale into a sandstone. The sandstone contains massive, laminated features. Faint cross-bedded is witnessed at the base of this unit. The shales in this section contain multiple conductive and resistive fractures. In addition, two possible micro-faults are identified also following the dominant strike trend of NE-SW.

- **Sagavanirktok E (1920 – 2060 ft MD; Figure A1.3)** - The base of this formation consists of a thick (60 ft) mostly laminated shale. The unit coarsens upward into a laminated sandstone. Two faults with localized drag features are identified in this section.

- **Sagavanirktok F (1571.2 – 1920 ft MD; Figures A1.3 and A1.4)** – This zones contains two coarsening upward sequences. The bottom of the formation contains laminated and massive shales that coarsen upward into siltstones and finally into a sandstone at 1740 ft MD. The siltstones in this formation contain a large amount of fractures. The sandstone is identified by its low gamma ray values, but there is also a large amount of washout in this section. After 1700 ft MD, the formation consists of a massive and laminated shales that coarsen upward into a massive sandstone.

- **Mid-Eocene Shale (1490-1571.2; Figures A1.4)** – Shale formation with lenses of more conductive mud.

3. RT SCANNER

3.1 Introduction

Laminated shale-sand or thin-bedded sand formations exhibit strong resistivity anisotropy. That is, resistivity measured perpendicular to the bedding (Rv) is significantly higher that the resistivity measured parallel to the bedding (Rh) due to the thin low resistivity (conductive) shale layers. Water saturation is over estimated by the conventional resistivity tools in thinly bed reservoirs. The triaxial induction tool (called Rt Scanner) provides several 3x3 tensor measurements that are sensitive to Rh, Rv and formation dip.

3.2 Rt Scanner Interpretation model

A forward –model (1D) inversion algorithm returns horizontal and vertical resistivity (Rh and Rv, respectively) as well as dip and azimuth of the formation. The inverted resistivity is dip-corrected, and shoulder bed corrected.
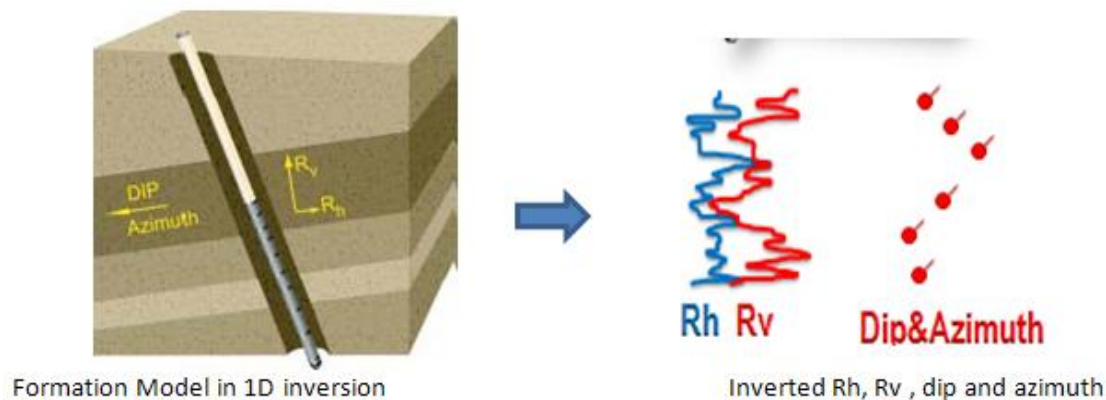
Figure 3.1: Theoretical examples of Rv and Rv.

3.3 Results

Rt scanner data was logged in open hole with oil base mud from 1473-2580 ft. The data quality was excellent except for one receiver. The data was reprocessed removing the receiver which was out of tolerance. Overall the results show resistivity anisotropy, Rv is higher than Rh. In the low resistivity, low dip zones, Rh is very close to AIT 90, the difference between Rv and Rh (or Rv/Rh) indicates strong resistivity anisotropy in the laminated shaley sand formations. In the high resistivity zones,1570 -1620, 2242 - 2272 ft, Rv is equal to Rh, because the tool is not sensitive to anisotropy in high resistivity zones.
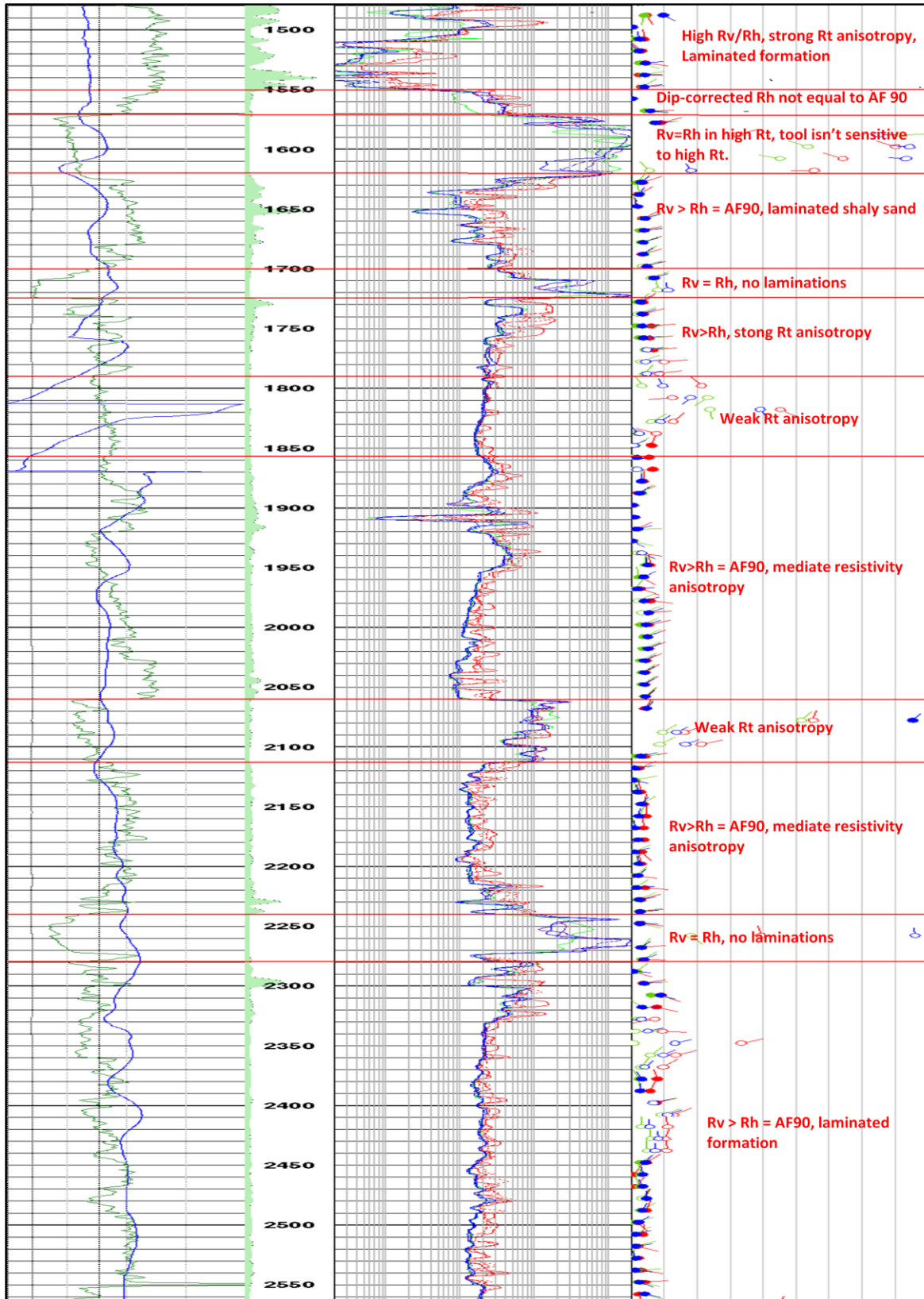
Figure 3.2: Rv, Rh, and Calculated dips from the Rt Scanner

4. Sonic Scanner

4.1 Introduction & Background

The Sonic Scanner* acoustic scanning platform provides a true 3D representation of the formations surrounding the borehole by scanning both orthogonally and radially. The latest acoustic technology is used to acquire borehole-compensated monopole with long and short spacings, and cross-dipole measurements. In addition to making axial and azimuthal measurements, the fully characterized tool radially measures the formation for both near-wellbore and far-field slowness. The typical depths of investigation are 2 to 3 times the borehole diameter.

The wide frequency spectrum used by the Sonic Scanner* tool captures data at a high signal-to-noise ratio, regardless of the formation slowness, and eliminates the need for multiple logging passes. The combination of a longer azimuthal array than on conventional acoustic tools—13 stations with 8 azimuthal receivers each—and multiple transmitter-receiver spacings enables the measurement of a radial monopole profile across the near-wellbore altered zone.

A 3D anisotropy algorithm is used to transform Sonic Scanner compressional, fast- and slow-shear, and Stoneley slowness measurements with respect to the borehole axes to referenced anisotropic moduli. The formation can then be classified as isotropic or anisotropic, along with determining the type and cause of the anisotropy—intrinsic or stress induced from the drilling process (figure 4.1).
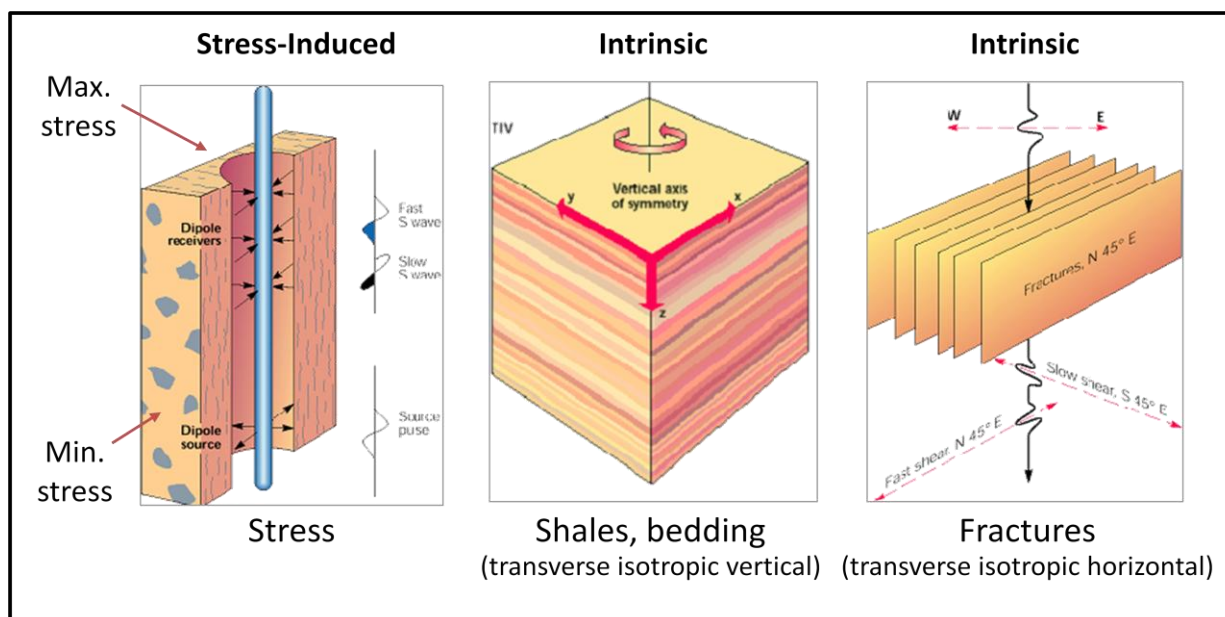
Figure 4.1: Graphical representation of both stress induced and intrinsic anisotropy mechanisms. Stress induced anisotropy velocity varies in both radius and azimuth, while shales and fractures are intrinsic anisotropy and the velocities vary only azimuthally.

4.2 Sonic Scanner Results for Ignik Sikumi #1

Schlumberger Sonic Scanner tool was run on ConocoPhillips Alaska, Inc. well Ignik Sikumi 1 on 17-APR-2011. The Sonic Scanner tool was run in P&S mode and Cross Dipole mode across the interval from 1472 ft to 2611 ft MD.

The Sonic Scanner data was acquired in P&S (monopole) mode and cross dipole mode. Compressional and shear travel times were rush processed by Schlumberger Data and Consulting Services (DCS) on the day of acquisition with the results transmitted to DCS Houston for planning of the XPT and MDT runs.

Quality control review of the Sonic Scanner data is outlined below:

The Sonic Scanner data for this well was obtained in open hole over the interval from 1472 ft to 2611 ft MD with cased hole data acquired to 1228 ft MD.

The borehole appears to be in very good shape over most of the wellbore with the exception of two intervals located within the permafrost section. The interval from 1709 ft to 1726 indicates two inches of washout while the interval from 1520 ft to 1626 ft indicates ¼ in to ½ in washout.

In general the open hole section shows high quality waveform and Slowness Time Coherence (ST) for all modes (monopole, dipole and low frequency monopole). The interval above the casing shoe indicates a strong casing signal with little to no monopole compressional data. The dipole signal in casing is also severely affected by the casing signal. As a result only the open hole sections will be processed.

The dipole signals exhibit high frequency compressional components which was filtered out during processing (See Figures below)
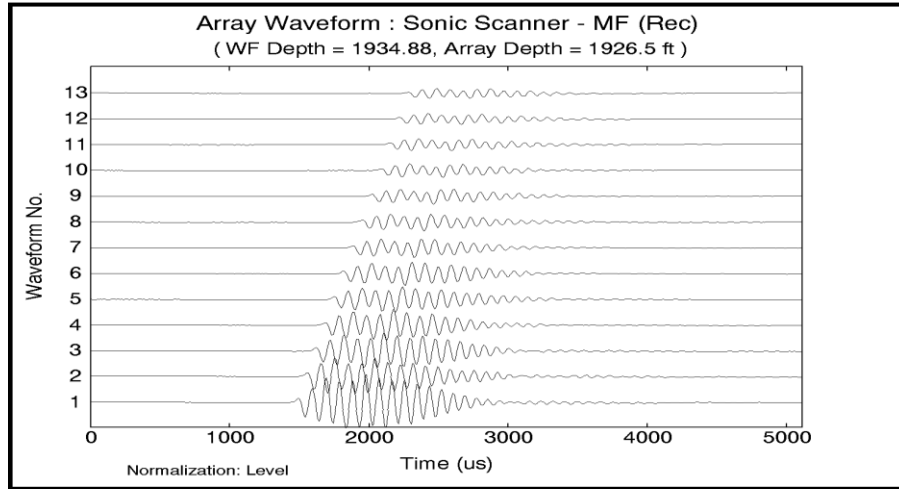
Figure 4.2 - Monopole Far waveform data 1926 MD (Hydrate section)

The waveforms depicted in Figure 4.2 are from the monopole mode and are from one of the apparent hydrate intervals. Note the very clean monopole waveform data from this depth.
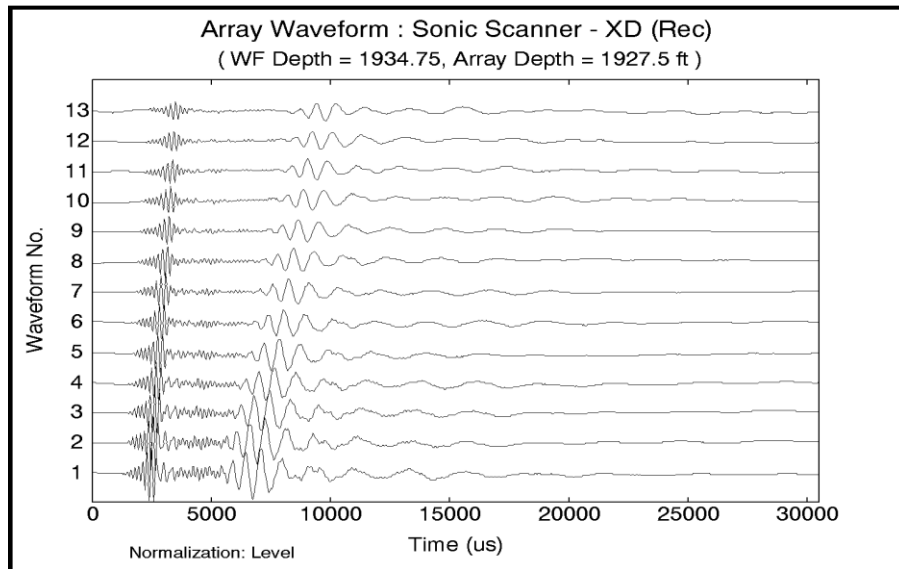
Figure 4.3 - Dipole waveform data from 1927 ft MD (Hydrate section)

Figure 4.3 presents the dipole waveforms from one of the apparent hydrate zones. This dipole waveform signal exhibits high frequency compression signal before the low frequency high amplitude dipole shear signal.
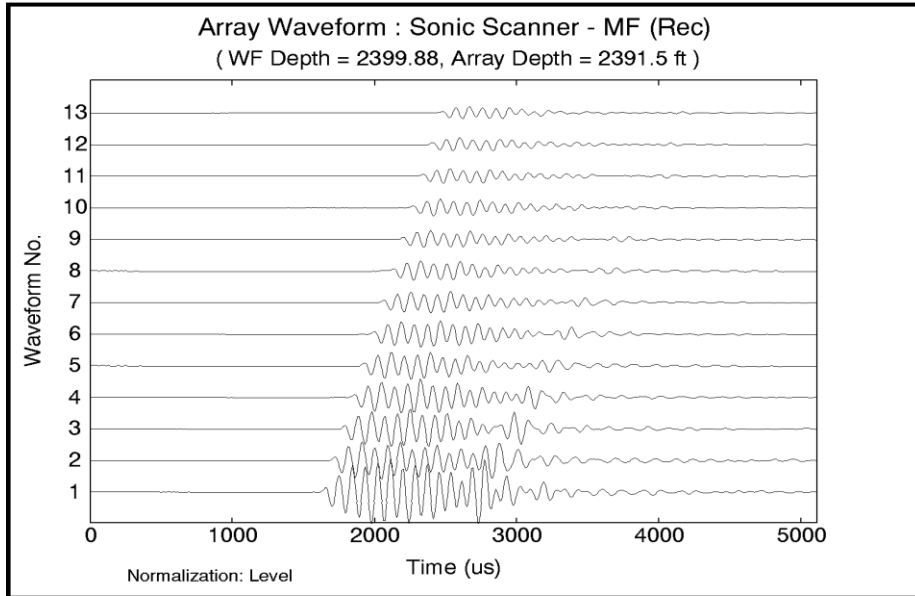
Figure 4.4 - Monopole Far waveform from 2391 MD, (non-hydrate formation)

Figure 4.4 is the monopole mode waveform from a non-hydrate interval. Note the very clean monopole waveform data from this depth.
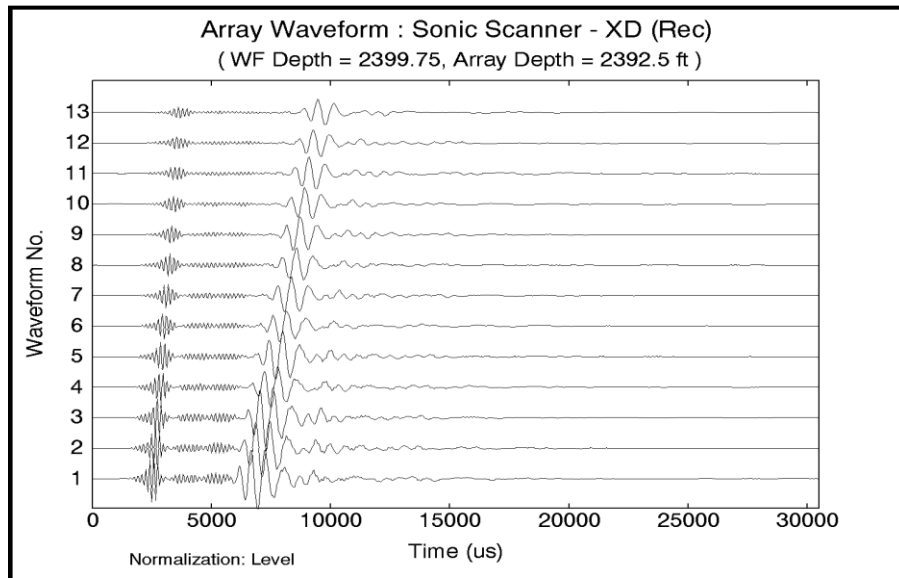
Figure 4.5 - Dipole waveform from 2392 ft MD (non-hydrate formation)

Note as with the dipole waveform in the apparent hydrate interval this section shows high frequency monopole signal before the low frequency high amplitude shear signal. This is below the apparent hydrate interval.

The apparent hydrate zones exhibit faster travel times than the shale and water filled zones. The shale and water filled zones are considered slow formations relative to processing while the apparent hydrate zones are considered intermediate to slow.

The Slowness Dispersion Plots (SWDA) presented below show frequency (x axis) verses slowness in usec/ft (y axis). These plots are used to understand the nature of the sonic signals to identify various conditions impacting the recorded waveforms. These plots include modeled response for shear travel time as solid lines with measured results as circles.

The SWDA plot from 1849 (figure 4.6) is from the shale above the upper hydrate Note the fast and slow shear results (red and blue circles) do not match the modeled results exhibiting a steeper slope. This is indicative of formation damage. By applying a filter to the lower frequency section of the dipole signal the true shear can be processed in this case.   The anisotropy plot from this interval clearly shows a different fast and slow shear signal with an orientation of the fast shear signal of NW 50 degrees.
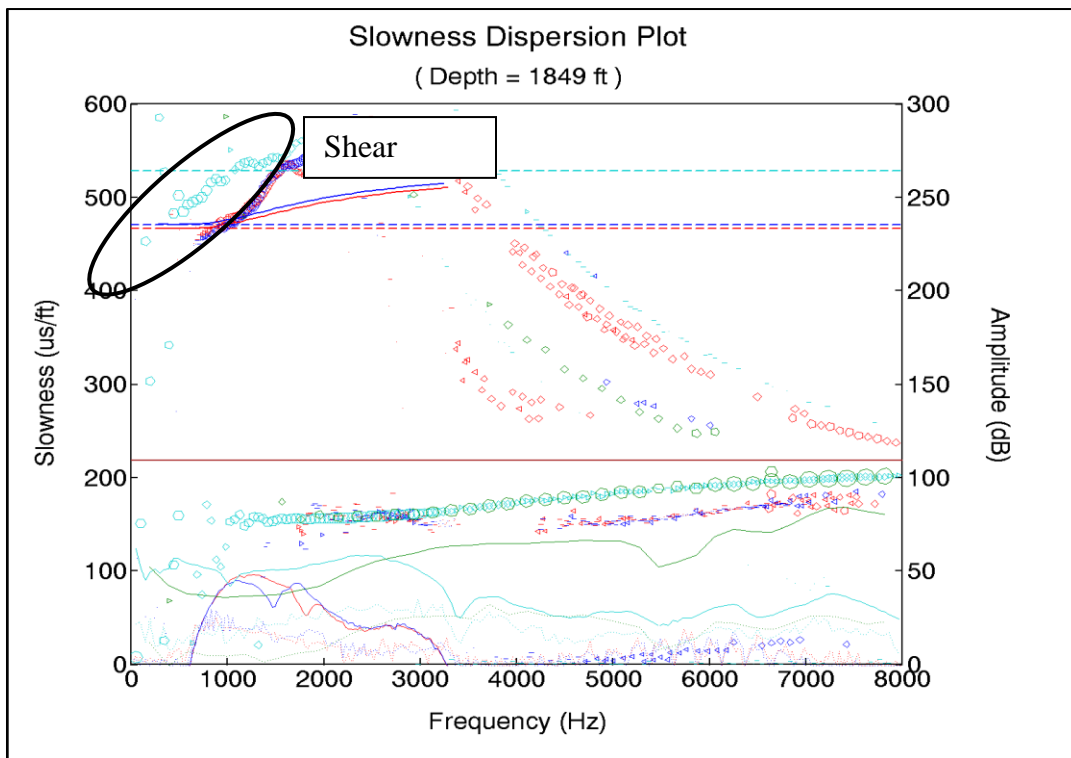
Figure 4.6: Slowness Dispersion Plot at 1849
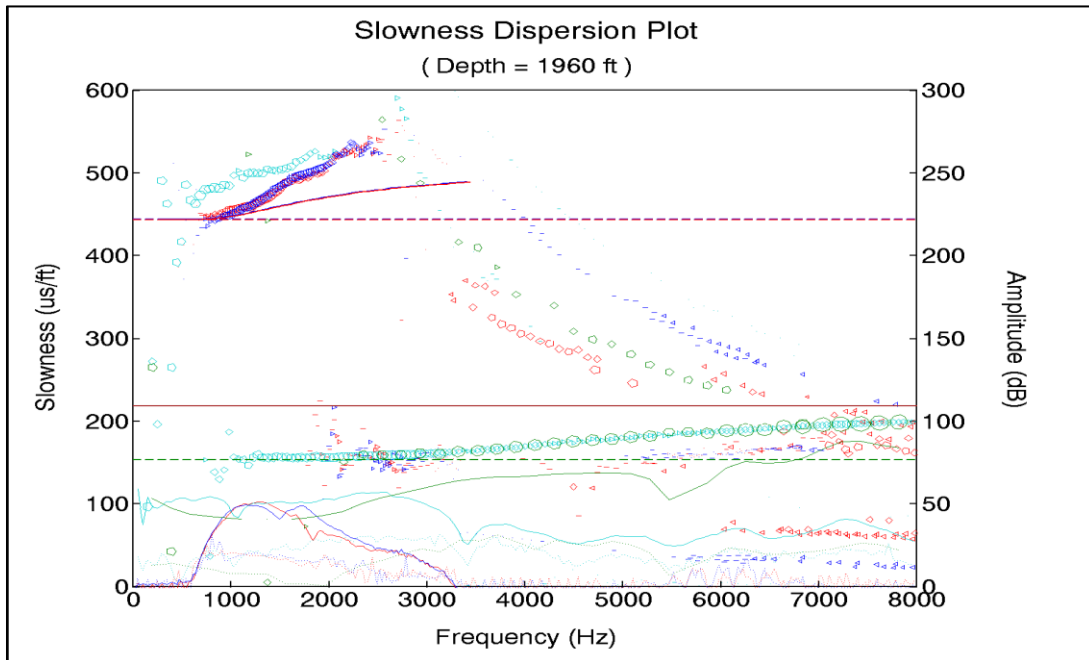
Figure 4.7 Slowness Dispersion plot at 1960

The SWDA figure from 1960 indicates formation damage due to the high slope on the shear signals. The anisotropy plot presented above across this interval clearly identifies differing travel times (fast and slow) with an orientation of around North 50 West. The waveform presented at this depth shows differing fast and slow shear travel times.

Over much of this well the fast shear azimuth tracks the tool rotation indicating that there is little to no anisotropy present. In intervals with anisotropy (indicated by the green shading in the left track the fast shear azimuth does reflect formation anisotropy.

The complete display of the monopole compressional, dipole shear and anisotropy results are presented in graphic format included with this report.
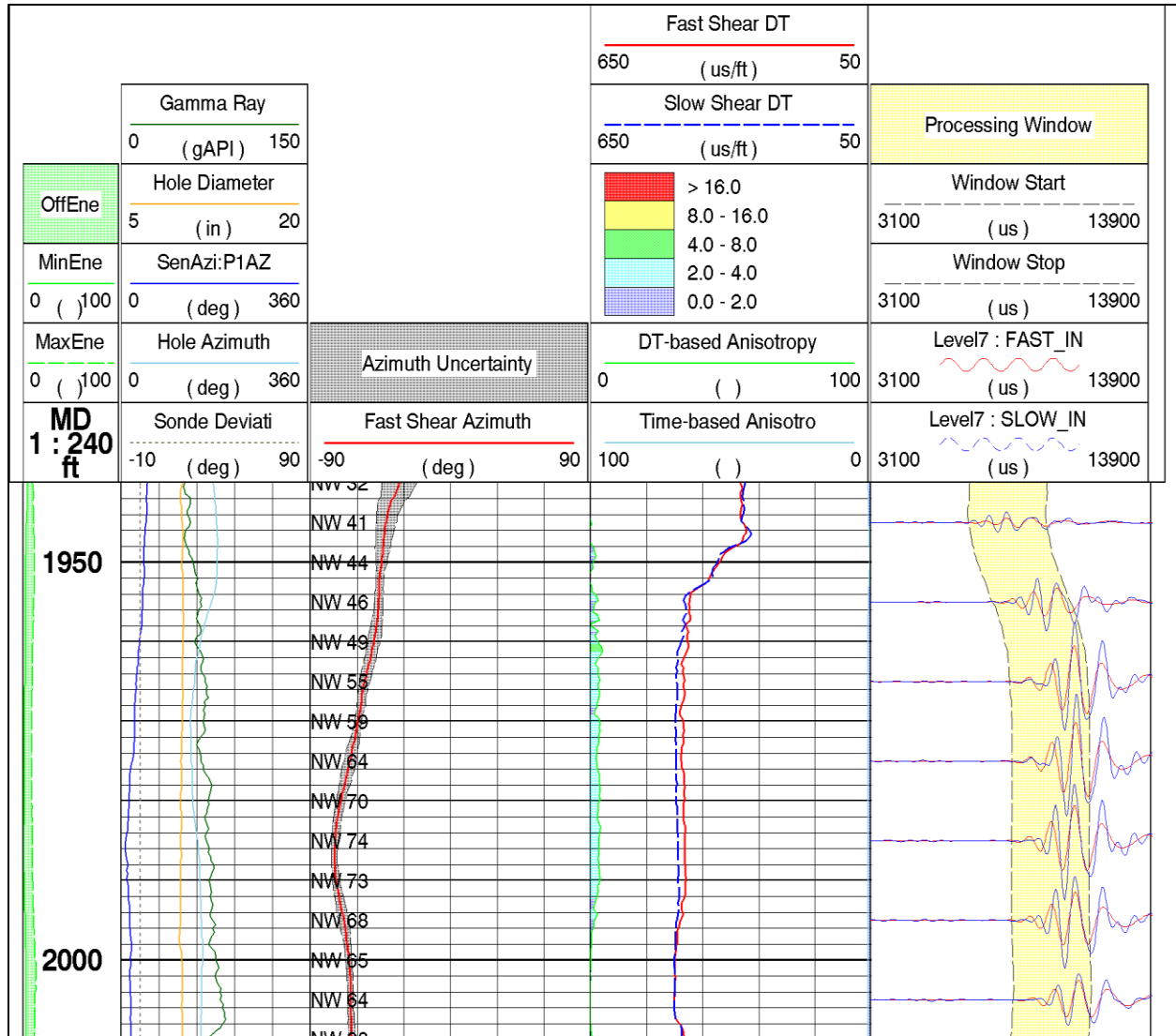
Figure 4.8: Anisotropy between the fast and slow shear waves.

The slowness dispersion plot from 2400 ft indicates clean signals with multiple modes present in the compressional data. Note the dispersive monopole signal from 2500 Hz to 10000 Hz. This is indicative of Leaky-P borehole mode. Note at higher frequency the non-dispersive monopole signal is available. The Leaky-P signal is characteristic of very slow formation and can be processed for compressional travel time by focusing on the low frequency portion of the signal. Also note that the low frequency Leaky-P signal and the non-dispersive monopole signal indicate the same travel time.   This interval exhibits little to no anisotropy.

The two rose plots presented below identify two distinct anisotropy directions.
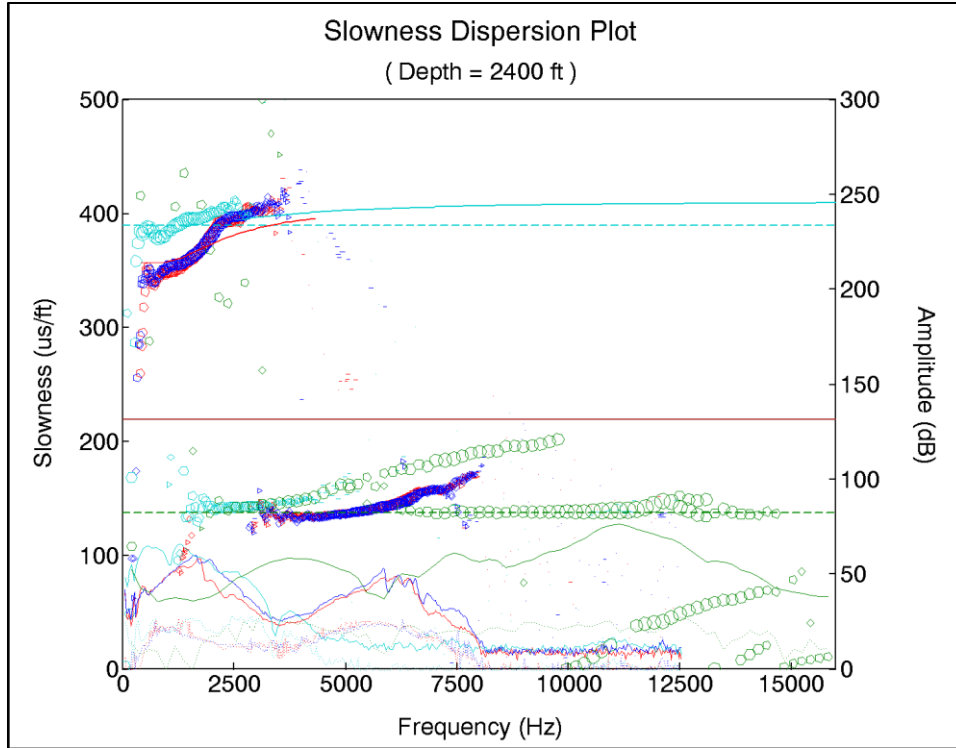
Figure 4.9: Slowness dispersion plot at 2400
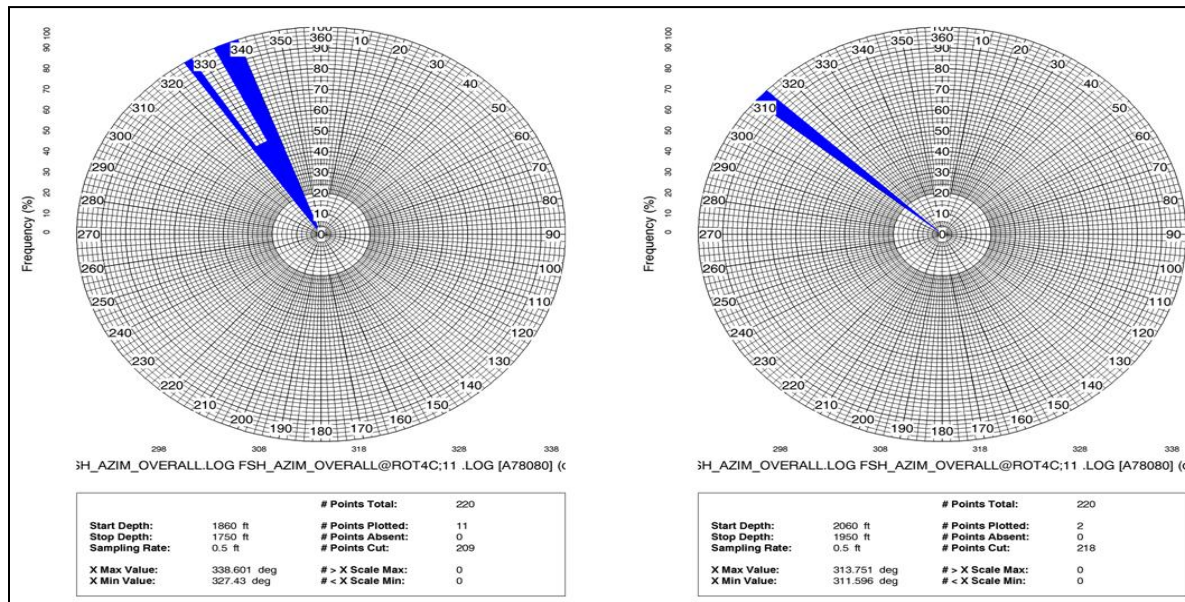
Figure 4.10: Rose plots indicating direction of anisotropy

The upper rose diagram (on left) indicates a fast shear direction with an azimuth of approximately 320 degrees while the lower section (on right) indicates a fast shear azimuth of approximately 312 degrees.

The figure below presents the Anisotropy plot over the openhole section of this well.
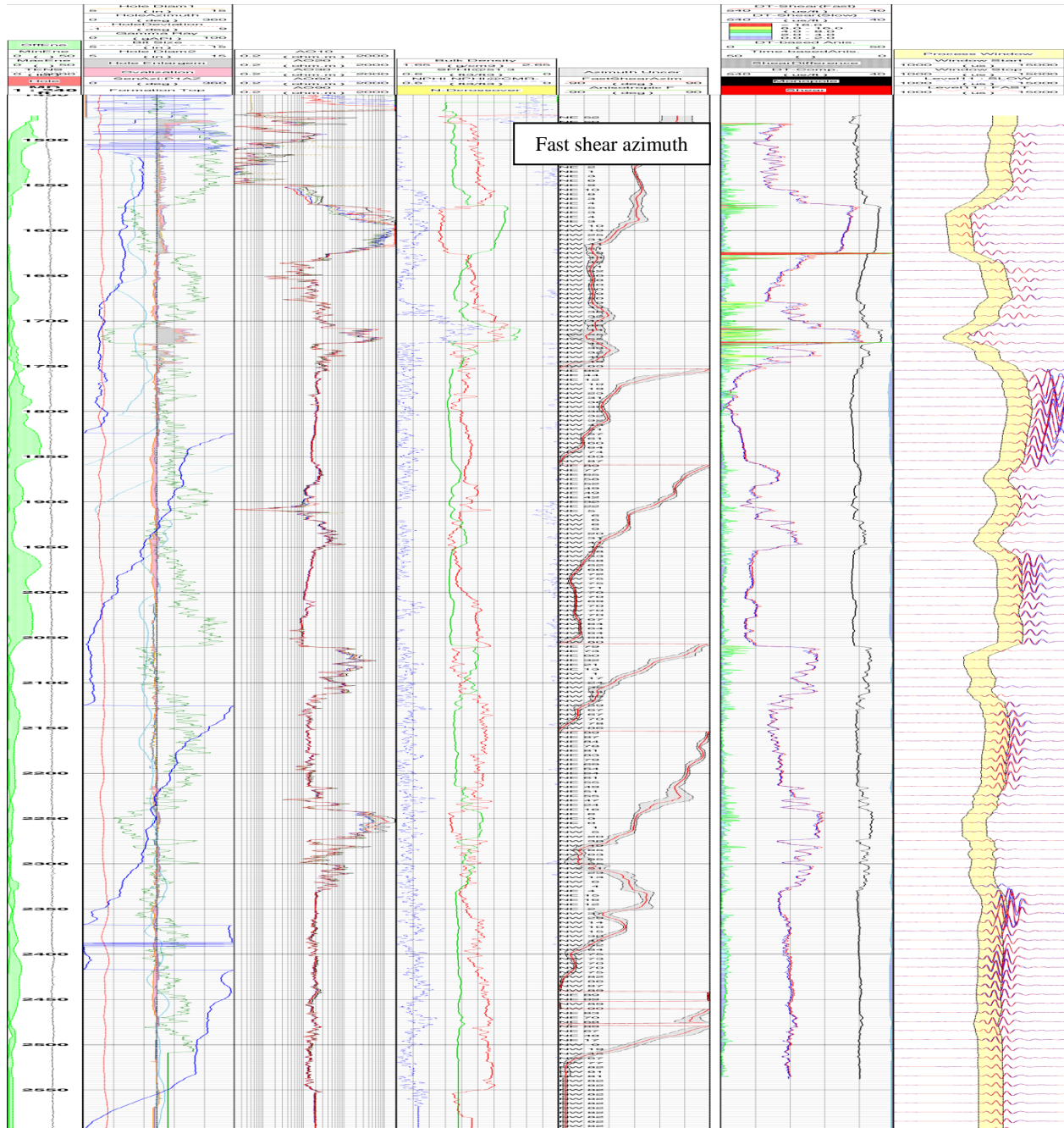
Figure 4.11: Anisotropy plot for the openhole section.

In summary the compressional and shear travel times are of high quality. This well exhibits acoustic anisotropy primarily in the shale sections of this well mainly in the intervals from 1760 ft to 1860 ft MD, 1900 ft to 2000 ft MD and 2400 ft to 2470 ft MD. The hydrate intervals exhibit lower amplitude on the waveforms.

5. ELAN*

Schlumberger performed an ELANPlus petrophysical analysis of the wireline data from ConocoPhillips Alaska, Inc. (CP) well Ignik Sikumi 1. The goal of this petrophysical study was to analyze the hydrate saturations within the interval from 1850 ft to 2540 ft md. Additionally ice saturation was identified above 1850 ft MD.

The ELAN* petrophysical analysis provides a level by level quantitative evaluation utilizing a simultaneous equation solver to identify the minerals and fluids within the interval analyzed. The specific minerals and fluids solved for in this evaluation included quartz, illite, ice, natural gas hydrate and liquid water. Well logging tools used in this model included:

- Bulk Density (RHOZ)
- Bound Fluid Volume (BVV)
- Gamma Ray (GR)
- Resistivity (AO90)

Selected parameters used in this evaluation include:

Parameter	Value
Rw	3 at 42 degF
Matrix Density	2.65
Hydrate Density	0.91
Ice Density	0.91
Water Density	1.0
CMR* HI of Hydrate	0

Table 5.1: Selected parameters

Water Resistivity (Rw) was determined using Rwa calculations from the apparent water sand located between 2330 ft and 2360 ft.

Based on this analysis three main hydrate sands were identified within this borehole. These are located at the following intervals:

- 1920 ft to 1955 ft MD
- 2060 ft to 2110 ft MD
- 2240 ft to 2330 ft MD

Minor hydrates were also located at 1860 ft to 1880 ft MD. Ice was identified at 1570 ft to 1625 ft MD with possible ice at 1708 ft to 1715 ft MD. This second ice interval was not quantitatively analyzed due to borehole conditions (washout) affecting the well log values.

6. CMR*

The CMR* uses magnetic resonance measurements to determine irreducible water saturation, pore size distribution, porosity, and permeability.

6.1 CMR* Bound Fluid Volume

The CMR* bound fluid volume is estimated by integrating the T2 distribution up to an analyst defined cutoff value. The T2 cutoff value used for is 33 ms.

The CMR-Plus* will characterize T2 decays as early as 0.3 ms. The clay bound water existing in the micro pores normally decay at this rate and this ensures that the clay bound water is sensed by the tool. The amount of the clay bound water is proportional to the volume of clay and is a direct indication of the volume of the clay.

An assumption is made that all porosity with a T2 time between 0.3 and 3 ms is associated with clay bound water. All porosity between 0.3 ms and the BFV cutoff of 33ms is capillary bound water. The CMR* tool uses short echo spacing of 200 microseconds, so diffusion affects are minimized.

Also, most common producible hydrocarbons have their T2 response in the higher ranges and do not affect the computation of BFV. This leads to high confidence in the CMR* BFV calculation. The BFV volume that the CMR* processing outputs includes both clay-bound water and capillary-bound water. The mnemonic for this volume is BFV.

6.2 CMR* Porosity

The porosity estimation from the CMR* is lithology independent, responding only to the pore fluids. The polarization of the pore fluid and its hydrogen index determine the response of the CMR* to the pore volumes occupied by each fluid.

Given that the depth of investigation of the CMR* is approximately around 2 inches, the fluids being measured are primarily mud filtrate, unflushed formation fluid (water and hydrocarbon) and clay and capillary bound water.   In the CMR* porosity processing, a polarization correction is applied whenever the wait time is insufficient for complete polarization of the fluid in the pore volume. This normally will occur in zones where there is gas, or where most of the pore space is flushed by the oil base mud filtrate.

The T1/T2 ratio used for the polarization correction is 2. Total CMR* porosity (TCMR) represents integration of the calculated T2 distribution from 0.3 ms to 3000ms. Comparison of density porosity and total CMR* porosity in water bearing zones shows a reasonable match of both porosities.

Schlumberger CMR* outputs relating to porosity are as follows:

TCMR	Total CMR Porosity
CMRP_3ms	All porosity greater than 3ms (TCMR – clay bound) also referred to as CMR* effective porosity.
BFV	All CMR* porosity less than the 20ms cutoff, contains clay bound and capillary bound fluid
CMFF	CMR* free fluid porosity, all porosity greater than 20ms cutoff.
T2LM	logarithmic mean of the CMR* T2 distribution

The CMR* was processed on GeoFrame Processing Platform using the T2 cut off equal to 33ms across logged interval (1490-2565 ft). This cut off was used in the computation of the free and bound fluid volumes, which also were used in the Timur Coates permeability equation. A three-levels averaging was applied to the processing (7.5 inch sampling rate) giving a 22.5-inch vertical resolution for the total, effective and capillary bound porosity.

6.3 CMR* Permeability

The permeability outputs K-Timur coats and K-SDR are also calculated and presented in standard resolution plot.

K-Timur is calculated using the following equation.
$KTIM = 10000 * TCMR^4 * (FFV / BFV)^2$

Where:
      TCMR: Total CMR porosity
      FFV: Free fluid volume ms)
      BFV: Total bound fluid volume

K-SDR is calculated using the following equation.
$KSDR = 4 * TCMR^4 * T2LM^2$

Where:
      TCMR: Total CMR Porosity
      T2LM: T2 Log Mean

6.4 Pore Size Distribution (Facies Correlations)

The CMR* provides qualitative textural information. Several cut off values are chosen to divide the T2 distribution to give the Bin porosity. The CMR* Bin porosity distribution gives an indication of pore size and differentiates rocks of identical porosity and mineral composition. It also shows variations of texture with depth, such as fining or coarsening upward sequences.

The cuttoffs used for MB-2 are:

Bin	1	2	3	4	5	6	7	8
T2 Cutoff	1	3	10	33	100	300	1000	3000

Table 6.1: T2 Cutoffs for Bin Processing

6.5 CMR* Discussion

- The CMR* Porosity is in good agreement with the density porosity except in the gas hydrate zones and the washed out sections.
- In the gas hydrate zone the porosity and T2 distribution is low because the CMR* does not see the ice or hydrate (hydrate MNR HI=0).
- The lower water sand at 2,330 ft MD has a large T2 distribution bin percentages (corresponding to larger pore sizes; Appendix Figure A2.3) indicating higher relative permeability compared to a shale (Appendix Figure A2.2) or gas hydrate (Appendix Figure A2.3)
- The ice at 1,570 ft MD has large bin percentages. This is thought to be caused by melting of the ice and invasion of the oil based mud due to the oil based mud signature (Appendix Figure A2.3).

Appendix A – OBMI* Figures

Figures Illustrating the Principal Facies and Main Features Observed on the OBMI* Images of the Logged Interval

Figures A2 – Scale 1:400

Figures A3 – Scale 1:20
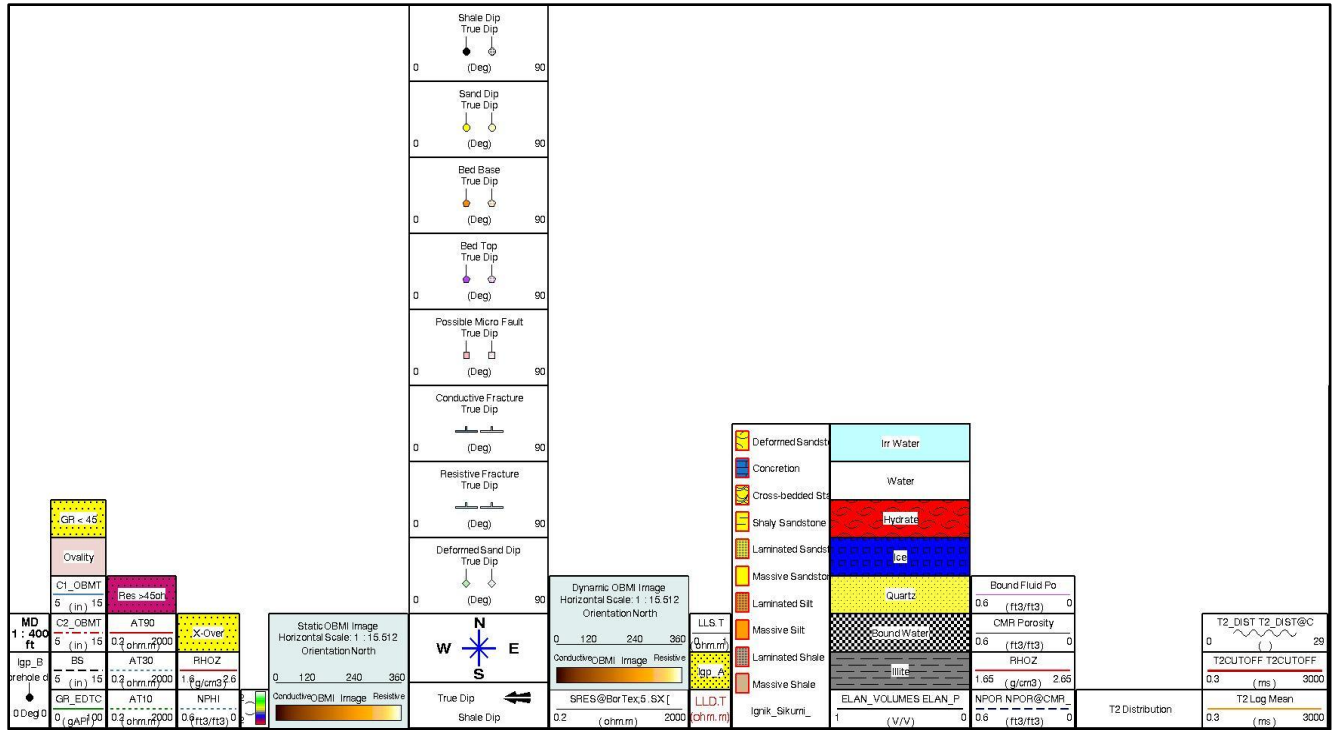
Figure A1.1: Log Header for figures Appendix figures A1
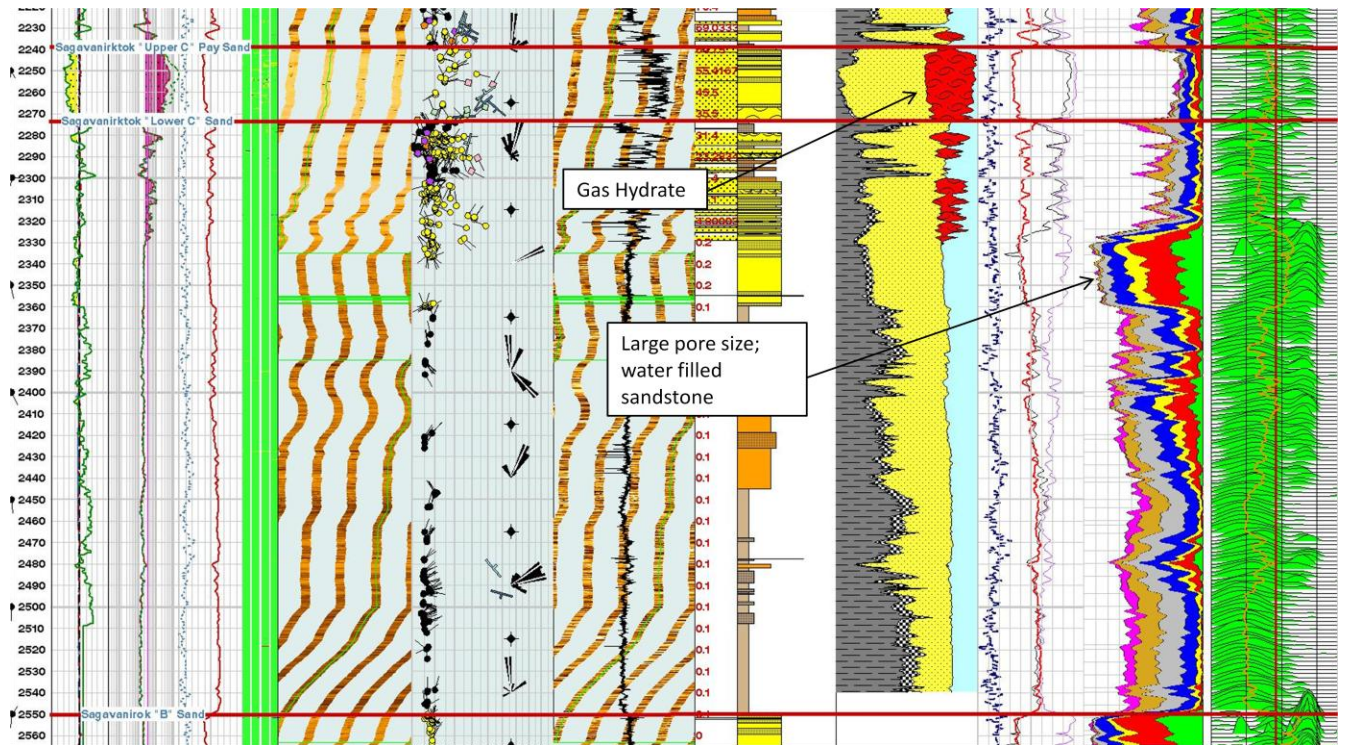
Figure A1.2: 2220 – 2565 ft MD of the Ignik Sikumi #1 well.
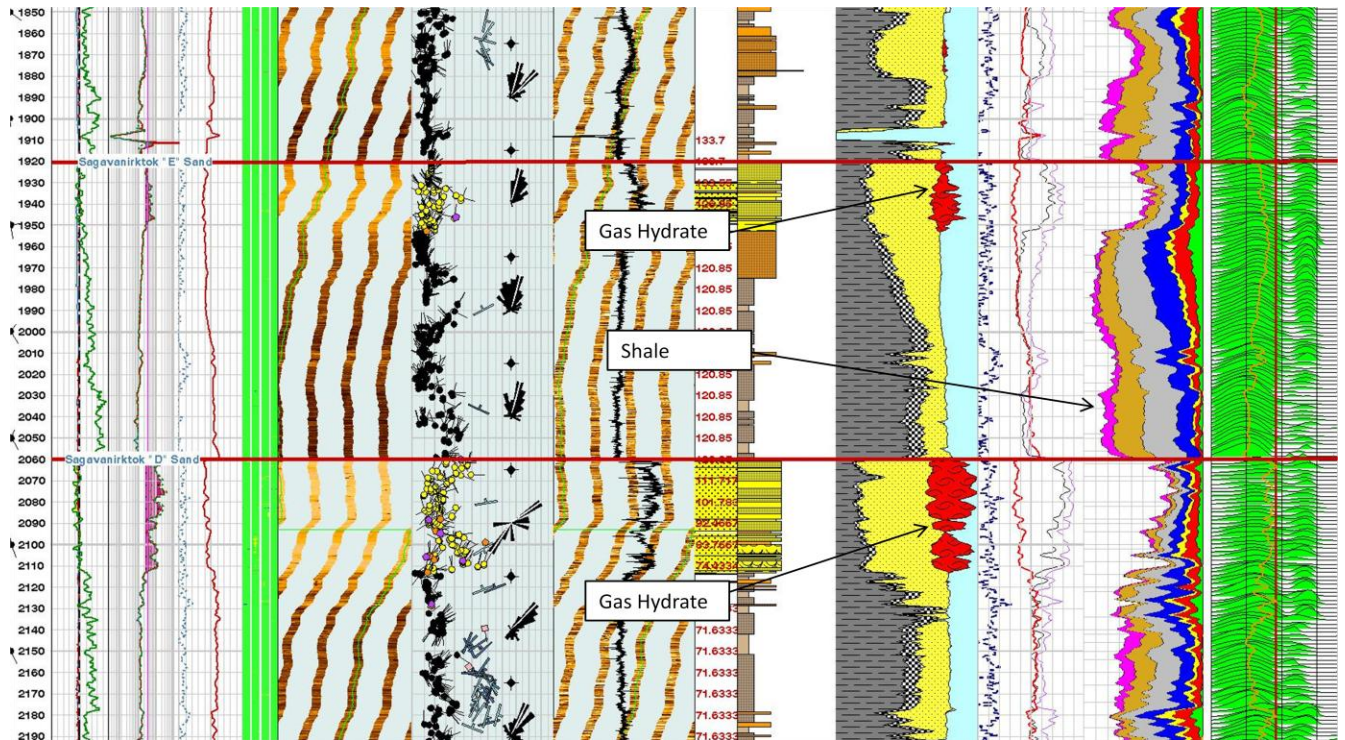
Figure A1.3: 1850 - 2190 ft MD of the Ignik Sikumi #1 well.
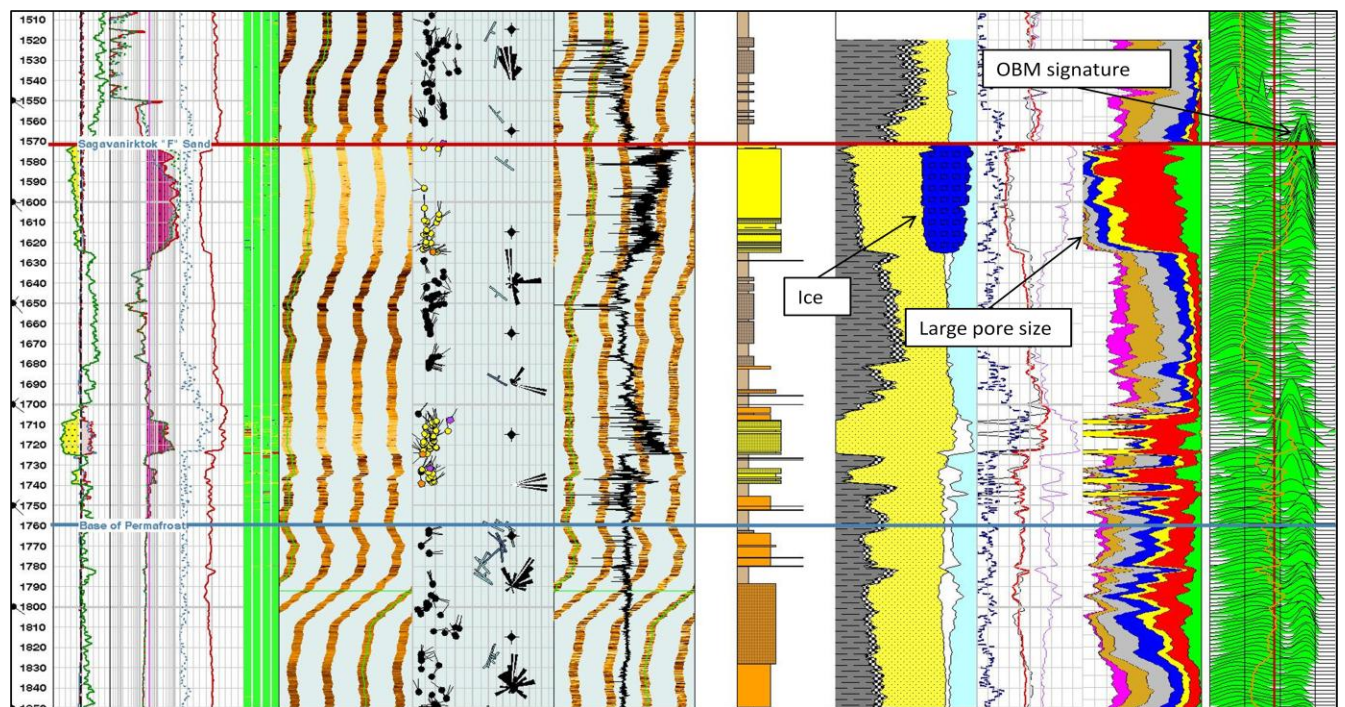
Figure A1.4: 1490 – 1850 ft MD of the Ignik Sikumi #1 well.
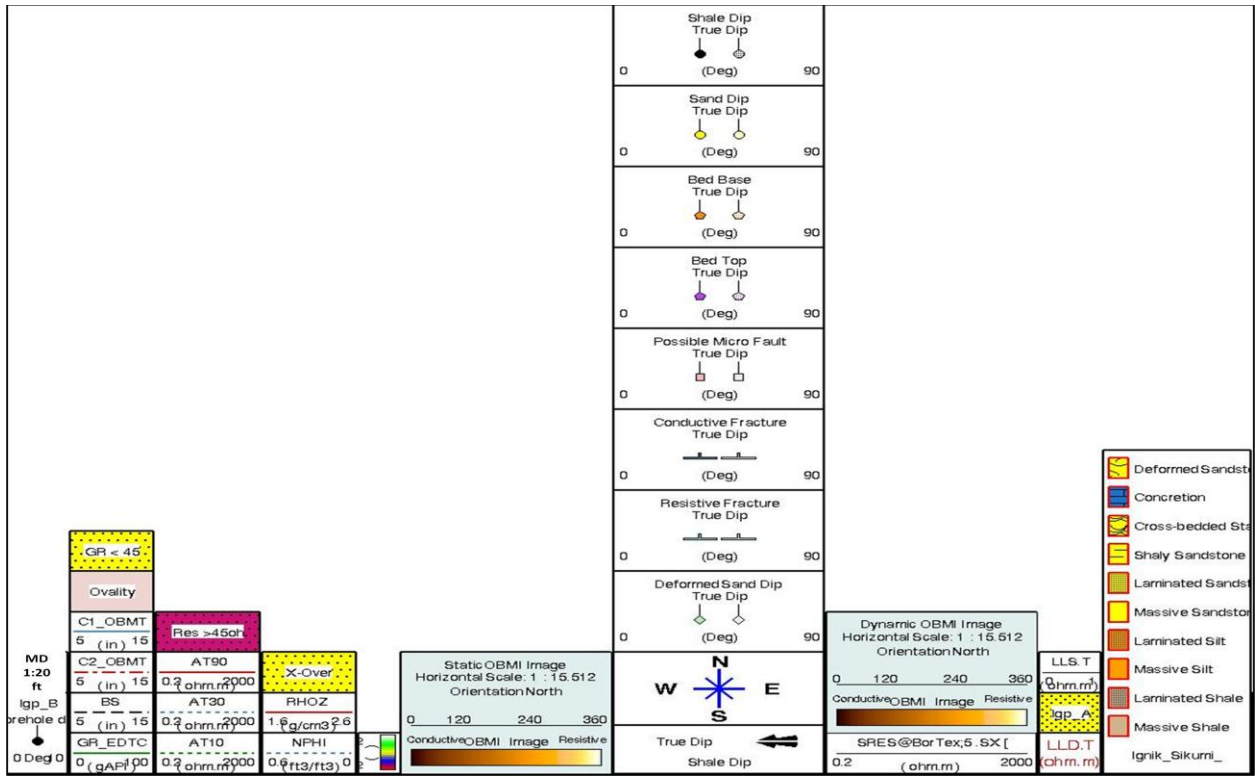
Figure A2.1: Log Header for appendix figures A2
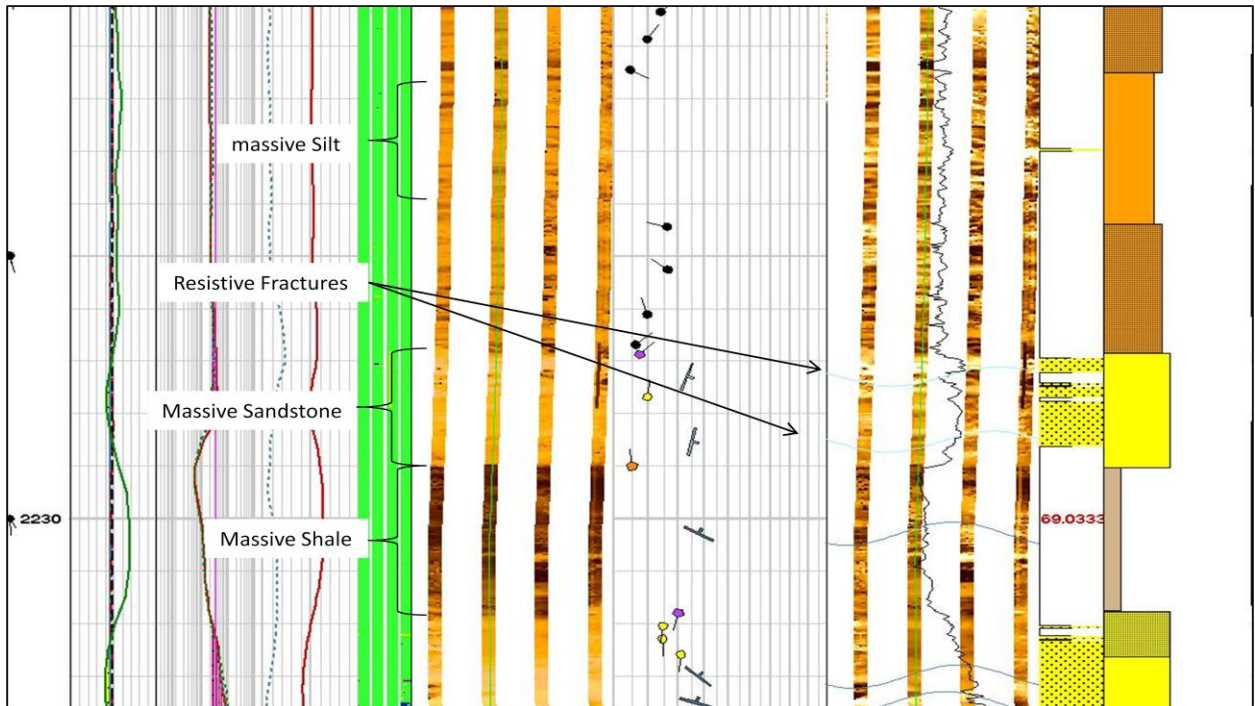
Figure A2.2: Example of the Massive Sand, Massive Shale, and Laminated shale facies.
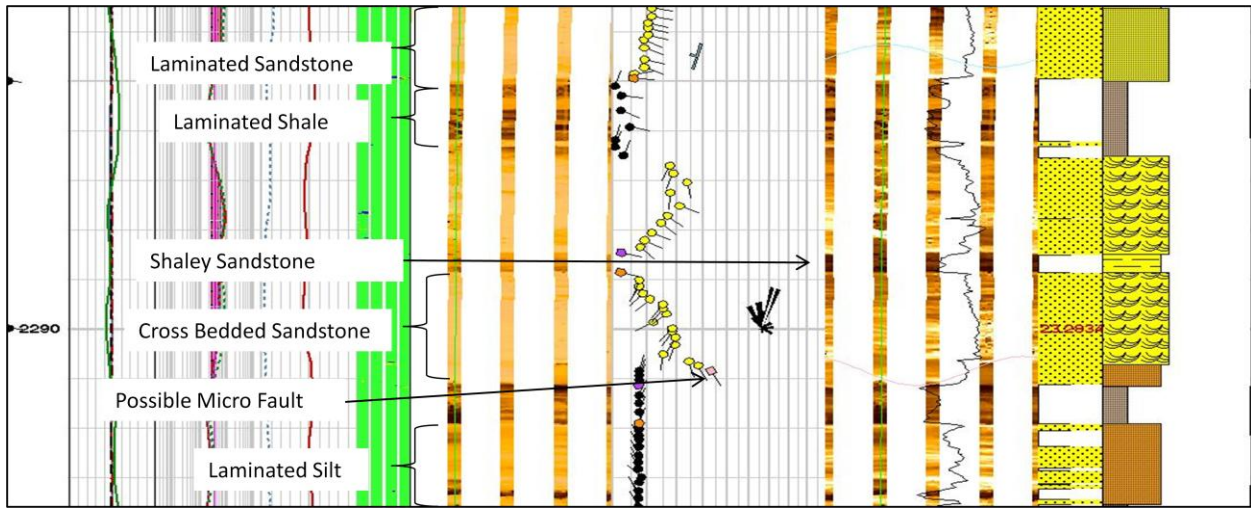
Figure A2.3: Example of the shaley sandstone, laminated sandstone, and concretion facies.
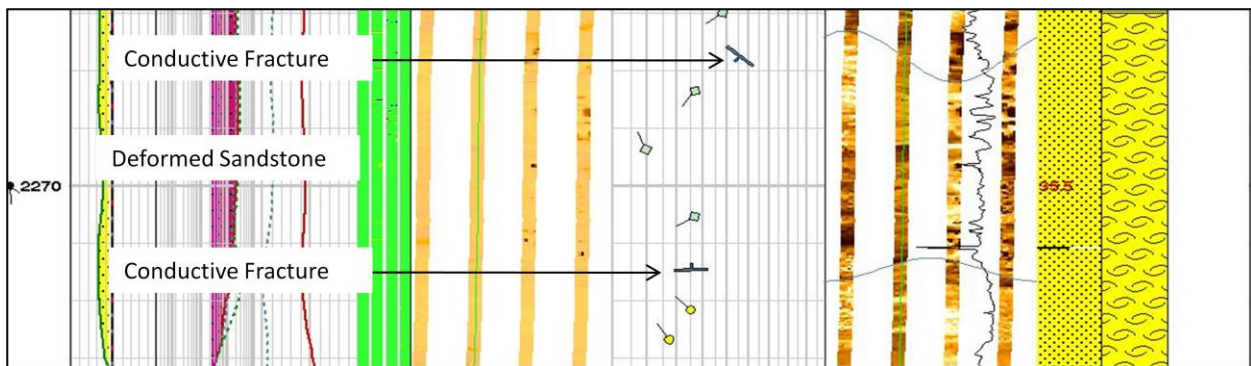
Figure A2.4: Example of the Deformed Sandstone and conductive fractures
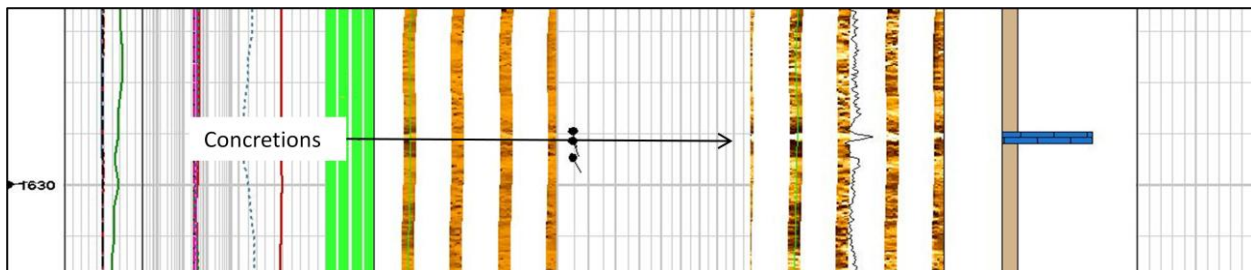
Figure A2.5: Example of the Concretions.

Appendix B - ELAN* elp file

```
session elan {
        temperature ( 10.000000 , 1.266359 ) ;
        boreholeTemp ( 42.900002 , 2598.000000 ) ;
        dataInterval ( 2595.000000 , 1348.125000 ) ;
        processingInterval ( 2540.000000 , 1520.000000 )  ;
        samplingRate 0.500000 ;
        uncertaintyChannel FALSE ;
        clayInput WET ;
        WetDryClayConvert WCLP ;
        bindingPrefer CODE_ONLY ;
        LCPS "Petrophysical";
        queryByCurveSet NO;
        queryByProducer NO;
        queryByCopyNumber NO;
        outputCurveSet "ELANPlus_107445";
        searchPrefer SESSION_FILE_FIRST ;
        mode RESISTIVITY ;
        referenceIndex MD ;
        visibilityLevel LOW ;
        specialFluids WATER ;
process Solve 1 {
        label "SOLVE" ;
        location (92, 57) ;
        solverUsed STANDARD ;
        weightPercentage RELATIVE_C ;
        display AUTO ;
        reconDisplay AUTO ;
        saveOutput ON ;
        equations RHOB CXDC_DWA GR ;
        volumes QUAR ILLI SMI2 XIWA ;
        constraintZoning {
                ( "UNDEFINED"  2595.000000 -999.250000 ) };
};
process Solve 2 {
        label "SOLVE" ;
        location (261, 59) ;
        solverUsed STANDARD ;
        weightPercentage RELATIVE_C ;
        display AUTO ;
        reconDisplay AUTO ;
        saveOutput ON ;
        equations RHOB BFV GR ;
        volumes QUAR ILLI XWAT XIWA ;
        constraintZoning {
                ( "UNDEFINED"  2595.000000 -999.250000 ) };
```

```
};
process Solve 3 {
        label "SOLVE" ;
        location (390, 138) ;
        solverUsed STANDARD ;
        weightPercentage RELATIVE_C ;
        display AUTO ;
        reconDisplay AUTO ;
        saveOutput ON ;
        equations RHOB BFV GR ;
        volumes QUAR ILLI SMI1 XIWA ;
        constraintZoning {
                ( "UNDEFINED"  2595.000000 -999.250000 ) };
};
process Combine 1 {
        label "COMBINE" ;
        location (159, 193) ;
        display AUTO ;
        reconDisplay AUTO ;
        saveOutput ON ;
        combineMethod {
                ( "UNDEFINED" 2595.000000 INT_AVE ) ,
                ( "Permafrost" 1850.000000 2 "SOLVE" ) ,
                ( "A" 1625.000000 3 "SOLVE" ) ,
                ( "B" 1570.000000 2 "SOLVE" ) };
        combineOrder SOL_1 SOL_2 SOL_3  ;
        expressions "wa_elan/hupp_cp_ignik_sikumi-1_elan_v01_COMBINE_1.prob"
        {prob(SOL.2,linear(GR_CH,75,0,90,1))};
};
dependency {
        ( SOL_3 , COM_1 ) ,
        ( SOL_2 , COM_1 ) ,
        ( SOL_1 , COM_1 ) };
zoning {
        ( "UNDEFINED" 2595.000000 42.862011 False NULL 0 G ) };
zone_color {
        ( "UNDEFINED" "Blue" 0.000000 0.000000 1.000000 1.000000 ) };
parameters {
        ( RHOB_QUAR "UNDEFINED" 2.650000 -999.250000) ,
        ( RHOB_ILLI "UNDEFINED" 2.610000 -999.250000) ,
        ( RHOB_SMI1 "UNDEFINED" 0.910000 -999.250000) ,
        ( RHOB_SMI2 "UNDEFINED" 0.910000 -999.250000) ,
        ( RHOB_XWAT "UNDEFINED" 0.910000 -999.250000) ,
        ( RHOB_UWAT "UNDEFINED" 1.013040 -999.250000) ,
        ( RHOB_XIWA "UNDEFINED" 1.009813 -999.250000) ,
        ( RHOB_XOIL "UNDEFINED" 0.910000 -999.250000) ,
        ( RHOB_UOIL "UNDEFINED" 0.910000 -999.250000) ,
```

(RHOB_XBWA "UNDEFINED" 1.000000 -999.250000) ,
(BFV_QUAR "UNDEFINED" 0.000000 -999.250000) ,
(BFV_ILLI "UNDEFINED" 0.100000 -999.250000) ,
(BFV_SMI1 "UNDEFINED" 0.000000 -999.250000) ,
(BFV_SMI2 "UNDEFINED" 0.000000 -999.250000) ,
(BFV_XWAT "UNDEFINED" 0.000000 -999.250000) ,
(BFV_UWAT "UNDEFINED" 1.000000 -999.250000) ,
(BFV_XIWA "UNDEFINED" 1.000000 -999.250000) ,
(BFV_XOIL "UNDEFINED" 0.000000 -999.250000) ,
(BFV_UOIL "UNDEFINED" 0.000000 -999.250000) ,
(CXDC_ILLI "UNDEFINED" -999.250000 -999.250000) ,
(CXDC_XWAT "UNDEFINED" 0.500000 -999.250000) ,
(CXDC_XIWA "UNDEFINED" 0.333333 -999.250000) ,
(CXDC_XBWA "UNDEFINED" -999.250000 -999.250000) ,
(CUDC_ILLI "UNDEFINED" -999.250000 -999.250000) ,
(CUDC_UWAT "UNDEFINED" 0.499715 -999.250000) ,
(CUDC_UBWA "UNDEFINED" -999.250000 -999.250000) ,
(GR_QUAR "UNDEFINED" 40.000000 -999.250000) ,
(GR_ILLI "UNDEFINED" 150.000000 -999.250000) ,
(GR_SMI1 "UNDEFINED" 0.000000 -999.250000) ,
(GR_SMI2 "UNDEFINED" 0.000000 -999.250000) ,
(GR_XWAT "UNDEFINED" 0.000000 -999.250000) ,
(GR_UWAT "UNDEFINED" 0.000000 -999.250000) ,
(GR_XIWA "UNDEFINED" 0.000000 -999.250000) ,
(GR_XOIL "UNDEFINED" 0.000000 -999.250000) ,
(GR_UOIL "UNDEFINED" 0.000000 -999.250000) ,
(CT1_QUAR "UNDEFINED" 0.000000 -999.250000) ,
(CT1_ILLI "UNDEFINED" 0.000000 -999.250000) ,
(CT1_XWAT "UNDEFINED" 1.000000 -999.250000) ,
(CT1_UWAT "UNDEFINED" -1.000000 -999.250000) ,
(CT1_XOIL "UNDEFINED" 0.000000 -999.250000) ,
(CT1_UOIL "UNDEFINED" 0.000000 -999.250000) ,
(CT2_QUAR "UNDEFINED" 0.000000 -999.250000) ,
(CT2_ILLI "UNDEFINED" 0.000000 -999.250000) ,
(CT2_XWAT "UNDEFINED" 0.000000 -999.250000) ,
(CT2_UWAT "UNDEFINED" 0.000000 -999.250000) ,
(CT2_XOIL "UNDEFINED" 1.000000 -999.250000) ,
(CT2_UOIL "UNDEFINED" -1.000000 -999.250000) ,
(ARHOB_ILLI "UNDEFINED" 2.794000 -999.250000) ,
(WCLP_ILLI "UNDEFINED" 0.173417 -999.250000) ,
(CBWA_ILLI "UNDEFINED" 2.081580 -999.250000) ,
(CECA_ILLI "UNDEFINED" 0.160000 -999.250000) ,
(RMF "UNDEFINED" 10000.000000 -999.250000) ,
(MST "UNDEFINED" 42.862000 -999.250000) ,
(RW "UNDEFINED" 2.000000 -999.250000) ,
(RWT "UNDEFINED" 42.900002 -999.250000) ,
(SALIN_ISOL "UNDEFINED" -999.250000 -999.250000) ,

```
        ( SALIN_PARA "UNDEFINED" -999.250000 -999.250000) ,
        ( SALIN_XWAT "UNDEFINED" 0.000000 -999.250000) ,
        ( SALIN_UWAT "UNDEFINED" 4.266850 -999.250000) ,
        ( SALIN_XIWA "UNDEFINED" 0.000738 -999.250000) ,
        ( SALIN_UIWA "UNDEFINED" -999.250000 -999.250000) ,
        ( SALIN_XOIL "UNDEFINED" 0.000000 -999.250000) ,
        ( SALIN_UOIL "UNDEFINED" 0.000000 -999.250000) ,
        ( SALIN_XGAS "UNDEFINED" 0.000000 -999.250000) ,
        ( SALIN_UGAS "UNDEFINED" 0.000000 -999.250000) ,
        ( SALIN_XSFL "UNDEFINED" -999.250000 -999.250000) ,
        ( SALIN_USFL "UNDEFINED" -999.250000 -999.250000) ,
        ( CT1_ZP "UNDEFINED" 0.000000 -999.250000) ,
        ( CT2_ZP "UNDEFINED" 0.000000 -999.250000) ,
        ( RHOB_UNC_ZP "UNDEFINED" 0.027000 -999.250000) ,
        ( BFV_UNC_ZP "UNDEFINED" 0.015000 -999.250000) ,
        ( CXDC_UNC_ZP "UNDEFINED" 0.000325 -999.250000) ,
        ( CUDC_UNC_ZP "UNDEFINED" 0.021147 -999.250000) ,
        ( GR_UNC_ZP "UNDEFINED" 2.250000 -999.250000) ,
        ( CT1_UNC_ZP "UNDEFINED" 0.015000 -999.250000) ,
        ( CT2_UNC_ZP "UNDEFINED" 0.015000 -999.250000) ,
        ( VOLS_UNC_ZP "UNDEFINED" 0.015000 -999.250000) ,
        ( RHOB_UNC_WM "UNDEFINED" 1.000000 -999.250000) ,
        ( BFV_UNC_WM "UNDEFINED" 1.000000 -999.250000) ,
        ( CXDC_UNC_WM "UNDEFINED" 0.500000 -999.250000) ,
        ( CUDC_UNC_WM "UNDEFINED" 0.670000 -999.250000) ,
        ( GR_UNC_WM "UNDEFINED" 0.300000 -999.250000) ,
        ( CT1_UNC_WM "UNDEFINED" 1.000000 -999.250000) ,
        ( CT2_UNC_WM "UNDEFINED" 1.000000 -999.250000) ,
        ( VOLS_UNC_WM "UNDEFINED" 1.000000 -999.250000) ,
        ( RHOB_IFAC_ZP "UNDEFINED" 0.300000 -999.250000) ,
        ( A_ZP "UNDEFINED" 1.000000 -999.250000) ,
        ( N_ZP "UNDEFINED" 2.000000 -999.250000) ,
        ( C_DWA "UNDEFINED" 1.000000 -999.250000) ,
        ( M_DWA "UNDEFINED" 1.738000 -999.250000) };
visibility {
        ( RHOB_QUAR, LOW ) ,
        ( RHOB_ILLI, LOW ) ,
        ( RHOB_SMI1, HIGH ) ,
        ( RHOB_SMI2, HIGH ) ,
        ( RHOB_XWAT, HIGH ) ,
        ( RHOB_UWAT, LOW ) ,
        ( RHOB_XIWA, LOW ) ,
        ( RHOB_XOIL, HIGH ) ,
        ( RHOB_UOIL, HIGH ) ,
        ( RHOB_XBWA, LOW ) ,
        ( BFV_QUAR, LOW ) ,
        ( BFV_ILLI, HIGH ) ,
```

(BFV_SMI1, LOW) ,
(BFV_SMI2, LOW) ,
(BFV_XWAT, HIGH) ,
(BFV_UWAT, LOW) ,
(BFV_XIWA, HIGH) ,
(BFV_XOIL, HIGH) ,
(BFV_UOIL, LOW) ,
(CXDC_ILLI, LOW) ,
(CXDC_XWAT, HIGH) ,
(CXDC_XIWA, LOW) ,
(CXDC_XBWA, LOW) ,
(CUDC_ILLI, LOW) ,
(CUDC_UWAT, LOW) ,
(CUDC_UBWA, LOW) ,
(GR_QUAR, HIGH) ,
(GR_ILLI, HIGH) ,
(GR_SMI1, HIGH) ,
(GR_SMI2, HIGH) ,
(GR_XWAT, LOW) ,
(GR_UWAT, LOW) ,
(GR_XIWA, LOW) ,
(GR_XOIL, LOW) ,
(GR_UOIL, LOW) ,
(CT1_QUAR, HIGH) ,
(CT1_ILLI, HIGH) ,
(CT1_XWAT, HIGH) ,
(CT1_UWAT, HIGH) ,
(CT1_XOIL, HIGH) ,
(CT1_UOIL, HIGH) ,
(CT2_QUAR, HIGH) ,
(CT2_ILLI, HIGH) ,
(CT2_XWAT, HIGH) ,
(CT2_UWAT, HIGH) ,
(CT2_XOIL, HIGH) ,
(CT2_UOIL, HIGH) ,
(ARHOB_ILLI, LOW) ,
(WCLP_ILLI, HIGH) ,
(CBWA_ILLI, HIGH) ,
(CECA_ILLI, HIGH) ,
(RMF, HIGH) ,
(MST, HIGH) ,
(RW, HIGH) ,
(RWT, HIGH) ,
(SALIN_ISOL, LOW) ,
(SALIN_PARA, LOW) ,
(SALIN_XWAT, LOW) ,
(SALIN_UWAT, LOW) ,

```
                ( SALIN_XIWA, LOW ) ,
                ( SALIN_UIWA, LOW ) ,
                ( SALIN_XOIL, LOW ) ,
                ( SALIN_UOIL, LOW ) ,
                ( SALIN_XGAS, LOW ) ,
                ( SALIN_UGAS, LOW ) ,
                ( SALIN_XSFL, HIGH ) ,
                ( SALIN_USFL, HIGH ) ,
                ( CT1_ZP, HIGH ) ,
                ( CT2_ZP, HIGH ) ,
                ( RHOB_UNC_ZP, LOW ) ,
                ( BFV_UNC_ZP, LOW ) ,
                ( CXDC_UNC_ZP, LOW ) ,
                ( CUDC_UNC_ZP, LOW ) ,
                ( GR_UNC_ZP, HIGH ) ,
                ( CT1_UNC_ZP, HIGH ) ,
                ( CT2_UNC_ZP, HIGH ) ,
                ( VOLS_UNC_ZP, LOW ) ,
                ( RHOB_UNC_WM, HIGH ) ,
                ( BFV_UNC_WM, HIGH ) ,
                ( CXDC_UNC_WM, HIGH ) ,
                ( CUDC_UNC_WM, HIGH ) ,
                ( GR_UNC_WM, HIGH ) ,
                ( CT1_UNC_WM, HIGH ) ,
                ( CT2_UNC_WM, HIGH ) ,
                ( VOLS_UNC_WM, HIGH ) ,
                ( RHOB_IFAC_ZP, HIGH ) ,
                ( A_ZP, HIGH ) ,
                ( N_ZP, HIGH ) ,
                ( C_DWA, HIGH ) ,
                ( M_DWA, HIGH ) };
binding {
                ( TEMP_CH "TEMP"  0 ) ,
                ( RHOB_IFAC_CH "IFRH"  0 ) ,
                ( RHOB_CH "RHOZ"  61886 ) ,
                ( BFV_CH "BFV"  62134 ) ,
                ( CXDC_CH "AO90"  56366 ) ,
                ( GR_CH "GR"  61491 ) ,
                ( PRB1_CH "PRB1"  0 ) ,
                ( PRB2_CH "PRB2"  0 ) ,
                ( PRB3_CH "PRB3"  0 ) ,
                ( M_CH "MXP"  0 ) ,
                ( N_CH "SXP"  0 )};

displayToolOrder {
                RHOB 1.500000 3.500000
                NPHI 0.500000 0.000000
```

NPHU 0.500000 0.000000
ENPI 0.500000 0.000000
TCMR 0.500000 0.000000
CMFF 0.500000 0.000000
BFV 0.500000 0.000000
BMK 0.000000 10.000000
VELC 7.500000 25.000000
DT 140.000000 40.000000
U 2.000000 22.000000
PHIT 0.500000 0.000000
CXDC 5.000000 0.000000
CUDC 5.000000 0.000000
CXDC_DWA 5.000000 0.000000
CUDC_DWA 5.000000 0.000000
CXDC_WS 5.000000 0.000000
CUDC_WS 5.000000 0.000000
CXDC_SIM 5.000000 0.000000
CUDC_SIM 5.000000 0.000000
CXDC_IND 5.000000 0.000000
CUDC_IND 5.000000 0.000000
QVSP_N 0.000000 5.000000
GR 0.000000 200.000000
CSI 0.000000 0.500000
CCA 0.000000 1.000000
CHY 0.000000 0.250000
CFE 0.000000 0.500000
CSUL 0.000000 0.500000
CCHL 0.000000 1.000000
CGDM 0.000000 0.500000
CK 0.000000 0.250000
CTI 0.000000 0.100000
DWSI 0.000000 0.500000
DWCA 0.000000 0.500000
DWFE 0.000000 0.150000
DWSU 0.000000 0.500000
DWK 0.000000 0.050000
DWAL 0.000000 0.200000
DWMG 0.000000 0.150000
DWTI 0.000000 0.010000
DWGD 0.000000 0.200000
DWTH 0.000000 20.000000
DWU 0.000000 0.100000
WWSI 0.000000 0.500000
WWCA 0.000000 0.500000
WWFE 0.000000 0.150000
WWSU 0.000000 0.500000
WWK 0.000000 0.050000

```
          WWAL 0.000000 0.200000
          WWMG 0.000000 0.150000
          WWTI 0.000000 0.010000
          WWGD 0.000000 0.200000
          WWTH 0.000000 20.000000
          WWU 0.000000 0.100000
          EATT 1000.000000 0.000000
          TPL 20.000000 5.000000
          SIGM 5.000000 50.000000
          EX1 0.000000 1.000000
          EX2 0.000000 1.000000
          EX3 0.000000 1.000000
          EX4 0.000000 1.000000
          EX5 0.000000 1.000000
          EX6 0.000000 1.000000
          EX7 0.000000 1.000000
          EX8 0.000000 1.000000
          EX9 0.000000 1.000000
          EX10 0.000000 1.000000
          CT1 -0.100000 0.100000
          CT2 -0.100000 0.100000
          CT3 -0.100000 0.100000
          CT4 -0.100000 0.100000
          CT5 -0.100000 0.100000
          CT6 -0.100000 0.100000
          };

displayVolumeOrder {
          CHLO
          ILLI
          KAOL
          MONT
          GLAU
          CLA1
          CLA2
          SHAL
          XBWA
          SILT
          COAL
          QUAR
          SAND
          ORTH
          ALBI
          FELD
          MUSC
          BIOT
          SIDE
```

```
PYRI
IGNE
META
SMI1
SMI2
HALI
GYPS
ANHY
EVAP
CALC
DOLO
CARB
ISOL
PARA
XGAS
XOIL
XSFL
XWAT
XIWA
};

}
```